UNIVERSIDAD DE GRANADA

DEPARTAMENTO DE MECÁNICA DE ESTRUCTURAS E INGENIERÍA HIDRÁULICA

PROGRAMA OFICIAL DE POSGRADO EN ESTRUCTURAS

SEISMIC BEHAVIOR OF EXISTING REINFORCED CONCRETE FRAMES AND ITS SEISMIC UPGRADING USING ENERGY DISSIPATION DEVICES

COMPORTAMIENTO SÍSMICO DE PÓRTICOS EXISTENTES DE HORMIGÓN ARMADO Y SU REACONDICIONAMIENTO SÍSMICO MEDIANTE DISPOSITIVOS DE DISIPACIÓN DE ENERGÍA

Memoria presentada por

Elena Oliver Saiz

Para la obtención del
grado de Doctor por la Universidad de Granada con Mención de Doctorado Internacional

Director: Dr. Amadeo Benavent Climent

GRANADA, 2015

Editorial: Universidad de Granada. Tesis Doctorales
Autora: María Elena Oliver Sanz
ISBN: 978-84-9125-286-3
URI: http://hdl.handle.net/10481/40942

La doctorando Elena Oliver Saiz y el director de la tesis Dr. Amadeo Benavent Climent garantizamos, al firmar esta tesis doctoral, que el trabajo ha sido realizado por la doctorando bajo la dirección de el director de la tesis y hasta donde nuestro conocimiento alcanza, en la realización del trabajo, se han respetado los derechos de otros autores a ser citados, cuando se han utilizado sus resultados o publicaciones.

Granada, Junio de 2015

Director de la Tesis	Doctorando
	
Fdo.: Dr. Amadeo Benavent Climent	Fdo.: Elena Oliver Saiz

This Thesis received financial support from the Spanish Government under a FPU fellowship of the Ministerio de Educacion, Spain (AP2009-0533).

The research stay at the University of California, Berkeley was funded by the Fulbright Schuman Program 2013-2014.

The research stay at the Università degli Studi di Napoli Federico II was funded by the PAP Program–Erasmus de Movilidad Internacional de Estudiantes de Posgrado, awarded by the University of Granada.

This work was developed at the Department of Structural Mechanics and Hydraulic Engineering of the University of Granada.

A mis padres,

y a Álvaro

Por otro lado, Cecil Balmond, el ingeniero de Ove Arup que colaboró en la Serpentine Gallery, es un genio que tiene su propia y excepcional lógica. Justo hace poco tuve una larga conversación telefónica con él sobre un proyecto que estamos haciendo en Inglaterra y le pregunté: "¿no podríamos simplemente dibujar líneas al azar sin girar el cuadrado como hicimos en la Serpentine Gallery?". Pero él insistía: "No, necesitas un algoritmo. Tienes que girar el cuadrado de acuerdo con alguna regla". Es extraño, incluso las líneas dibujadas al azar recurren a las costumbres.

Las reglas hacen algoritmos. Al manipular las reglas obtienes cosas que nunca hubieras pensado.

Extracto del libro "Toyo Ito - Conversaciones con estudiantes", de Akira Suzuki

Agradecimientos

Siempre me ha asombrado la enorme generosidad del que enseña, el que con enorme paciencia guía los pasos del aprendiz y comparte uno de sus bienes más preciados: su conocimiento sobre el mundo. Son muchas las deudas que he adquirido a lo largo de estos años y que me han permitido terminar escribiendo esta memoria, pero mis primeras palabras han de ser para mi director de tesis, Dr. Amadeo Benavent-Climent. A él quiero expresarle mi mayor gratitud por guiar con paciencia y constancia mis pasos, por confiar en mí, siempre, y por poner a mi alcance su valioso conocimiento sobre las estructuras. La deuda contraída con él es impagable.

También guardo un recuerdo enormemente especial para el Prof. Filip C. Filippou, que tuvo la generosidad de acogerme, de compartir su conocimiento verdaderamente único y de guiar mis investigaciones, con dedicación y entusiasmo, durante una inolvidable estancia en la Universidad de California, en Berkeley.

Mi gratitud también hacia el programa Fulbright-Schuman y todas las personas que lo hacen posible y que me permitieron hacer posible mi sueño de realizar esa estancia. En especial, al Prof. Guillermo Rus por su decidido apoyo. Y también a Ali Edelstein su inestimable ayuda con la gestión. A lo largo de todo mi viaje, me sentí feliz y agradecida por la calurosa acogida del programa

Fulbright, que me brindó también la oportunidad de compartir sueños y experiencias con otros Fulbrighters.

Asimismo, me gustaría expresar mi más sincero agradecimiento al Prof. Gaetano Manfredi y al Prof. Andrea Prota por acogerme en la Università degli Studi di Napoli Federico II. En especial, quiero mostrar mi agradecimiento al Prof. Marco Di Ludovico por guiar con atención mis investigaciones y por compartir sus valiosos conocimientos sobre el reacondicionamiento con materiales tipo composite.

También quiero mostrar mi agradecimiento al Prof. Ángel Vallecillo Capilla, por guiar con paciencia y dedicación mis pasos en mi iniciación a la docencia y por proporcionarme una base sólida en el conocimiento de los fundamentos de estructuras, sin los cuales no habría podido progresar en mis investigaciones. También por enseñarme la importancia del conocimiento profundo de las estructuras que hay detrás de una buena obra de Arquitectura.

De un modo especial, guardo enorme gratitud hacia mis profesores de Arquitectura, que me guiaron durante tantos años y me animaron a progresar en el conocimiento de la geometría y las estructuras. En especial al Prof. Antonio Cayuelas Porras, porque fue primero profesor, pero también un buen jefe y mejor amigo. Por su enorme generosidad al compartir su visión contemporánea sobre la Arquitectura, y por guiarme en el aprendizaje del rigor y la precisión.

Guardo también un recuerdo especial de los profesores Ubaldo y Marisol García Torrente, por transmitirme una visión entusiasta de la rehabilitación y por enseñarme a reinterpretar de manera contemporánea el legado arquitectónico.

Por supuesto, este trabajo no habría sido posible sin el apoyo de mis compañeros. Cuando entré a formar parte del equipo del Prof. Benavent-Climent, me acogió un grupo de personas competentes y entusiastas, y puedo decir que de todos he aprendido algo valioso. Con muchos de ellos comparto también algunos de los trabajos de investigación que han hecho posible esta memoria. Gracias Leandro, Jesús, David, Alberto y Ana Luisa.

Finalmente, son tantas las emociones y tan profundo mi agradecimiento, que me temo que es imposible recoger en unas líneas la gratitud que siento hacia las personas más importantes de mi vida, mi familia y mis amigos.

En especial, es muy difícil expresar palabras de agradecimiento hacia mis padres, porque les debo, nunca mejor dicho, toda una vida. A mi madre, que confió siempre en mí y me animó a luchar por alcanzar mis sueños con trabajo y tesón. También por enseñarme la importancia de seguir mi propio criterio y de perseguir con esfuerzo la satisfacción personal que produce el trabajo bien hecho. A mi padre, por enseñarme la felicidad que produce el satisfacer mi infatigable curiosidad mediante el estudio y la investigación. Por transmitirme

los valores que debe reunir un buen profesor, con su ejemplo, generosidad y dedicación.

Quiero dedicar estas últimas y más especiales palabras de gratitud para el mejor compañero de viaje que se puede tener y con el que espero compartir toda mi vida. Porque sin su paciencia, su comprensión y su apoyo durante todo este tiempo, no me habría sido posible terminar esta memoria. Gracias Álvaro por acompañarme, siempre.

Summary

Earthquake engineering has progressed significantly in the last few decades. However, a high proportion of the building stock located in earthquake-prone regions still exhibits serious seismic deficiencies. In fact, many of these buildings were designed before the appearance of seismic codes, in view of rudimentary anti-seismic design criteria and/or by using obsolete seismic hazard maps. A significant number of the structures that still remain under-designed have reinforced concrete (RC) frames as the main system of lateral resistance. Recent seismic events revealed the poor performance of under-designed RC frame structures (L'Aquila 2009, Lorca 2011 and Emilia 2012), accentuating the need for seismic assessment and retrofitting. In this sense, it is necessary to develop retrofitting strategies that increase the seismic capacity of existing structures and that control the level of structural and non-structural damage, within the framework of performance-based seismic design. To this end, the addition of energy dissipation devices is an effective technique that provides not only the strength and deformation capacity required to protect human life, but also the supplemental energy dissipation capacity necessary to reduce

structural and non-structural damage. Among the different types of energy dissipation devices that are commercially available or under development, the so-called "hysteretic" dampers are particularly popular because of their low cost, in comparison with viscous fluid dampers or viscoelastic solid dampers. For this reason, the use of brace-type hysteretic dampers for the seismic upgrading of existing frames has increased exponentially in the past two decades. Nevertheless, adding hysteretic dampers to an under-designed RC frame structure is not straightforward and some important issues must be addressed. On one hand, the connection of the hysteretic dampers to the existing frame requires special attention. The brace may develop high axial loads and the design of the anchoring system to the existing beam-column joint may be costly and difficult to execute. On the other hand, the dampers require the frame to have a minimum lateral deformation capacity, in order to develop their inherent energy dissipation capacity. Under-designed RC frames may not posses this minimum deformation capacity required for an efficient combination of frame and dampers. For this reasons, this Thesis is focused on investigating two main issues: (i) a solution for connecting brace-type hysteretic dampers to the existing RC frame; and (ii) a hybrid retrofitting solution with hysteretic dampers that considers the possibility of including local strengthening procedures (e.g. FRP/SRP), in order to increase the lateral deformation capacity of the main frame.

Regarding the first issue, a new solution for connecting concentric braces to beam-column joints of existing RC frames is investigated in Chapter 3. This solution is suitable for connecting either a conventional concentric steel brace or a brace-type hysteretic damper. It consists of (i) two shear-key steel plates fixed to the concrete with anchor bolts —which restrain the displacements of the end-plates of the steel brace— and (ii) a device for minimizing friction forces between the shear-key plates and the end-plates. Minimizing friction produces the effect of eliminating tension forces on the anchor bolts and of reducing the bending moments on the shear-key plates. Consequently, this solution allows using thin plates without stiffeners and avoids brittle failure modes on the anchors, thus reducing the number of anchors, as well as the required effective anchorage depth. To clarify the influence of some parameters (such as the initial gaps between the steel plates and the thickness of the Teflon sheets) a 3D finite element model is developed. As a result, execution provisions and design criteria of the brace-frame connection are proposed. Finally, the efficiency and validity of the proposed brace-frame connection is evaluated through shaking-table tests conducted on a 3x3x3 m^3 scaled RC frame retrofitted with brace-type hysteretic dampers. Experimental results show that the braces installed with the proposed brace-frame connection successfully controlled the damage on the main frame and that the hysteretic dampers dissipated most of the energy input by the earthquake. Thus, the proposed brace-frame

connection was effective in mobilizing the energy dissipation capacity of the hysteretic dampers.

Second, a retrofitting solution with hysteretic dampers is presented in Chapter 4, which considers the addition of local strengthening procedures (e.g. FRP/SRP) to enhance the flexural strength and/or the lateral deformation capacity of the main frame. As explained above, a minimum lateral deformation capacity of the main RC frame is required for the hysteretic dampers (displacement-based devices) to develop their intrinsic energy dissipation capacity. An energy-based method proposed by Benavent-Climent in past research for retrofitting RC frame structures with hysteretic dampers, is extended in this Thesis to consider the possibility of locally strengthening the main frame (e.g. adding FRP/SRP). In this way, the proposed procedure ensures the existence of a solution for the design of the dampers that meets the inter-story drift requirements at each floor. In addition, this procedure is capable of predicting the maximum inter-story drift for different mean return periods, thus being possible to evaluate the solution for different performance objectives. Finally, the energy-based seismic design procedure is tested by means of nonlinear time history analysis, as described in Chapter 5. For this purpose, a retrofitting solution is designed for each earthquake scenario (near-fault and far-field) to upgrade a six-story prototype RC frame structure —representative of pre-70 residential buildings. The performance of these solutions is evaluated

for three levels of seismic hazard (corresponding to mean return periods 95, 475 and 2475 years). Later, a numerical model is developed, and subjected to two sets of 20 natural acceleration records —far-field and near-fault. Results show good agreement between the overall performance obtained from the dynamic response analysis, and the behavior anticipated in the design. As intended in the design procedure, there was no concentration of damage and the dampers dissipated most of the energy input by the earthquake

Resumen

La ingeniería sísmica ha evolucionado significativamente en las últimas décadas. Sin embargo, una elevada proporción de las construcciones existentes, ubicadas en zonas de riesgo sísmico, todavía presenta serias deficiencias en cuanto a su diseño sismorresistente. De hecho, muchos de estos edificios se construyeron con anterioridad a la aparición de códigos sísmicos, siguiendo criterios de diseño sismorresistente rudimentarios, y/o utilizando mapas de peligrosidad sísmica que han quedado obsoletos. Un número elevado de estas estructuras existentes fue construido con pórticos de hormigón armado (HA), que constituyen su principal sistema de resistencia lateral. Recientemente, varios eventos sísmicos han puesto de manifiesto el mal comportamiento de este tipo de estructuras de HA (L'Aquila 2009, Lorca 2011 y Emilia 2012), enfatizando la necesidad de evaluar su comportamiento sísmico y de llevar a cabo las medidas necesarias para su reacondicionamiento. En este sentido, se deben desarrollar estrategias de reacondicionamiento capaces de mejorar la capacidad sismorresistente de las estructuras existentes, pero también de controlar el nivel de daño, tanto estructural como no-estructural,

en el marco del diseño sismorresistente basado en prestaciones. Para ello, la instalación de dispositivos de disipación de energía se revela como una técnica efectiva que proporciona la resistencia y la rigidez lateral necesarias para asegurar la protección de vidas humanas, pero también la capacidad adicional de disipación de energía necesaria para reducir el daño tanto estructural como no-estructural. Entre los distintos tipos de dispositivos de disipación de energía que están disponibles en el mercado o en desarrollo, los llamados disipadores "histeréticos" son especialmente populares debido a su bajo coste, en comparación con los disipadores de fluido viscoso o con los disipadores visco-elásticos sólidos. Por este motivo, el uso de disipadores histeréticos para el reacondicionamiento sísmico de estructuras existentes, que se instalan como barras de arriostramiento convencionales en el interior de estructuras porticadas, ha aumentado exponencialmente en las ultimas dos décadas. No obstante, añadir disipadores histeréticos a una estructura porticada de HA carente de la necesaria capacidad sismorresistente, requiere tener en cuenta algunos aspectos importantes. Por un lado, la conexión de disipadores histeréticos a la estructura porticada existente requiere especial atención. Los disipadores tipo barra pueden desarrollar fuerzas axiles elevadas y el diseño de su sistema de anclaje a la unión viga-columna de HA existente puede ser cara y difícil de ejecutar. Por otro lado, los disipadores requieren que el pórtico existente posea una mínima capacidad de deformación lateral para que puedan desarrollar adecuadamente su inherente capacidad de disipación de energía. Las

estructuras porticadas de HA que no cumplen la normativa sismorresistente pueden no poseer esta mínima capacidad de deformación lateral, necesaria para que la solución estructural que combina pórtico y disipadores sea eficiente. Por estas razones, la presente Tesis se centra en investigar dos cuestiones importantes: (i) una solución para conectar disipadores histeréticos tipo barra a estructuras existentes porticadas de HA; y (ii) una solución de reacondicionamiento híbrida con disipadores de tipo histerético que considera la posibilidad de reforzar localmente el pórtico principal (por ejemplo, mediante materiales tipo composite FRP/SRP), para incrementar su capacidad de deformación lateral.

En primer lugar, en el Capítulo 3 se investiga una solución nueva para conectar barras de tipo concéntrico a las uniones viga-columna de pórticos existentes de HA. Esta solución es adecuada tanto para conectar una barra de acero de arriostramiento convencional, como para conectar un disipador histerético tipo barra. Consiste en (i) dos placas de cortante de acero (*shear-key plates*), fijadas a la superficie de hormigón con tornillos de anclaje, que restringen el desplazamiento de las placas soldadas en el extremo de la barra de acero (*end-plates*); y (ii) un dispositivo que permite minimizar las fuerzas de fricción entre las placas de cortante y las placas extremas. De esta manera, al minimizar la fricción entre las placas se consigue eliminar las fuerzas axiles de tensión en los tornillos de anclaje y reducir el momento flector en las placas de cortante. En consecuencia, esta solución

permite emplear placas delgadas sin rigidizadores y evita el desarrollo de modos de fallo frágiles en los anclajes, reduciendo así el número de tornillos de anclaje y la profundidad de anclaje efectiva necesaria. Para determinar la influencia de algunos parámetros (tales como la separación inicial entre las placas de acero o el grosor de las láminas de Teflón) se ha desarrollado un modelo de elementos finitos en 3D. Como resultado, se proponen disposiciones de ejecución y criterios de diseño para la solución de conexión propuesta. Finalmente, la eficiencia y validez de esta conexión barra-pórtico se evalúa mediante ensayos dinámicos en mesa sísmica de un espécimen a escala, formado por una estructura porticada de HA con dimensiones 3x3x3 m^3 y reacondicionado con disipadores histeréticos tipo barra. Los resultados experimentales muestran que las barras diagonales instaladas con la solución de conexión propuesta controlaron satisfactoriamente el daño en el pórtico principal y que la mayor parte de la energía introducida por el terremoto fue disipada por los disipadores histeréticos. Por tanto, la solución de conexión propuesta fue efectiva en movilizar la capacidad de disipación de energía de los disipadores histeréticos.

En segundo lugar, en el Capítulo 4 se presenta una solución de reacondicionamiento con disipadores histeréticos que considera la posibilidad de reforzar localmente el pórtico principal (p. ej. FRP/SRP) para mejorar su resistencia a flexión y su capacidad de deformación lateral. Como se ha explicado anteriormente, el pórtico principal debe poseer una mínima capacidad de deformación lateral

para que los disipadores histeréticos (dispositivos basados en el desplazamiento) desarrollen su capacidad intrínseca de disipación de energía. Esta Tesis extiende el método basado en energía propuesto por Benavent-Climent en investigaciones previas, para el reacondicionamiento de estructuras porticadas de HA con disipadores de tipo histerético, incluyendo la posibilidad de reforzar localmente el pórtico existente (p. ej. FRP/SRP). De esta manera, el procedimiento propuesto asegura la existencia de una solución para el diseño de los disipadores que permita controlar el valor de la desviación entre plantas (*inter-story drift*) en todas las plantas del edificio. Además, este procedimiento es capaz de predecir la máxima desviación entre plantas para niveles de peligrosidad sísmica correspondientes a distintos periodos de retorno medio, siendo posible alcanzar diferentes objetivos de prestaciones. Finalmente, este procedimiento de diseño sismorresistente basado en energía se valida mediante análisis dinámicos directos, como se describe en el Capítulo 5. Para ello, se diseña una solución de reacondicionamiento para un prototipo de pórtico de HA de 6 plantas, representativo de edificios residenciales construidos con anterioridad a 1970, para dos escenarios sísmicos distintos: cerca y lejos de falla. La respuesta de estas soluciones se evalúa bajo tres niveles de peligrosidad sísmica (correspondientes a periodos de retorno medio de 95, 475 y 2475 años). Para ello, se realizan cálculos dinámicos directos con dos conjuntos de 20 acelerogramas históricos —cerca y lejos de falla. Los resultados muestran una buena correspondencia entre la respuesta global

obtenida en los análisis numéricos y el comportamiento predicho por el procedimiento propuesto. Tal como pretendía el procedimiento de diseño, los resultados muestran que no hubo concentración de daño y que los disipadores disiparon la mayor parte de la energía introducida por el terremoto.

Contents

1

Introduction

Seismic design is a relatively recent development that has evolved constantly in the last few decades. As a result, a high proportion of the building stock located in earthquake-prone regions (such as the Mediterranean area) was designed before the appearance of seismic codes or in view of rudimentary anti-seismic design criteria (Masi, 2003). Recent earthquakes have revealed the poor performance of existing reinforced concrete (RC) buildings, accentuating the need for seismic assessment and retrofitting, e.g. L'Aquila (Italy 2009, M_w=6.3), Lorca (Spain 2011, M_w=5.1) and Emilia (Italy 2012, M_w=6.0). At the same time, the seismic hazard of some Mediterranean countries has been updated, as indicated in the official Italian hazard data (available at http://esse1-gis.mi.ingv.it) and in the updated seismic hazard map of Spain (Instituto Geográfico Nacional, 2012). The latter increases by up to about three times the seismic hazard in some regions. Consequently, a large number of

structures have probably become under-designed and need to be retrofitted. Retrofitting strategies should focus not only on increasing the seismic capacity of existing buildings, but also on attaining the corresponding performance objectives described in the latest standards published in Europe (EN 1998-3:2005, 2005; NTC 2008, 2008).

1.1 Seismic vulnerability of RC frame structures in Spain

Seismic assessment of existing structures is a difficult task that was considered in few standards (FEMA 178, 1992; JBDPA, 1977) before the appearance of the Eurocode 8-Part 3 (EN 1998-3:2005, 2005). A major challenge is linked to the uncertainty about the configuration and the structural data of the existing structure (e.g. material strength, localization of reinforcement, quality of the execution process, etc.), since technical documentation is not always available and most of the data is based in limited field investigations. For this purpose, the age of construction is considered a key-aspect to determine the structural characteristics of a building.

The age of the existing building stock is a useful parameter to quantify the amount of structures that remain under-designed nowadays. In Italy, Crowley et al. (2009) used the data from the 13th General Census of Population and Dwellings (Istituto Nazionale di Statistica, 1991) to study the vulnerability of the building stock. They

concluded that, although the vulnerability of the masonry buildings is clearly superior to the RC structures, the vulnerability of non-seismically designed RC structures is also a concern. In Spain, the Census of Population and Dwellings 2011 (Instituto Nacional de Estadística, 2013), gives the percentage rate of primary dwellings for each period of construction, as shown in Table 1.1. It can be observed that 60.3% of the primary dwellings were built between 1941 and 1991. It is precisely in the 1940s when masonry structures started to be progressively substituted by frame structures and the use of reinforced concrete became widespread (Monjo Carrió, 2005). In particular, 26.2% of primary dwellings were built between 1941 and 1970, approximately before the publication of the first seismic codes in Spain (PDS-1, 1974; PGS-1, 1968). A percentage of 34.1% were built between 1970 and 1991, before the appearance of modern seismic codes (NCSE-02, 2002; NCSE-94, 1994). Only 15% of primary dwellings were built after 2002 (with the current seismic code).

Period	Primary residence (%)
2002-2011	15.0
1991-2001	16.0
1981-1990	13.0
1971-1980	21.1
1961-1970	15.3
1951-1960	7.8
1941-1950	3.1
Before 1941	8.6

Table 1.1: Primary residence in Spain classified by year of construction (Instituto Nacional de Estadística, 2013)

The data described for Spain are representative of the situation in many Spanish cities, such as the city of Lorca, recently affected by the earthquake in 2011 (Álvarez Cabal, Díaz-Pavón Cuaresma, & Rodríguez Escribano, 2013). However, the proportion of old buildings constructed before the publication of the first Spanish seismic code PGS-1 (1968), can be greater in big and historical cities such as Barcelona, where this percentage reaches 80% (Barbat, Pujades, & Lantada, 2006).

1.1.1 Evolution of seismic provisions in Spain

The first seismic code was published in Spain in 1968, PGS-1 (1968), as provisional. In 1974, the publication of the definitive code PDS-1 (1974) lead to the repeal of the 7th chapter about seismic actions of the standard MV 101-1962 (1963). These standards were based on pure-strength methods and did not pay attention to the plastic deformation capacity of the structural elements. Furthermore, the equivalent lateral seismic forces prescribed by these codes were quite low, resulting in a poor lateral strength design (Benavent-Climent, Akiyama, Lopez-Almansa, & Pujades, 2004).

In the 90s, significant regulatory changes produced an improvement of the lateral strength and lateral deformation capacity of the new buildings. The new seismic code NCSE-94 (1994) introduced important modifications in both the definition of seismic actions and structural design (Blázquez Martínez, 1997). First, the

seismic hazard map was represented in terms of horizontal ground acceleration associated with a return period of 500 years, instead of macroseismic intensity (MKS). Second, the elastic response spectrum is defined in the body of the code, depending on the ground type. Third, although the design method is still strength-based, the concept of ductility was included for the first time (Benavent Climent, 2010b). The ductility factor, μ, reduced the elastic forces obtained from the elastic response spectra to obtain the design forces. Finally, the use of wide beams was banned in seismic areas with design PGA, a_c>0.16g, and the ductility factor was limited to a value of 2 in regions with a_c< 0.16g.

It is also worth mentioning that the appearance of the code on structural concrete, EH-98 (1998), enhanced the concrete strength by increasing its minimum design strength, f_{ck}, from 17.5 (EH-91, 1991) to 25 MPa. Before 1998, concrete with $f_{\mathrm{ck}} = 17.5$ MPa was frequently used due to its lower cost.

In 2002, the current code NCSE-02 (2002) was published. In this code, different limit states –as contained in Eurocode 8-Part 3 (EN 1998-3:2005, 2005)– are still not explicitly considered, although they are implicitly taken into account through the specification of the maximum ductility factor (Benavent Climent, 2010b). In case very high ductility is considered (μ=4), this code enforces the formation of stable energy dissipation mechanisms (such as beam-sway

mechanisms). To this end, the strong-column/weak-beam principle is applied to prevent a soft-story mechanism. Later, this principle was explicitly included in the current version of the code on structural concrete, EHE-08 (2008), which requires that the sum of column ultimate flexural-strengths, M_{cu}, exceed the sum of beam ultimate flexural-strengths, M_{bu}, at each beam-column connection ($\sum M_{cu} \geq \gamma_{SR} \sum M_{bu}$). The factor γ_{SR} accounts for possible overstrength, and is equal to 1.35 in EHE-08 and to 1.3 in Eurocode 8. The current seismic code, NCSE-02, also changed the restriction adopted by the former code for wide beams, by allowing their use in regions with $a_c \geq$ 0.16g. However, it imposed several restrictions to such structures, by limiting the ductility factor to μ=2, and prescribing special requirements about the dimensions of the beams and the location of the reinforcement. In addition, the current seismic code also included the consideration of the amplification effect of the ground type on the seismic design acceleration.

Finally, an updated version of the seismic hazard maps in Spain has been published (Instituto Geográfico Nacional, 2012). It modifies the design PGA in some regions by increasing it up to three times.

1.1.2 Evolution of concrete construction practice in Spain

Several studies describe the structural characteristics of the Spanish building stock in earthquake-prone regions, such as the

recently affected city of Lorca (Álvarez Cabal et al., 2013; Feriche, Vidal, Alguacil, Navarro, & Aranda, 2012; Cabañas et al., 2011). The construction practices observed in Lorca are representative of the ones that can be found in other Spanish earthquake-prone cities. The data exposed by (Álvarez Cabal et al., 2013) confirm that most of the buildings were constructed between the 1940s and the 1990s. In addition, they analyzed the distribution of buildings by type of structure, showing that most of the buildings used RC moment resisting frames with deep beams, followed by masonry structures and RC frames with wide beams.

A detailed description of the evolution of structural practices can be found in (Álvarez Cabal et al., 2013) and is summarized below. The use of RC frame structures for residential buildings became widespread in the 1940s, gradually replacing masonry structures (Monjo Carrió, 2005). In the early years, RC buildings were constructed with confined masonry technology. It consists of masonry walls confined by horizontal and vertical RC members. The confining elements resist only gravity loads, while the masonry walls provide most of the earthquake resistance (although they were not designed for that purpose). These buildings ranged in height from four to five stories. Story heights were not much greater than 2 meters and beam-span lengths were not longer than 4 meters. These buildings were constructed with poor quality materials, smooth reinforcement bars and usually with poor quality control.

In a short time, the number of stories increased, as well as the length of the beam span and the story height. At the end of the 1970s, buildings were more than 8-story height and most of them used RC frames in one direction with wide beams supporting one-way slabs, without compression layer. They were designed only for gravity loads. Thus, they did not have any lateral resistance elements in the direction perpendicular to the frames, apart from the masonry infill walls, which were designed as partitions.

In the 1980s, the use of wide beams and compression layer became widespread. However, the seismic code NCSE-94 banned the use of wide beams in regions with $a_c \geq 0.16g$ (which was not the case of Lorca, with $a_c = 0.11g$ at that time). It was not until 2002, that the use of wide beams was allowed in seismic regions with $a_c \geq 0.16g$, but with some restrictions, as explained in previous section 1.1.1. Regarding the seismic criteria that lead to stable energy dissipation mechanisms (such as the strong-column/weak-beam principle), they have not been incorporated in most cases to the construction practice, although it is compulsory according to current codes (EHE-08, 2008; NCSE-02, 2002). Today a considerable amount of buildings also have deficiencies in seismic design, such as plan and vertical irregularities, discontinuities in the load path, under-designed squat-columns, etc.

1.1.3 Observed damage to RC frames

The performance of RC buildings have been analyzed from the data extracted in field campaigns carried out after recent seismic events, which affected several Mediterranean earthquake-prone regions (e.g. Molise 2002, L'Aquila 2009, Emilia 2012 and Lorca 2011).

In the case of Molise earthquakes (31 October and 1 November 2002, M_w=5.8), only 10% of the affected buildings were RC frame structures. Most of them suffered none to slight damage, although few of them were severely damaged (Decanini et al., 2004). These structures had been built in the absence of seismic codes and with poor quality materials, thus showing several deficiencies (poor concrete, smooth reinforcing bars, insufficient transverse reinforcement, etc.). In the Emilia area, most of the buildings affected by the earthquake (20 May 2012, M_w=6.0) had also been designed only for gravity loads. In this case, RC frame structures suffered slight to moderate damage and only rare situations of collapse in the epicentral area (Ioannou et al., 2012; Verderame, De Luca, Ricci, & Manfredi, 2011; Verderame, Ricci, De Luca, Del Gaudio, & De Risi, 2014). In the area affected by L'Aquila earthquake (6 April 2009, M_w=6.3), most of the damaged RC structures had been designed according to old seismic codes, not aimed at providing the proper energy dissipation capacity and were ineffective to prevent brittle failure mechanisms (Ricci, De Luca, &

Verderame, 2011). Furthermore, plan and vertical irregularities, as well as the interaction between infills and frame structures, played a key role in documented building collapses.

In Spain, a recent seismic event hit the city of Lorca (11 May 2011, M_w=5.1). In a narrow range of vibration periods, this event exceeded by about four times the energy input implicit in the Spanish seismic code NCSE-02 (Benavent-Climent, Escobedo, Donaire-Ávila, Oliver-Saiz, & Ramírez-Márquez, 2013), affecting 80% of the building stock (Donaire-Ávila et al., 2011). In this case, a significant part of the buildings that had to be demolished after the earthquake (Feriche et al., 2012), were RC frame structures (in particular, 150 out of 328). The distribution of damage level by the seismic code in force (De Luca, Verderame, Gómez-Martínez, & Pérez-García, 2013) showed that the majority of the buildings that suffered heavy and very heavy structural damage were designed according to the old code PDS-74, although the design codes did not affect significantly the attained level of damage. Again, a substantial part of damage was related to vertical irregularities (open-plan ground floors, squat columns) and to the interaction between infills and frame structures. In addition, old RC buildings were usually constructed with smooth reinforcing bars, poor quality construction materials and insufficient transverse reinforcement (Álvarez Cabal et al., 2013; De Luca et al., 2013; Feriche et al., 2012; Cabañas et al., 2011). Finally, Benavent-Climent et al. (2013) studied the influence of masonry infills and the proneness

of the frames to concentrate damage in a specific story. To this end, they performed nonlinear dynamic response analyses of two prototype RC frame structures with wide beams, designed in two time periods (1994–2002 and 2003–2008) with the seismic codes in force at that time. Results corroborated the extremely negative effect of vertical irregularities caused by an uneven distribution of masonry infills, which made the structure very prone to damage concentration. These authors stated that this negative effect can be avoided by establishing special gaps between structural and non-structural elements (Architectural Institute of Japan, 1994) or by providing sufficient energy dissipation capacity at the story where damage concentration is expected, e.g. by adding energy dissipators (Benavent-Climent, 2011). They also pointed out the importance of controlling the damage distribution among the stories. In the case of conventional RC frames this can be accomplished by adopting the strong-column/weak-beam principle (EHE-08, 2008), or by providing a lateral strength distribution close to the "optimum" one that makes the normalized cumulative plastic strain energy, η_i, approximately equal in all stories (Akiyama, 1985).

1.2 Seismic assessment

Earthquake engineering research and seismic provisions has mainly been focused on new construction, although under-designed existing buildings are considered to be the major earthquake threat to

human life and property (Fardis, 2009). A possible explanation is that many policy makers expect the problem to be solved by urban renewal, which is a tolerable solution in case the rate of building renewal was higher than the rate of occurrence of moderate earthquakes. However, this is not the case of many European cities, which tend to consolidate the existing urban fabric. One of the main drawbacks is the cost of retrofitting an existing building, even comparable to the cost of constructing a new one because seismic design increases very little the cost of a new structure. Furthermore, the cost of retrofitting should consider not only the cost of the structural measures, but also should take into account other factors such as the disruption in use and the relocation of occupants. For this reasons, the existence of seismic risk mitigation policies is of major importance, to assess the building stock and promote the application of retrofitting strategies that ensure the safety of existing buildings. These programs can be classified between "active" —if the assessment and possible retrofitting of an existing building is required by a specific deadline—, and "passive" —if assessment and retrofitting measures are motivated by an event, such as a change in use or the need of repairing the damage caused by a seismic event— (Fardis, 2009).

In Spain, the Royal Decree-Law 8/2011 established the obligation of assessing the residential buildings that are more than 50 years old. Among other aspects, this mandatory inspection evaluates the

structural safety, in global terms. The ITE Observatory (iteweb.es) publishes statistics about the outcome of the inspections performed. The annual statistical reports for 2013 and 2014 (Observatorio ITE, 2013, 2014) shows that only 1.9% and 5.6% —respectively— of the buildings inspected obtained a negative outcome due to structural causes. These report also show that the number of buildings under the obligation of being inspected that year is similar to the number of inspected buildings (thus indicating that most of the inspected buildings were older than 50 years). Clearly, there is a lack of accurate data, which explicitly quantify the number of buildings in seismic regions and the proportion of them that need to be retrofitted due to seismic deficiencies. Nevertheless, it is worth mentioning that the percentages provided by the cited reports seem to be quite low, noting that buildings older than 50 years were constructed in the absence of seismic codes, and before the publication of PGS-1 (1968).

1.2.1 Assessment provisions

A detailed seismic assessment is the first step towards determining the convenience of retrofitting an existing building, as well as selecting the correct retrofitting strategy. The assessment of an existing structure is a complicated task that involves many aspects (Villaverde, 2007): (1) the characteristics of the ground motion; (2) the geometry and constructive details of the existing structure, (3) the mechanical properties of the elements; (4) the dynamic properties

of the existing structure; (5) the postelastic and cyclic degradation behavior of the elements; (6) the interaction of the structure with non-structural elements; (7) second order effects; and (8) soil-structure interaction. For this purpose, it is essential to develop specific seismic provisions focused on the assessment of existing structures. An old under-designed structure is unlikely to meet the rigorous requirements of modern codes (such as vertical and horizontal regularity, continuity of the load path, member detailing, etc.). Thus, the acceptance criteria should be less stringent for existing structures than for the construction of new ones, in order to avoid magnifying the cost of retrofitting measures (Fardis, 2009).

Rapid screening procedures are a useful guide in seismic risk mitigation programs to assess the seismic risk of a certain area and identify the priority buildings (Fardis, 2009). The FEMA 154 (2002) handbook provides a rapid visual screening procedure aimed at identifying the buildings that are potentially seismic hazardous and need further study. Following, the ASCE 41-13 (ASCE/SEI 41-13, 2014; Pekelnicky & Poland, 2012), which combined the ASCE 31-03 Seismic Evaluation of Existing Buildings and the ASCE 41-06 Seismic Rehabilitation of Existing Buildings, provides a procedure to inspect in detail a given building and to assess its seismic performance. This standard retains the three–tier assessment approach of ASCE 31-03 (2002): (1) Tier 1 Screening, is the first step towards the assessment but it is not valid for retrofit design; (2) Tier 2 Deficient-Based, to

study in detail the deficiencies identified in the previous Tier 1 and/or chose a retrofit strategy; and (3) Tier 3, to systematically analyze the building through different types of analysis (Linear Static, Linear Dynamic, Nonlinear Static, and Nonlinear Dynamic), useful either for assessment or retrofitting. A three-tier approach is also described in the Japanese standard JBDPA (2001).

In Europe, the Eurocode 8-Part 3 (EN 1998-3:2005, 2005) is the first standard focused on the assessment and retrofitting of existing buildings. It describes the performance requirements and criteria, the information required for structural assessment, the applicability and criteria for the use of the different methods of analysis, and provides guidance on the selection and design of the structural intervention. This code establishes different knowledge levels (KL1-Limited knowledge, KL2-Normal knowledge, and KL3-Full knowledge) depending on the structural data available of the existing building (geometry, structural details, mechanical properties of the materials, etc.). It also relates the knowledge level to the type of analysis that can be performed, by limiting the analysis of buildings with knowledge level KL1 to the use of the Lateral Force and Modal Response Spectrum (MRS) analysis methods. For the rest of knowledge levels, other analysis methods are also accepted: Non-linear static (pushover) analysis and non-linear time history analysis.

1.3 Evolution of the analysis methods

1.3.1 From strength-based to displacement-based design

Traditionally, the application of seismic provisions has been the responsibility of legal authorities, for whom the main purpose was the protection of human life (Fardis, 2010). Hence, seismic design was focused on preventing the collapse of buildings under a rare seismic event. In the early years, design codes prescribed lateral inertia forces, corresponding to value of about 10% of the building weight. During the 1940s and 1950s, a better understanding of dynamic properties led the definition of period-dependent design lateral force levels. From around 1960, a growing concern on the inelastic behavior of the buildings was developed. This concept explained that many structures with a reduced strength, resisted earthquakes of certain intensity (Priestley, 2007b). Thus, the concept of ductility gained importance. Allowing the development of inelastic deformations, led to more economic solutions by reducing the demanded elastic strength. To this end, some researchers (Veletsos & Newmark, 1960) studied the relation between the maximum deformation attained by an elastic system, and the maximum deformation attained by an elastoplastic system with similar initial stiffness and damping ratio. Based on these results, they derived the relation between the displacement ductility ratio and the force-reduction factor. Veletsos & Newmark studied two approaches: the “equal displacement approximation”, which considers

that maximum deformations of both elastic and elastoplastic systems are equal, and the "equal energy approximation", which considers that the absorbed energy is equal in both systems. Recent studies (Ruiz-García & Miranda, 2003), validated the first approach for SDOF systems with certain values of fundamental period and lateral strength ratio, ($R = mS_a / Q_y$, where m is the mass of the system, S_a is the acceleration spectral ordinate and Q_y is the lateral yielding strength). For a lateral strength ratio of 2, Ruiz-García & Miranda (2003) state that the equal displacement rule is approximately correct for periods longer than 0.45, 0.65 and 0.8s for structures on NEHRP site classes (FEMA 302, 1997) B (rock), C (very dense soil and soft rock) and D (stiff soil), respectively. For greater lateral strength ratios (up to 6), the equal displacement rule is applicable for periods longer than 1.2 s.

During the 1970s and 1980s, extensive research was carried out to determine the ductility factor of different structural systems, and the concept of capacity design became a fundamental part of seismic design (Park & Paulay, 1975). Although seismic design was focused on displacement capacity, the calculation procedure was still made in terms on strength, and displacement capacity was only checked at the end of the process (Priestley, 2007b).

In the last decades, some authors have reviewed the fundamentals of displacement-based design, and developed an approach that

requires little or no iteration, termed "Direct Displacement Based Design" (DDBD). This approach was introduced in 1993 (Priestley, 1993) and it is fully described in (Priestley, Calvi, & Kowalsky, 2007). Unlike force-based seismic design, which of characterizes the structure by its elastic properties (initial stiffness, elastic damping), DDBD uses the secant stiffness at maximum displacement and the equivalent viscous damping. The equivalent viscous damping represents ductility and energy dissipation capacity, by using relationships based on time-history analyses.

1.3.2 Performance-based seismic design (PBSD)

From the 1960s, earthquake-engineering researchers became concerned about the economic losses caused by frequent earthquakes. In 1968, the Structural Engineers Association of California (SEAOC) proposed a number of recommendations, which laid the foundations for the performance-based seismic design (PBSD). These recommendations connected the earthquake intensity level —minor, moderate or major— with the level of damage attained by the structure —without damage, without structural damage but possibly with some nonstructural damage, or without collapse but with some structural and nonstructural damage, respectively— (Fardis, 2010).

In the 1980s and 1990s, several seismic events took place in developed countries (Loma Prieta 1989, Northridge 1994 and Kobe 1995), emphasizing the need for controlling the level of structural and

nonstructural damage. These events caused severe damage in code-compliant buildings and produced substantial material losses. The Loma Prieta earthquake in 1989, was considered to be a moderate event but caused $8 billion in direct damage (Bertero, 2000). For this reason, the SEAOC Board of Directors founded the Vision 2000 Committee in 1992, to establish the framework for a new seismic code based on performance-based design. This committee assumed the assignment of publishing a final document that contained a set of seismic design provisions by the year 2000. In 1994, a new seismic event caused extensive losses (Northridge earthquake), being recognized as the most expensive earthquake of U.S. history (FEMA 445, 2006). Therefore, performance-based seismic design was brought to the forefront, and the SEAOC developed the SEAOC Vision 2000 Committee report (SEAOC Vision 2000 Committee, 1995) to be used immediately (Bertero, 2000). Later, the FEMA 273 (1997) Report was published, focused on reducing the seismic hazards of existing buildings. This report provided the guidelines for the seismic rehabilitation of buildings according to performance-based seismic design philosophy.

In this way, traditional seismic design (focused only on preventing collapse) was replaced by a multi-level design that defined the performance objectives by coupling the expected maximum damage state of a building (performance level) with a specific level of seismic demand (ground-motion hazard level) that corresponded to a

particular annual probability of exceedance. FEMA 273 (1997) defined four building performance levels: Operational, Immediate Occupancy, Life Safety and Collapse Prevention. In particular, damage suffered by vertical elements of concrete frames was associated with maximum transient-drift values for each structural performance level: 1% (Immediate Occupancy), 2% (Life Safety) and 4% (Collapse Prevention). These building performance levels were related to different earthquake hazard levels through a matrix, so that each cell represented a single rehabilitation objective. Rehabilitation Objectives were classified in Basic Safety Objectives (BSO) —for which buildings were expected to suffer little damage under frequent to moderate earthquakes and severe damage for the most infrequent earthquake that could occur—, Enhanced Rehabilitation Objectives —superior than BSO— and Enhanced Rehabilitation Objectives —inferior than BSO—. Ground-motion hazard levels were defined in terms of the probability that a more demanding seismic event occured in a 50-year period (probability of exceedance). In particular, two levels of earthquake hazard were defined as especially useful: the Basic Safety Earthquake 1 (BSE-1) —typically with a probability of exceedance of 10% in a 50-year period— and the Basic Safety Earthquake 2 (BSE-2) —usually 2%/50 year—. Finally, the first generation of PBSD procedures, also defined four different analysis methods (Linear Static, Linear Dynamic, Nonlinear Static and Nonlinear Dynamic procedures) for which they provided specific guidance and acceptance criteria.

Based on the experience gained with the application of FEMA 273 (1997) and the case studies contained in FEMA 343 (1999), a reviewed document for the rehabilitation of existing buildings was published: FEMA 356 (2000). This is considered the second generation of PBSD procedures, and is widely accepted in engineering practice nowadays.

In Europe, PBSD was introduced for new and existing buildings through the Eurocode 8 (EN 1998-1:2004, 2004; EN 1998-3:2005, 2005), which identify the performance levels as limit states. EN 1998-1 asks explicitly for two levels of seismic design: Damage Limitation (DL) requirement and No-Collapse (NC) requirement. Additionally, EN 1998-1 requires the satisfaction of a number of pertinent measures that are implicictly equivalent to the specification of a thrid performance requirement, which intends to guarantee the No-Global Collapse (NGC) during a very strong and rare earthquake. On the other hand, EN 1998-3 defines three limit states: Damage Limitation (DL), similar to Immediate Occupancy; Significant Damage (SD), similar to Life Safety; and Near Collapse (NC), similar to Collapse Prevention. It does not determine the return period for the design seismic action corresponding to each limit state, which should be determined in the National Annex. However, Eurocode 8 recommends some values. For new buildings (EN 1998-1), DL limit state is associated with 95 years of return period, while NC limit state is associated with 475 years and NGC with 1500-2000 years. For

existing buildings (EN 1998-3), DL limit state is associated with 225 years, SD limit state with 475 years and NC limit state with 2475 years. As cited in the previous section, the Eurocode 8-Part 1 addresses two types of linear-elastic analysis: lateral force method (restricted to buildings whose response is mainly governed by the fundamental mode) and modal response spectrum analysis. In addition, it also defines two non-linear methods: non-linear static (pushover) analysis and non-linear time history (dynamic) analysis.

In recent years, researchers and practitioners have highlighted the limitations of the second generation of PBSD procedures (FEMA 445, 2006): concerns about the accuracy of analysis methods, the conservatism of the acceptance criteria, the difficulties to adapt these procedures to the design of new buildings and the difficulties in communicating engineering decisions to the stakeholders. For these reasons, the Applied Technology Council (ATC) was contracted by FEMA in 2001 for the development of a next-generation of performance-based seismic design guidelines for new and existing buildings, under the projects designed as ATC-58/ATC 58-1. The planning phase document was published in 2006 as the FEMA 445 (2006) Report, which defined the framework for the new methodology. This probabilistic approach quantified the uncertainties associated to the prediction of the response and allowed to assess its behavior in terms that also fit the necessities of the decision-making skateholders (such as disruption of use, repairing and reconstruction

costs, environmental impact, etc.). The response is evaluated in terms of: human losses, direct economic losses (e.g. repair and replacement costs) and indirect losses (e.g. repair time). The basis of this methodology was developed between 1997 and 2010 by researchers of the Pacific Earthquake Engineering Research Center (PEER). Moehle and Deierlein defined the framework of this methodology by applying the total probability theorem to the PBSD and structuring the design process in logical elements (Moehle & Deierlein, 2004): IM, Intensity Measures (which define in probabilistic terms the main characteristics of the seismic hazard); EDP, Engineering Demand Parameters (which describe the structural response), DM, Damage Measures (which describe the state of the structure) and DV, Decision Variables (which express the damage in probabilistic terms that enter into risk management decisions). Earthquake performance is calculated as a multi-level integral of "the probability of incurring earthquake effects of differing intensity, over all intensities; the probability of experiencing building response of different levels, given an intensity of shaking; the probability of incurring damage of different types, given building response; and the probability of incurring specific consequences given that damage occurs" (FEMA P-58-1, 2012). Finding a closed form solution of the multi-level integral is difficult for real buildings, and a modified Monte Carlo approach was developed for that purpose.

The completion of the first phase of the project ended with the publication of the document FEMA P-58 for the seismic assessment of buildings, which contains a description of the new methodology (FEMA P-58-1, 2012), an implementation guide (FEMA P-58-2, 2012) and supporting electronic materials (FEMA P-58-3). Currently, the second phase of the project is in process, which consists on the development of the performance-seismic design guidelines and stakeholder guidelines.

1.3.3 Energy-based approach

Several authors have highlighted the shortcomings of displacement-based design methods (Bertero & Bertero, 2002), highlighting the necessity to develop a rational seismic design that includes a more general definition of damage. On one hand, although a direct relation can be established between ductility demand and damage, the former does not yet give an appropriate idea about the amount of energy that a structure will dissipate through the hysteretic behavior during an earthquake. Park and Ang expressed the level of damage as a linear function of the maximum deformation and the repeated cyclic loading effect (Park & Ang, 1985). On the other hand, though it may at first seem that designing structures with the maximum ductility lead to the most economic solution, there are several reasons for limiting the drift and ductility of a structure: (1) prevent structural damage, (2) reduce non-structural damage, (3)

reduce second order effects, (4) reduce the concentration of damage in a critical story, which is greater as the structure goes deeper inelastic deformations and (5) avoid human discomfort under frequent seismic events of a reduced intensity level (Bertero & Bozorgnia, 2004; Bertero, 1992a). For this reasons, it is important to consider not only the demand of strength and deformation, but also their combined effect on the energy dissipation capacity of the whole structure.

The energy-based method was first proposed by Housner (1956) and gained wide attention with the contributions of Akiyama (1985), who developed the current theoretical framework of energy-based methods (Bertero, 1995). This method is based on the assumption that the energy input by an earthquake can be reliable predicted, and must be lower that the energy dissipation capacity of the structure to attain a satisfactory performance.

Furthermore, the characterization of the potential damage caused by an earthquake can be done in terms of the energy input by the earthquake. The total input energy E of an MDOF damped inelastic system (Akiyama, 1985; Housner, 1956), is a very stable parameter that approximately coincides with that of an equivalent elastic SDOF system with mass M equal to the total mass of the MDOF system and period T equal to that of the fundamental mode. This has been proved in numerical (Akiyama, 1999) and experimental (Uang & Bertero, 1990) studies.

The nonlinear behavior of a structure excited by an earthquake can be know by solving the highly nonlinear equation of motion for an MDOF system:

$$\mathbf{M}\ddot{\mathbf{y}}+\mathbf{C}\dot{\mathbf{y}}+\mathbf{Q}=-\mathbf{M}\mathbf{r}\ddot{z}_g \tag{1.1}$$

where $\mathbf{M}$ is the mass matrix, $\mathbf{C}$ the damping matrix, $\mathbf{Q}(t)$ is the restoring force vector, $\dot{\mathbf{y}}(t)$ and $\ddot{\mathbf{y}}(t)$ are the velocity and acceleration vectors relative to the ground, and $\mathbf{r}$ is the displacement vector $\mathbf{y}(t)$ resulting from a unit support displacement. An effective way to reduce the complexity of this process consists of transforming Eq. (1.1) into an equation of energy balance (Akiyama, 1985), by integrating over the duration of the ground motion (from t=0 to t=t_0):

$$W_k+W_\xi+W_s=E \tag{1.2}$$

where W_k is the kinetic energy, W_ξ the damping energy, W_s the absorbed energy, and E is the (relative) input energy, given by:

$$W_k=\int_0^{t_0}\dot{\mathbf{y}}^{\mathrm{T}}\mathbf{M}\ddot{\mathbf{y}}\,dt;\ W_\xi=\int_0^{t_0}\dot{\mathbf{y}}^{\mathrm{T}}\mathbf{C}\dot{\mathbf{y}}\,dt;\ W_s=\int_0^{t_0}\dot{\mathbf{y}}^{\mathrm{T}}\mathbf{Q}\,dt;\ E=-\int_0^{t_0}\dot{\mathbf{y}}^{\mathrm{T}}\mathbf{M}\mathbf{r}\ddot{z}_g\,dt \tag{1.3}$$

On the other hand, the absorbed energy, W_s, can be expressed as the sum of the recoverable elastic strain energy, W_{se}, and the irrecoverable plastic energy, W_p, (W_s= W_{se}+ W_p). The sum of the

kinetic energy W_k and the elastic strain energy, W_{se}, is the elastic vibrational energy W_e (= $W_k + W_{se}$). Therefore, Eq. (1.2) can be rewritten as follows:

$$W_e + W_\xi + W_p = E \tag{1.4}$$

Housner (1956) defined $W_e + W_p = E - W_\xi$ as the energy attributable to damage. This definition is very useful to illustrate that the energy input by the earthquake can be compensated by just the elastic behavior of the structure (strength-based approach) or by dissipating as much energy as possible in the form of plastic energy, W_p. Nowadays, a common practice is to increase the amount of W_p by increasing the ductility of a structure, which implies damaging the main structure. A possible alternative consists of concentrating the dissipation of energy in specific parts of the structure, such as energy dissipation devices (EDDs). In this way, the structure is composed by two parts: the flexible part (which remains elastic) and the stiff part (which absorbs most of the energy input). This solution is known as flexible-stiff mixed structure. Another option is to concentrate the dissipation of energy through base isolation techniques, which reduce the energy demand of the main structure. Therefore, the energy-based approach is considered a rational and clear methodology for the selection of retrofitting strategies (Bertero, 1992b).

1.4 Retrofitting techniques

As explained above, the energy-based approach is a powerful tool for evaluating the effect of upgrading seismic techniques. Form this point of view, different main strategies can be defined: (1) reduce the earthquake demand of the main structure, (2) improve the elastic properties of the existing structure (strength and stiffness), (3) improve the inelastic properties of the existing structure, increasing the energy dissipation capacity of the structure (e.g. provide higher ductility, install EDDs, etc.) and (4) any combination of the previous options (Bertero, 1992b). Traditional techniques have been usually focused on improving the strength and stiffness of the existing structure, by adopting either a global (e.g. adding structural walls or steel braces) or a local (e.g. concrete o steel jacketing) modification scheme (Moehle, 2000). However, besides life safety, there are a number of objectives that must be considered in the choice and design of the seismic upgrading within the framework of the Performance Based Design (PBD): (i) control of damage; (ii) minimum disruption of building use during upgrading; (iii) proper performance of the building after upgrading; and (iv) minimum cost. Control of damage means protecting structural and non-structural components and building contents, to protect investment, or to maintain building function following an earthquake. Damage control is often a major consideration and involves the control of displacements of the (i.e. story drift) to values that can be tolerated by non-structural

components, and the reduction of seismic building absolute accelerations (which might damage special machinery or artifacts). For these purposes, innovative techniques have undergone recent development; because they can not only enhance the inelastic deformation capacity of the elements (e.g. FRP jacketing), but also can directly increase the energy dissipation capacity of the structure (i.e. by installing energy concentration devices). Thus, innovative techniques can reduce the cost of retrofitting, making the new and existing components to act compositely and eliminating the need for foundation upgrading or extensive structural upgrading.

1.4.1 Traditional techniques

Traditional techniques have been applied for many years and their performance is demonstrated by this large experience of use. They use conventional materials (steel, concrete) and conventional construction procedures that do not require particularly qualified manpower. Despite these advantages, traditional techniques normally do not lead to optimized design solutions, since they are usually focused on increasing the strength and stiffness of the structure —i.e. as shown by the energy balance equation Eq. (1.4) this means increasing only W_e. Thus, this approach presents important shortcomings: (1) the severe disruptions of the activity of the building that they can cause, and (2) the significant reduction of the net floor area, jeopardizing of the use of the building. In addition, increasing strength and stiffness

means also increasing the response acceleration, and thus producing nonstructural damage (e.g. damage suffered by building facilities, machines, etc.). This is a problem which specially affects buildings that are less than 30-stories height (Akiyama, 1999). A more rational solution consists on providing ductility by improving the confinement pressure of concrete elements, which can be attained through different jacketing systems. However, increasing ductility implies allowing a certain level of damage in the main structure. A description about the application of these techniques on concrete structures can be found in (Moehle, 2000).

These techniques include the in-filling with shear walls —cast in place (Jirsa & Kreger, 1989) or precast (Frosch, Li, Jirsa, & Kreger, 1996)—, the addition of conventional bracing systems —X-type or K-type steel braces (Goel & Masri, 1996)— or side-walls, and the strengthening of columns and beams with concrete (Karayannis, Chalioris, & Sirkelis, 2008) and wire jacketing, with steel jacketing (Aboutaha, Engelhardt, Jirsa, & Kreger, 1996) or with wire winding.

1.4.2 Innovative techniques

The innovative techniques provide a wider range of possibilities. Advanced composite materials allow improving the elastic and inelastic properties of the elements without increasing the stiffness or adding mass. In particular, Fibre Reinforced Polymer laminates (FRP) mainly improve the ductility, while the addition of Steel

Reinforced Polymer spikes (SRP) also increases the flexural strength. Another solution consists on supplementing energy dissipation capacity by installing energy dissipating devices such as viscous, friction or hysteretic dampers. In addition, base isolation systems can also represent an interesting retrofitting option. This solution can be costly for conventional buildings but specially useful for historical buildings, since their original uniqueness and aesthetic value remain unaltered (Matsagar & Jangid, 2008).

1.4.2.1 FRP/SRP

Innovative strengthening techniques based on the use of FRP have strongly grown due to their numerous advantages: easy and fast installation procedure, durability, light weight, high strength, high elastic modulus, corrosion and environmental resistance, and impact resistance (ACI 440R-96, 1996). In particular, ease of installation and minimum space requirements make the solution with FRP sheets a very efficient alternative in the seismic retrofit of existing buildings. There are several types of FRP products (GFRP, AFRP, CFRP, etc.) whose common link is the use of continuous fibers (glass, aramid, carbon, respectively) embedded in a resin matrix that makes the fibers to work together. The resin matrix can be made of thermoset (polyester, vinyl ester, etc.) or thermoplastic (nylon, PET, etc.). Analytical and experimental results (Di Ludovico, Prota, Manfredi, & Cosenza, 2008; Galal, Arafa, & Ghobarah, 2005; Karabinis & Rousakis, 2002; Mirmiran & Shahawy, 1997) have shown that,

wrapping structural components with FRP sheets improve their shear strength and ductility without adding stiffness to the elements.

However, the implementation of a flexural strengthening technique that requires less intensive labor than the traditional ones (such as concrete or steel jacketing) still remains a challenging task (Fardis, 2010). For this purpose, two techniques of similar nature have been recently proposed. On one hand, a combined solution with FRP laminates and SRP spikes allows a global improvement of the performance of the structure under both gravity and seismic loads. SRP spikes increase the bending capacity of RC columns without enlarging their cross section, while FRP wrapping prevents existing steel vertical reinforcement and SRP spikes from buckling (Cuzzilla, Di Ludovico, Prota, & Manfredi, 2011; Huang, Birman, Nanni, & Tunis, 2005). Also, FRP improves the concrete compressive strength owing to the passive confinement generated by the FRP jacket as the concrete dilates under axial, shear and moment load combination. On the other hand, the use of a near-surface mounted (NSM) technique has been also recently developed (Bournas & Triantafillou, 2010). NSM reinforcement consists on cutting of grooves into the concrete cover and bonding rebars (CFRO strips, GFRP bars, stainless steel rebars) inside them by using a specific filler (epoxy resin, cement-based mortar). Nevertheless, the main shortcoming of these FRP/SRP techniques is the cost that is typically high due to both the materials used and the need of qualified manpower.

1.4.2.2 Energy Dissipation Devices (EDDs)

Innovative strengthening techniques based on the installation of Energy Dissipation Devices (EDDs) seek to transfer most of the energy input by the earthquake to the dampers in order to reduce the inelastic energy dissipation demands and to limit the damaging deformations on the main framing system. This passive control system is an effective upgrading strategy for existing RC frame structures that has gained considerable attention in recent years (Di Sarno & Manfredi, 2012; Khampanit, Leelataviwat, Kochanin, & Warnitchai, 2014; Oviedo, Midorikawa, & Asari, 2010; Di Sarno & Manfredi, 2008). Although great effort has been carried out in high seismicity countries such as Japan, USA and New Zealand (JBDPA, 2005; Symans et al., 2008), passive systems are still rarely applied in low-to-moderate earthquake-prone countries other than Italy. Some examples of installing passive structural control systems in the Mediterranean area are described in (Benavent-Climent, 2008).

A number of mechanisms have been used for dampers in seismic retrofitting (Soong & Spencer Jr, 2002): phase transformation of metals, friction sliding, fluid orificing, deformation of viscoelastic solids or liquids, and yielding of metals. Among them, the so-called "hysteretic" dampers are particularly popular because of their low cost in comparison with viscous fluid dampers or viscoelastic solid dampers. In particular, metallic dampers based on the yielding of metals are one of the most popular that have been proposed and

installed. This is due to their stable hysteretic behavior, low-cycle fatigue property, and long-term reliability regardless of the ambient temperature (Soong & Spencer Jr, 2002). In hysteretic dampers, yielding of metals can be achieved by different ways (Martínez-Rueda, 2002). Some of the most popular are the X-shaped added damping and stiffness (ADAS) damper (Bergman & Goel, 1987) or its triangular-plate variant the TADAS damper (Tsai, Chen, Hong, & Su, 1993). They consist on yielding metallic plates by out-of-plane bending. Other devices consists of a metallic plate with a several openings that is subjected to in-plane shear deformations. Some examples of this type are the honeycomb damper (Kobori et al., 1992), the slit damper (Benavent-Climent, Oh, & Akiyama, 1998; Chan & Albermani, 2008; Oh, Kim, & Ryu, 2009) and the recently developed tube-in-tube (TTD) damper (Benavent-Climent, 2010a). In other devices energy is dissipated through plastic shear deformations of a metallic panels, welded inside an inclosing steel frame (Nakashima et al., 1994). Finally, one of the most common metallic devices is the Buckling Restrained Brace (Watanabe, Hitomi, Saeki, Wada, & Fujimoto, 1988; Xie, 2005) that is installed as a conventional concentric brace. The BRB damper is based on the yielding of a metal core encased in a concrete-filled steel tube, which avoids buckling when the brace is subjected to axial deformations. One of the advantages of the hysteretic dampers is the cost that can be markedly lower than that of friction or viscous dampers. In the recent years, new brace-type hysteretic dampers (Benavent-Climent,

Morillas, & Vico, 2011) have been developed with the aim of lowering their cost as much as possible so that they can be used in earthquake-prone developing countries.

1.5 Seismic retrofitting of existing RC frames by adding hysteretic dampers

The design of EDDs for the seismic retrofit of existing RC structures must address several aspects. First, the main structure should remain elastic or suffer light damage, unless the configuration, design details and mechanical properties of the existing frame were completely known, being possible to carry out a reliable collapse assessment. Second, it is important to account for the consequences of the mass added, the need of new foundations, and the possibility of causing damage to the existing structural and non-structural components (Fardis, 2009).

In particular, two specific problems arise when designing a retrofitting solution with hysteretic dampers: (i) the forces transferred by the dampers to the existing frame may require strengthening the existing frame in the connection region, and (ii) the main frame must have a minimum lateral deformation capacity so that the dampers can deform in the plastic range and develop efficiently their intrinsic energy dissipation capacity.

First, the study of the connection between the EDDs and the existing frame is particularly important in hysteretic dampers that are installed as conventional concentric braces (FEMA 547, 2006). In fact, the connection between the old RC beam-column joints and the damper devices has been pointed out as the key challenge of this retrofitting technique (Fardis, 2009). For this reason, a new connection is proposed in Chapter 3, and its performance is evaluated with numerical and experimental tests. A revision of the solutions proposed in the past for brace-frame connections is described in the Introduction of Chapter 3, which justifies the need of developing of the new connection.

Second, the main frame requires a minimum lateral deformation capacity to remain elastic, while the EDDs develop plastic deformations and dissipate enough amount of energy. In this way, the frame and the new hysteretic dampers act compositely as a "flexible-stiff mixed structure" (FSMS). The FSMS mixed structures are composed of two parts that work in parallel: the flexible part and the stiff part. The former has low lateral stiffness and is designed to remain basically elastic (i.e. main frame). The later has high lateral stiffness, low strength, and large energy dissipation capacity through plastic deformations (i.e. EDDs). Past research (Akiyama, 1999) has shown that under seismic actions, the flexible part stabilizes the response of the stiff part and as a result the efficiency of the entire system in terms of energy absorption with respect to maximum

deformation is high, and the residual deformation on the structure after the earthquake is very small. In addition, damage is concentrated in the EDDs (which must be designed to be easily inspected and replaced) while minimum damage is caused to the existing frame (whose seismic performance is usually known with a considerable degree of uncertainty and is expected be very limited). To this end, a hybrid retrofitting technique is proposed in Chapter 4 of the present Thesis, which combines the addition of hysteretic dampers with a limited strengthening of the existing frame with FRP/SRP. The level of strengthening with FRP/SRP is the minimum necessary to ensure that the existing frame has enough lateral deformation capacity. In this way, the strengthened existing frame is able to play the role of the "flexible part" in the FSMS, while the new hysteretic dampers constitute the "stiff part". Chapter 4 presents an energy-based method to design the proposed solution, and points out the main parameters that control the response. Finally, the proposed hybrid retrofitting technique is validated through numerical simulations in Chapter 5.

1.5.1 Design of hysteretic EDDs for the seismic retrofit of existing RC structures

The design of energy dissipation devices (EDDs) for the seismic retrofit of existing structures was first introduced in the guidelines FEMA 273 (1997) and commentary FEMA 274 (1997). After, an updated version was published as FEMA 356 (2000). These

documents address several aspects: (1) spatial distribution of the EDDs, (2) redundancy of the EDDs, and (3) the condition that the EDDs and their connections must remain elastic (FEMA 273, 1997; Symans et al., 2008). In addition, these documents describe four analysis methods, which directly or indirectly consider the contribution of EDDs: (1) Linear Static procedure, (2) Linear Dynamic procedure, (3) Nonlinear Static procedure and (4) Nonlinear Dynamic procedure. Only the fourth method explicitly considers the supplemental dissipated energy, the cumulative damage and load-history effects.

The linear procedures apply very restrictive conditions to the use of EDDs, since they tend to oversimplify the highly nonlinear response of the structure (Benavent-Climent, 2011). They are applicable only if the framing system exclusive of the EDDs remains elastic, and limit the effective damping afforded by the EDDs to 30% of the critical damping in the fundamental mode (FEMA 273, 1997; FEMA 356, 2000). The linear procedures indirectly account for the energy dissipation capacity supplemented by the EDDs, by reducing the design seismic loads or the response spectrum through a factor that depends on an equivalent effective viscous damping. Further requirements are imposed for the design of displacement-dependent devices (e.g. hysteretic dampers): (1) the ratio of the maximum resistance in each story to the story shear demand, must range between 80% and 120% of the average value of the ratio for all stories

and; (2) the total resistance of the EDDs in a story, must be lower than 50% of the resistance of the main frame.

The Nonlinear Static procedure (pushover analysis) accounts for the contribution of EDDs either (1) by increasing the global stiffness of the structure and by reducing the target displacement as a result of reducing the effective fundamental period of the structure, or (2) by defining an equivalent effective viscous damping. Benavent-Climent (2011) described the shortcomings of using this procedure for the design of a retrofitting solution with EDDs. First, they substitute the hysteretic damping provided by the EDDs by an equivalent viscous damping, although no physical evidence supports that relationship, especially for highly inelastic systems. Second, cyclic degradation is considered in an implicit way. Since no explicit criteria is given to determine the relation between the number of cycles at a given design ductility, it is difficult to include the effect of duration-related cumulative damage. In fact, Kunnath & Chai (2004) demonstrated that inelastic cyclic demand depends not only on the ductility-based force reduction factor, but also on the earthquake characteristics and the force-deformation characteristics of the structure.

Recently, the European Norm on Anti-seismic EN 15129:2009 (2009) devices came officially into force (1 August, 2011). It is focused on standardization of the seismic hardware, since design is must be done in accordance to Eurocode 8 (EN 1998-1:2004, 2004). However, the latter gives specific guidance for base isolation devices but not for

EDDs. The EN 15129 is the most up-to-date document in this field at present, and a description of its development process can be found in (Medeot, 2014). This standard provides two types of requirements for anti-seismic devices: (1) no failure requirement and (2) damage limitation requirement. These requirements are referred to the seismic intensities defined in Eurocode 8-Part 1 (EN 1998-1:2004, 2004): Ultimate Limit State and Damage Limitation State, respectively. The first one is intended to avoid failure while the second one focuses on limiting the damage to avoid disproportionately high costs of repairing or replacement. In addition, specific emphasis is made on the ease of inspecting and replacing the devices and their connections to the structure. Finally, specific guidance is provided about the technical validation procedure and about the type tests required for acceptance.

In the past, several studies have proposed methods for designing RC frame structures with supplemental EDDs. Uetani, Tsuji, & Takewaki (2003) presented an optimum structural design method for new building frames with hysteretic dampers. This method was able to find the minimum weight design such that satisfied member-end strain and interstory-drift constraints. However, the retrofitting of existing structures must consider a specific RC frame design as a starting point, usually with poor seismic performance. In the literature there are several methods that can be used for retrofitting. Gluck, Reinhorn, Gluck, & Levy (1996) proposed a design method for

the design of supplemental passive dampers, based on optimal linear control theory. They proved the efficiency of this method for structures dominated by a single mode of vibration. Mazza (2014) applied the displacement-based design method (Priestley, 2007a) for the retrofitting of RC frame structures with hysteretic dampers. They extended this method to structures with in-elevation irregularities, to obtain an even distribution of strength and stiffness.

Other authors proposed computational design approaches. Although these approaches require performing several time-consuming nonlinear time-history analyses, they rely on the advance of parallel computing. Moreschi & Singh (2003) determined the optimal design parameters for yielding-metallic and friction dampers. In the case of metallic dampers, they stated that the optimum parameters were: the yield displacement of the device, the stiffness of the device and the stiffness of the bracing system that supports the device. They also proposed a method based on nonlinear time-history analyses that uses a genetic algorithm, which obtained the optimal solution that satisfied a specific performance objective. Karami Mohammadi, El Naggar, & Moghaddam (2004) proposed an iterative method for shear buildings with hysteretic dampers, based on time-history nonlinear dynamic analyses, to find the optimum strength (and stiffness) distribution pattern that could lead to a uniform story-drift distribution. It depended on the number of stories, design ground motion, strain-hardening ratio and viscous damping ratio. Dargush &

Sant (2005) also employed a genetic algorithm for the optimization of passive devices. They studied several cases with three different types of passive dampers (metallic plate dampers, viscous fluid dampers and viscoelastic dampers).

Recently, some authors have developed energy-based procedures that avoid the use of intensive nonlinear time history analyses, and directly account for the energy dissipation capacity supplemented by the EDDs. They are based on the energy-based methods proposed by Housner (1956) and developed by Akiyama (1985). This energy-based design methodology has been widely accepted (Fajfar, Vidic, & Fischinger, 1992; Uang & Bertero, 1990) and has been recently included in the Japanese seismic code (BSL, 2009). Benavent-Climent (2011) proposed a practical energy-based design method, for the seismic upgrading of conventional low to medium-rise existing structures by adding hysteretic EDDs. This method determined the lateral stiffness, the lateral strength and the energy dissipation capacity of the EDDs, so that the existing frame does not exceed a specific limit of drift, beyond which the existing RC frame would develop plastic deformations. This method uses the parameters proposed by Manfredi, Polese, & Cosenza (2003) and Manfredi (2001) to characterize the ground motion. Manfredi et al. 2003 characterized the seismic input through the I_D index and established a relation between this index and the equivalent number of plastic cycles, n_{eq}. The equivalent number of cycles, n_{eq}, is defined as the number of

plastic cycles at the maximum value of plastic excursion, that the structure must develop to dissipate the total amount of hysteretic energy E_H.

An extension of the method proposed by Benavent-Climent is presented in Chapter 4 of the present Thesis. As discussed later, for some under-designed RC frames with low lateral deformation capacity, it may not be sufficient to add EDDs for controlling the drift response at each story. For this reason, it may be convenient to strength the existing frame (e.g. by adding SRP/FRP) in order to increase the lateral deformation capacity at a specific floor. Thus, the previous method is modified such that a minimum strengthening of the existing frame is considered and the dampers succeed in controlling the drift response at each floor. In addition, the maximum inter story drift at each story can be predicted, for different return periods, being possible to evaluate the retrofitting solution for different performance objectives.

2

Objectives

Recent seismic events in the Mediterranean area have revealed the vulnerability of the building stock located in moderate earthquake-prone regions and the poor performance of RC frame under-designed buildings, accentuating the need for seismic assessment and retrofitting. New retrofitting techniques should focus not only in life safety, but also in controlling the damage and the economic cost of repairing measures after the earthquake. For this reasons, the present Thesis proposes a retrofitting technique based on the use of hysteretic dampers that also considers the possibility of locally strengthening the main frame. This aims to increase the flexibility of the retrofitting measures and to reduce the cost of the final solution. The performance of the proposed solution is evaluated for different seismic hazard levels, within the framework of performance-based seismic design.

To this end, the Thesis addresses the following particular objectives:

1. Investigate a solution for connecting brace-type hysteretic dampers to the existing RC frame. The proposed brace–frame connection is suitable for connecting either a conventional concentric steel brace or a brace-type hysteretic damper. The steel brace may develop high axial loads, and its influence on a possibly damaged frame is a matter of major concern. For this reason, an alternative solution is investigated, aimed at reducing the number and anchorage height of the anchors and the dimensions of the shear-key plates (Chapter 3).
2. Propose execution provisions and design criteria based on numerical analyses of the brace-frame connection that determine the influence of specific parameters on its performance (Chapter 3).
3. Evaluate the efficiency and validity of the proposed brace-frame connection by means of shaking-table tests conducted on a 3x3x3 m^3 scaled reinforced concrete frame retrofitted with brace-type hysteretic dampers. In particular, the following main aspects are studied: the level of damage suffered by the main frame, the effects of the brace-frame connection in the efficiency of the hysteretic damper and the effectiveness of the new connection in

reducing tension forces on the anchor bolts and bending moments on the shear-key plates (Chapter 3).

4. Develop an energy-based seismic design procedure, based on a previous method proposed by Benavent-Climent (2011) for retrofitting existing RC frame structures with hysteretic dampers that includes the possibility of locally strengthening the main frame (e.g. by adding FRP/SRP). In this way, the retrofitting design process is more flexible, opening the range of retrofitting measures. This ensures the existence of a solution for the design of the dampers that meets the drift requirements at each floor, for different performance objectives (Chapter 4).

5. Validate the new energy-based seismic design procedure and the proposed retrofitting solution by means of nonlinear time history analysis. To this end, a retrofitting solution will be designed for a six-story prototype RC frame structure —representative of pre-70 residential buildings— and three levels of seismic hazard, through the addition of hysteretic dampers and FRP/SRP strengthening at particular locations. Afterward, a numerical model capable of reproducing the performance of the under-designed RC frame structure upgraded with the proposed solution will be developed, and subjected to two sets of natural acceleration records —far-field and near-fault. In particular, this numerical study will be focused

not only on evaluating the agreement between the overall performance obtained from the dynamic response analyses and the behavior anticipated in the design, but also on paying particular attention to the concentration of damage and the distribution of dissipated energy (Chapter 5).

3

New connection between RC building frames and concentric braces

Part of the contents of this Chapter has been recently published in (Benavent-Climent, Oliver-Saiz & Donaire-Avila, 2015).

This Chapter investigates a solution for connecting concentric steel braces and brace-type dampers to existing reinforcing concrete frames subjected to lateral loads. These braces may develop high axial tension forces, and transferring them appropriately to the existing beam-column joints is a key challenge. The proposed solution connects the end-plate of the steel brace with the frame, using (1) shear-key plates fixed to the concrete with anchor bolts, and (2) a low friction material inserted between the end-plates and the shear-key

plates. The addition of a low friction material impedes the development of tension forces in the anchor bolts and ensures that they are basically subjected to shear forces. This prevents brittle types of failure (concrete cone failure, pull-out/pry-out failure), and results in a reduction of the number of anchors required as well as anchorage height. The efficiency and validity of the proposed brace-frame connection is studied with (1) FEM numerical simulations and (2) shaking table tests conducted on a $3\times3\times3m^3$ scaled reinforced concrete frame retrofitted with brace-type hysteretic dampers.

3.1 Introduction

One of the key challenges of retrofitting reinforced concrete frames with concentric steel braces is the connection between the ends of the steel braces and the existing frame (Fardis, 2009), briefly referred to as "brace-frame connection" herein. The steel brace may develop high axial loads, and its influence on a possibly damaged frame is a matter of major concern.

Several solutions have been proposed for the brace-frame connection in the past. The simplest one consists of using steel anchors to connect the end-plate of the brace directly to the concrete, as shown in Fig. 3.1.a. The anchors are thereby subjected to shear V_i and tension forces N_i. A second proposal (Ichikawa, Okayasu, Nakamura, Yamada, & Wada, 2005; Ozaki, Harada, & Murakami,

2008) is to use shear-key plates to fasten the end-plate of the brace, as shown schematically in Fig. 3.1.b. The shear-key plate is adhered to the surface of the concrete with epoxy resin and fixed with anchor bolts. In this second solution, there is a direct metal-to-metal contact between the end-plate of the brace and the shear-key plate. When the brace is in tension, the direct metal-to-metal contact induces forces perpendicular to the plane of the shear-key plate (denoted by V_c in Fig. 3.1.b) that tend to uplift and detach it from the concrete surface. Because these contact forces also induce large tension forces N_i in the anchors and bending moments in the shear-key plates, there is a need for thicker plates or the addition of stiffeners. Sustaining high tension forces with bolts anchored in the concrete calls for considerable anchoring height and a greater number of anchors. Hence, this solution can prove costly or technically unfeasible. In addition, the typical failure modes exhibited by anchor bolts subjected to tension loads (concrete cone failure, pull-out/pry-out failure) are brittle.

This chapter investigates an alternative solution for the brace-frame connection that improves upon the one shown in Fig. 3.1.b, reducing the number and anchorage height of the anchors and the dimensions of the shear-key plates. The proposed solution aims to minimize or cancel the tension forces N_i acting on the anchor bolts, and the subsequent bending moments developed on the shear-key plates. The proposed brace-frame connection is suitable for connecting either a conventional concentric steel brace or a brace-type hysteretic

damper. The validity and efficiency of the new connection is assessed through (1) FEM numerical analyses and (2) shaking table tests conducted on a one-story one-bay frame structure. Shaking table tests can capture the strain-rate effects associated with dynamic loading, as well as the cumulative damage to the anchoring system caused by the successive cycles of deformation that take place in structures actually subjected to seismic motions. Past research has shown (Otani, Kaneko, & Shiohara, 2003) that strain rates anticipated in earthquake excitation (about 0.3 mm/mm×s) produce the following effects: (i) a conspicuous enhancement of the yield stress of steel materials (about 13%), and (ii) an increase of the flexural resistance of members (by 7%~20%) in comparison with the strength under static loading.

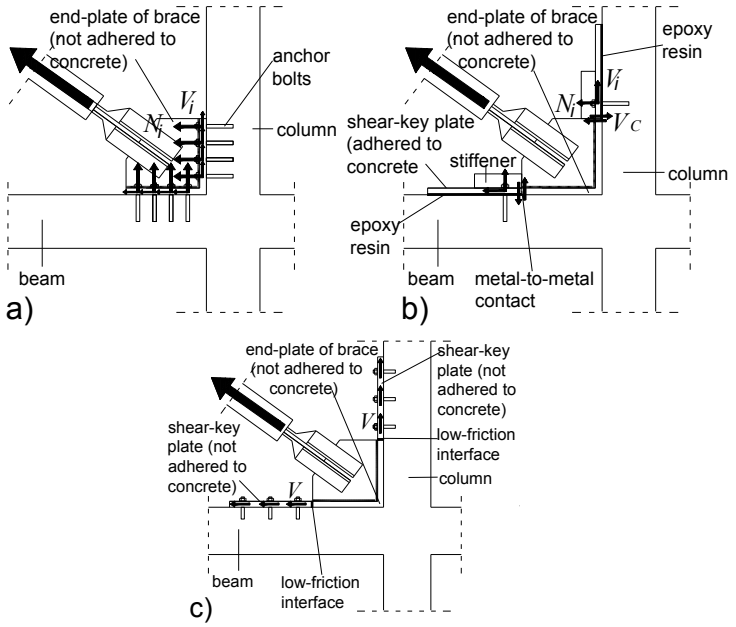

Fig. 3.1: Existing (a, b), and proposed (c) solutions for brace-frame connections

3.2 Proposed brace-frame connection

Fig. 3.1.c illustrates the proposed brace-frame connection. It consists of two shear-key plates fixed to the concrete only with anchor bolts (i.e. without epoxy resin), plus a device for reducing the friction between the end-plates and the shear-key plates. This device forms a low friction interface intended to minimize the contact forces (denoted with V_c in Fig. 3.1.b), the subsequent tension forces N_i on the anchor bolts, and the bending moments on the shear-key plates. The device consists of two sheets of polytetrafluoroethylene (simply Teflon hereafter), or else one sheet of Teflon in contact with a stainless steel surface polished to mirror finish (i.e. with less than $0.1\mu m$ surface roughness). Past experimental investigations (Dolce, Cardone, & Croatto, 2005) have shown that the friction coefficient μ_c of this type of device decreases along with an increase in the contact pressure. For contact pressures of about 25MPa, μ_c is between 0.03 and 0.1. This range of μ_c can be further reduced to about 0.01-0.02 if the interface is lubricated. By limiting μ_c, the proposed brace-frame connection ensures that the anchors are basically subjected to shear forces.

Using anchors subjected basically to shear loads makes the proposed solution (Fig. 3.1.c) less demanding than the conventional ones (Fig. 3.1.a and b) in terms of the number and effective anchorage depth h_{ef} of the anchors, as explained next. The guidelines for metal anchors in concrete —ETAG 001-Annex C (1997) in

Europe, for example— distinguish several modes of failure and provide equations for estimating the resistance limited by each one of them. The following failure modes are considered for anchors subjected to tension loads: (i) steel failure; (ii) pull-out failure; (iii) concrete cone failure; and (iv) splitting failure. For anchors subjected to shear loads, the failure modes are: (i) steel failure; (ii) concrete pry-out failure; and (iii) concrete edge failure. According to the above-mentioned guidelines, the resistance of an anchor governed by steel failure depends on the anchor cross-section area A_s and on the steel´s ultimate tensile strength f_{uk}, and it is two times larger under tension loads than under shear loads. For the proposed brace-frame connection the failure of the steel is not a concern, however, because f_{uk} and A_s can be made large enough to prevent this mode of failure. The splitting failure under tension loads and the concrete edge failure under shear loads can also be avoided by using appropriate edge distances for the shear-key plates. The failure modes of concern with the proposed brace-frame connection would be those that depend on the concrete compression strength f_{ck}: pull-out failure and concrete cone failure under tension loads, and concrete pry-out failure under shear loads. For these failure modes the resistance of an anchor subjected to shear loads is twice that of an anchor subjected to tension loads. In addition, minimizing the contact forces V_c (see Fig. 3.1.b) makes it possible to use thinner shear-key plates without stiffeners. Since the proposed solution entails anchor bolts that are

subjected basically to shear forces, brittle modes of failure such as anchor pull out/through failure or concrete cone failure are prevented.

The installation process of the proposed connection is schematized in Fig. 3.2. It necessarily involves the occurrence of initial gaps of width t_g between the end-plates of the dampers and the shear-key plates ($t_{g,h}$, and $t_{g,v}$ in Fig. 3.3). In turn, the mechanism to transfer tension forces from the end-plates of the brace to the reinforced concrete members is activated by the geometric relationship between the thickness of the shear-key plate t_p and the relative distance t_g. It is clear from Fig. 3.3.a that for the above transfer mechanism to develop the width t_g in both the horizontal, $t_{g,h}$, and vertical, $t_{g,v}$, directions, it must satisfy the following:

$$t_{g,h} < \left(t_{p,h} / \tan\alpha\right); \quad t_{g,v} < \left(t_{p,v} / \tan\alpha\right) \tag{3.1}$$

where $t_{p,h}$ and $t_{p,v}$ are the thickness of the horizontal and vertical shear-key plates, and α is the angle that the axis of the brace forms with the horizontal. t_g should be much smaller than the limit given in Eq. (3.1) to control (minimize or cancel) the amount of lateral displacement required on the frame to mobilize axial forces in the brace. Besides t_g, the thickness t_t of the Teflon sheets might also have some influence on the effectiveness of the proposed solution.

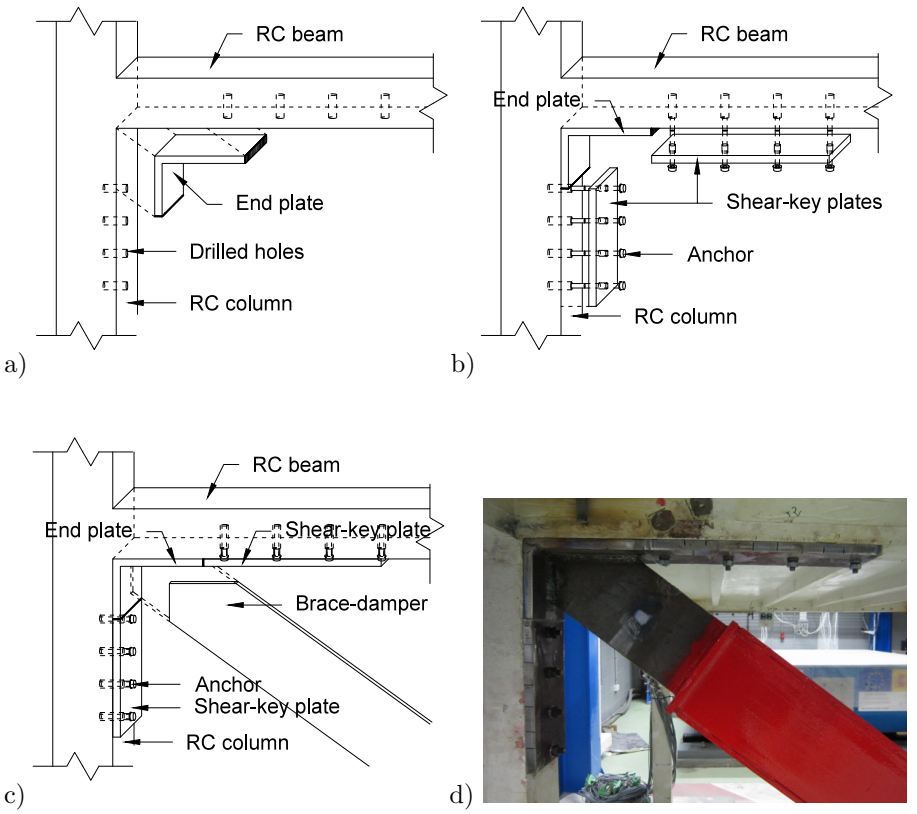

Fig. 3.2: Assembly diagram of the proposed brace-frame connection: (a) drilled holes are prepared and end-plate is placed (fixed with any provisional device), (b) shear-key plates are anchored, fixing the position of the end-plate, (c) the brace is welded to the end-plate and (d) picture of the final assembly in the tested specimen.

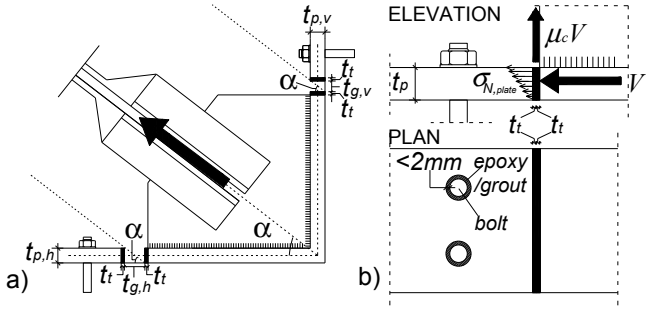

Fig. 3.3: Brace-frame connection: (a) before closing the gap t_g; (b) detail of the horizontal shear-key plate after closing the gap (t_g=0)

3.3 Finite element analysis of the brace-frame connection

To clarify the influence of t_g and t_t on the effectiveness of the proposed solution, a numerical study was conducted with the Finite Element Model shown in Fig. 3.4 by using the software ANSYS (2007). The values of t_g investigated are 0, 1 and 2 mm, and those for t_t are 4 and 8mm.

3.3.1 Description of the FEM model

The model was subjected to a lateral force F of increasing magnitude and the corresponding lateral displacement δ was computed (see Fig. 3.4). The nodes at the base of the column and at the base of the brace were fully constrained. The nodes at half-length of the beam were constrained only in z-direction. To save CPU-time, half of the frame was modeled, enforcing symmetry in the XZ plane.

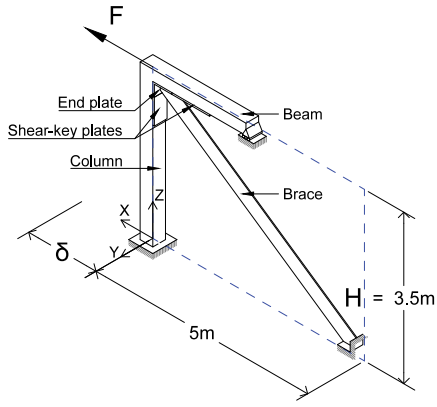

Fig. 3.4: Overall view of the FEM model

As shown in Fig. 3.5, the frame was modeled by using an eight-node solid element (SOLID65) for concrete, capable of cracking in tension and crushing in compression. Steel reinforcement was modeled with beam elements (BEAM188). Damper and joint structure were also modeled with the eight-node solid element (SOLID65). Mesh size equal to 20 mm was used for the concrete frame and for the brace damper, and finer mesh for the joint structure (5mm). Large deformation effects were taken into account.

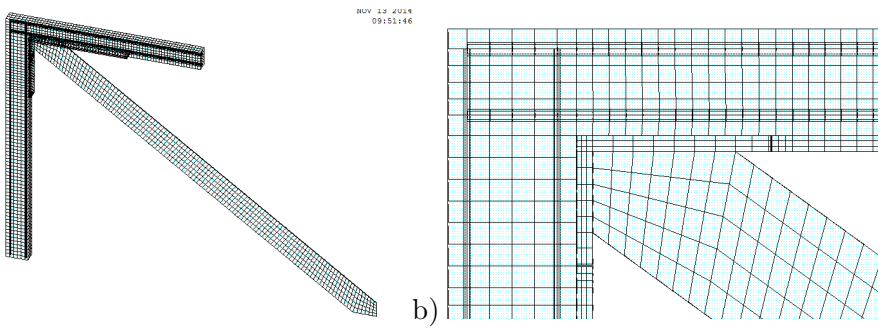

Fig. 3.5: Element discretization in joint structure: (a) overall view and (b) detail of the upper connection. Note: translucency was activated to show the steel reinforcement.

A bilinear isotropic hardening constitutive model was used for the steel reinforcement, the brace and the Teflon sheets, with the parameters described in Table 3.1. The properties of the Teflon material were defined according to past experimental tests (Rae & Dattelbaum, 2004). Part of the brace of 1m length was defined with a damper material such that the resulting yield strength, Q_{yd}, tangent stiffness K_{td}, and yield displacement, δ_{yd}, matched the experimental results of the hysteretic brace-damper (Q_{yd}=39.4 kN,

K_{td}=(1/30)(Q_{yd}/δ_{yd}), δ_{yd}=1.88 mm) obtained in previous tests (Benavent-Climent, Morillas, & Vico, 2011). The rest of the brace-damper and the plates of the joint structure were defined with a linear elastic material model.

The frame was modeled by using the concrete material model with the parameters described in Table 3.1 and the compressive uniaxial stress-strain relationship defined in Table 3.2. As recommended by Kachlakev, Miller, Yim, Chansawat, & Potisuk (2001), the crushing capability was turned off to attain convergence. For the same reason, the shear transfer coefficient for open cracks was assumed to be 0.3 and 1.0 for closed cracks. The stress-strain curve was determined by using the uniaxial compression model for cracked concrete proposed by Maekawa, Pimanmas, & Okamura (2003), with uniaxial compressive strength f_c=35MPa and uniaxial strain at f_c equal to ε_c=0.002.

As shown in Fig. 3.6, surface-to-surface contact was created at the areas between the Teflon sheet and the shear-key plates, with friction coefficient μ_c=0.03 and pairs of elements TARGE170 (for target surfaces) and CONTA174 (for contact surfaces). To save CPU time, the minimum number of contact areas was defined, where significant normal forces between the contact surfaces were expected. Thus, surface-to-surface contact was also defined at the areas between the end-plate and the RC frame, with friction coefficient μ_{sc}=0.57.

Table 3.1: Material properties of the FEM model

Constitutive Model	Part of the FEM model	Elastic modulus *(MPa)*	Poisson's ratio	Yield stress *(MPa)*	Tangent modulus *(MPa)*
Linear Elastic	Steel plates and brace	210000	0.3		
Bilinear isotropic hardening	Steel reinforcement	210000	0.3	500	21000
	Teflon	1000	0.47	15	30.93
	Damper	18712	0.3	35.18	623.73

Constitutive Model	Elastic modulus	Poisson's ratio	Ultimate uniaxial compressive strength	Ultimate uniaxial tensile strength	Shear transfer coefficient
Concrete	33796 MPa	0.2	35 MPa	7 MPa	0.3

Table 3.2: Compressive uniaxial stress-strain relationship for concrete

Strain	0.00025	0.0005	0.00075	0.001	0.00125	0.0015	0.00175	0.002
Stress (Mpa)	8.45	15.96	22.20	27.10	30.68	33.09	34.50	35.08

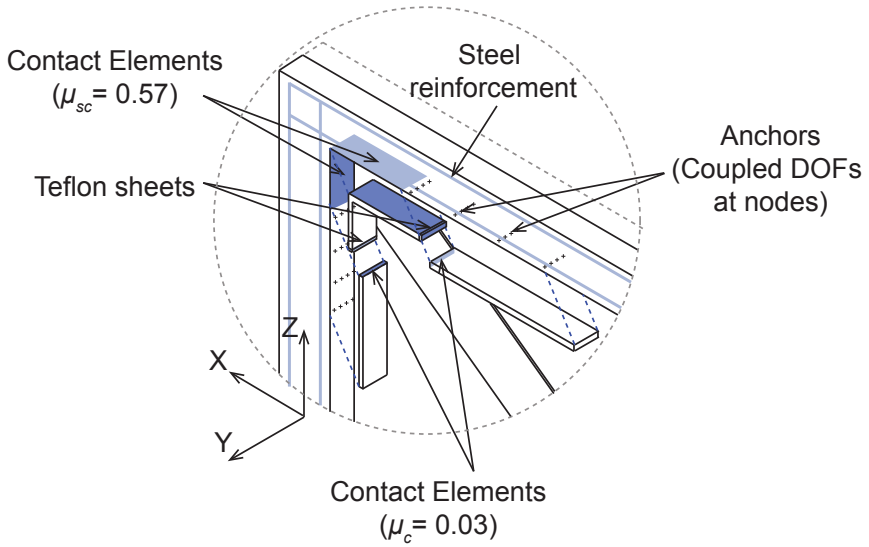

Fig. 3.6: Detail of the upper connection of the FEM model

3.3.2 Results of the FEM analysis

The overall deformation pattern of the FEM model is shown in Fig. 3.7. Fig. 3.8 shows a detail of the deformation pattern of the connection and the distribution of axial compressive stresses along the thickness of the bolted plates.

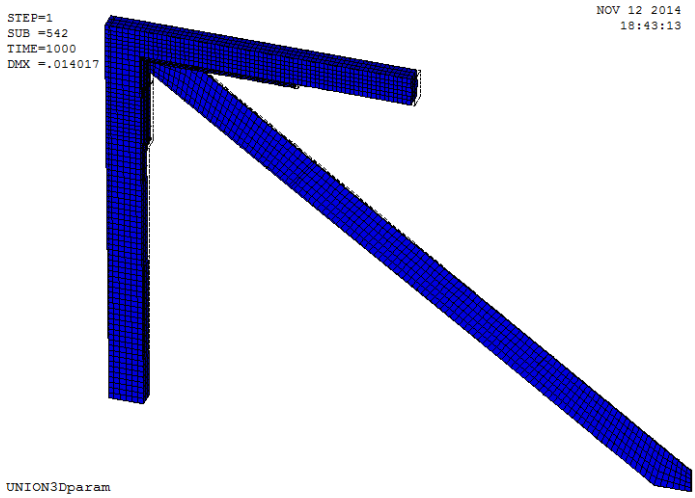

Fig. 3.7: Deformed shape of the FEM model

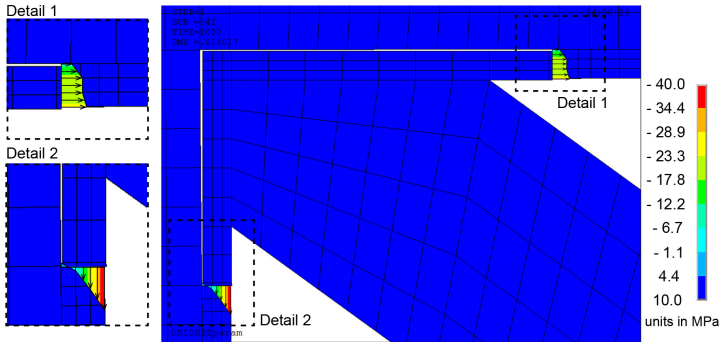

Fig. 3.8: Detail of the brace-frame connection of the FEM model: deformation pattern and axial compressive stresses along the thickness of the bolted plates

Fig. 3.9 shows the normalized curves F-F_y vs. δ/H for several combinations of t_g and t_t. Here F_y is the lateral force corresponding to the yielding of the brace, and H the total height of the frame. As is seen in Fig. 3.9: (i) the thickness t_t of the Teflon sheets has no influence on the behavior of the proposed connection; and (ii) the lateral displacement required to mobilize the damper increases with t_g, but it is relatively small (about 0.1%) even for the largest value of t_g that can be reasonably tolerated (2mm).

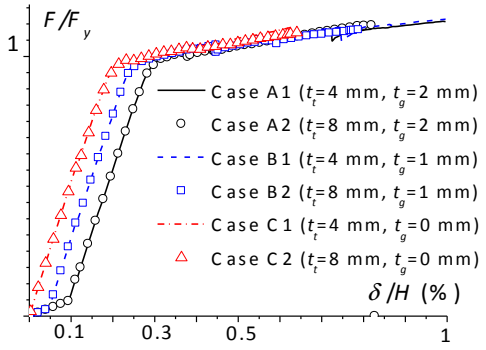

Fig. 3.9: Results of the numerical analyses

3.4 Proposal of execution provisions and design criteria

Based on numerical results and in order to facilitate execution, it is proposed to observe the following provisions when connecting the brace to the frame applying the proposed solution. First, to facilitate the installation of the shear-key plates, a clearance of up to 2 mm shall be allowed between the diameter of the holes and the diameter

of the anchor bolts, and this clearance should be filled with epoxy or high strength cement grout to prevent relative movements between the shear-key plates and the concrete, as shown in Fig. 3.3.b. Second, the width t_g of the initial gap between the shear-key plates and the end-plate of the brace must satisfy the limits given by Eq. (3.1), and should be less than 2mm.

The following design criteria of the brace-frame connection is proposed. The maximum axial force to be developed by the brace, F_u, is decomposed into the horizontal $V_H = F_u \cos\alpha$ and vertical $V_V = F_u \sin\alpha$ components. Each component applies to each shear-key plate a shear force V (see Fig. 3.3.b) that is transferred to the concrete through a group of n anchors. Since relative movements between the shear-key plate and the concrete are prevented by filling the possible clearance with epoxy or cement grout, it can be assumed that V is distributed equally among the anchors and therefore the shear force acting in each anchor is V/n. The anchors are also subjected to (small) tension loads due to the force $\mu_c V$ (normal to the shear-key plate; see Fig. 3.3.b) and the bending moment $\mu_c V e_N$ acting on the fixture. Here e_N is the eccentricity of the normal force $\mu_c V$ measured as prescribed by the guideline in use, i.e. ETAG 001 (1997) in Europe. The relevant guideline is also used to determine the characteristics of the anchors required, the dimensions of the shear-key plate and the position of the holes. For this purpose, the design method A, as described in the cited ETAG 001-Annex C (1997), was followed. It implies considering

all loading directions (tension, shear) as well as all failure modes (steel failure, pull-out failure, concrete cone failure, splitting failure, concrete edge failure and concrete pry-out failure). The geometrical restrictions due to the escalation of the specimen, forced us to use different anchoring system: HSC-A M10X40, in beams and, HILTI HIT-RE 500-SD with HIT-V (8.8) M10, in foundations.

The proposed beam-frame connection cannot be applied when the quality of the concrete is too poor, because a reliable anchorage of the shear-key plates with anchors cannot be guaranteed. This limits the applicability of the proposed solution in (old) existing structures with very low-strength concrete. Regarding the integrity of the contact surfaces of the low-friction interface during and after seismic events, past research (Dolce et al., 2005) concluded that: (i) the wear is not a problem under seismic conditions, as an earthquake produces only a few cycles at the maximum displacement amplitudes; (ii) the wear of nonlubricated Teflon surfaces does not significantly affect their frictional behavior; and (iii) the wear of lubricated Teflon surfaces is practically negligible. Finally, it is worth noting that the risk of the brace “running away”, when it is subjected to high-tension forces, can be eliminated by making the thickness of the shear-key plates large enough. Also, the flexural deformations of beams and columns when the damper is in tension have a beneficial fastening effect that reduces this risk.

3.5 Experimental study: shake table tests

3.5.1 Design of the prototype building and test structure

A prototype reinforced concrete frame structure consisting of a three-story 3×3 bay was designed to support only gravity loads, as shown in Fig. 3.10. The prototype represented an existing structure not designed for seismic loads, and thus lacking the ductile reinforcement details and the strength hierarchy between beams and columns prescribed by modern seismic codes. The floor system consisted of one-way joists spaced 800mm apart. These joists were supported by the main beams (joist-band floor system) and in turn, the joists supported a thin concrete slab 60mm thick. The weight of one square meter of this floor system was 2.1kN/m^2. To this value, the self-weight of ceramic flooring (1 kN/m^2) and the self-weight of a light plaster ceiling (0.12 kN/m^2) were added to obtain the total dead load of the floor 3.22 kN/m^2. In the case of the roof, the self-weight of the coating considered was 0.85 kN/m2, giving a total dead load of 2.95 kN/m^2. Additional dead loads of 1 kN/m^2 were considered for the partitions. The self-weight of beams and columns was also included, assuming a specific weight for reinforced concrete of 25 kN/m^3. These loads were multiplied by factor 1.35 for dead loads and by 1.5 for live loads. The concrete compressive strength f_{ck} assumed in calculations was 25MPa, and the yield strength for reinforcing steel was 500MPa.

The prototype structure was retrofitted with brace-type hysteretic dampers. The overall view, geometry and details of the dampers used are shown in Fig. 3.11. They were constructed by assembling segments of steel I-sections (European I-beam type IPE-140), which constitute the energy-dissipating device, and steel U-section members (European channel type U-140) that remain elastic and function as auxiliary bars. The assemblage is arranged in such a way that when the brace is subjected to forced deformations in the axial direction, the web of the I-shape section undergoes out-of-plane flexural deformations. A detailed description of this type of brace can be found in reference (Benavent-Climent et al., 2011). The mechanical properties, lateral stiffness ${}_sk$ and lateral strength ${}_sQ_y$ of the dampers were determined by applying an energy-based method (Benavent-Climent, 2011). This method calls for characterizing the ground motion in terms of input energy expressed by an equivalent velocity $V_{D,p}$, and fixing the maximum allowed inter-story drift δ_{max}. In this study, $V_{D,p}$=80cm/s and δ_{max}=0.01h (h being the story height) were adopted. The value $V_{D,p}$=80cm/s, proposed in the past (Benavent-Climent, Pujades, & Lopez-Almansa, 2002) for Spain, corresponds to a peak ground acceleration of a_b=0.23g (here g is the gravity acceleration) and soft soil conditions. It is worth noting that a_b=0.23g is the reference peak ground acceleration prescribed by the current Spanish seismic code NCSE-02 (2002) in stiff soil for a design earthquake having a 500-year mean return period T_R. According to NCSE-02, for soft soil and for a building of ordinary importance, a_b

must be multiplied by 1.34 to obtain the design peak ground acceleration, PGA, giving $1.34a_b$=0.31g. $\delta_{max}=0.01h$ is the limit proposed by ATC-40 (1996) and FEMA-356 (2000) to guarantee a performance of the frame within the "Immediate Occupancy" level.

From the prototype structure a partial structural model was separated (shaded area in Fig. 3.10). Fig. 3.12 shows the partial structural model with the brace dampers. The partial structural model is one bay and a half, in the direction of the main beams. It consists of two frames connected by the joists, by the thin slab reinforced with a steel mesh, and by perpendicular secondary beams. From the partial structural model, a reduced-scale test structure was defined by applying scale factors that were obtained as follows. The π Buckingham theorem states that any dimensionally homogeneous equation $F=(X_1,X_2 \ldots X_n)=0$ involving a set of n physical quantities $X_1,X_2 \ldots X_n$, can be reduced to an equivalent equation $G(\pi_1,\pi_2 \ldots \pi_m)=0$ involving a complete set of $\pi_1,\pi_2 \ldots \pi_m$ independent dimensionless products of the physical quantities (Harris & Sabnis, 1999). Here, the number of dimensionless products is $m=n-r$, where r is the number of fundamental measures involved. Physical systems that differ only in the magnitudes of the units used to measure the X_n quantities, e.g. the quantities for a prototype structure and its reduced-scale model, will have identical functionals $G(\pi_1,\pi_2 \ldots \pi_m)=0$, that can be also expressed as $\pi_1=\phi(\pi_2 \ldots \pi_m)$. Similarity requirements for modeling result from forcing the π_i terms to be equal in the model and prototype as

follows. The functional $\pi_1=\phi(\pi_2 \ldots \pi_m)$ can be written once for the prototype and once for the model to form the following ratio:

$$\frac{\pi_{1p}}{\pi_{1m}}=\frac{\phi\left(\pi_{2p}\ldots\pi_{mp}\right)}{\phi\left(\pi_{2m}\ldots\pi_{mm}\right)} \tag{3.2}$$

Here, the second subindex p in π_{ip} refers to the prototype and the second subindex m in π_{im} refers to the model. Complete similarity is defined to be the condition in which $\pi_{ip}=\pi_{im}$ for all of the π_i terms. The similarity relations can be derived from $\pi_{ip}=\pi_{im}$ by solving for the scaling factor S_i of each quantity i. The scale factor S_i is defined as the quotient between the value of quantity i in the prototype and the value of quantity i in the model. The experimental investigation conducted in this research addresses a dynamic mechanical problem, thus r=3. The development of scaling factors for structural dynamics under seismic motions can be based on the following physical quantities (Dove & Bennett, 1986): (i) the response acceleration at any point on the structure *a;* (ii) the stress strain characteristic of the material given by the modulus E; (iii) the mass m; (iv) the length l; (v) the acceleration input to the base a_b; (vi) the time t; (vii) and the force f. These quantities can be gathered together (Dove & Bennett, 1986) in the following π_i terms:

$$\frac{a}{a_b}=\phi\left(\frac{El^2}{ma_b},\frac{l}{a_bt^2},\frac{f}{ma_b}\right) \tag{3.3}$$

Given that the maximum number of dimensionally independent quantities equals r, only three scale factors (i.e. for only three quantities) may be arbitrarily chosen. In this experimental study, the quantities selected were l, E and a, and the corresponding scale factors are denoted by $S_l=l_p/l_m$, $S_E=E_p/E_m$ and $S_a=a_p/a_m$, respectively. Here l_p, E_p and a_p are the quantities for the prototype, and l_m, E_m and a_m are the quantities for the model. The scale factors S_i for the rest of quantities are obtained by making $\pi_{ip}=\pi_{im}$ and solving for S_i, giving:

$$\pi_{1p}=\pi_{1m}:\ \frac{a_p}{a_{bp}}=\frac{a_m}{a_{bm}}\rightarrow\frac{a_p}{a_m}=\frac{a_{bp}}{a_{bm}}\rightarrow S_{a_b}=S_a \tag{3.4}$$

$$\begin{aligned}\pi_{2p}=\pi_{2m}:\ \frac{E_p l_p^2}{m_p a_{bp}}=\frac{E_m l_m^2}{m_m a_{bm}}\rightarrow\frac{E_p l_p^2}{E_m l_m^2}=\frac{m_p a_{bp}}{m_m a_{bm}}\\ \rightarrow S_E S_l^2=S_m S_{a_b}\rightarrow S_m=\frac{S_E S_l^2}{S_a}\end{aligned} \tag{3.5}$$

$$\begin{aligned}\pi_{3p}=\pi_{3m}:\ \frac{l_p}{a_{bp}t_p^2}=\frac{l_m}{a_{bm}t_m^2}\rightarrow\frac{l_p}{l_m}=\frac{a_{bp}t_p^2}{a_{bm}t_m^2}\rightarrow S_l=S_{a_b}S_t^2\\ \rightarrow S_l=S_a S_t^2\rightarrow S_t=\sqrt{S_l/S_a}\end{aligned} \tag{3.6}$$

$$\begin{aligned}\pi_{4p}=\pi_{4m}:\ \frac{f_p}{m_p a_{bp}}=\frac{f_m}{m_m a_{bm}}\rightarrow\frac{f_p}{f_m}=\frac{m_p a_{bp}}{m_m a_{bm}}\rightarrow S_f=S_m S_{a_b}\\ \rightarrow S_f=S_m S_a\rightarrow S_f=S_E S_l^2\end{aligned} \tag{3.7}$$

In this experimental study, the scale factors adopted were $S_l=5/2$, $S_E=1$, and $S_a=1$. The scaling factor for length was set to $S_l=5/2$ in order to make the dimensions of the test model compatible with the

size of the shaking table. The scale factor for the stress strain characteristic of the material was set to S_E=1, because it is considered (Harris & Sabnis, 1999) the only practical way to conduct true modeling of reinforced concrete structures. More precisely, bond stresses developed between concrete and reinforcing steel in the model must be identical to those developed in the prototype for true models, and this is only possible when S_E=1 (Zia, White, & Van Horn, 1970). S_E=1 results automatically when the same material is used in the model and prototype (as in the present study). The scale factor for response acceleration was set to S_a=1 to have equal scale factors for force and mass and not distort the gravity force. Substituting S_l=5/2, S_E=1, and S_a=1 in Equations (4)-(7) gives the scaling factors for the input acceleration S_{ab}=1, for mass S_m=$(5/2)^2$, for time S_t=$(5/2)^{0.5}$ and for force S_f=$(5/2)^2$.

The geometry and reinforcing details of one of the two identical main frames that formed the test structure are shown in Fig. 3.13. The test structure was built at the Laboratory of Dynamics of Structures of the University of Granada. The total mass was m=11295kg, which is the sum of the mass of the floor diaphragm with its added weight, plus the added weight put on top of the columns. The yield stress of the steel obtained from tension tests was 551MPa for the longitudinal bars and 636MPa for the stirrups. The concrete strength at the 28th day, obtained by means of compression tests, was 35MPa. The brace-frame connections of the test specimen were

designed as described in Section 2 for F_u=64kN, α=0.61rad, μ_c=0.03 and the actual strength of the concrete f_{ck}=35MPa. This resulted in shear-key plates of 210×120×15mm fixed with four anchors of cross section area A_s=78.5mm^2, and effective anchorage depth h_{ef}=40mm.

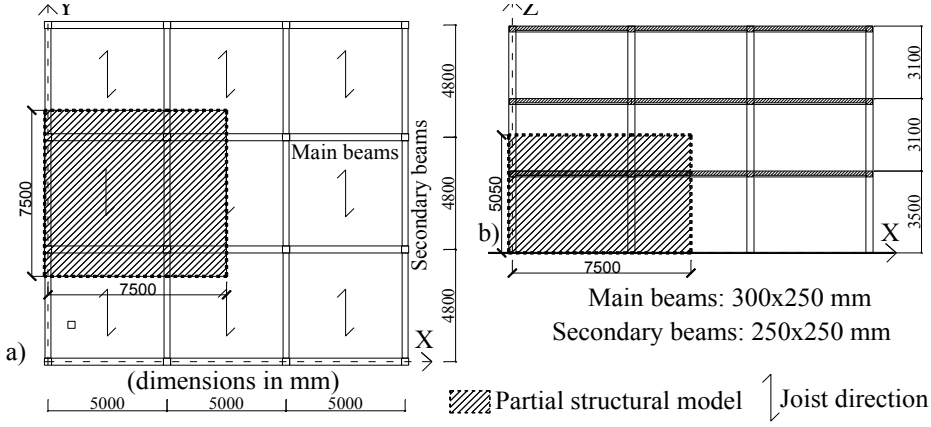

Fig. 3.10: Prototype structure (units: mm): a) plan; b) elevation

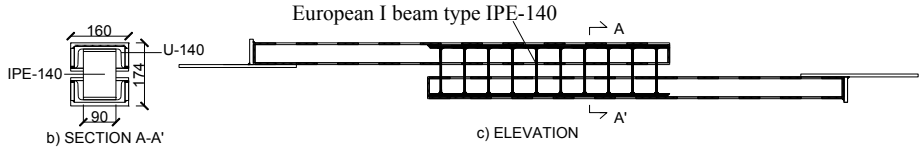

Fig. 3.11: Brace-type damper (units: mm): (a) section; (b) elevation

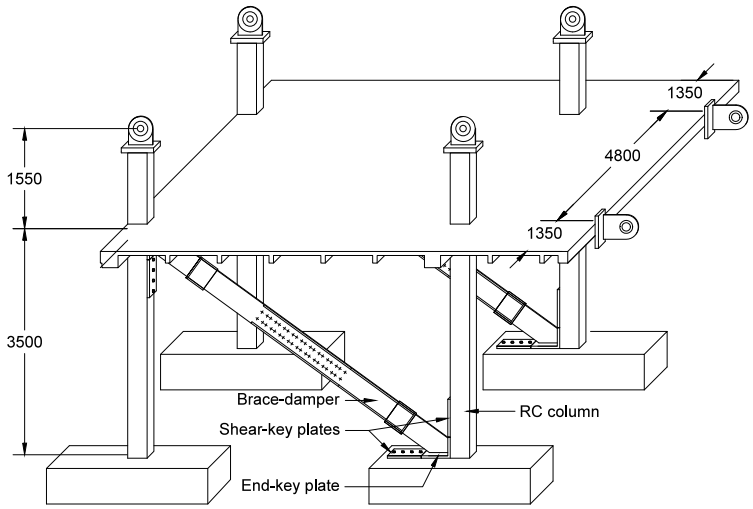

Fig. 3.12: 3D representation of the partial structural model (units: mm)

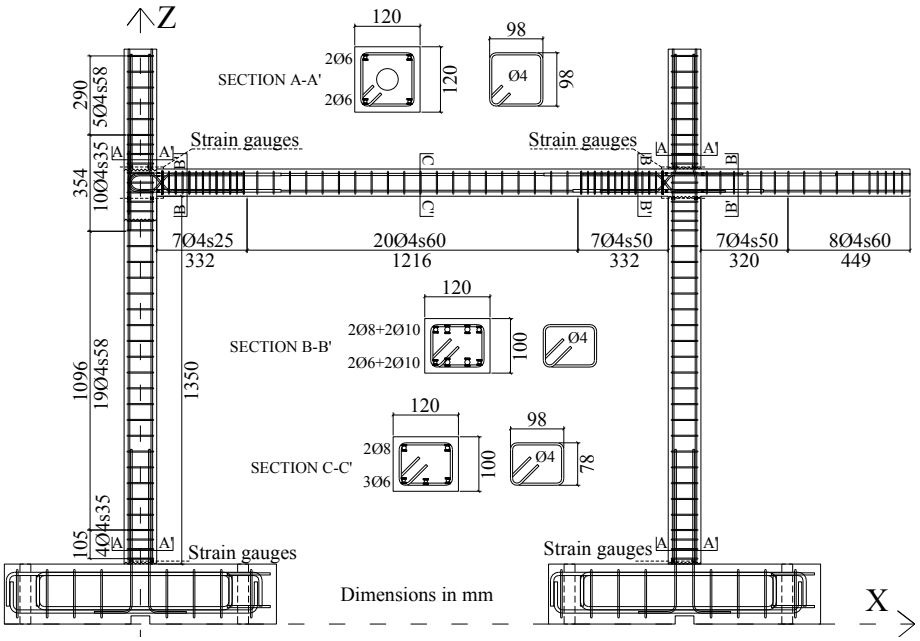

Fig. 3.13: Test structure before retrofitting (units: mm)

3.5.2 Test set-up

The tests conducted in this investigation were meant to reproduce the actual stress and deformation conditions on a real brace-frame connection subjected to seismic actions. Figs. 3.14 and 3.15 show the test structure placed on the uniaxial MTS $3\times3m^2$ shaking table. Steel blocks were attached to the top of the slab and to the top of half columns of the second story (indicated in Fig. 3.15.a as "added weight"). In order to simplify the experimental set-up, the upper half-story of the test structure was stiffened with diagonal bars (Fig. 3.15.a), so that the lateral displacement was concentrated in the first (lower) story. The seismic retrofit consisted of installing two brace-type hysteretic dampers in the first story, referred to as "Damper 1" and "Damper 2" in Fig. 3.15.b. In order to investigate the influence of the presence of a low-friction material between the shear-key plates and the end-plates of the damper, the Teflon sheets were not inserted in all connections. More precisely, the Teflon sheets were inserted in the brace-frame connection of the lower end of Damper 1 and in the upper end of Damper 2. For the upper end of Damper 1 and for the lower end of Damper 2 the brace-frame connection shown in Fig. 3.1.c was also used, but without the low friction material (i.e. with direct metal-to-metal contact). In Fig. 3.15.b the brace-frame connections with Teflon sheets are identified as "w/ Teflon", and those without Teflon as "w/o Teflon". The reason for inserting Teflon sheets only in one end of each brace damper, instead of using one brace damper

with Teflon in both ends and another brace damper without Teflon sheets, was to maintain the symmetry of the test structure in the direction of loading. The horizontal and vertical shear-key plates were anchored to the concrete with anchor bolts.

3.5.3 Instrumentation

Several longitudinal bars were instrumented with strain gauges located at member end sections where potential plastic hinges might develop, as shown in Fig. 3.13. Strain gauges were also attached to the shear-key plates of the four brace-frame connections, and to the ends of the braces in order to calculate the axial force sustained by each one of them, as shown in Fig. 3.15.a.

Fig. 3.15.a also shows: (i) the transducer (LVDT2) that measured the horizontal displacements of the floor mass; (ii) the accelerometers that measured the absolute accelerations of the floor mass and of the steel blocks added on the top of the specimen; (iii) the transducers (LVDTs 6 to 15) that measured the relative displacements of the shear-key plates and of the end-plates of the dampers with respect to the reinforced concrete elements to which they were attached; and (iv) the transducer that measured the axial deformations of the brace (LVDT 5). The data acquisition system was initialized to 0 before the onset of the first seismic simulation conducted on the retrofitted test structure.

3.5.4 Seismic simulations

The ground motion recorded at Calitri (Italy) during the Campano-Lucano earthquake (1980) was chosen for the seismic simulations. This record corresponds to an earthquake of intensity VII in the MSK scale and a moment magnitude of 6.9. The accelerogram is the horizontal NS component of the ground motion recorded at a distance of 16 km from the epicenter, in stiff soil (shear wave velocity v_s=529 m/s), and the maximum acceleration was 0.16g. Fig. 3.16.a shows the time history and Fig. 3.16.b the normalized response spectrum of the original (unscaled) Calitri record for 5% damping. Also shown in Fig. 3.16.b is the design spectrum prescribed by the Spanish seismic code for stiff soil with $400 \leq v_s \leq 750$m/s, together with the unscaled fundamental period of the tested structure.

The Calitri record was chosen because, as seen in Fig. 3.16.b: (i) in a wide range of periods Calitri's response spectrum is close to the design spectrum of the Spanish seismic code, and (ii) the corner periods of the Calitri spectrum enclose the range of possible periods of vibration of the test structure, thus guaranteeing maximum amplification of motion as the period elongates during testing. For the tests, the Calitri record was scaled in time by the scale factor $S_t=(5/2)^{0.5}$ to fulfill the similarity laws. Further, to guarantee progressive damage to the test structure, it was subjected to six seismic simulations, referred to as C50, C100, C200, C300, C350 and

C400, in which the Calitri record was scaled in amplitude multiplying by 0.5, 1, 2, 3, 3.5 and 4, respectively. The corresponding PGAs are shown in the second column of Table 3.3. Each PGA represents a different seismic hazard level at the site (Granada), and can be associated with mean return periods T_R of 17, 97, 500, 1435, 2032 and 2828 years, respectively. For relating T_R with PGA the following expression taken from the Spanish seismic code NCSE-02 (2002) was used: $PGA_{TR}=PGA_{500}(T_R/500)^{0.4}$. Here, PGA_{500} is the peak ground acceleration of an earthquake with T_R=500 years, and PGA_{TR} is the peak ground acceleration for an earthquake with a given return period T_R.

Before and after each simulation, free vibration tests were conducted to determine the period T_1 and damping fraction ξ of the first vibration mode. It is worth noting that the PGA of seismic simulation C200 represents the design PGA (0.31g) at the site (Granada). As explained in Section 3.1, the difference between 0.31g and the reference peak ground acceleration 0.23g is justified through the influence of the soil type, characterized in terms of the shear-wave velocity $v_{s,30}$ averaged in the layers existing in the top 30 m. The value 0.31g corresponds to a soft soil with $v_{s,30}$<200m/s.

Table 3.3 shows the values of relevant parameters used to characterize ground motions. They were calculated for the scaled record used in each seismic simulation. In Table 3.3, D_s is the significant duration (Trifunac & Brady, 1975), AI is Arias intensity

(Arias, 1970), a_{rms} the root-mean square acceleration, and SI is Housner's spectrum intensity, defined by:

$$AI = \frac{\pi}{2g}\int_0^{t_t} a_b^2(t)dt; \quad a_{rms} = \sqrt{\left(\int_{t_5}^{t_{95}} a_b^2(t)dt\right)\Big/\left(t_{95}-t_5\right)}; \qquad SI = \int_{0.1}^{2.5} SV(T,\xi)dT \tag{3.8}$$

where a_b(t) is the acceleration time history of total duration t_t; t_5 and t_{95} are the instants that define the interval between 5% and 95% of AI (Trifunac & Brady, 1975); SV is the velocity spectrum; T is the period of vibration; and ξ the damping ratio. It can be seen that the values of these parameters in all seismic simulations are realistic, that is, they fall within the range of real earthquake motions. Finally, in Fig. 3.16.b the response spectrum of Calitri record scaled in time (dash lines) is superimposed on the response spectrum of the original (unscaled) record. The obtained spectrum is seen to retain the characteristics of real records, and it is close to the design spectrum of the Spanish seismic code.

Finally, it is worth noting that prior to retrofitting with brace-type hysteretic dampers, the frame of the test structure was damaged by subjecting it to several shakings with the Calitri record (Benavent-Climent, Morillas, & Escolano-Margarit, 2014). The health of the frame at the end of these preliminary seismic simulations can be summarized as follows. Plastic hinges developed at the base of the columns of the first story, and the index of Park & Ang (1985) ranged

between 0.19 and 0.43, which corresponds to moderate (reparable) damage (Park & Ang, 1985). The average strains at member end sections of the rest of the frame ranged from 0.4 to 0.9 times the yield strain in columns, and from 0.16 to 0.23 times the yield strain in beams. The width of the concrete cracks ranged between 0.08 and 0.2 mm. The permanent drift displacement was 0.1%.

Fig. 3.14: Overview of the test set-up

3.5.5 Test results and interpretation

3.5.5.1 Overall response

For the sake of convenience in the forthcoming discussions, the test structure was idealized with a single degree of freedom system of mass m, whose dynamic equilibrium is governed by:

$$m\ddot{y}^t + C\dot{y} + Q_B = 0 \tag{3.9}$$

where $\ddot{y}^t$ is the absolute acceleration, C is the damping coefficient, $\dot{y}$ is the relative velocity and Q_B is the restoring force exerted by the structure. Since m is known and $\ddot{y}^t$ was measured with the accelerometers, the total shear force $F_{I,B}$ exerted by the inertial force, i.e. $F_{I,B} = m\ddot{y}^t = -\left(c\dot{y} + Q_B\right)$, can be readily calculated and is shown in Figs. 3.17 and 3.18 against the horizontal displacement of the center of mass of the floor diaphragm δ_T, for each seismic simulation. The figure reflects a stable energy dissipation behavior with minor pinching in the loops. In the instants of zero velocity (i.e. $\dot{y} = 0$), the damping force $c\dot{y}$ is null and $F_{I,B}$ coincides with the restoring force carried out by the structure Q_B. Values of $F_{I,B}$ when $\dot{y} = 0$ and thus $F_{I,B}$=Q_B were calculated for each seismic simulation and are plotted with solid symbols in Figs. 3.17 and 3.18. An approximate bilinear envelope of these points is drawn with thin dotted lines in the figure; it can be interpreted as the "capacity curve" of the structure obtained from the dynamic tests.

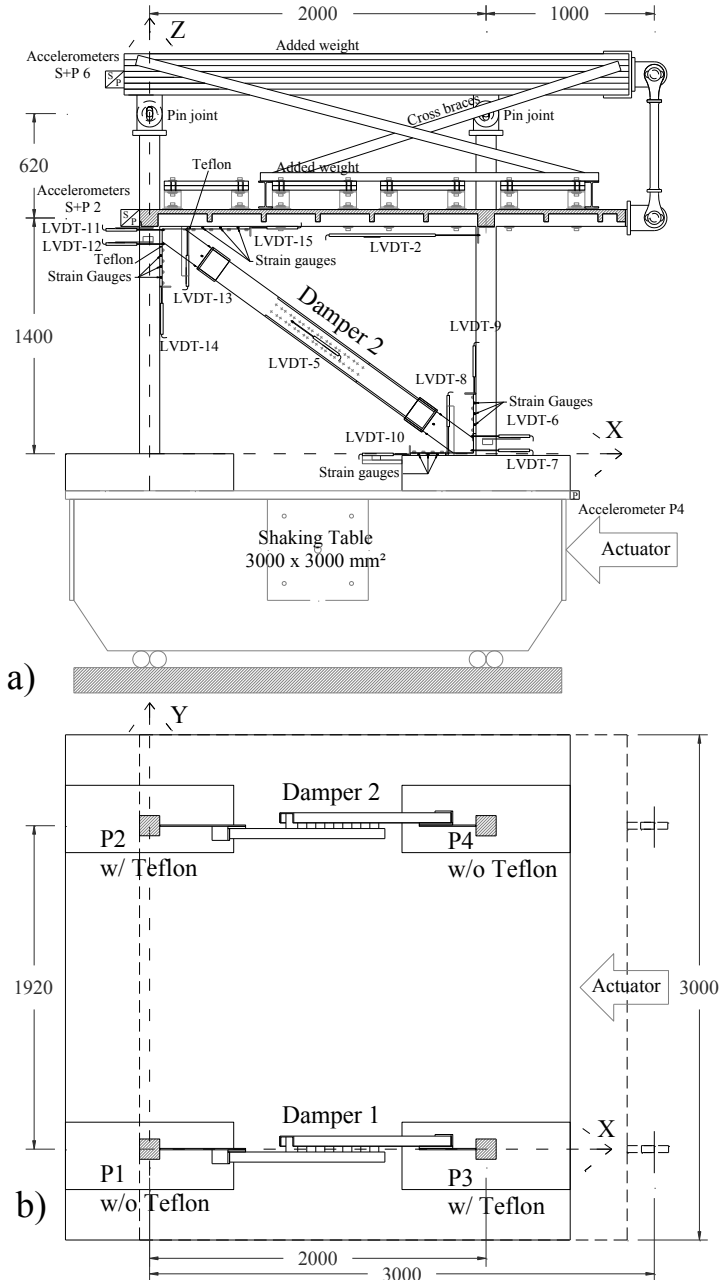

Fig. 3.15: Test structure; set-up and instrumentation (units: mm): a) elevation; b) plan

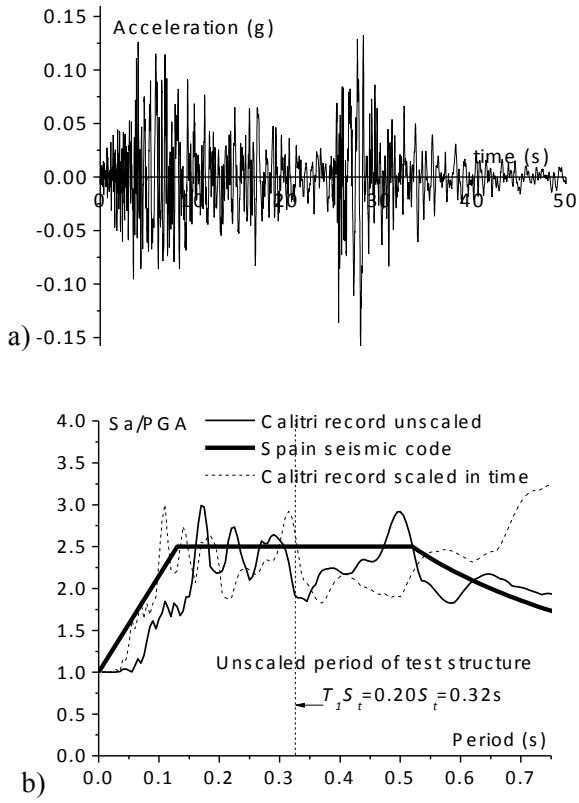

Fig. 3.16: Time history (a) and response spectrum (b) of Calitri record

Table 3.3: Parameters that characterize the records used for tests

Seismic simulation	*PGA (g)*	*SI (m)*	a_{rms} *(g)*	*AI (m/s)*	D_s (s)
C50	0.08	0.40	0.02	0.17	30.07
C100	0.16	0.75	0.03	0.67	30.07
C200	0.31	1.50	0.08	2.7	30.07
C300	0.47	2.26	0.11	6.1	30.07
C350	0.54	2.64	0.13	8.2	30.07
C400	0.62	3.01	0.15	10.8	30.07

The overall response of the specimen is summarized in Table 3.4 and Table 3.5. For each seismic simulation, Table 3.4 shows, in columns two to six, the fundamental period T_1, the damping ratio ξ, the maximum absolute response acceleration $\ddot{y}^t_{\max}$, the maximum

inter-story drift ratio *ID*, and the residual inter-story drift ratio ID_r. The seventh column indicates the seismic performance level determined according to the IDs established by ATC-40 (1996) and FEMA-356 (2000) that are shown in columns eight and nine. T_1 and ξ were determined from free vibration tests conducted at the end of the seismic simulations. Table 3.5 summarizes the normalized maximum strain ε_{max} measured in the longitudinal bars located at the member end sections of columns and beams identified in Fig. 3.19. The yield strain of the steel ε_y was 2625 μm/m. For seismic simulations C50, C100 and C200, the structure exhibited *ID*s below 1%, ID_rs were zero or negligible, and ε_{max} was in general below ε_y at the base of the columns. This corresponds to a performance level of "immediate occupancy" according to ATC-40 and FEMA-356 criteria, and a light or very light level of damage in the structure. For the seismic simulations C300, C350 and C400, the structure exhibited *ID*s between 1.05% and 1.5%, ID_rs between 0.12% and 0.16%, and ε_{max} ranged from ε_y to $5.1\varepsilon_y$ at the base of the columns. According to ATC-40 and FEMA-356 criteria for reinforced concrete frames, this corresponds to a seismic performance level of "life safety" and a moderate level of damage. This indicates that the addition of braces with the proposed brace-frame connection was effective in controlling the response of the retrofitted structure.

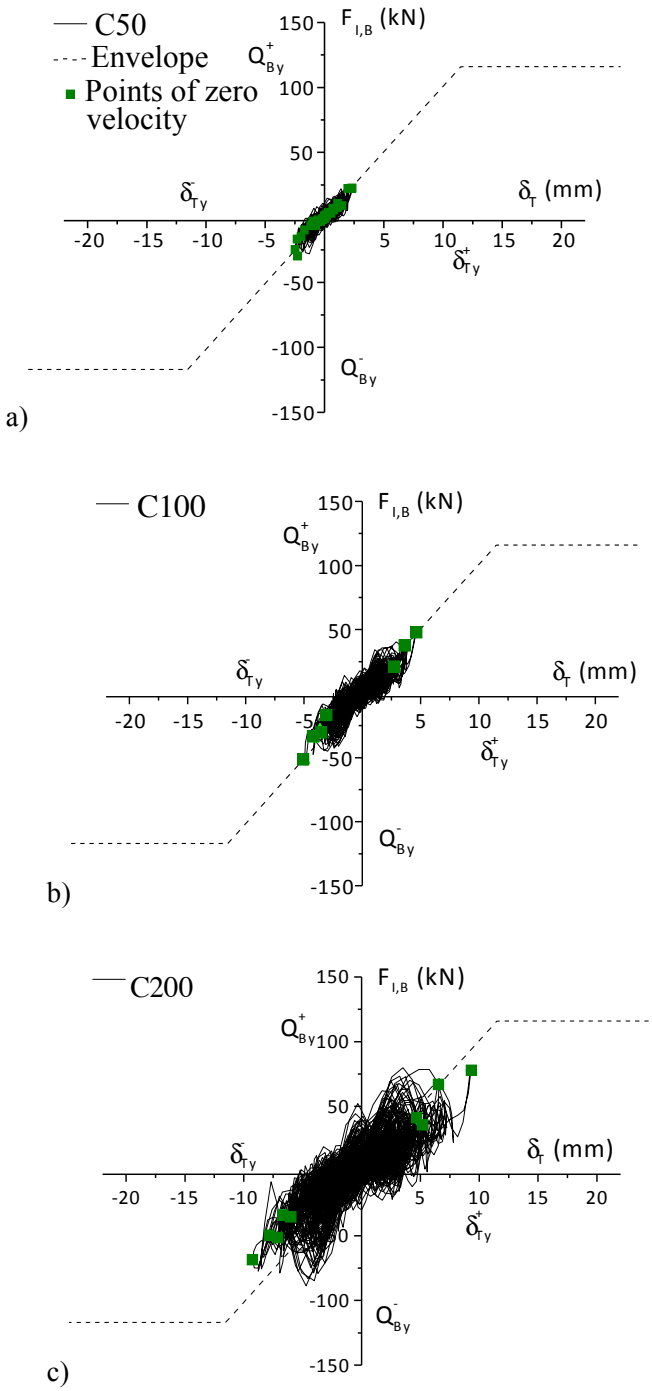

Fig. 3.17: Base shear force vs. top displacement, with indication of points with zero velocity, for simulations: a) C50, b) C100, c) C200.

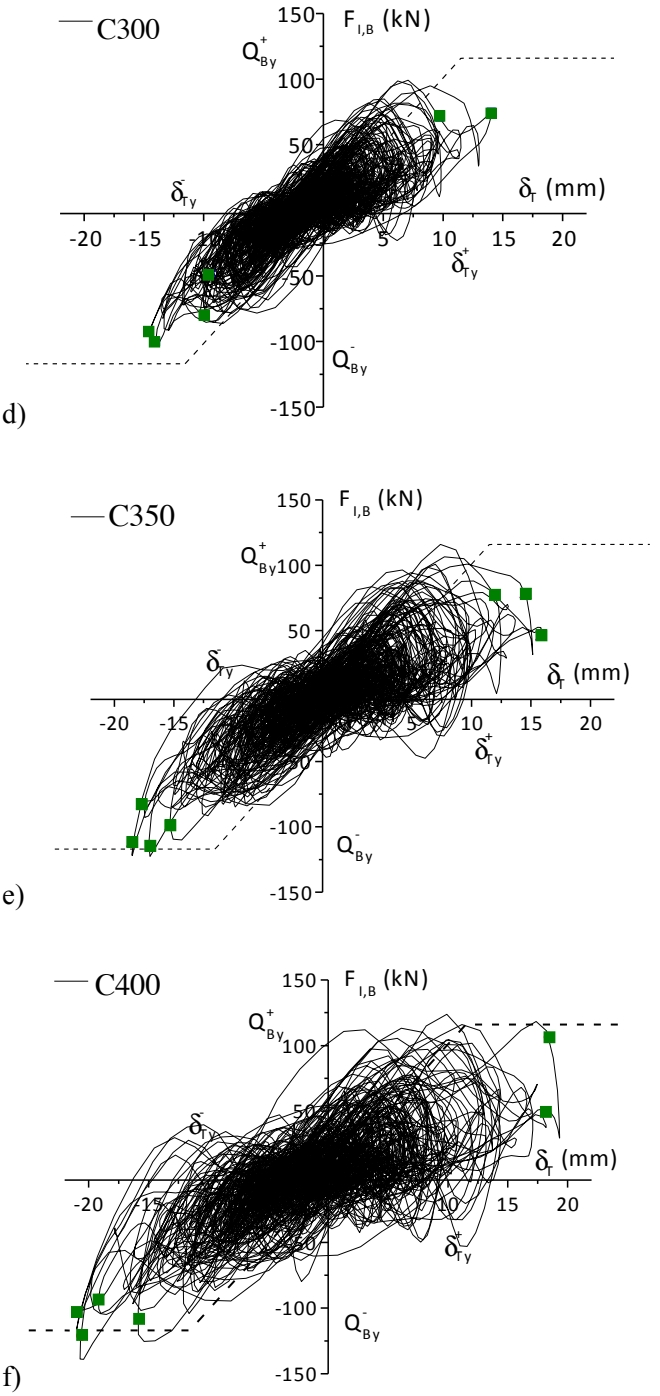

Fig. 3.18: Base shear force vs. top displacement, with indication of points with zero velocity, for simulations: a) C300, b) C350, c) C400

Table 3.4: Overall response

Seismic simulation	T_1 s	ξ %	$\ddot{y}^t_{max}$ g	ID %	ID_r %	Seismic performance	ATC ID(%)	FEMA ID(%)
c50	0.20	1.26	0.21	0.18	0.00	Immediate Occupancy	<1	<1
c100	0.20	0.96	0.44	0.35	0.00	Immediate Occupancy	<1	<1
c200	0.21	1.04	0.72	0.66	0.03	Immediate Occupancy	<1	<1
c300	0.21	1.31	1.17	1.05	0.12	Life Safety	1-2	1-2
c350	0.21	1.30	1.21	1.32	0.16	Life Safety	1-2	1-2
c400	0.21	1.34	1.32	1.50	0.12	Life Safety	1-2	1-2

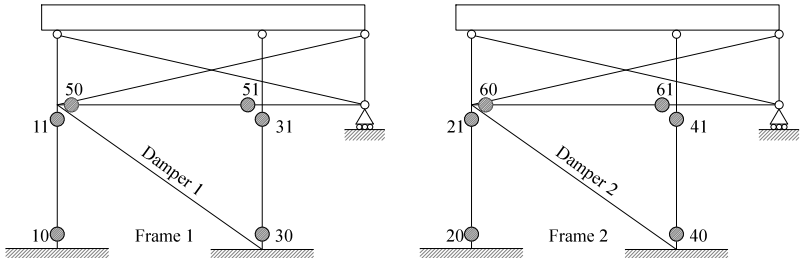

Fig. 3.19: Identification of potential plastic hinges in members

Table 3.5: Strains in longitudinal rebars

Seismic simulation:		C50	C100	C200	C300	C350	C400
	Hinge	$\varepsilon_{max}/\varepsilon_y$	$\varepsilon_{max}/\varepsilon_y$	$\varepsilon_{max}/\varepsilon_y$	$\varepsilon_{max}/\varepsilon_y$	$\varepsilon_{max}/\varepsilon_y$	$\varepsilon_{max}/\varepsilon_y$
BASE COLUMN	10	0.21	0.35	0.87	1.3	1.3	1.6
	20	0.29	0.40	0.67	1.0	1.1	2.9
	30	0.28	0.48	0.82	1.4	3.1	5.1
	40	0.31	0.50	1.09	2.0	2.8	3.6
UPPER END COLUMN	11	0.10	0.20	0.55	0.84	0.93	2.0
	21	0.07	0.14	0.41	0.58	0.72	0.83
	31	0.08	0.16	0.53	0.77	0.94	1.0
	41	0.04	0.13	0.40	0.56	0.66	0.69
BEAMS	50	0.13	0.25	0.47	0.65	0.73	0.81
	51	0.04	0.07	0.13	0.16	0.17	0.25
	60	0.16	0.28	0.49	0.73	0.84	0.89
	61	0.08	0.12	0.17	0.20	0.22	0.24

3.5.5.2 Modal Analysis

A numerical elastic model was developed in OpenSEES and subjected to a modal analysis, in order to compare some parameters obtained from experimental data with the ones obtained from numerical analysis. These parameters are: (1) the initial fundamental period, T_1, computed from free vibration tests conducted at the end of the seismic simulations, (2) the initial lateral stiffness of the global structure, K_T, obtained from the base shear-top displacement curves shown in Figs. 3.17 and 3.18 and, (3) the initial stiffness of the dampers, K_D, calculated from the load-displacement curves of the dampers shown in Fig. 3.23. Further, the initial stiffness of the reinforced concrete frame (without dampers), K_f, was numerically estimated through linear static analysis (LSA). As shown in Table 3.6, there is a good agreement between the numerical and the experimental data. The experimental value of K_f cannot be directly obtained from the test measures and consequently it is not included in Table 3.6.

Table 3.6: Comparison of experimental and numerical results

T_1 (s)		K_f (kN/mm)	K_D (kN/mm)		K_T (kN/mm)	
Tests	Numerical (MA)	Numerical (LSA)	Tests	Numerical (MA)	Tests	Numerical ($K_{f,LSA}$+$K_{D,MA}$)
0.20	0.21	1.78	8.87	8.32	10.60	10.10

3.5.5.3 Damage in the RC frame

3.5.5.3.1 Damage at a global level

As introduced in section 3.5.5.1, the dynamic equilibrium of an inelastic SDOF system subjected to a unidirectional horizontal ground motion is controlled by the following equation:

$$m\ddot{y}+C\dot{y}+Q_B=-m\ddot{z}_g \tag{3.10}$$

where m is the mass, C the damping coefficient, Q_B the restoring force, y the relative displacement, $\dot{y}$ and $\ddot{y}$ its first and second derivates with respect to time, and $\ddot{z}_g$ the ground acceleration. Multiplying Eq. (3.10) by $dy=\dot{y}dt$ and integrating over the duration of the earthquake, i.e. from $t=0$ to $t=t_o$, the equilibrium of forces of Eq. (3.10) is transformed in an equation of energy balance:

$$W_k+W_\xi+W_s=E \tag{3.11}$$

where W_k is the kinetic energy, W_ξ the damping energy, W_s the absorbed energy, and E is (by definition) the (relative) input energy, given by:

$$W_k=\int \dot{y}M\ddot{y}dt;\quad W_\xi=\int C\dot{y}^2dt;\quad W_s=\int Q_B\dot{y}dt;\quad E=\int -M\ddot{z}_g\dot{y}dt \tag{3.12}$$

W_s is composed of the recoverable elastic strain energy, W_{se}, and the irrecoverable plastic energy, W_p, i.e. $W_s = W_{se} + W_p$:

$$E = W_\xi + W_p + W_{se} + W_k \tag{3.13}$$

The sum of the kinetic and the elastic strain energies gives the elastic vibrational energy $W_e = W_{se} + W_k$. The difference $E - W_\xi = W_p + W_e$ is what Housner (1956) called the energy that contributes to damage and will be denoted by $E_D = E - W_\xi$ hereafter.

According to Eq. (3.13), the total input energy E can be split in two parts: the so-called total absorbed energy ($W_\xi + W_p$), and the energy "stored" by the system ($W_{se} + W_k$) $= W_e$. The former represents the energy that is cumulatively dissipated by the system, and therefore its time history is always a monotonically increasing curve (i.e. $W_\xi + W_p$ at a given instant t is always larger than at previous instants). The other part, W_e, is the energy stored by the system in the form of vibrational elastic energy, and its time history —in a system subjected to forced vibrations— is typically an oscillating curve. Therefore, the total absorbed energy ($W_\xi + W_p$) can be easily estimated from the time history of E by taking a lower bound curve, as shown in Fig. 3.20. The difference between the curve E-t and the lower bound curve is the history of W_e. Fig. 3.20 shows the histories of total input energy E, the sum of the plastic and elastic strain

energy $W_{p,d}+W_{se,d}$ dissipated by the dampers, the sum of the plastic and elastic strain energy $W_{p,f}+W_{se,f}$ of the RC frame (without dampers), and the total absorbed energy $W_{\xi}+W_{p}$ accumulated in the sequence of seismic simulations. The initial energies (i.e. when the pseudotime is 0) are the values accumulated in previous tests, prior to the installation of the hysteretic dampers, and described in (Benavent-Climent et al., 2014). Damping energy was estimated with Eq. (3.14), where $\dot{y}$ is the relative horizontal velocity of the SDOF system and $C=\xi 2m\omega_n$ is the damping coefficient. The damping ratio ξ was obtained for each simulation, as described in Table 3.4. These values of ξ are similar to the values recommended by Martinelli & Filippou (2009).

$$W_{\xi}=\int_0^t \dot{y}^T C\dot{y}\,dt \tag{3.14}$$

Finally, Table 3.7 summarizes the cumulated energy input in the test specimen, E_j, at the end of each simulation j, in terms of equivalent velocity V_E (defined by $V_E=\sqrt{2E/m}$) and calculated with Eq. (3.15). The corresponding equivalent velocity in the prototype, $V_{E,p}$, was computed by dividing by the scaling factor for velocity $\lambda_v=\frac{\lambda_L}{\lambda_t}=0.63$. Table 3.7 shows also the energy that contributed to damage, E_D, expressed in terms of equivalent velocity for both the test specimen, V_D, and for the prototype, $V_{D,p}$. The values of V_E, V_D,

$V_{E,p}$ and $V_{D,p}$ were computed at the end of the tests conducted prior to retrofitting with brace-type hysteretic dampers, already mentioned in section 3.5.4 —see reference (Benavent-Climent et al., 2014). As described previously, in estimating W_ξ with Eq. (3.14), the damping ratio ξ measured during the tests, for each simulation, was used (see Table 3.4).

$$V_E = \sqrt{2\sum_{j=1}^{s} E_j / m} \tag{3.15}$$

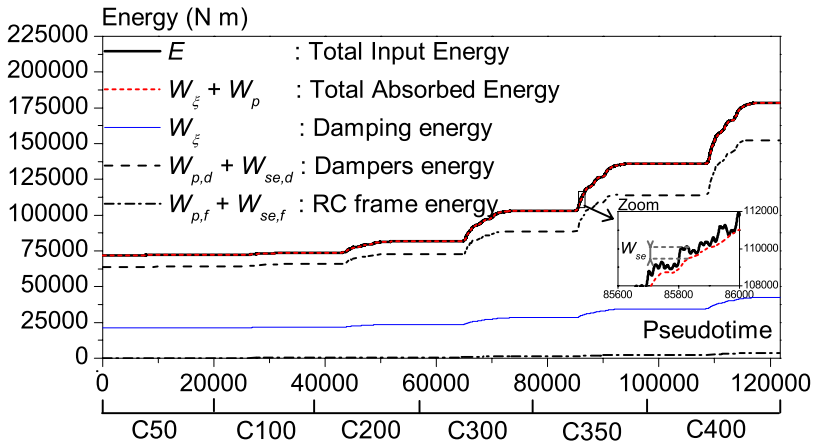

Fig. 3.20: Histories of accumulated energy

Table 3.7: Cumulative input energy

Simulation	Test Specimen (cm/s)		Prototype (cm/s)	
	V_E	V_D	$V_{E,\,p}$	$V_{D,\,p}$
Previous tests	340	285	537	450
C50	358	300	568	476
C100	362	304	575	483
C200	380	320	603	508
C300	427	363	678	576
C350	490	424	778	673
C400	562	491	892	779

3.5.5.3.2 Damage at a local level

The elastic and plastic strain energy absorbed by a given plastic hinge k of the structure during the cyclic loading, $W_{se,k}+W_{p,k}$, is the sum of the energy dissipated by the concrete, $W_{C,k}$, and the energy dissipated by the longitudinal reinforcement, $W_{S,k}$ (Park & Eom, 2006). The stress in the steel reinforcement, $\sigma_S(t)$, is approximated from the corresponding strain data $\varepsilon_S(t)$ measured by the strain gauges, by using the steel model described in (Benavent et al. 2011). The strain at each fiber of the concrete section, $\varepsilon_C(t)$, is approximated from the strain measured by the gauges at the steel rebars, by considering the well-known assumption of plane sections remaining plane (Bernoulli's principle). The corresponding stress $\sigma_C(t)$ is approximated from $\varepsilon_C(t)$ by using the uniaxial material model developed by Maekawa et al. (2003), by assuming no tensile strength.

The plastic hinge length was calculated using the empirical formulae for cyclic loading proposed by Fardis (2009), as detailed in Chapter 5 (section 5.2.1.2).

Finally, the elastic and plastic strain energy absorbed/dissipated by the existing RC structure is computed as the sum of the contributions of the p plastic hinges:

$$W_{se,k}+W_{p,k}=\sum_{k=1}^{p}\left(W_{S,k}+W_{C,k}\right) \tag{3.16}$$

Fig. 3.21 shows the energy absorbed/dissipated accumulated in the successive seismic simulations by the hinges of the RC frame. This energy was grouped and summed up as follows: energy absorbed/dissipated at the base of the columns (i.e. hinges 10, 20, 30, 40 in Fig. 3.19), energy absorbed/dissipated at the upper ends of the columns of the first story (i.e. hinges 11, 21, 31, 41 in Fig. 3.19) and, energy absorbed/dissipated at the beams ends (i.e. hinges 50, 51, 60, 61 in Fig. 3.19). It is worth emphasizing that the initial values when the pseudotime is 0 are the accumulated energies attained at the end of the tests conducted prior to the installation of the dampers, as described in (Benavent-Climent et al., 2014).

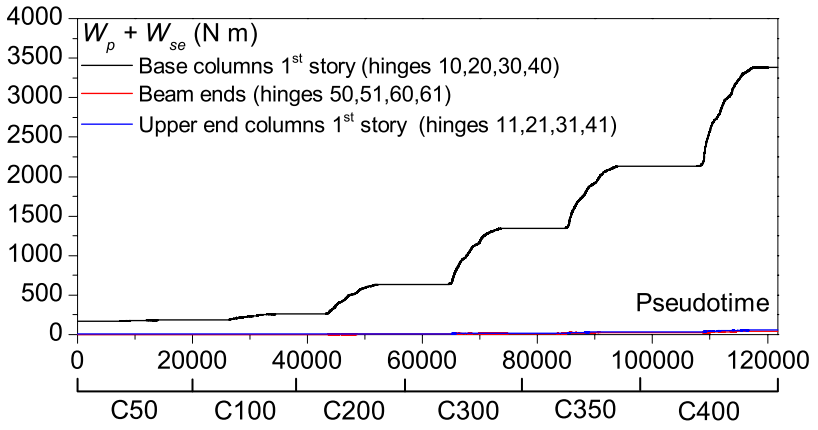

Fig. 3.21: Energy absorbed/dissipated by the hinges of the RC frame

The damage at the level of each individual hinge k of the columns was estimated in terms of maximum chord rotation demand θ_m in relation to chord rotation at ultimate capacity θ_u, that is,

$\theta_m/\theta_u = \max\left\{\left|\theta_m^+/\theta_u^+\right|, \left|\theta_m^-/\theta_u^-\right|\right\}$, the energy-based damage index D_i proposed by Darwin and Nmai (1986) and the well-known index of damage DI_{PA} developed by Park and Ang (1985). Results are shown in Table 3.8.

The chord rotation demand θ_m was estimated from the measurements provided by displacement transducers. The chord rotation capacities at ultimate θ_u and the chord rotation at yielding θ_y were predicted using the equation recommended by Fardis (2009). The damage index D_i, and the Park and Ang index of damage D_{PA} at a given hinge k were calculated as follows:

$$D_i = \frac{W_{p,k}}{0.5\left(M_y^+\theta_y^+ + \left|M_y^-\right|\left|\theta_y^-\right|\right)} \tag{3.17}$$

$$D_{PA} = \max\left\{\frac{\theta_m^+ - \theta_y^+}{\theta_u^+ - \theta_y^+}, \frac{\left|\theta_m^-\right| - \left|\theta_y^-\right|}{\left|\theta_u^-\right| - \left|\theta_y^-\right|}\right\} + \beta\frac{W_{p,k}}{0.5\left(M_y^+\theta_u^+ + \left|M_y^-\right|\left|\theta_u^-\right|\right)} \tag{3.18}$$

The parameter β was taken $\beta = 0.1$. The yielding moments under positive and negative bending, M_y^+ and M_y^- were estimated according to the formula proposed by Fardis (2009):

$$M_y = bd^3\varphi_y\left\{E_c\frac{\xi_y^2}{2}\left(\frac{1-d_1/d}{2} - \frac{\xi_y}{3}\right) + \frac{E_s\left(1-d_1/d\right)}{2}\left[\left(1-\xi_y\right)\rho_1 + \left(\xi_y - d_1/d\right)\rho_2 + \frac{\rho_v}{6}\left(1-d_1/d\right)\right]\right\} \tag{3.19}$$

where φ_y is the yielding curvature proposed by Fardis (a detailed description is given in Chapter 5, section 5.2.1.3); ξ_y is the neutral axis depth at yielding (normalized to the section effective depth, d); b is the width of the section, E_c is the moduli of the concrete; d_1 equal to the distance from the centre of the compression reinforcement to the extreme compression fibres; the set ρ_1, ρ_2 and ρ_v are the geometric reinforcement ratios of the tension, compression and web reinforcement. The variable ξ_y is defined as $\xi_y = \left(\zeta^2 A^2 + 2\zeta B\right)^{1/2} - \zeta A$ where $\zeta = E_s / E_c$ with E_s the steel strain moduli; A and B are variables which depend on the reinforcement ratios stated before, the yield strength of the reinforcement f_y and the axial load N in the column.

The results of Table 3.8 indicate that the RC frame remained basically elastic (i.e. the rotation demand was far below yielding and the Park and Ang damage index was very small (below 0.2 during seismic simulations C50, C100, and C200). During seismic simulations C300, C350 and C400, the rotation demand slightly exceeded the yield rotation (up to 81%) and the Park and Ang damage index was very small, except at the bottom end of the columns when this index reached 1.29. In general, and excepting the bottom ends of the columns, the RC frame experienced minor plastic deformations (small damage).

Table 3.8: Rotation demand θ_m/θ_u, θ_m/θ_y and damage indexes of column hinges.

	C50				C100			
Hinge	θ_m/θ_y	θ_m/θ_u	D_i	DI_{PA}	θ_m/θ_y	θ_m/θ_u	D_i	DI_{PA}
10	0.25	0.05	1.29	0.03	0.41	0.09	2.05	0.04
20	0.28	0.06	3.54	0.08	0.44	0.10	4.61	0.10
30	0.25	0.05	1.03	0.02	0.41	0.09	1.62	0.04
40	0.28	0.06	3.40	0.07	0.44	0.10	3.52	0.08
11	0.25	0.05	0.05	0.00	0.41	0.09	0.05	0.00
21	0.28	0.06	0.05	0.00	0.44	0.10	0.05	0.00
31	0.25	0.05	0.08	0.00	0.41	0.09	0.09	0.00
41	0.28	0.06	0.05	0.00	0.44	0.10	0.05	0.00

	C200				C300			
Hinge	θ_m/θ_y	θ_m/θ_u	D_i	DI_{PA}	θ_m/θ_y	θ_m/θ_u	D_i	DI_{PA}
10	0.87	0.19	4.59	0.10	1.25	0.27	8.73	0.26
20	0.87	0.19	6.56	0.14	1.17	0.26	8.02	0.23
30	0.87	0.19	8.87	0.19	1.25	0.27	25.72	0.64
40	0.87	0.19	4.02	0.09	1.17	0.26	4.91	0.16
11	0.87	0.19	0.06	0.00	1.25	0.27	0.06	0.07
21	0.87	0.19	0.07	0.00	1.17	0.26	0.11	0.05
31	0.87	0.19	0.17	0.00	1.25	0.27	0.40	0.08
41	0.87	0.19	0.06	0.00	1.17	0.26	0.07	0.05

	C350				C400			
Hinge	θ_m/θ_y	θ_m/θ_u	D_i	DI_{PA}	θ_m/θ_y	θ_m/θ_u	D_i	DI_{PA}
10	1.43	0.31	17.14	0.50	1.78	0.39	30.10	0.88
20	1.50	0.33	9.89	0.36	1.81	0.40	23.92	0.75
30	1.43	0.31	39.38	0.99	1.78	0.39	48.78	1.29
40	1.50	0.33	6.96	0.29	1.81	0.40	11.55	0.48
11	1.43	0.31	0.09	0.12	1.78	0.39	0.21	0.22
21	1.50	0.33	0.16	0.14	1.81	0.40	0.23	0.23
31	1.43	0.31	0.70	0.14	1.78	0.39	1.07	0.24
41	1.50	0.33	0.17	0.15	1.81	0.40	0.32	0.23

3.5.5.3.3 Section forces

The section forces developed during the seismic simulations at the hinges located in the columns were estimated. Table 3.9 shows the values for each simulation at the time step corresponding to

maximum moment in each column. To this end, the cross-section response was obtained by integrating the stress–strain response of the materials (Spacone, Filippou, & Taucer, 1996), as defined in previous section 3.5.5.3.2. The strain at each fiber of the section was calculated from the strain measures at the steel rebars and, regarding the plane sections-remain-plane assumption.

Table 3.9: Internal forces at the hinges

	C50		C100		C200	
	M kN m	*V* kN	*M* kN m	*V* kN	*M* kN m	*V* kN
10	3.68	2.89	5.09	3.82	6.92	4.94
11	-0.37		-0.26		0.00	
20	3.47	2.29	5.21	3.24	6.13	3.69
21	0.27		0.68		0.97	
30	1.94	1.95	3.97	3.61	5.04	3.93
31	-0.80		-1.09		-0.46	
40	1.89	1.26	2.29	1.67	3.77	2.58
41	0.12		-0.05		0.16	

	C300		C350		C400	
	M kN m	*V* kN	*M* kN m	*V* kN	*M* kN m	*V* kN
10	7.98	5.68	8.60	6.16	8.78	6.22
11	0.03		-0.01		0.08	
20	6.37	3.61	-4.95	-4.80	-7.71	-6.66
21	1.32		1.77		1.62	
30	5.37	4.43	4.64	2.56	5.29	1.94
31	-0.84		1.06		2.57	
40	3.52	2.35	-1.23	-0.96	-5.77	-4.74
41	0.23		0.11		0.87	

On the other hand, the design shear resistance of the columns without shear reinforcement, $V_{Rd,c}$, was evaluated by following art. 6.2.1. of EN 1992-1-1:2004 (2004). Results obtained are 10.76 kN for the exterior columns and 12.64 kN for the interior columns. As shown

in Table 3.9, the shear values attained during the tests were considerably lower than the shear resistance of the global member without shear reinforcement, showing that there was no need to increase the global shear resistance of the existing column. As explained in 5.4.3.2.1 of EN 1998-1:2004 (2004), this requirement is applicable also for medium and high ductility sections.

However, the concentrated action at the top of the external columns during the severest seismic simulation C400, probably caused a diagonal crack shown in Fig. 3.22. These diagonal cracks can be prevented, if necessary, by retrofitting the existing joint with mono-directional steel fibre fabric placed in the same direction of the damper. Details for the design of a convenient reinforcement can be found in (Dolce & Manfredi, 2011), considering the horizontal action applied by the damper similar to the diagonal one applied by a wall on the existing external beam-column joint.

a)

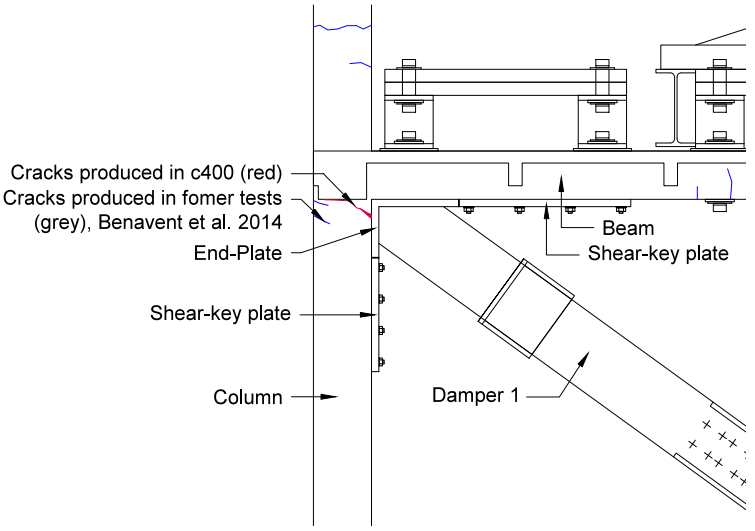

b)

Fig. 3.22: Crack pattern in the connection of dampers at the end of c400

3.5.5.4 Response of the braces

In contrast to the frame, the braces underwent severe plastic deformations. Fig. 3.23 shows the axial force N measured in one of the braces (Damper 2) versus the horizontal displacement of the floor

mass expressed in percentage of story height. The shape of the hysteretic loops for large plastic deformations is close to a rhomboid, thus indicating that the proposed brace-frame connection is effective in mobilizing the inherent energy dissipation capacity of the damper. The histories of horizontal displacements of the floor mass measured by transducer LVDT-2 (see Fig. 3.15.a) were compared with the histories of the horizontal component of the displacement measured along the axis of the brace by the transducer LVDT-5 (see Fig. 3.15.a). Table 3.12 summarizes the peak values and the residual values at the end of each seismic simulation. Both histories followed the same pattern and the minor differences are attributable to: (i) the elastic (axial) deformations of the auxiliary parts of the braces that were not captured by LVDT-5, and (ii) possible relative movements between the ends of the brace and the frame. This means that the proposed brace-frame connection was effective in preventing or minimizing relative movements between the ends of the dampers and the frame.

To corroborate the experimental data shown in Fig. 3.23, characteristic parameters of the dampers were calculated using the formula described in (Benavent-Climent et al., 2011). In this way, the axial yield load was Q_{yd}=39.83kN, the axial maximum apparent load was Q_{Bd}=51.67kN and, the axial yield displacement was δ_{yd}=1.88mm. The total lateral stiffness was calculated from the unloading part of the experimental load-lateral displacement curves K_{D1}=4.97kN/mm,

for the damper 1, and K_{D2}=3.90kN/mm, for the damper 2. It can be seen that the actual maximum axial force endured by the dampers (about 60 kN) is above the predicted maximum apparent strength (Q_{Bd}=51.67kN), which was calculated by using the yield stress of the steel obtained from static tests. This increment of strength (about 16%) can be attributable, at least partially, to strain rate effects.

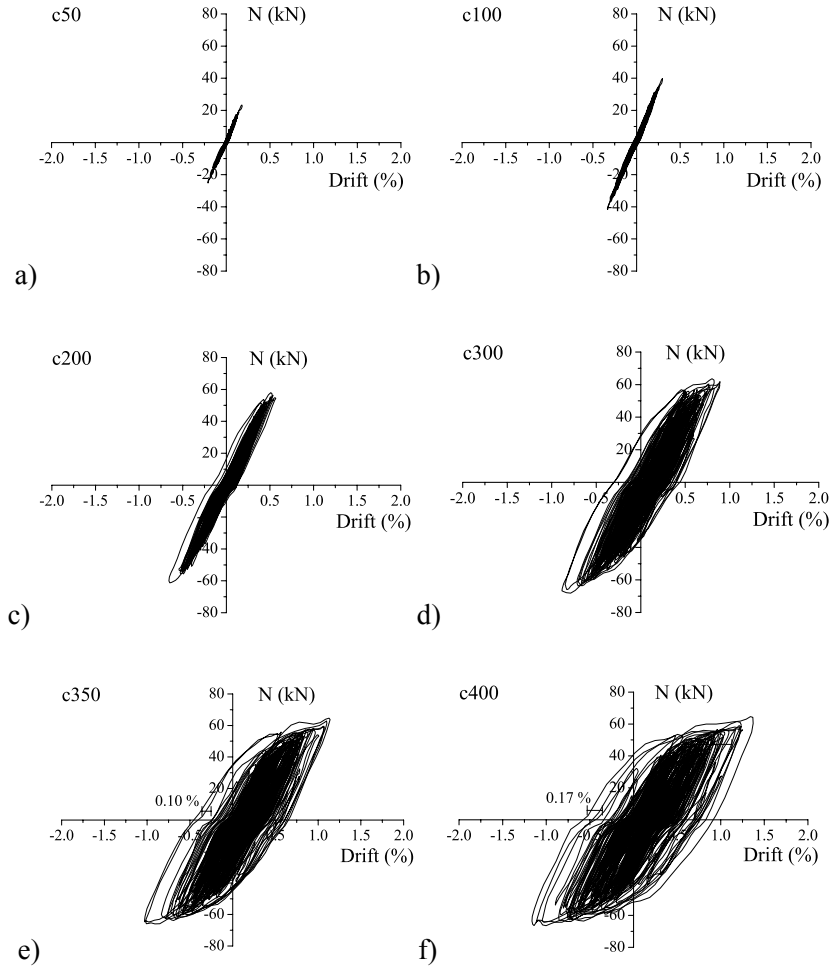

Fig. 3.23: Axial force in damper 2 vs. lateral displacement of the structure for seismic simulations (a) c50, (b) c100, (c) c200, (d) c300, (e) c350, (f) c400

3.5.5.4.1 Damage evaluation at local level in the EDDs

The damage in the hysteretic-type EDDs was characterized by the index $\overline{ID}$ proposed by Benavent-Climent (2007) which was experimentally evaluated with shake-table tests. The damage index $\overline{ID}$ measures the level between 0 (no damage) and 1 (failure). It is important to note that the index $\overline{ID}$ is calculated for the positive $\overline{ID}^{+}$ and negative $\overline{ID}^{-}$ domain. Benavent-Climent (2007) proposed to take the maximum value between the two values, as the global damage index $\overline{ID}$. In order to calculate the damage index $\overline{ID}$, the *N*-axial displacement curves corresponding to damper 2 (similar to the curves shown in Fig. 3.23, expressed in terms of lateral displacement, δ_T, in percentage of story height) were decomposed into the so-called "Skeleton Part" and "Bauschinger Part". The area enveloped by each domain of loading in the Skeleton curve was called ${}_{S}W_{u}^{+}$ and ${}_{S}W_{u}^{-}$ for positive and negative domain, respectively. Similarly, the area enveloped by each domain of loading in the Bauschinger curve was called ${}_{B}W_{u}^{+}$ and ${}_{B}W_{u}^{-}$. Maximum displacements attained in Skeleton Part are noted as ${}_{S}\delta_{u}^{+}$ and ${}_{S}\delta_{u}^{-}$. These parameters were expressed in nondimensional form as follows:

$$
\begin{aligned}
&{}_S\overline{\eta}^{+} = \frac{{}_S W_u^{+}}{Q_{yd}\delta_{yd}}; \quad {}_S\overline{\eta}^{-} = \frac{{}_S W_u^{-}}{Q_{yd}\delta_{yd}}; \quad {}_S\eta = \left|{}_S\overline{\eta}^{+}\right| + \left|{}_S\overline{\eta}^{-}\right| \\
&{}_B\overline{\eta}^{+} = \frac{{}_B W_u^{+}}{Q_{yd}\delta_{yd}}; \quad {}_B\overline{\eta}^{-} = \frac{{}_B W_u^{-}}{Q_{yd}\delta_{yd}}; \quad {}_B\eta = \left|{}_B\overline{\eta}^{+}\right| + \left|{}_B\overline{\eta}^{-}\right| \\
&{}_{ep}\overline{\eta}^{+} = \frac{{}_S\delta_u^{+}}{\delta_{yd}}; \quad {}_{ep}\overline{\eta}^{-} = \frac{{}_S\delta_u^{-}}{\delta_{yd}}; \quad {}_{ep}\eta = \left|{}_{ep}\overline{\eta}^{+}\right| + \left|{}_{ep}\overline{\eta}^{-}\right| \\
&\overline{\eta}^{+} = {}_S\overline{\eta}^{+} + {}_B\overline{\eta}^{+}; \quad \overline{\eta}^{-} = {}_S\overline{\eta}^{-} + {}_B\overline{\eta}^{-}; \quad \eta = {}_S\eta + {}_B\eta
\end{aligned}
\tag{3.20}
$$

where ${}_{ep}\eta$ is the apparent ultimate cumulative plastic deformation ratio on the Skeleton Part; ${}_S\eta$ is the ultimate cumulative plastic deformation ratio on the Skeleton Part; ${}_B\eta$ is the ultimate cumulative plastic deformation ratio on the Bauschinger Part and η is the ultimate total cumulative plastic deformation ratio, as defined by Benavent-Climent et al. (2011). Resulting ratios for damper 2 are shown in Table 3.10.

Table 3.10: Nondimensional ratios

${}_S\overline{\eta}^{+} =$	7.51	${}_S\overline{\eta}^{-} =$	3.62	${}_S\eta =$	11.13
${}_B\overline{\eta}^{+} =$	649.36	${}_B\overline{\eta}^{-} =$	207.81	${}_B\eta =$	857.17
${}_{ep}\overline{\eta}^{+} =$	7.06	${}_{ep}\overline{\eta}^{-} =$	5.79	${}_{ep}\eta =$	12.85
$\overline{\eta}^{+} =$	656.87	$\overline{\eta}^{-} =$	211.43	$\eta =$	868.30
${}_B\overline{\eta}^{+}/{}_S\overline{\eta}^{+} =$	86.47	${}_B\overline{\eta}^{-}/{}_S\overline{\eta}^{-} =$	57.41	${}_B\eta/{}_S\eta =$	77.03

Table 3.11 shows the results of the damage index at the end of each simulation i, which are computed as $\overline{ID}^{+} = \overline{\eta}^{+}/\overline{\eta}_u^{+}$; $\overline{ID}^{-} = \overline{\eta}^{-}/\overline{\eta}_u^{-}$ for each loading domain. The ultimate limit state points $\overline{\eta}_u^{+}, \overline{\eta}_u^{-}$ were determined with the equations described by Benavent-Climent (2007)

and the parameters corresponding to the type of hysteretic damper (WPD) obtained by Benavent-Climent et al. (2011).

Table 3.11: Damage index $\overline{ID}$ in damper 2

	C50	C100	C200	C300	C350	C400
$\overline{ID}^{+}$	0.02	0.08	0.30	0.62	0.89	1.07
$\overline{ID}^{-}$	0	0.01	0.03	0.05	0.26	0.58
$\overline{ID}=\max\left\{\overline{ID}^{+};\overline{ID}^{-}\right\}$	0.02	0.08	0.30	0.62	0.89	1.07

Furthermore, the load path in the $_{ep}\eta$-η space obtained from the test and the predicted failure curve is shown in Fig. 3.24. It was calculated by following the procedure described in (Benavent-Climent et al., 2011). It is worth mentioning that this figure represents the values of $_{ep}\eta$ and η corresponding to the sum of the positive and negative domains of loading.

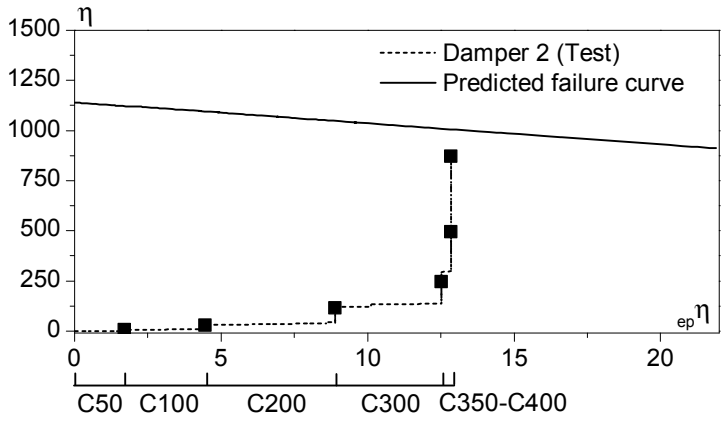

Fig. 3.24: Energy consumption path in the $_{ep}\eta$-η space obtained from the test and predicted failure curve for damper 2.

3.5.5.5 Behavior of the brace-frame connection

The following sub-sections analyze the effect of inserting a low friction material (Teflon) between the shear-key plates and the end-plates of the brace in terms of: (i) the normal stress distributions along the shear-key plates and their relative displacement with respect to the reinforced concrete members; and (ii) movements of the end-plates of the braces relative to the reinforced concrete members to which they are fastened.

3.5.5.5.1 Stress distribution along the shear-key plates

As shown in Fig. 3.15.a, each brace has two ends (referred to as "upper" and "lower" ends hereafter), and each end is connected to the frame with two shear-key plates (referred to as "horizontal" and "vertical" shear-key plates in the following discussion). The normal stresses $\sigma_{N,plate}$ (see Fig. 3.3.b) in several cross-sections of each shear-key plate were measured by gauges located at midpoint between the anchor bolts as shown in Fig. 3.15.a.

Figs. 3.25 and 3.26 compare the distributions of $\sigma_{N,plate}$ in the shear-key plates of the upper end of Damper 1 (without Teflon sheets), with those in the shear-key plates of the upper end of Damper 2 (with Teflon sheets). Fig. 3.25 refers to the horizontal shear-key plates and Fig. 3.26 to the vertical ones. The values of $\sigma_{N,plate}$ are taken at the instant of maximum axial force in Damper 2, N_{D2}. At this instant, the axial force in Damper 1, N_{D1}, was in general

similar to N_{D2}. The horizontal axis in Figs. 3.25 and 3.26 represents the distance x measured from the contact surface of the shear-key plate. As seen in Fig. 3.25, in the proximity of the contact surface (x=0) $\sigma_{N,plate}$ is larger for the horizontal shear-key plate with Teflon sheet than for the horizontal shear-key plate without Teflon. In contrast, it is seen in Fig. 3.26 that in the vertical shear-key plates, $\sigma_{N,plate}$ remains approximately constant or decreases in the vicinity of the contact surface when Teflon sheets are inserted. This means that the inclusion of Teflon sheets causes the in-plane forces (named V in Fig. 3.1.c) acting in the horizontal shear-key plates to increase, and those in the vertical shear-key plates to decrease or to remain approximately constant. Figs. 3.25 and 3.26 show the results for the seismic simulations C200, C300, C350, C400; similar trends were found for simulations C50 and C100.

3.5.5.5.2 Displacements of the horizontal shear-key plates

For Damper 2, Figs. 3.27 and 3.28 compare the horizontal displacements, relative to the concrete, of the horizontal shear-key plate located at the upper end (with Teflon sheets), with that of the horizontal shear-key plate at the lower end (without Teflon). These displacements were measured by the displacement transducers LVDT 15 and LVDT 10 in Fig. 3.15.a. Both histories of displacement start from zero at the onset of simulation C50 (Fig. 3.27.a) but develop in a different way in the successive seismic simulations. The range of displacements experienced by the shear-key plate with Teflon sheets

is wider than that of the shear-key plate without Teflon, but the residual deformation of the former at the end of seismic simulations following C50 is about one half that of the latter. In any case, the maximum displacements are small (less than 1mm) and very similar for both horizontal shear-key plates (i.e. with and without Teflon sheets). Hence, the effect of including a low friction material on the maximum relative displacements experienced by the horizontal shear-key plates is negligible.

Table 3.12: Horizontal frame displacement and horizontal component of brace displacement

Simulation	Maximum horizontal displacement		Residual horizontal displacement	
	Frame (mm)	Brace (mm)	Frame (mm)	Brace (mm)
c50	-2.69	-2.98	0.00	0.00
c100	-4.30	-4.77	0.00	-0.03
c200	-8.47	-10.09	0.56	0.54
c300	-11.39	-15.03	1.69	3.10
c350	-13.08	-17.00	2.40	4.46
c400	17.67	20.95	2.23	4.47

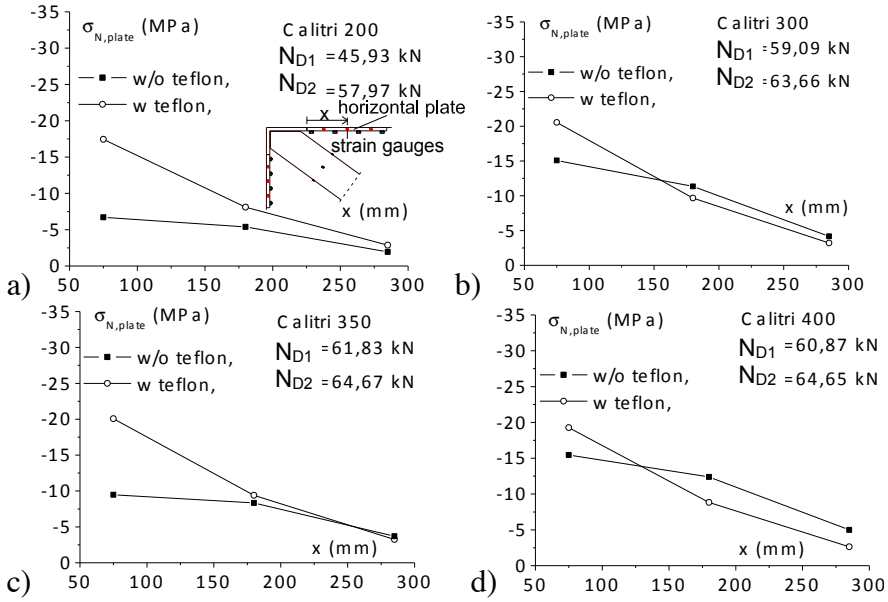

Fig. 3.25: Distribution of normal stresses in the upper horizontal shear-key plates, for seismic simulations: a) C200; b) C300; c) C350; d) C400

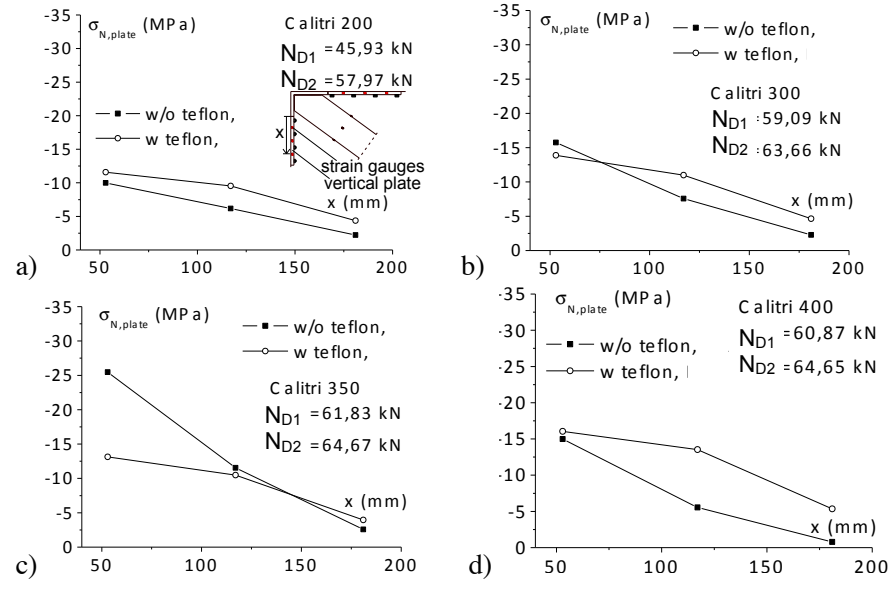

Fig. 3.26: Distribution of normal stresses in the upper vertical shear-key plates for seismic simulations: a) C200; b) C300; c) C350; d) C400

3.5.5.5.3 Displacement of the vertical shear-key plates

For Damper 2, Figs. 3.29 and 3.30 compare the vertical displacements, relative to the concrete, of the vertical shear-key plate located at the upper end (with Teflon), with that of the vertical shear-key plate at the lower end (without Teflon). These displacements were measured by LVDTs 14 and 9, respectively, in Fig. 3.15.a. It can be seen that the residual deformations at the end of each seismic simulation are smaller than those observed in the horizontal shear-key plates in the previous sub-section. Also, similarly to the horizontal shear-key plates, in any case the maximum displacements are small (less than 1.5mm) and in the same range for both shear-key plates. Again, the presence of the low friction material does not seem to significantly affect the minor maximum relative displacements of the vertical shear-key plates. The results of sub-sections 3.5.5.5.2 and 3.5.5.5.3 are relevant, as they indicate that the presence of the low friction material does not jeopardize the behavior of the brace-frame connection in terms of the relative displacements of the shear-key plates.

3.5.5.5.4 Displacement of the ends of the damper in the direction of its axis

Figs. 3.31 and 3.32 compare the displacement of the upper end-plate of Damper 2 relative to the beam-column joint, with the displacement of the lower end-plate of the same damper relative to

the foundation-column connection. Both displacements are measured in the direction of the axis of the damper and are taken as positive when the end-plate moves away from the beam-column joint, or from the foundation-column connection. Referring to Fig. 3.15.a, these axial displacements were obtained from the readings provided by LVDTs 11, 12 and 13 for the upper end-plate, and from LVDTs 6, 7 and 8 for the lower end-plate. It is worth recalling that the brace-frame connection that fixed the upper end of the damper had Teflon sheets and that of the lower end of the damper did not. As seen in Figs. 3.31 and 3.32, for the low and design levels of the seismic action (simulations C50, C100 and C200), the displacement of the upper end-plate (with Teflon) is small (up to about 1mm), yet larger than that of the lower end-plate (without Teflon). However, the trend reverses as the severity of the ground motion increases and the number of accumulated cycles of displacement grows (simulations C300, C350 and C400). During the last and most severe seismic simulation, C400, the axial displacement of the upper end-plate is about one half that of the lower one. Therefore, the insertion of the low friction material does not have a negative effect from the standpoint of the maximum gap between the end-plate of the damper and the beam-column joint or foundation-column connection.

3.5.5.5.5 Rotation of the end-plates of the damper

Figs. 3.33 and 3.34 compare the rotation of the upper and lower end-plates of Damper 2 about an axis perpendicular to the plane of

the frame. Both rotations are taken as positive when they are counter-clockwise. Referring to Fig. 3.15.a, the rotations were obtained from the readings provided by LVDTs 11, 12 and 13 for the upper end-plate, and from LVDTs 6, 7 and 8 for the lower end-plate of the damper. The same pattern of movements discussed in sub-section 3.5.5.5.4 for the displacement of the end-plates in the direction of the axis of the damper can be observed for the rotations. That is, for low and design levels of the seismic action (simulations C50, C100 and C200), the rotation of the upper end-plate (with Teflon) is larger than that of the lower end-plate (without Teflon), but the trend reverses for more severe earthquakes (simulations C300, C350 and C400). In any case, the rotations are small. Therefore, the insertion of the low friction material does not have a negative effect on the amount of rotation of the end-plates of the damper.

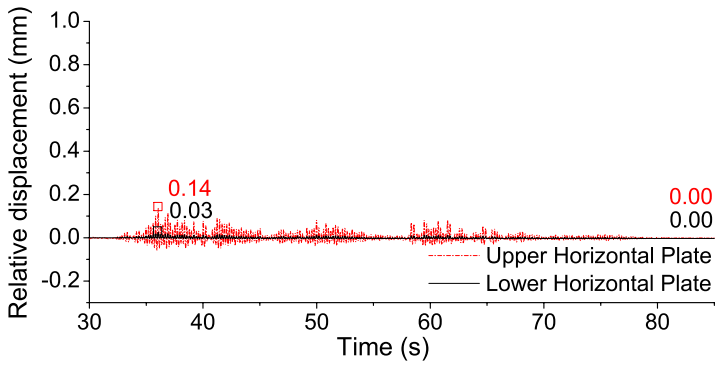

a)

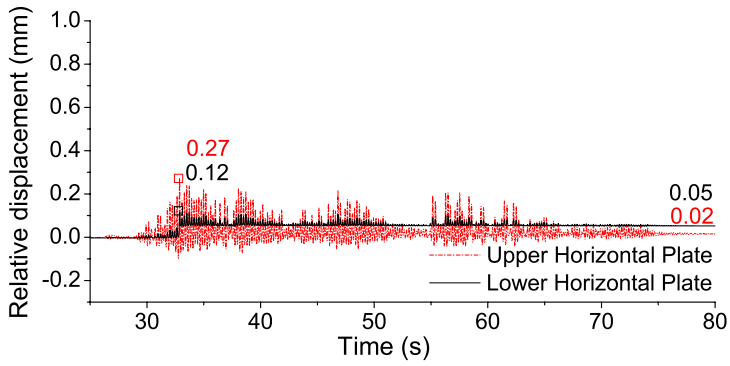

b)

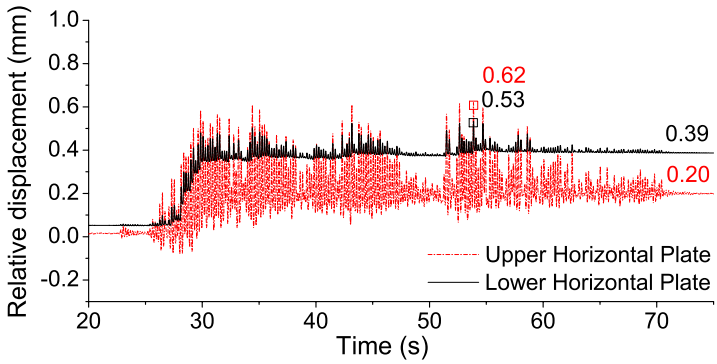

c)

Fig. 3.27: Relative horizontal displacements of upper (with Teflon) and lower (without Teflon) horizontal shear-key plates of Damper 2 for: a)C50; b)C100; c)C200.

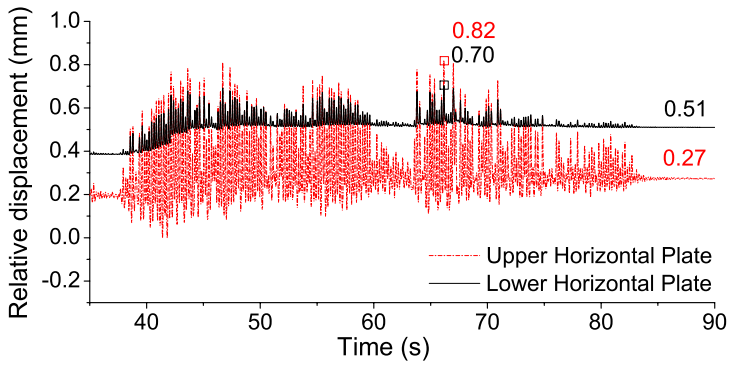

a)

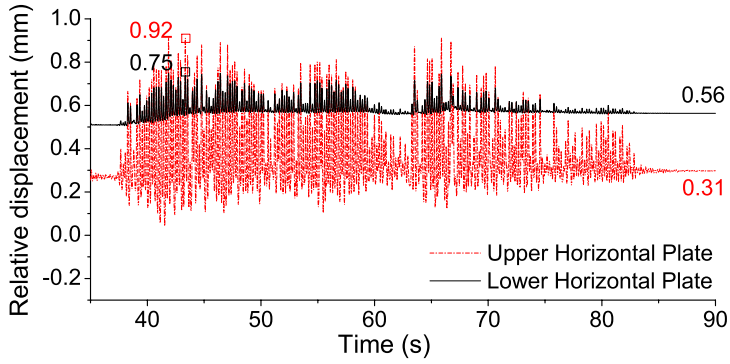

b)

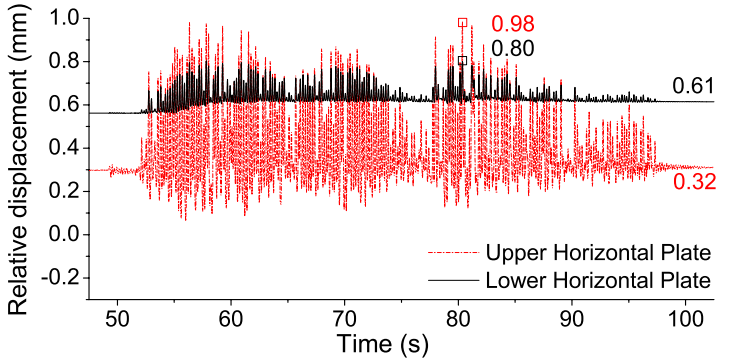

c)

Fig. 3.28: Relative horizontal displacements of upper (with Teflon) and lower (without Teflon) horizontal shear-key plates of Damper 2 for: a)C300; b)C350; c)C400.

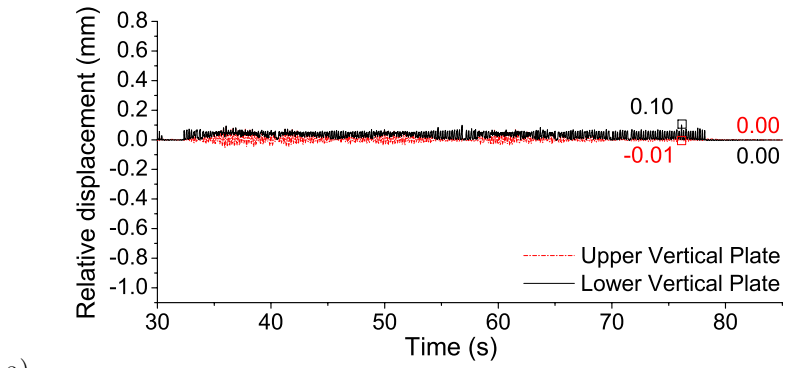

a)

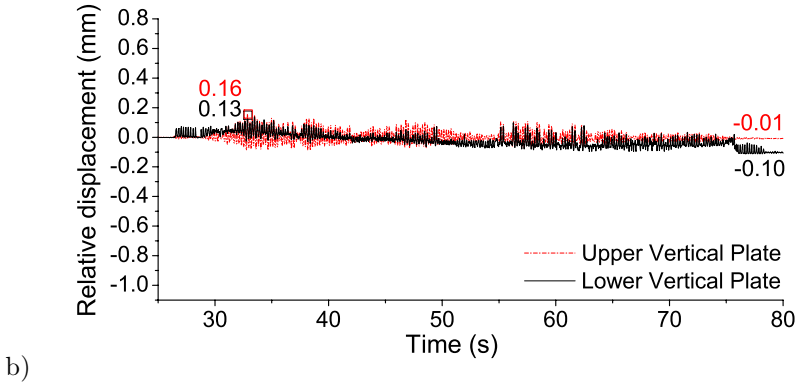

b)

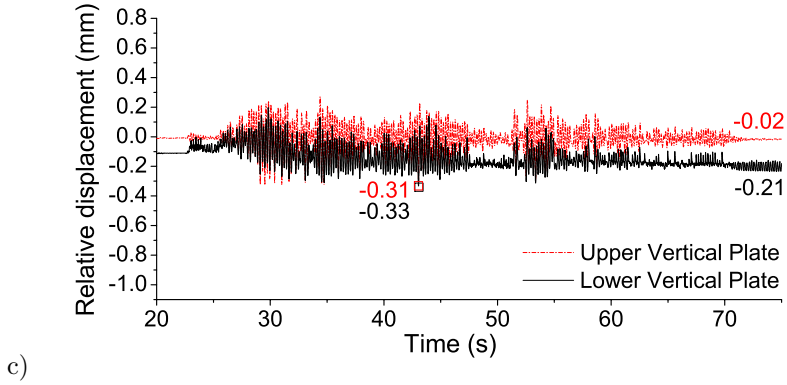

c)

Fig. 3.29: Relative vertical displacements of upper (with Teflon) and lower (without Teflon) vertical shear-key plates of Damper 2 for: a) C50; b) C100; c) C200.

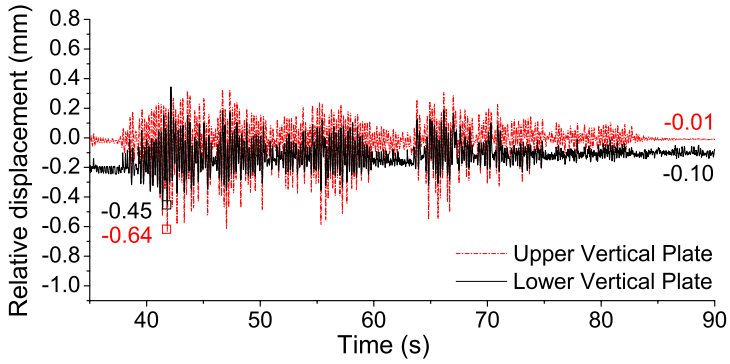

a)

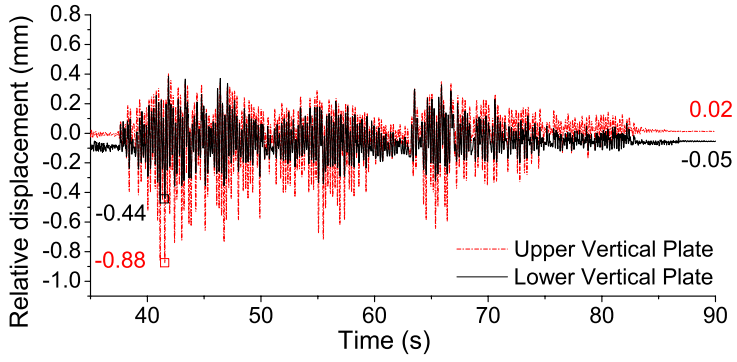

b)

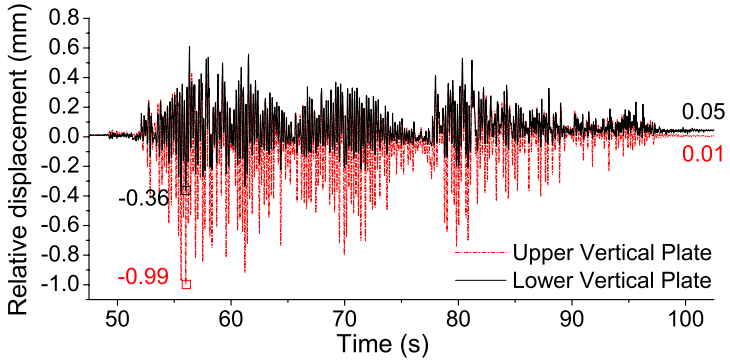

c)

Fig. 3.30: Relative vertical displacements of upper (with Teflon) and lower (without Teflon) vertical shear-key plates of Damper 2 for: a) C300; b) C350; c) C400.

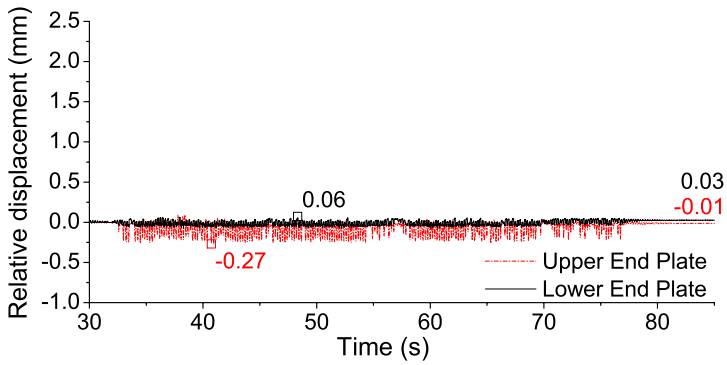

a)

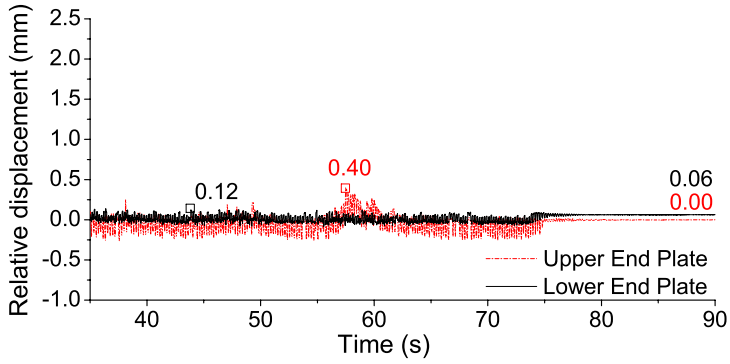

b)

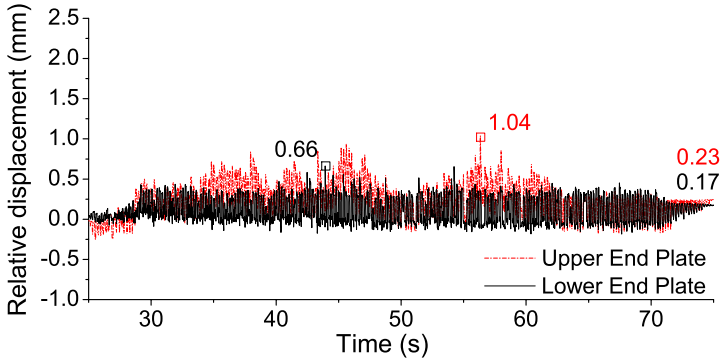

c)

Fig. 3.31: Relative displacement of the end-plates of Damper 2 in the direction of the axis of the damper, for seismic simulations: a) C50; b) C100; c) C200.

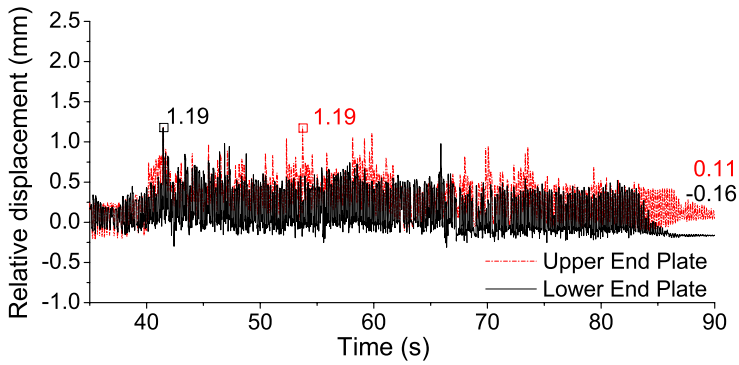

a)

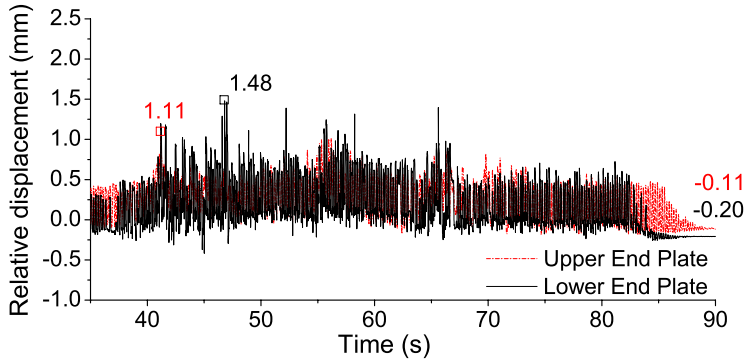

b)

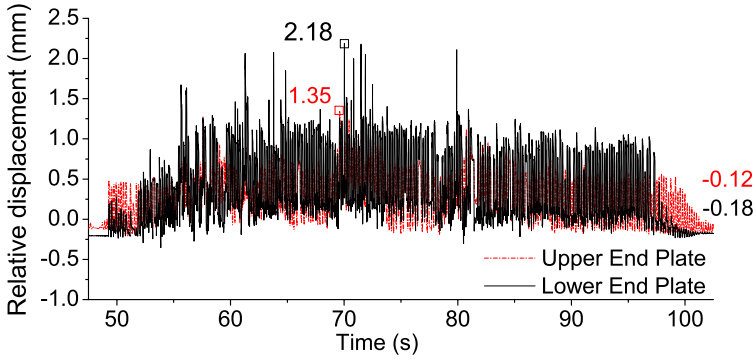

c)

Fig. 3.32: Relative displacement of the end-plates of Damper 2 in the direction of the axis of the damper, for seismic simulations: a) C300; b) C350; c) C400.

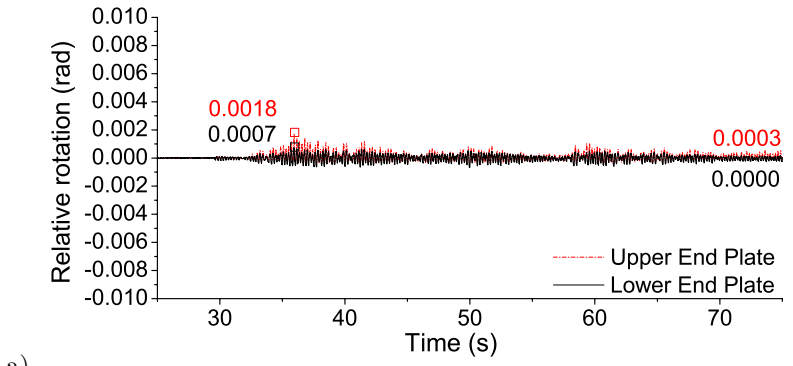

a)

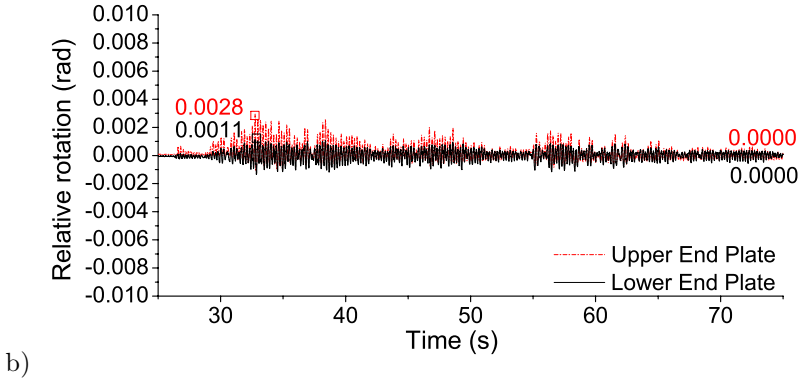

b)

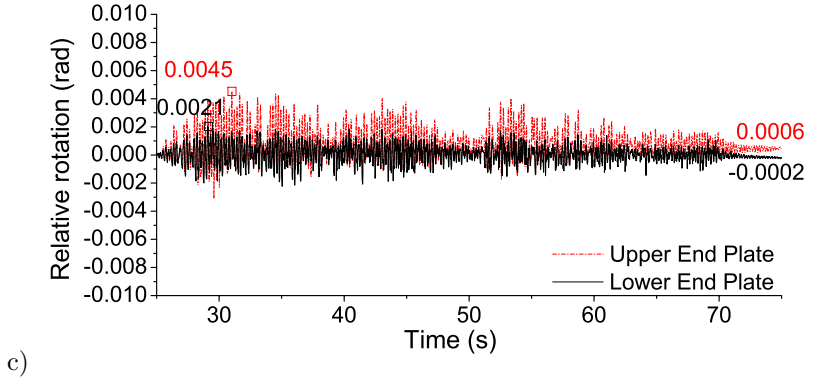

c)

Fig. 3.33: Relative rotation of the end-plates of Damper 2 about an axis perpendicular to the frame for seismic simulations: a) C50; b) C100; c) C200.

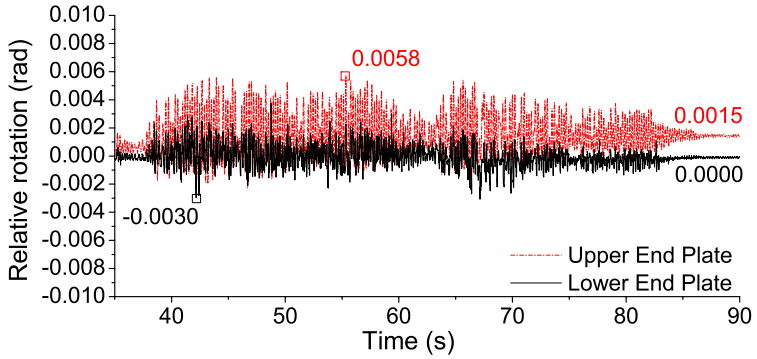

a)

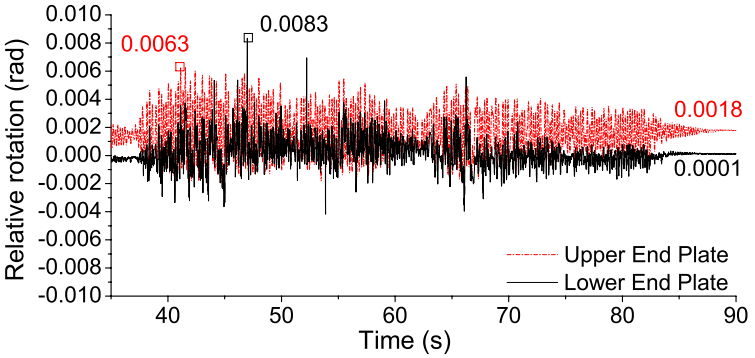

b)

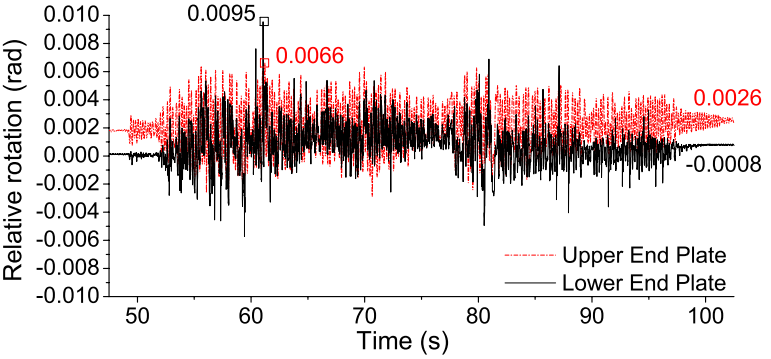

c)

Fig. 3.34: Relative rotation of the end-plates of Damper 2 about an axis perpendicular to the frame for seismic simulations: a) C300; b) C350; c) C400.

4

Seismic upgrading of existing structures by combining the addition of hysteretic dampers with local strengthening procedures (FRP/SRP)

The poor performance exhibited by many (under-designed) existing reinforced concrete frames during recent earthquakes has underlined the need of seismic retrofitting. Innovative technologies such as strengthening with advanced composite materials (i.e. Fiber Reinforced Polymer laminates FRP and Steel Reinforced Polymer spikes SRP), or by adding passive devices (hysteretic dampers) have been used for retrofitting purposes in the past. However, an extensive structural upgrading with (only) FRP/SRP can be cost prohibitive, and installing hysteretic dampers in an existing frame that lacks a

minimum quasi-elastic deformation capacity can jeopardize the efficiency of the energy dissipators, leading to dampers of excessive size and cost. This study proposes a hybrid solution that combines a limited strengthening with FRP/SRP with the addition of hysteretic dampers. This chapter discusses the structural variables involved in the design of this hybrid solution and states the desirable range of their values. On this basis, and using an energy-based approach, a method for seismic retrofitting RC frames with FRP/SRP strengthening and hysteretic dampers is developed.

4.1 Introduction

Nowadays, building codes are moving from prescriptive to objective based, within the framework of the Performance Based Design (PBD). Besides life safety, there are a number of objectives that must be considered in the choice and design of the seismic upgrading: (i) control of damage; (ii) minimum disruption of building use during upgrading; (iii) proper performance of the building after upgrading; and (iv) minimum cost. Control of damage means protecting structural and non-structural components and building contents, to protect investment, or to maintain building function following an earthquake. Damage control is often a major consideration and involves the control of displacements of the (i.e. inter-story drift) to values which can be tolerated by non-structural components, and the reduction of seismic building accelerations

(which might damage special machinery or artifacts). Cost can be reduced by using new structural components that make the new and existing components act compositely, and eliminating the need for foundation upgrading or extensive structural upgrading.

In this context, a hybrid retrofit technique is proposed here that combines the addition of hysteretic dampers with a limited strengthening of the existing frame with FRP/SRP. The level of strengthening with FRP/SRP is the minimum that allows the existing frame and the new hysteretic dampers to act compositely as a "flexible-stiff mixed structure" (FSMS). The FSMS are composed of two parts that work in parallel: the flexible part and the stiff part. The former has low lateral stiffness and is designed to remain basically elastic. The later has high lateral stiffness, low strength, and large energy dissipation capacity through plastic deformations. Past research (Akiyama, 1999) has shown that under seismic actions, the flexible part stabilizes the response of the stiff part and as a result the efficiency of the entire system in terms of energy absorption with respect to maximum deformation is high, and the residual deformation on the structure after the earthquake is very small. In the hybrid retrofit technique proposed here, the existing frame is strengthened to play the role of the "flexible part" in the FSMS, while the new hysteretic dampers constitute the "stiff part". This study presents an energy-based method to design the proposed solution, and points out the main parameters that control the response. Finally, the

proposed solution is validated through numerical simulations in the next Chapter.

4.2 Idealization of the structure

Regular buildings can be modeled as multi-degree-of-freedom (MDOF) systems with lumped masses m_i and equivalent shear springs. The type of building structure dealt with here are RC frames working in parallel with hysteretic dampers installed in each story. This structure is idealized with a lumped mass MDOF system with two elastic-perfectly-plastic shear springs at each story level. One represents the existing (main) frame and the other the hysteretic dampers, as shown in Fig. 4.1.

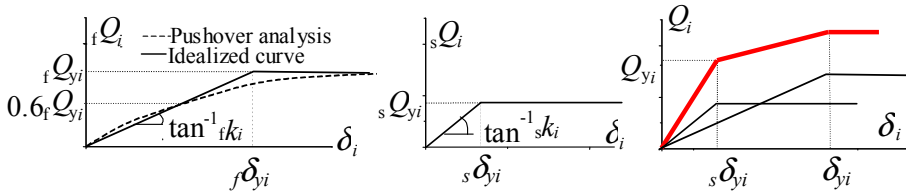

a) Existing (main) structure b) Energy dissipating device c) Dual system

Fig. 4.1: Idealized interstory drift-shear force curve of each story

The lateral load-displacement relationship, ${}_fQ_i$-δ_i, of a given i-th story of the main structure —without dampers— is represented with the curve shown with dot lines in Fig. 4.1.a, and it can approximated with the elastic-perfectly plastic model shown with solid line in Fig. 4.1.a. The first segment of this bilinear model can be taken as a line passing through the origin and the point of the selected ${}_fQ_i$-δ_i curve

for which ${}_fQ_i=0.6{}_fQ_{y,i}$. Here ${}_fQ_{y,i}$ is the yielding shear force of the bare frame and it is taken as the maximum of the ${}_fQ_i$-δ_i curve. The second segment is horizontal at ${}_fQ_i={}_fQ_{y,i}$. The abscissa of the intersection point of these two segments is taken as yielding interstory drift of the bare frame ${}_f\delta_{y,i}$. The elastic stiffness of the bare frame is thus ${}_fk_i={}_fQ_{y,i}/{}_f\delta_{y,i}$. The contribution of the hysteretic dampers to the lateral load-displacement relationship, ${}_sQ_i$-δ_i, in a given i-th story is represented by a spring characterized by the lateral strength ${}_sQ_{yi}$ and stiffness ${}_sk_i$ or yielding interstory drift of the dampers, ${}_s\delta_{y,i}$ $(={}_sQ_{y,i}/{}_sk_i)$, as shown in Fig. 4.1.b. The shear force-interstory drift relationship of the entire structure Q_i-δ_i, is obtained by summing up the forces sustained by each element as shown in Fig. 4.1.c. Accordingly, the lateral yield strength of the entire building-device structure at the i-th story, Q_{yi}, is:

$$Q_{y,i} = {}_sQ_{y,i} + {}_s\delta_{y,i}\,{}_fk_i \tag{4.1}$$

For convenience, hereafter $Q_{y,i}$, ${}_fQ_{y,i}$, ${}_sQ_{yi}$ and ${}_fk_1$ will be expressed in non-dimensional form by:

$$\begin{aligned} \alpha_i &= \frac{Q_{y,i}}{\sum_{k=i}^{N} m_k g}; \qquad {}_f\alpha_i = \frac{{}_fQ_{y,i}}{\sum_{k=i}^{N} m_k g} \\ {}_s\alpha_i &= \frac{{}_sQ_{y,i}}{\sum_{k=i}^{N} m_k g}; \qquad \chi_i = \frac{{}_fk_1}{k_{eq}} \end{aligned} \tag{4.2}$$

where, N is the total number of stories, g is the acceleration of the gravity, and k_{eq} is the stiffness of an equivalent single-degree-of-freedom (SDOF) system of mass $M=\Sigma m_i$ and period equal to the fundamental period of the main structure (without dampers), ${}_fT_1$, i.e. $k_{eq}=4\pi^2 M/{}_fT_1{}^2$.

4.3 Structural variables governing the design

The design of a frame with hysteretic dampers in governed by several parameters defined at each story level i, whose interrelations and most appropriate values have been addressed in different ways in the literature.

4.3.1 Strength ratio

The first variable relates the lateral force developed by the main frame and by the dampers. Akiyama (1999) characterized this relation with the ratio $r_{q,i}$ defined by:

$$r_{q,i} = \frac{{}_f\overline{Q}_{m,i}}{{}_sQ_{y,i}} \tag{4.3}$$

where ${}_f\overline{Q}_{m,i}$ is the mean value of the maximum shear force sustained by the main frame in the positive and negative domains. Inoue & Kuwahara (1998), and Oviedo, Midorikawa & Asari (2010) used a different ratio called β_i, defined by:

$$\beta_i = \frac{{}_sQ_{y,i}}{{}_sQ_{y,i} + {}_fQ_{y,i}} = \frac{{}_s\alpha_i}{{}_s\alpha_i + {}_f\alpha_i} \tag{4.4}$$

The level of knowledge of an existing RC structure (amount of steel, reinforcing details etc.) is often limited, and therefore ${}_fQ_{y,i}$, or the corresponding inter story drift at yield ${}_f\delta_{y,i}$, must be estimated conservatively. On the other hand, the larger the maximum inter story drift allowed $\delta_{m,i}$ is, the smaller is the size (and hence the cost) of the dampers and the forces that they exert on the existing structure. It is also advisable not to exceed ${}_f\delta_{y,i}$ since existing frames designed according to old seismic codes or without any seismic calculation and detailing are very likely to have a small (or null) plastic deformation capacity. In sum, in seismic upgrading existing RC frames with hysteretic dampers it is reasonable to design the dampers so that $\delta_{m,i}={}_f\delta_{y,i}$. If the strength ${}_fQ_{y,i}$ or lateral the deformation capacity ${}_f\delta_{y,i}$ of the existing frame is too small, seismic upgrading the frames only with hysteretic dampers might not be feasible. In this case, ${}_fQ_{y,i}$ and ${}_f\delta_{y,i}$ should be increased before installing the dampers and one solution is to use SRP/FRP. Combining the dampers with some strengthening using SRP/FRP can be also useful to improve/optimize the performance of the overall retrofitted structure and to reduce the size of the dampers. Base on previous discussion, herein the design condition ${}_f\overline{Q}_{m,i} = {}_fQ_{y,i}$ will be adopted and thus:

$$r_{q,i} = \frac{{}_f Q_{y,i}}{{}_s Q_{y,i}} = \frac{{}_f \alpha_i}{{}_s \alpha_i} \tag{4.5}$$

From Eqs. (4.4) and (4.5) it follows that $r_{q,i}$ and β_i are simply related by:

$$\beta_i = \frac{1}{1 + r_{q,i}} \tag{4.6}$$

4.3.2 Yield deformation ratio

The second structural variable relates the yield inter story drift of the dampers installed in the i-th story, ${}_s\delta_{y,i}$ to ${}_f\delta_{y,i}$. Oviedo et al. (2010) defined for this purpose the ratio ν_i given by:

$$\nu_i = \frac{{}_s \delta_{y,i}}{{}_f \delta_{y,i}} \tag{4.7}$$

ν_i must be always less than 1 to guarantee a minimum protection to the main frame. Oviedo et al. (2010) showed that the lower ν_i is, the wider is the range of the strength ratio β_i at which the protection of the main frame with the dampers is maximized and kept almost invariant. Oviedo et al. (2010) recommended:

$$\nu_i \leq 0.4 \tag{4.8}$$

because this makes the structural performance of the entire system less sensitive (i.e. less affected) in case of modifications to the

design caused by uncertainties such as mechanical properties of the existing structure, on-site installation practices of the dampers and/or material strength reliability.

4.3.3 Stiffness ratio

A third structural variable commonly used in the design of frames with hysteretic dampers is the ratio K_i between the lateral elastic stiffness of the dampers, ${}_sk_i$, and the elastic stiffness of the frame, ${}_fk_i$. When $\delta_{m,i}={}_f\delta_{y,i}$, it is simply related to β_i and ν_i by:

$$K_i=\frac{{}_sk_i}{{}_fk_i}=\frac{{}_sQ_{y,i}/{}_s\delta_{y,i}}{{}_fQ_{y,i}/{}_f\delta_{y,i}}=\frac{1}{r_{q,i}\nu_i}=\frac{\beta_i}{\nu_i\left(1-\beta_i\right)} \tag{4.9}$$

Inoue and Kuwahara (1998) proposed an optimum value for β_i, $\beta_{opt,i}$, which maximizes the equivalent viscous damping ratio of the entire structural system (i.e. frame+dampers), that is given by:

$$\beta_{opt,i}=1-\frac{1}{\sqrt{K_i+1}} \tag{4.10}$$

Replacing β_i with $\beta_{opt,i}$ given by Eq. (4.10) in Eq. (4.6) and taking into account Eq. (4.9) gives the following relations applicable when $\beta_i=\beta_{opt,i}$:

$$K_i=\frac{1-2\nu_i}{\nu_i^2} \tag{4.11}$$

$$r_{q,i} = \frac{v_i}{1-2v_i} \tag{4.12}$$

4.3.4 Equivalent number of yield excursions

The plastic strain energy (hysteretic energy), $W_{p,i}$, and the maximum plastic deformation experienced by the hysteretic dampers $(\delta_{m,i}\text{-}\delta_{y,i})$ at a given story i, can be expressed in non-dimensional form by the following ratios:

$$\eta_i = \frac{W_{p,i}}{{}_sQ_{y,i}\,{}_s\delta_{y,i}}; \quad \mu_{m,i} = \frac{\left(\delta_{m,i} - {}_s\delta_{y,i}\right)}{{}_s\delta_{y,i}} \tag{4.13}$$

The quotient $n_{e,i}$ between η_i and $\mu_{m,i}$, i.e. $n_{e,i}=\eta_i/\mu_{m,i}$, is a structural variable of primer importance in the energy-based seismic design methodology. $\eta_i/\mu_{m,i}$ is named "equivalent number of yield excursions" and its estimation has been addressed in different ways in the past (Cosenza & Manfredi, 1997; Manfredi, 2001; Uang & Bertero, 1990). On the basis of numerous nonlinear dynamic response analysis, Akiyama (1999) related $r_{q,i}$ with $\eta_i/\mu_{m,i}$ for flexible-stiff mixed systems:

$$For \quad r_{q,i} < 1: \quad n_{e,i} = \frac{\eta_i}{\mu_{m,i}} = 4\left(1 + r_{q,i}\right) \tag{4.14}\text{a}$$

$$For \quad r_{q,i} \geq 1: \quad n_{e,i} = \frac{\eta_i}{\mu_{m,i}} = 8 \tag{4.14}\text{b}$$

In Eqs. (4.14) the parameter $r_{q,i}$ accounts for the influence on $\eta_i/\mu_{m,i}$ of the presence of an elastic element working in parallel with the elastic-perfectly plastic element. Past research (Akiyama, 1999) has shown that the presence of this elastic element improves notably the response of the mixed structure because: (i) reduces of the maximum displacement for a fixed amount of hysteretic energy $W_{p,i}$ input by the earthquake; and (ii) makes the maximum displacement in the positive and negative domain almost equal, thus minimizing the residual plastic deformation on the structure. The case $r_{q,i}$=0, Eq. (4.14) represents a pure elastic-perfectly plastic system and it can be interpreted from Eq. (4.14) that the existence of the elastic element magnifies $\eta_i/\mu_{m,i}$ by $(1+r_{q,i})$ times with an upper bound limit of 2 times. However, Akiyama's expression does not take into account the influence of seismological parameters and the type of ground motion (i.e. near-fault or far-field) on $\eta_i/\mu_{m,i}$. The later aspects were investigated by Manfredi, Polese, & Cosenza (2003) for an elastic-perfectly plastic SDOF system, who proposed the following expression based on the results of regression analyses performed with 128 near-fault and 122 far-field earthquake records:

$$\frac{\eta}{\mu_m} = 1 + c_1 I_d \sqrt{\frac{T_{NH}}{T}} \left(R-1\right)^{c_2} \tag{4.15}$$

Here T_{NH} is the initial period of medium period region in the Newmark and Hall spectral representation (Newmark & Hall, 1982). R is a parameter that characterizes the plastic response of the

structure given by $R=mS_a/Q_y$, where m is the mass of the SDOF system, S_a is the elastic spectral acceleration and Q_y the yield strength of the SDOF system. Further, I_d is a seismological parameter defined by (Cosenza & Manfredi, 1997):

$$I_d = \frac{\int_0^{t_0} \ddot{z}_g^2 dt}{PGA \cdot PGV} \tag{4.16}$$

where $\ddot{z}_g$ is the ground acceleration, t_o is the duration of the ground motion, and PGA and PGV the peak ground acceleration and velocity, respectively. In Eq. (4.15), Manfredi et al. (2003) proposed to take c_1=0.23, c_2=0.4 for near-fault earthquakes; and c_1=0.18, c_2=0.6 for far-field earthquakes. Manfredi et al.'s equation can be applied to each story of a multi-story frame with hysteretic dampers, by assimilating the later to an equivalent SDOF system with elastic period T equal to the fundamental period of the main frame ${}_fT_1$, mass m equal to the total mass M of the structure, and yield strength Q_y equal to $Q_y={}_sQ_{y1}+{}_fk_1\cdot{}_s\delta_{y1}={}_sQ_{y,1}(1+1/K_1)$, taking into account Eq. (4.9) and the ratios defined in Eq. (4.12) this gives:

$$\frac{\eta}{\mu_m} = 1 + c_1 I_d \sqrt{\frac{T_{NH}}{{}_fT_1}} \left(\frac{S_a}{{}_s\alpha_1 g\left(1+\nu_1 r_{q,1}\right)} - 1 \right)^{c_2} \tag{4.17}$$

As indicated above, Eqs. (4.14) indicate that the presence of an elastic element working in parallel with the elastic perfectly plastic system magnifies $\eta_i/\mu_{m,i}$ by $(1+r_{q,i})$ times, with an upper limit of 2

times. In this study, this magnification derived by Akiyama is adopted to modify Eq. (4.17) in order to include the presence of an elastic element, giving:

$$For\ r_{q,i}<1: n_{e,i}=\frac{\eta_i}{\mu_{m,i}}=\left(1+r_{q,i}\right)\left[1+c_1 I_d\sqrt{\frac{T_{NH}}{{}_fT_1}}\left(\frac{S_a}{{}_s\alpha_1 g\left(1+v_1 r_{q,1}\right)}-1\right)^{c_2}\right] \quad (4.18)\text{a}$$

$$For\ r_{q,i}\geq 1: n_{e,i}=\frac{\eta_i}{\mu_{m,i}}=2\left[1+c_1 I_d\sqrt{\frac{T_{NH}}{{}_fT_1}}\left(\frac{S_a}{{}_s\alpha_1 g\left(1+v_1 r_{q,1}\right)}-1\right)^{c_2}\right] \quad (4.18)\text{b}$$

If the optimum $\beta_{opt,i}$ proposed by Inoue and Kuwahara is used, taking into account Eq. (4.12), ${}_s\alpha_1$ is:

$${}_s\alpha_1=\frac{{}_sQ_{y,1}}{Mg}=\frac{{}_fQ_{y,1}}{Mgr_{q,1}}=\frac{{}_f\alpha_1\left(1-2v_1\right)}{v_1} \quad (4.19)$$

and Eqs. (4.18) can be specialized for $\beta_{opt,i}$ by substituting $r_{q,i}$ given by Eq. (4.12) and using (4.19):

$$For\quad r_{q,i}=\frac{v_i}{1-2v_i}<1:\quad n_{e,i}=\frac{\eta_i}{\mu_{m,i}}=$$
$$=\left(\frac{1-v_i}{1-2v_i}\right)\left[1+c_1 I_d\sqrt{\frac{T_{NH}}{{}_fT_1}}\left(\frac{S_a v_1}{{}_f\alpha_1 g\left(v_1-1\right)^2}-1\right)^{c_2}\right] \quad (4.20)\text{a}$$

$$For \quad r_{q,i} \geq 1: \quad n_{e,i} = \frac{\eta_i}{\mu_{m,i}} = 2\left[1 + c_1 I_d \sqrt{\frac{T_{NH}}{{}_f T_1}} \left(\frac{S_a \nu_1}{{}_f \alpha_1 g \left(\nu_1 - 1\right)^2} - 1 \right)^{c_2}\right] \qquad (4.20)\text{b}$$

Finally, it is worth emphasizing that the term $S_a\nu_1/[{}_f\alpha_1 g(\nu_1-1)^2]$ in Eqs. (4.20) represents the reduction factor R and it must be larger than 1 for the response of the entire structure being on the plastic range. The condition $R>1$ yields then:

$$\frac{S_a \nu_1}{{}_f \alpha_1 g \left(\nu_1 - 1\right)^2} > 1 \rightarrow \nu_1 > \left[\left(\frac{S_a}{2\,{}_f \alpha_1 g} + 1 \right) - \sqrt{\left(\frac{S_a}{2\,{}_f \alpha_1 g} + 1 \right)^2 - 1}\right] \qquad (4.21)$$

4.3.5 Strength distribution among stories

The lateral strength distribution of the entire frame-damper structure, Q_{yi}/Q_{y1}, expressed in terms of the shear-force coefficients defined in Eq. (4.2) will be referred to by $\bar{\alpha}_i$ ($=\alpha_i/\alpha_1$) herein. The criterion adopted in the proposed method to determine $\bar{\alpha}_i$ is to attain an even distribution of damage among the hysteretic dampers, as characterized by the parameter η_i. Past studies (Akiyama, 1985) showed that the strength distribution $\bar{\alpha}_i$ that makes η_i approximately equal in all stories ($\eta_i=\eta$) in a low-to-medium rise multi-story building subjected to seismic loads coincides approximately with the maximum shear-force distribution in an equivalent elastic undamped shear strut with similar lateral stiffness

distribution along its height. The derivation of the "exact" shear-force coefficient distribution $\bar{\alpha}_i$ can be found elsewhere (Benavent-Climent, 2011), and it can be approximated for design purposes by (Benavent-Climent, 2011):

$$\bar{\alpha}_i = \exp\left[\left(1-0.02\frac{{}_f k_1}{{}_f k_N}-0.16\frac{{}_f T_1}{T_G}\right)\bar{x}-\left(0.5-0.05\frac{{}_f k_1}{{}_f k_N}-0.3\frac{{}_f T_1}{T_G}\right)\bar{x}^2\right] \quad (4.22)$$

Here $\bar{x}=(i-1)/N$; ${}_fk_1$ and ${}_fk_N$ and the lateral stiffness of the base and uppermost stories of the main frame; ${}_fT_1$ the fundamental period of the main frame; T_G is the predominant period of the ground motion. Of course, instead of Eq. (4.22), a more refined lateral strength distribution could be derived from dynamic analysis by applying a trial and error iterative method. This would not alter the proposed method at all. However, it implies selecting a set of earthquake records, conducting many non-linear dynamic response analyses, and averaging the distribution derived for each record, which can be a very cumbersome process.

4.4 Energy balance of the structure

As described in Chapter 3 (section 3.5.5.1) the equation of energy balance for an inelastic SDOF system is given by:

$$W_k + W_\xi + W_s = E \quad (4.23)$$

where W_k is the kinetic energy, W_ξ the damping energy, W_s the absorbed energy, and E is (by definition) the (relative) input energy, given by:

$$W_k = \int \dot{y} M \ddot{y} dt; \quad W_\xi = \int C \dot{y}^2 dt; \quad W_s = \int Q_B \dot{y} dt; \quad E = \int -M \ddot{z}_g \dot{y} dt \qquad (4.24)$$

W_s is composed of the recoverable elastic strain energy, W_{se}, and the irrecoverable plastic energy, W_p, i.e. $W_s = W_{se} + W_p$. On the other hand, E can be expressed in the form of an equivalent velocity V_E by:

$$V_E = \sqrt{\frac{2E}{M}} \qquad (4.25)$$

Since $W_k + W_{se}$ is the elastic vibrational energy W_e ($= W_k + W_{se}$), Eq. (4.23) can be rewritten as:

$$W_e + W_p = E - W_\xi \qquad (4.26)$$

Further, $W_e + W_p$ can also be expressed in the form of an equivalent velocity V_D so that:

$$W_e + W_p = \frac{M V_D^2}{2} \qquad (4.27)$$

Frame structures can be modeled as multi-degree-of-freedom (MDOF) systems with lumped masses and equivalent shear springs. As introduced in Chapter 1 (section 1.3.3), Eq. (4.23) holds also for

general MDOF systems if the above expressions for W_k, W_ξ, W_s and E are replaced by:

$$W_k = \int \dot{\mathbf{y}}^{\mathrm{T}} \mathbf{M} \ddot{\mathbf{y}} dt\,;\quad W_\xi = \int \dot{\mathbf{y}}^{\mathrm{T}} \mathbf{C} \dot{\mathbf{y}} dt\,;\quad W_s = \int \dot{\mathbf{y}}^{\mathrm{T}} \mathbf{Q} dt\,;\quad E = -\int \dot{\mathbf{y}}^{\mathrm{T}} \mathbf{M} \mathbf{r} \ddot{z}_g dt \quad (4.28)$$

where $\mathbf{M}$ is the mass matrix, $\mathbf{C}$ the damping matrix, $\mathbf{Q}(t)$ is the restoring force vector, $\dot{\mathbf{y}}(t)$ and $\ddot{\mathbf{y}}(t)$ are the velocity and acceleration vectors relative to the ground, and $\mathbf{r}$ is the displacement vector $\mathbf{y}(t)$ resulting from a unit support displacement. Past studies have shown numerically (Akiyama, 1999) and experimentally (Uang & Bertero, 1990) that in general MDOF damped inelastic systems, the total input energy E —and consequently V_E— coincides approximately with that of an equivalent elastic SDOF system with mass M equal to the total mass of the MDOF system and period T equal to that of the fundamental mode. It has been also shown that E is a very stable quantity scarcely affected by the level of plastic deformations or damping, neither by the hysteretic rules followed by the shear springs. This constitutes the basis of the energy-based approach of seismic design. In this approach, the loading effect of the earthquake is characterized by a V_E -T or a V_D -T spectrum. Various empirical expressions have been proposed that allow us to obtain V_D from V_E (Akiyama, 1985; Benavent-Climent, Pujades, & Lopez-Almansa, 2002; Fajfar & Vidic, 1994; Kuwamura & Galambos, 1989). In addition, attenuation relationships have been established for use in energy-based seismic design (Chou & Uang, 2000) that directly

provide W_s —the absorbed energy— for a given earthquake magnitude, source-to-site distance, site class and ductility factor, in terms of an equivalent velocity V_a defined by

$$V_a = \sqrt{\frac{2W_s}{M}} \tag{4.29}$$

4.5 Design criteria

Strengthening the beams and columns of a frame with SRP/FRP does not modify significantly the lateral stiffness ${}_fk_i$ and the mass m_i of each story, but increases the initial lateral strength ${}_fQ_{yi}{}^o$ (or yielding interstory drift ${}_f\delta_{yi}{}^o={}_fQ_{yi}{}^o/{}_fk_i$). Therefore, ${}_fk_i$, m_i (and thus ${}_fT_1$) can be considered as constant parameters of the existing structure that will not be modified by the proposed seismic upgrading strategy. On this basis, the problem to solve is stated as follows. Given an existing frame which mass m_i, lateral stiffness ${}_fk_i$, initial lateral yield force ${}_fQ_{yi}{}^o$ (or initial lateral yielding interstory drift ${}_f\delta_{yi}{}^o={}_fQ_{yi}{}^o/{}_fk_i$) and fundamental period ${}_fT_1$, determine at each story level i the lateral stiffness ${}_sk_i$ and yielding interstory drift ${}_s\delta_{yi}$ (or yield strength ${}_sQ_{yi}={}_s\delta_{yi}$ ${}_sk_i$) that must be provided by the dampers, and the increment of lateral strength Δ_fQ_{yi} (or lateral yielding interstory drift $\Delta_f\delta_{yi}=\Delta_fQ_{yi}/{}_fk_i$,) to be attained with SRP/FRP, so that the main frame remains elastic, i.e. $\delta_{m,i}\leq({}_f\delta_{yi}{}^o+\Delta_f\delta_{yi})$, under a seismic hazard level characterized by V_D and the seismological parameters I_d, c_1, c_2, T_G, T_{NH}. In other words, since ${}_fk_i$, m_i and ${}_fT_1$ are kept constant, the goal is

determining ${}_sk_i$, ${}_s\delta_{yi}$ and ${}_fQ_{yi}$ (=${}_fQ_{yi}{}^o$+Δ_fQ_{yi}), that define the seismic upgrading solution. The first two parameters, ${}_sk_i$ and ${}_s\delta_{yi}$ can be normalized by ${}_fk_i$ and by the lateral yielding interstory drift of the main frame strengthen with SRP/FRP, ${}_f\delta_{yi}$ (=${}_f\delta_{yi}{}^o$+$\Delta_f\delta_{yi}$) by means of the parameters K_i and ν_i defined with Eqs. (4.9) and (4.7). Further, the lateral yield strength of the frame strengthened with SRP/FRP, ${}_fQ_{yi}$=${}_fQ_{yi}{}^o$+Δ_fQ_{yi}, can be expressed in terms of the shear force coefficient ${}_f\alpha_i$ defined by Eq. (4.2). Therefore, the non-dimensional parameters to be determined are K_i,ν_i and ${}_f\alpha_i$. These parameters are determined in order to attain the following goals: (i) making the damage on the hysteretic dampers, in terms of η_i, approximately equal in all stories; (ii) maximizing the equivalent viscous damping ratio of the entire structural system; and (iii) making the performance of the entire system relatively insensitive to construction uncertainties. To this end, the following design criteria are adopted: (i) the distribution of strength among the stories will follow the law given by Eq. (4.22); (ii) ν_i and K_i must satisfy the relation given by Eq. (4.11); and (iii) ν_i is limited to 0.4 as stated by Eq. (4.8). These design criteria are implemented in the formulation as explained in next section.

4.6 Formulation

The $3N$ unknown non-dimensional parameters ${}_f\alpha_i$, ν_i and K_i, that define the seismic retrofit solution with dampers and SRP/FRP are determined as follows.

4.6.1 Relation between ν_1 and the yield displacement ratios of the rest of stories ν_i ($i \neq 1$)

The condition that the distribution of strength among stories $\bar{\alpha}_s$ must follow the law given by Eq. (4.22) is imposed and this yields (N-1) relations between ν_1 and the yield displacement ratios of the rest of stories ν_i ($i \neq 1$), as explained below.

If the optimum strength $\beta_{opt,i}$ proposed by Inoue & Kuwahara (1998) is adopted, the ν_i of a given story i that makes the distribution of the shear force coefficient among the stories equal to the optimum distribution $\bar{\alpha}_s$ is obtained as follows. The total base yield shear force coefficient α_1 can be expressed in terms of ν_1 as follows:

$$\alpha_1 = \frac{{}_sQ_{y,1} + {}_fk_1\,{}_s\delta_{y,1}}{Mg} = \frac{{}_fQ_{y,1}}{Mg}\left(\frac{1}{r_{q,1}} + \nu_1\right) = {}_f\alpha_1\left(\frac{1}{r_{q,1}} + \nu_1\right) \qquad (4.30)$$

Since the optimum strength ratio $\beta_{opt,i}$ is adopted, $r_{q,i}$ is given by Eq. (4.12) and substituting in Eq. (4.30) gives:

$$\alpha_1 = \frac{{}_f\alpha_1 \left(\nu_1 - 1\right)^2}{\nu_1} \tag{4.31}$$

Also, from Eq. (4.31) and Eq. (4.12) the optimum distribution of the yield shear force coefficient is:

$$\bar{\alpha}_i = \frac{{}_sQ_{y,i} + {}_fk_i\,{}_s\delta_{y,i}}{\alpha_1 \sum_{j=i}^{N} m_j g} = \frac{\left({}_fQ_{y,i}/r_{q,i}\right) + {}_fk_i\nu_i\,{}_f\delta_{y,i}}{\alpha_1 \sum_{j=i}^{N} m_j g} = \frac{{}_f\alpha_i}{\alpha_1}\left(\frac{1}{r_{q,1}} + \nu_1\right) = \frac{{}_f\alpha_i}{\alpha_1}\frac{\left(\nu_i - 1\right)^2}{\nu_i} \tag{4.32}$$

Solving for ν_i in Eq. (4.32) and taking into account that α_1 is given by Eq. (4.31), yields the (N-1) relations between ν_1 and the yield displacement ratios of the rest of stories ν_i ($i \neq 1$):

$$\nu_i = \left(1 + \frac{\bar{\alpha}_i\,{}_f\alpha_1\left(\nu_1 - 1\right)^2}{2\,{}_f\alpha_i\nu_1}\right) - \sqrt{\left(1 + \frac{\bar{\alpha}_i\,{}_f\alpha_1\left(\nu_1 - 1\right)^2}{2\,{}_f\alpha_i\nu_1}\right)^2 - 1} \tag{4.33}$$

4.6.2 Relation between K_i and ν_i

The condition given by Eq. (4.11) is imposed to maximize the equivalent viscous damping ratio of the entire structural system, giving N relations between K_i and ν_i.

4.6.3 Expression for the maximum inter story drift of the *i-th* story

As indicated by Eq. (4.8), the yielding interstory drift of the dampers ${}_s\delta_{y,i}$ is forced to be much smaller than that of the main structure, ${}_f\delta_{y,i}$. If ${}_s\delta_{y,i}$ is very small in comparison to ${}_f\delta_{y,i}$ the elastic strain energy that can be stored by the dampers becomes negligible in comparison to that of the main structure, and consequently the elastic vibrational energy of the whole building, W_e, can be approximated by:

$$W_e = \frac{M g^2 {}_f T_1^2}{4\pi^2} \frac{{}_f \alpha_1^2}{2} \tag{4.34}$$

A detailed derivation of Eq. (4.34) can be found elsewhere (Benavent-Climent, 2011). From Eq. (4.13) and taking into account the coefficients defined in Eq. (4.2), $W_{p,i}$ can be expressed as follows:

$$W_{p,i} = \eta_i {}_s Q_{y,i} {}_s \delta_{y,i} = \eta_i \frac{{}_s Q_{y,i}^2}{{}_s k_i} = \eta_i {}_s \alpha_i^2 \left(\sum_{k=i}^{N} m_k g \right)^2 \frac{1}{{}_s k_i} \tag{4.35}$$

where ${}_s\alpha_i$ can be expressed in terms of K_i, ν_i and ${}_f\alpha_i$ as follows:

$${}_s\alpha_i = \frac{{}_s Q_{y,i}}{\sum_{k=i}^{N} m_k g} = \frac{{}_s k_i {}_s \delta_i}{\sum_{k=i}^{N} m_k g} = \frac{K_i {}_f k_i \nu_i {}_f \delta_i}{\sum_{k=i}^{N} m_k g} = K_i \nu_i {}_f \alpha_i \tag{4.36}$$

Using Eq. (4.35), the total plastic strain energy dissipated by the dampers of the whole structure, W_p, can be expressed in terms of the

plastic strain energy dissipated by the dampers of the first story, W_{p1}, by introducing a new ratio $\gamma_1 = W_p / W_{p1}$ given by:

$$\gamma_1 = \frac{W_p}{W_{p1}} = \frac{\sum_{i=1}^{N}\left[\eta_i \, {}_s\alpha_i^2 \left(\sum_{k=i}^{N} m_k g\right)^2 \Big/ {}_s k_i\right]}{\eta_1 \, {}_s\alpha_1^2 M^2 g^2 \Big/ {}_s k_1} \tag{4.37}$$

Since the strength distribution $\overline{\alpha}_i$ given by Eq. (4.22) is adopted the normalized plastic strain energy η_i can be assumed equal in all stories, i.e. $\eta_i = \eta$. For that purpose, and taking into account Eq. (4.9), Eq. (4.1) is rewritten as follows:

$$Q_{y,i} = {}_sQ_{y,i} + {}_s\delta_{y,i} \, {}_f k_i = {}_sQ_{y,i} + {}_s\delta_{y,i} \frac{{}_s k_i}{K_i} = {}_sQ_{y,i}\left(1 + \frac{1}{K_i}\right) \tag{4.38}$$

Dividing Eq. (4.38) by $\sum_{k=i}^{N} m_k g$ and recalling the ratios defined in Eq. (4.2), gives

$$\alpha_i = {}_s\alpha_i \left(1 + \frac{1}{K_i}\right) \tag{4.39}$$

which, particularized for the first story, yields:

$$\alpha_1 = {}_s\alpha_1 \left(1 + \frac{1}{K_1}\right) \tag{4.40}$$

Dividing Eq. (4.39) by Eq. (4.40), and taking into account that, by definition, $\overline{\alpha}_i = \alpha_i / \alpha_1$ gives:

$$\bar{\alpha}_i = \frac{{}_s\alpha_i K_1 \left(K_i + 1\right)}{{}_s\alpha_1 K_i \left(K_1 + 1\right)} \tag{4.41}$$

From Eq. (4.41):

$$\frac{{}_s\alpha_i}{{}_s\alpha_1} = \bar{\alpha}_i \frac{K_i \left(K_1 + 1\right)}{K_1 \left(K_i + 1\right)} \tag{4.42}$$

Substituting Eq. (4.42) in Eq. (4.37) and operating gives:

$$\gamma_1 = \sum_{i=1}^{N} \left\{ \left[\bar{\alpha}_i \left(\sum\nolimits_{j=i}^{N} \frac{m_j}{M} \right) \frac{\left(K_1 + 1\right)}{\left(K_i + 1\right)} \right]^2 \frac{{}_f k_1 K_i}{{}_f k_i K_1} \right\} \tag{4.43}$$

Thus

$$\begin{aligned} W_p = \gamma_1 W_{p,1} = \gamma_1 {}_s Q_{y,1} {}_s \delta_{y,1} \eta = \frac{\gamma_1 {}_s Q_{y,1}^2 \eta}{{}_s k_1} = \frac{\gamma_1 {}_s \alpha_1^2 M^2 g^2 \eta}{K_1 {}_f k_1} = \\ \frac{\gamma_1 {}_s \alpha_1^2 M^2 g^2 \eta}{K_1 \chi_1 k_{eq}} = \frac{\gamma_1 {}_s \alpha_1^2 M g^2 \eta {}_f T_1^2}{4\pi^2 K_1 \chi_1} \end{aligned} \tag{4.44}$$

Substituting Eqs. (4.34) and (4.44) in Eq. (4.27) gives:

$$\frac{M g^2 {}_f T_1^2}{4\pi^2} \left[\frac{{}_f \alpha_1^2}{2} + \frac{\gamma_1}{K_1 \chi_1} \eta {}_s \alpha_1^2 \right] = \frac{M V_D^2}{2} \tag{4.45}$$

For convenience, a new parameter α_e is introduced that is defined as the base shear-force coefficient that the main structure should have in order to absorb by itself —i.e. without hysteretic dampers— the

total input energy $MV_D^2/2$ supplied by the earthquake. The expression for α_e can be obtained placing ${}_s\alpha_1=0$ in Eq. (4.45) and solving for ${}_f\alpha_1(=\alpha_e)$, which gives:

$$\alpha_e = \frac{2\pi V_D}{g\,{}_f T_1} \tag{4.46}$$

Using Eq. (4.46), Eq. (4.45) is rewritten as follows:

$$\frac{{}_f\alpha_1^2}{2} + \frac{\gamma_1}{K_1\chi_1}\eta\,{}_s\alpha_1^2 = \frac{\alpha_e^2}{2} \tag{4.47}$$

Making ${}_s\alpha_1={}_sQ_1/Mg={}_sk_{1s}\delta_{y1}/Mg=K_{1f}k_1\nu_{1f}\delta_{y1}/Mg=K_1\nu_{1f}Q_{y1}/Mg$ $=K_1\nu_{1\,f}\alpha_1$ in Eq. (4.47) and solving for $\eta(=\eta_i)$:

$$\eta = \left[\frac{\alpha_e^2 - {}_f\alpha_1^2}{\left(K_1\nu_{1\,f}\alpha_1\right)^2}\right]\frac{K_1\chi_1}{2\gamma_1} \tag{4.48}$$

On the other hand, ${}_s\alpha_i$ can be expressed in terms of ${}_s\alpha_1$, solving for ${}_s\alpha_i$ in Eq. (4.41):

$${}_s\alpha_i = \bar{\alpha}_i\,{}_s\alpha_1\frac{K_i\left(K_1+1\right)}{K_1\left(K_i+1\right)} \tag{4.49}$$

Taking into account that $n_{e,i}=\eta/\mu_{m,i}$, $\mu_{m,i}=(\delta_{m,i}-{}_s\delta_{y,i})/{}_s\delta_{y,i}$, ${}_s\delta_{y,i}={}_sQ_{y,i}/{}_sk_i$, using Eqs. (4.19) ,(4.49) and solving for $\delta_{m,i}$ gives the following expression for the maximum inter story drift of the *i-th* story:

$$\delta_{m,i} = \frac{\bar{\alpha}_{i\,f}\,\alpha_1\left(1-2\nu_1\right)\left(K_1+1\right)\sum_{k=i}^{N} m_k g}{\nu_1 K_1\left(K_i+1\right)_f k_i}\left[1+\frac{\left(\alpha_e^2-{}_f\alpha_1^2\right)K_1\chi_1\nu_1^2}{2\gamma_1 n_{e,i\,f}\,\alpha_1^2\left(1-2\nu_1\right)^2}\right] \quad (4.50)$$

and substituting Eq. (4.11) in Eq. (4.50) gives:

$$\delta_{m,i} = \frac{\bar{\alpha}_{i\,f}\,\alpha_1\nu_1\left(\frac{1-2\nu_1}{\nu_1^2}+1\right)\sum_{k=i}^{N} m_k g}{\left(\frac{1-2\nu_i}{\nu_i^2}+1\right)_f k_i}\left[1+\frac{\left(\alpha_e^2-{}_f\alpha_1^2\right)\chi_1}{2\gamma_1 n_{e,i\,f}\,\alpha_1^2\left(1-2\nu_1\right)}\right] \quad (4.51)$$

Since ν_i is a function of ν_1 and ${}_f\alpha_i$, as given by Eq. (4.33), the maximum displacements $\delta_{m,i}$ predicted with Eq. (4.51) depend on the unknown (N+1) parameters ν_1 and ${}_f\alpha_i$.

In addition, it is worth mentioning that the maximum displacements $\delta_{m,i}$ can be predicted for a given FSMS (i.e. with fixed properties ν_1 and ${}_f\alpha_i$) at different performance levels (i.e. characterized with different values of PGA). This entails considering different α_e and $n_{e,i}$ in Eq. (4.51). The first parameter is proportional to V_D as stated by Eq. (4.46). The second parameter can be also related to V_D, by substituting in Eq. (4.20) the value of the spectral acceleration S_a. The spectral acceleration can be computed as $S_a=(2\pi/{}_fT_1)\,V_D$, since it has been shown (Akiyama, 1985; Housner, 1956) that V_D provides a good approximation of the spectral velocity S_v and therefore it can be taken as equal for the purposes of earthquake-resistant design. Thus, the maximum interstory drifts $\delta_{m,i}$ can be predicted for the same FSMS at different performance levels defined with different values of

V_D. Strictly speaking, the prediction holds as long as the flexible part remains elastic because this is the assumption made in the development of the method. However, on the basis of the well known "equal displacement rule", it is reasonable to expect that the prediction will be also satisfactory even when the flexible part undergoes some plastic deformation. Whether this expected response is true or not, will be addressed in the next Chapter 5 through numerical simulations.

4.7 Example of application

For illustrative purposes, a simple example an existing 3-storey frame is considered with the following mass and mechanical properties before any strengthening with SRP/FRP: m_i=*57000kg,* ${}_fT_1$=0.37*s,* ${}_fk_1$=6.2kN/mm; ${}_fk_2$=7.7kN/mm; ${}_fk_3$=9.7kN/mm, ${}_f\alpha_1$=0.055, ${}_f\alpha_2$=0.103, ${}_f\alpha_3$=0.260 (here, i=1, 2 and 3 denote the first –ground-, second and third stories respectively). The corresponding inter-story drifts of the frame at yielding are ${}_f\delta_{y1}$=${}_f\delta_{y2}$=${}_f\delta_{y3}$=15mm. The frame is subjected to two design earthquakes characterized by c_1=0.23, c_2=0.4, T_{NH}=0.65, T_G=0.52, I_d=7.5, and different values of V_D=450 and 1600 mm/s.

For the design earthquake with V_D=450 mm/s, several solutions for incremental values of ν_1 are shown in Table 4.1 and Fig. 4.2. It can be observed that a higher value of ν_1 leads to a more efficient solution characterized by lower values of ${}_s\alpha_i$, ${}_sk_i$ and ${}_sQ_{yi}$. However, it is important to note that the maximum interstory-drift values, $\delta_{m,i}$,

attain a minimum value for a certain ν_1, and tend to increase for greater values of ν_1.

For the design earthquake with V_D=1600 mm/s, the solutions with incremental values of ν_1 are described in Table 4.2 and Fig. 4.3. In this case, the greater value of input energy (V_D=1600 mm/s) produces greater values of the maximum interstory-drift, $\delta_{m,i}$, being not possible to find a solution for ${}_f\delta_{y1}$= ${}_f\delta_{y1}{}^o$=15mm. To clarify this aspect, the relation between δ_{m3} and ν_1, given by Eq. (4.51) and particularized for this design earthquake, is shown in Fig. 4.3

for different values of ${}_f\alpha_1$. If we try to retrofit the frame only with dampers (i.e. if the different values of ${}_f\alpha_i$ are kept constant at ${}_f\alpha_1$=0.055, ${}_f\alpha_2$=0.103, ${}_f\alpha_3$=0.260) it can be seen that there is no solution for ${}_f\alpha_1$=0.055 (that corresponds to ${}_f\delta_{y1}$=15mm) and ${}_f\delta_{y3}$=15mm. This means that the addition of dampers is not sufficient to control the response of the third story and it is necessary to strengthen the main frame with SRP/FRP, that is, to increase ${}_f\alpha_i$. Now, we can try to find a solution by strengthening only the first story, i.e. modifying only ${}_f\alpha_1$ by increasing ${}_f\delta_{y1} = {}_f\alpha_1 Mg / {}_fk_1$. Fig. 4.4 shows the ν_1-δ_{m3} curves for different levels of strengthening: (${}_f\alpha_1$=0.065, ${}_f\alpha_1$=0.074, ${}_f\alpha_1$=0.083, ${}_f\alpha_1$=0.092 and ${}_f\alpha_1$=0.102). It is found that there is set of solutions for ${}_f\alpha_1$=0.083 with ν_1 ranging between 0.031 and 0.047. This means that the response of the third story can be controlled by strengthening the first story of the main frame with

SRP/FRP up to ${}_f\alpha_1$=0.083, and installing dampers with the characteristics described in Table 4.2–Eqs.(4.33),(4.22),(4.11),(4.36), (4.8). It is worth mentioning that the greatest value of ν_1 in the cited range (ν_1=0.047), produces the most efficient solution characterized by lower values of ${}_s\alpha_i$, ${}_sk_i$ and ${}_sQ_{yi}$. As shown in Table 4.2 and Fig. 4.4, solutions with values of ν_1 greater than 0.047 lead to even more efficient solutions for the design of the dampers, but require a greater increase of ${}_f\alpha_1$ (by strengthening of the first story of the main frame with SRP/FRP). Thus, this method enables the designer to select the most economic solution either by optimizing the design of the dampers, or by reducing the level of strengthening with SRP/FRP.

Table 4.1: Possible solutions for incremental values of ν_1 and V_D=450 ($_f\delta_{y1}$=15mm).

Story i	ν_1	$\delta_{m,i}$	$_sk_i$	$_sQ_{yi}$	$_s\alpha_i$,	$n_{e,i}=\eta_i/\mu_{m,i}$	η
		mm	kN/mm	kN			
3	0.151	8.9	297.68	673.56	1.206	1.40	4.12
2	0.085	5.4	876.08	1121.90	1.004	1.27	
1	0.063	4.1	1383.67	1299.43	0.775	1.23	
3	0.161	6.8	254.54	613.91	1.099	2.33	4.20
2	0.092	4.1	744.98	1026.44	0.919	2.09	
1	0.068	3.1	1173.31	1189.74	0.710	2.03	
3	0.171	6.6	219.82	562.25	1.007	2.73	4.28
2	0.098	4.1	640.16	943.94	0.845	2.43	
1	0.073	3.1	1005.50	1094.99	0.653	2.35	
3	0.180	6.6	191.49	517.14	0.926	3.05	4.37
2	0.105	4.1	555.20	872.04	0.781	2.69	
1	0.078	3.1	869.81	1012.45	0.604	2.60	
3	0.189	6.6	168.06	477.37	0.855	3.33	4.45
2	0.111	4.2	485.42	808.80	0.724	2.92	
1	0.083	3.2	758.60	939.91	0.561	2.80	
3	0.198	6.7	148.47	442.05	0.791	3.59	4.54
2	0.117	4.3	427.43	752.75	0.674	3.12	
1	0.088	3.3	666.40	875.64	0.523	2.99	
3	0.207	6.9	131.92	410.45	0.735	3.85	4.63
2	0.124	4.5	378.73	702.73	0.629	3.31	
1	0.093	3.4	589.14	818.32	0.488	3.16	
3	0.216	7.0	117.80	382.01	0.684	4.09	4.73
2	0.130	4.6	337.46	657.79	0.589	3.48	
1	0.098	3.5	523.82	766.87	0.458	3.32	
3	0.225	7.1	105.66	356.26	0.638	4.34	4.82
2	0.136	4.7	302.18	617.22	0.552	3.66	
1	0.103	3.7	468.12	720.43	0.430	3.48	
3	0.233	7.3	95.14	332.84	0.596	4.59	4.92
2	0.142	4.9	271.81	580.38	0.519	3.83	
1	0.108	3.8	420.27	678.31	0.405	3.63	
3	0.242	7.4	85.96	311.43	0.558	4.83	5.03
2	0.148	5.0	245.48	546.80	0.489	3.99	
1	0.113	3.9	378.88	639.93	0.382	3.77	

Table 4.2: Possible solutions for incremental values of ν_1 and V_D=1600.

Story i	${}_f\delta_{yi}$ mm	${}_f\alpha_i$	ν_1	$\delta_{m,i}$ mm	${}_sk_i$ kN/mm	${}_sQ_{yi}$ kN	${}_s\alpha_i$,	$n_{e,i}=\eta_i/\mu_{m,i}$	η
3	15	0.260	0.058	14.9	2542.00	2214.39	3.964	2.09	33.65
2	15	0.103	0.030	8.0	8019.04	3613.62	3.235	2.02	
1	22.5	0.083	0.031	12.4	5903.10	4167.22	2.487	2.02	
3	15	0.260	0.059	14.7	2442.67	2168.00	3.881	2.17	33.70
2	15	0.103	0.031	7.8	7698.19	3538.33	3.167	2.10	
1	22.5	0.083	0.032	12.3	5667.19	4080.38	2.435	2.10	
3	15	0.260	0.068	14.1	1820.69	1853.21	3.318	2.66	34.16
2	15	0.103	0.035	7.6	5694.43	3027.58	2.710	2.56	
1	22.5	0.083	0.037	11.9	4193.72	3491.27	2.083	2.56	
3	15	0.260	0.076	14.3	1407.44	1613.17	2.888	3.02	34.62
2	15	0.103	0.040	7.8	4369.92	2638.45	2.362	2.89	
1	22.5	0.083	0.042	12.3	3219.50	3042.43	1.816	2.89	
3	15	0.260	0.085	14.7	1119.02	1424.03	2.549	3.32	35.09
2	15	0.103	0.045	8.2	3450.22	2332.12	2.087	3.16	
1	22.5	0.083	0.047	12.8	2542.87	2689.09	1.605	3.16	
3	15	0.260	0.085	13.5	1106.08	1415.01	2.533	3.33	31.88
2	15	0.103	0.045	7.5	3409.07	2317.51	2.074	3.17	
1	25	0.092	0.052	14.3	2054.44	2670.77	1.594	3.20	
3	15	0.260	0.093	14.0	914.83	1274.99	2.282	3.58	32.29
2	15	0.103	0.050	7.9	2802.38	2090.96	1.872	3.39	
1	25	0.092	0.057	14.9	1690.74	2409.30	1.438	3.42	
3	15	0.260	0.100	14.4	768.16	1157.45	2.072	3.81	32.71
2	15	0.103	0.054	8.2	2339.29	1900.97	1.702	3.59	
1	25	0.092	0.062	15.5	1412.90	2190.00	1.307	3.63	
3	15	0.260	0.108	14.9	653.25	1057.37	1.893	4.03	33.14
2	15	0.103	0.059	8.6	1978.17	1739.36	1.557	3.78	
1	25	0.092	0.067	16.2	1196.08	2003.43	1.196	3.82	
3	15	0.260	0.107	13.7	668.50	1071.12	1.918	4.00	30.10
2	15	0.103	0.058	7.8	2025.98	1761.56	1.577	3.75	
1	27.5	0.102	0.072	17.6	1023.77	2027.06	1.210	3.82	
3	15	0.260	0.114	14.1	579.65	988.64	1.770	4.20	30.49
2	15	0.103	0.062	8.2	1747.86	1628.49	1.458	3.92	
1	27.5	0.102	0.077	18.3	884.67	1873.29	1.118	4.00	

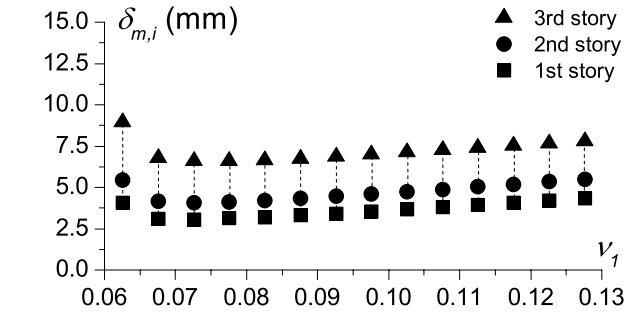

a)

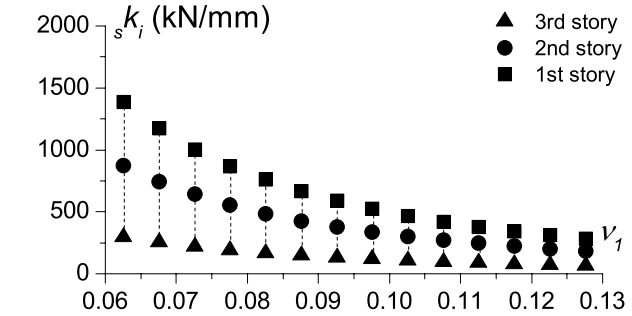

b)

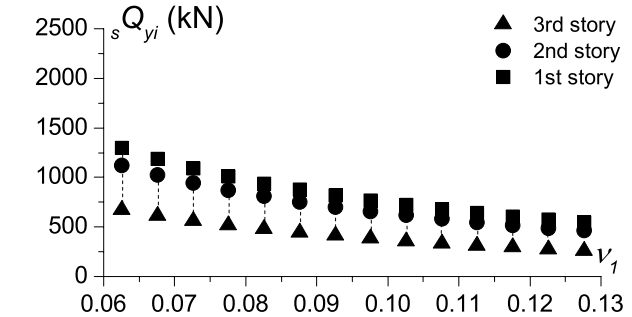

c)

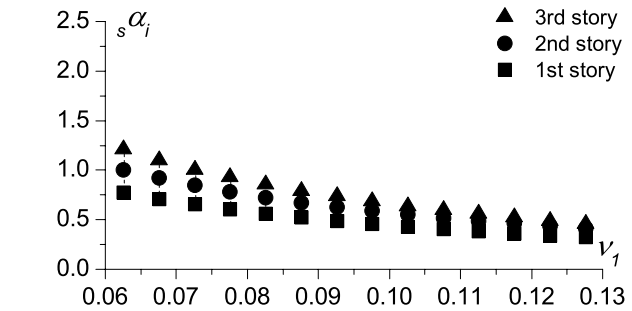

d)

Fig. 4.2: Values of a) $\delta_{m,i}$ b) $_sk_i$ c) $_sQ_{yi}$ and d) $_s\alpha_i$, corresponding to different solutions obtained for incremental values of ν_1 and V_D=450, ($_f\delta_{y1}$=15mm)

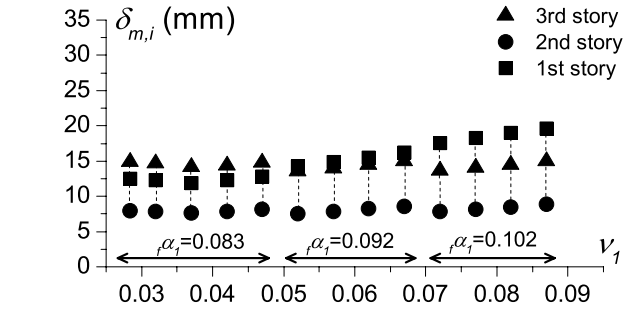

a)

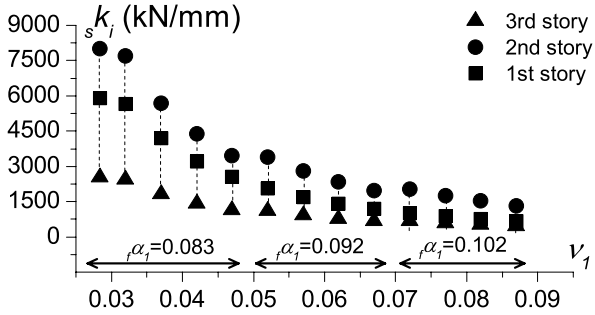

b)

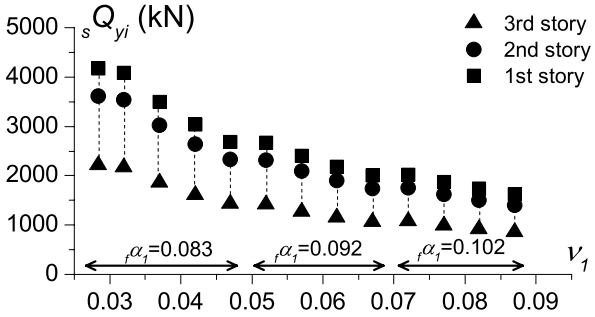

c)

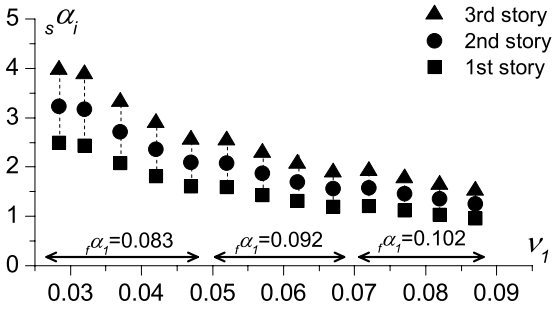

d)

Fig. 4.3: Values of a) $\delta_{m,i}$ b) $_sk_i$ c) $_sQ_{yi}$ and d) $_s\alpha_i$, corresponding to different solutions obtained for incremental values of ν_1 and V_D=1600.

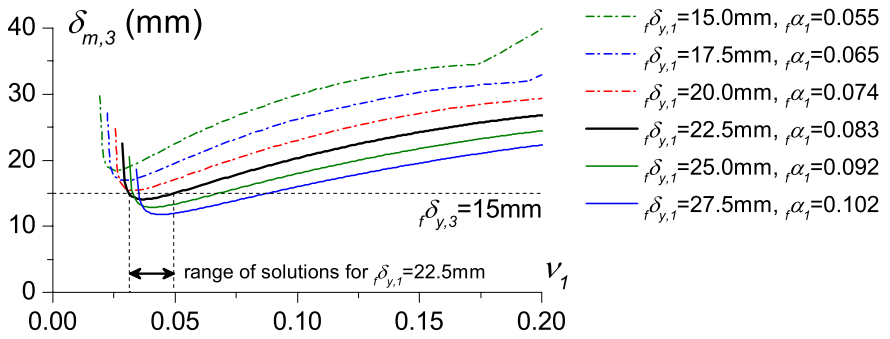

Fig. 4.4: Example of ν_1-$\delta_{m,i}$ curve

4.8 Procedure

In this section, a procedure is proposed to determine the mechanical properties of the hysteretic dampers and the required strengthening of the main frame with SRP/FRP, so that the upgraded structure can sustain a given level of ground motion without exceeding the elastic deformation capacity $_f\delta_{yi}$ of the frame. The proposed procedure is an iterative process that involves the several steps. In the first iteration, the possibility of seismic upgrading the frame without SRP/FRP strengthening is tried. If it is not possible, or if the strength/stiffness of the required dampers is to be reduced/minimized, in following iterations the values of $_f\alpha_i$ are increased with SRP/FRP. The stories to be strengthened and the level of strengthening is decided by the designer, based on architectural or minimum/cost considerations; some hints and recommendations are given later.

Step 1: Characterize the design earthquake in terms of a bilinear V_D-T spectrum defined by the maximum demand V_{Dmax} and the predominant period T_G —i.e. $V_D = T \cdot V_{Dmax} / T_G$ for $T < T_G$, $V_D = V_{Dmax}$ for $T \geq T_G$— and the values of the seismological parameters I_d, T_{NH}, c_1 and c_2.

Step 2: Develop a numerical model of the bare frame (without SRP/FRP strengthening) and conduct an eigenvalue analysis to determine the periods ${}_fT_n$ and corresponding vibration modes $\boldsymbol{\phi}_n$. The model should be able to capture possible flexural and shear modes of failure of the member sections, as well as the shear failure of the beam-column joints. Since SRP/FRP strengthening scarcely modifies the lateral stiffness and mass of the stories, the ${}_fT_n$ and $\boldsymbol{\phi}_n$ obtained are assumed to be also valid if the frame is strengthened with SRP/FRP.

Step 3: Perform a static pushover analysis for each n-mode of the structure applying the lateral load pattern $\mathbf{M}\boldsymbol{\phi}_n s$ until the main frame collapses. Here, $\mathbf{M}$ is the diagonal mass matrix of the structure, $\boldsymbol{\phi}_n$ is the n-th mode shape vector and s a scalar factor. Among the n story shear-interstory drift curves obtained for each story i, ${}_fQ_i$-δ_i, select the curve that reaches the largest δ_i. Approximate this curve with a bilinear elastic-perfectly plastic model as explained in section 4.2 (Fig. 4.1.a), and determine the lateral strength ${}_fQ_{yi}$, yielding interstory drift ${}_f\delta_{yi}$, ultimate interstory drift ${}_f\delta_{ui}$ and lateral stiffness ${}_fk_i$ of the initial frame (i.e. without SRP/FRP strengthening). From these pushover

analyses, the "weak" points of the structure (i.e. sections that exhibit a brittle failure) are identified, and this information can be used later to guide the strengthening strategy with SRP/FRP, if necessary.

Step 4: Calculate ${}_f\alpha_i$, χ_1 with Eq. (4.2), α_e with Eq. (4.46) and $\bar{\alpha}_i$ with Eq. (4.22). Note that in the first iteration ${}_f\alpha_i$ is calculated with ${}_fQ_{yi}={}_fQ_{yi}^o$, but if in subsequent iterations the frame is strengthened with SRP/FRP, the new lateral strength ${}_fQ_{yi}={}_fQ_{yi}^o+\Delta_fQ_{yi}$ must be used in Eq. (4.1).

Step 5: From i=1 to N proceed for each story i as follows:

a) fix a tentative value for ν_1 (<0.4) starting from small values (for example ν_1=0.01)
b) calculate the ν_s of the rest of stories ($s\neq1$) with Eq. (4.33) and check if $\nu_s\leq0.4$ is satisfied; if not, strengthen the main frame with SRP/FRP to increase ${}_f\alpha_1$ and restart the process in Step 4. Note that Eq. (4.33) formally is $\nu_s=a-(a-1)^{0.5}$ where:

$$a=1+\frac{\bar{\alpha}_s\,{}_f\alpha_1\left(\nu_1-1\right)^2}{2\,{}_f\alpha_s\,\nu_1} \tag{4.52}$$

Since ν_s decreases as a increases and noting that $\bar{\alpha}_i$ does not depend on the strength ${}_f\alpha_i$, to increase a for a given ν_1

it is necessary to enhance the strength of the first story of the main frame, ${}_f\alpha_1$.

c) calculate the K_s of each story s (from s=1 to s=N) with Eq.(4.11);

d) calculate γ_1 with Eq. (4.43);

e) calculate the $n_{e,i}$ for the story i under consideration with Eq. (4.20); in this equation, as explained in section 4.6.3, the spectral acceleration S_a can be taken as $S_a=(2\pi/{}_fT_1)\,V_D$, since it has been shown that the V_D is very close to the relative spectral velocity (Akiyama, 1985; Housner, 1956);

f) calculate the maximum inter story drift $\delta_{m,i}$ predicted for the story i with Eq. (4.50).

g) compare $\delta_{m,i}$ with ${}_f\delta_{y,i}$; if $\delta_{m,i}$ is larger than ${}_f\delta_{y,i}$ within an acceptable tolerance (i.e. 5%), increase ν_1 and return to (a). Note that in the first iteration ${}_f\delta_{y,i}= {}_f\delta_{y,i}{}^o$ but in subsequent iterations, if the frame has been strengthened with SRP/FRP ${}_f\delta_{y,i}= {}_f\delta_{y,i}{}^o+\Delta_f\delta_{y,i}$. If $\delta_{m,i}$ starts to increase with increasing values of ν_1, or if it is not possible to find a ν_1 in the range $\nu_1<0.4$ that makes $\delta_{m,i}$ less than ${}_f\delta_{y,i}$, then strengthen the frame with SRP/FRP and restart the process in Step 4.

h) Once the appropriate ν_1 that controls the lateral displacement of the i-th story under consideration is determined, keep it as $\nu_{1,i}=\nu_1$ and proceed with the next

story. The parameter $\nu_{1,i}$ represents the yield displacement ratio required on the dampers of the first story so that the maximum inter story drift at the i-th story meets ${}_f\delta_{y,i}$.

Step 6: Select the maximum of the $\nu_{1,i}$, i.e. $\nu_{1,max}=\max\{\nu_{1,i}\}$, which gives the required yield displacement ratio for the dampers of the first story. The required yield displacement ratio for the dampers of the rest of stories, ν_s ($s\neq1$), is calculated with Eq. (4.33). The required shear force coefficients ${}_s\alpha_i$ of the dampers to be installed in each story i is obtained with Eqs. (4.19) and (4.49), and the required stiffness ${}_sk_i$ from Eq. (4.11) taking into account that $K_i={}_sk_i/{}_fk_i$. The required yield strength, ${}_sQ_{y,i}$, and normalized energy dissipation capacity, η ($=\eta_i$), of the dampers is determined with Eqs. (4.2) and (4.48), respectively. This gives a strengthening level with SRP/FRP characterized by ${}_f\delta_{y,i}={}_f\delta_{y,i}{}^o+\Delta\,{}_f\delta_{y,i}$, and a possible solution for the dampers characterized by: ${}_s\alpha_i$, ${}_sk_i$ and η. This solution is not necessarily the only one possible for a given level of strengthening with SRP/FRP. In fact, in general it is possible to find different solutions for the dampers (i.e. different sets of values ${}_s\alpha_i$, ${}_sk_i$ and η) for a given ${}_f\delta_{y,i}$. To find a new solution for the dampers keeping invariable the level of strengthening with SRP/FRP, go back to step 5.a (with the same ${}_f\delta_{y,i}$) and repeat the process with a ν_1 slightly larger than $\nu_{1,max}$ (e.g. increments of 0.005 are reasonable). This will provide a new set of values (${}_s\alpha_i$, ${}_sk_i$ and η) that are also a solution of the problem. This process of increasing ν_1 will stop when $\nu_1=0.4$ is

reached or when the algorithm fails to find a solution. Then, for a given level of strengthening with SRP/FRP, the designer can choose among different sets of possible solutions for the dampers ($_s\alpha_i$, $_sk_i$ and η). One possible criterion for selecting the "optimum" solution is to take the one that provides the minimum value of the total base shear force coefficient, i.e. the minimum $_s\alpha_1 + _f\alpha_1$.

Once $_sk_i$, $_sQ_{yi}$ and $\eta_i = \eta$ are determined, the appropriate type, number and distribution of hysteretic dampers within each story is chosen by the designer. In choosing the type of damper, it is necessary to check that the normalized ultimate energy dissipation capacity of the damper η_{ui} is larger than the demand η_i ($=\eta$). The estimation of η_{ui} for a given type of hysteretic damper is beyond the scope of this paper; yet a procedure is proposed by Benavent-Climent et al. (2011). As for the number and distribution of dampers within a story, attention must be paid to the concentrated forces that they transfer to the existing frame, and to the need for strengthening the connection region.

4.8.1 Strengthening with SRP/FRP and Performance Based Design

The required level of FRP/SRP can be determined for different performance levels and earthquake scenarios (near-fault and far-field).

First, dampers are designed according to the procedure described above for a return period, T_R, equal to 475years.

Second, the solution of dampers and strengthening level obtained for the return period T_R=475years is checked for other return periods. To this end, the energy input spectra in terms of V_D, V_D-T, and the seismological parameters described in Step 1 of the procedure are determined for return periods T_R=95 and 2475years. In the case of Spain, the most recent seismic hazard map published in 2012 (Instituto Geográfico Nacional, 2012) provides the peak ground acceleration, PGA, for return periods of 95, 475, 975 and 2475years; and the absolute spectral acceleration, SA, for several points of the spectrum (i.e. 0.1, 0.2, 0.5, 1 and 2s) and return period 475years. Next, the maximum displacement $\delta_{m,i}$ for each return period is predicted by using Eq. (4.51) (it implies substituting the value corresponding of V_D in Eqs. (4.20) and (4.46) to calculate S_a, $n_{e,i}$ and α_e). It is worth noting that the design method proposed in previous sections assumes that the main frame remains elastic. This assumption is satisfied for the seismic hazard level corresponding to T_R=95 and 475years. However, for economic reasons, it can be reasonable to allow some (minor or moderate) plastic deformations on the main frame for more severe levels (i.e. T_R=975 and 2475years). Even then, although the assumption of the proposed method is not fulfilled, we suggest that the method is still applicable as long as the level of plastic deformations on the main frame is not excessive. This

suggestion is based on the well known “equal displacement rule”. The appropriateness of this suggestion will be validated later through numerical simulations.

The required performance of the structure for the seismic hazard levels characterized by T_R=95 and T_R=2475years is as follows: $\delta_{mi} <$ 0.5% for return period 95years and $\delta_{mi} < {}_f\delta_{ui}$ for return period 2475years. If these performance criteria are not satisfied, the strengthening level with SRP/FRP and the dimensioning of the dampers are recalculated.

5

Numerical validation of the proposed upgrading solution with FRP/SRP and hysteretic dampers

The validity of the method proposed in Chapter 4 is assessed through numerical simulations conducted on a six-story frame subjected to ground motions of different types (far-field and near-fault earthquakes). It is shown that the frames upgraded according to the proposed method exhibit the expected performance.

5.1 Design of the prototype building

A six-story prototype RC frame structure was designed that represents typical pre-70 residential buildings placed in the moderate-

seismicity southern part of Spain. The plan configuration and elevation are shown in Fig. 5.1. The (main) frames are denoted as PI and PII in the figure, and their beams support the joists that form the one way slab. The main frames are connected by transverse beams. In accordance with the regulations in force in Spain at that time (the 70's), the prototype was designed taking into account only gravity loads and without any seismic detailing. The size and reinforcing of the RC members was determined with a former Spanish Standard for RC structures, EH-91 (1991). Following the Spanish Standard NBE AE-88 (1988), the values corresponding to gravity loads are described in Table 5.1. The material properties were representative of the period considered: the concrete strength was f_c=17.5 MPa and the steel reinforcement yield-strength f_y=400MPa. The story height was equal in all stories (310 cm) except in the first story (350 cm). The resulting dimensions of beams and columns are summarized in Table 5.2. Beams and columns are identified in Fig. 5.1.

Table 5.1: Gravity loads

Permanent Actions		Variable Actions	
One-way joist slab	4 kN/m^2	Interior partitions	1 kN/m^2
Flooring	0.8 kN/m^2	Residential use	2 kN/m^2
Tile roofing system (over slab)	3 kN/m^2	Snow load	0.43 kN/m^2
Masonry cavity wall system	7 kN/m		

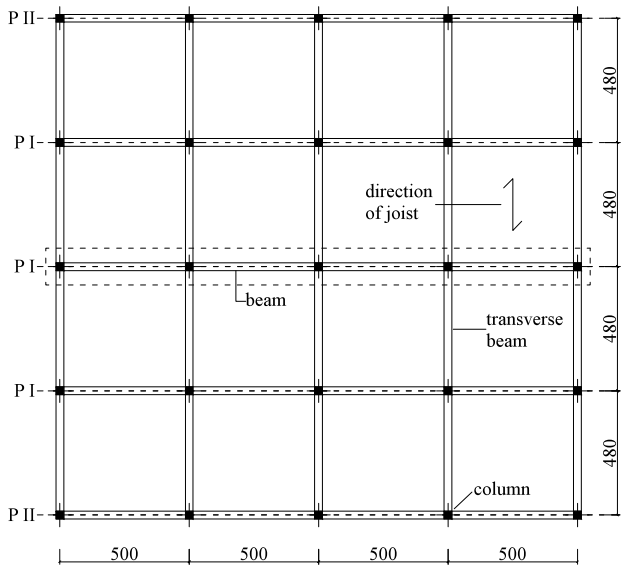

a)

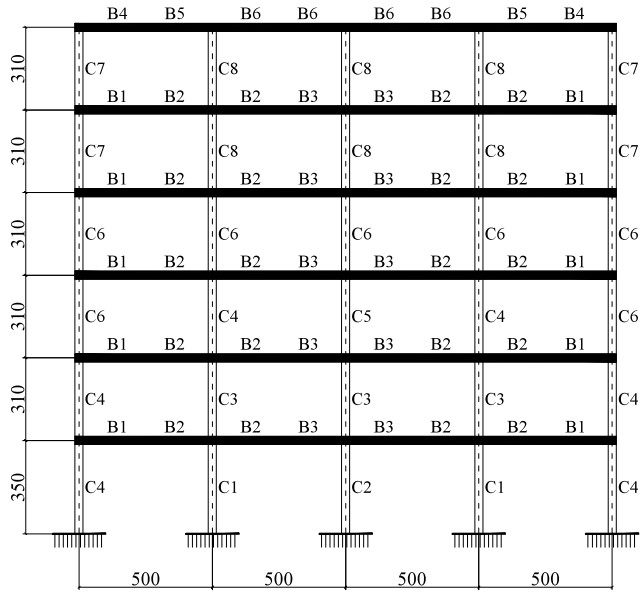

b)

Fig. 5.1: Prototype building: plan (a) and elevation (b). Dimensions in cm.

Table 5.2: Characteristics of the prototype building

Section	b	h	s_h	*Longitudinal*				*Transversal*
	cm	cm	cm	*Bars*	*Area* (cm^2)			*Bars*
C1	40	40	30	12ø20	37.70			2+1cø8
C2	40	40	20	16ø16	32.16			2+1cø8
C3	40	40	15	20ø12	22.60			2+1cø8
C4	40	40	30	4ø20	12.56			1cø8
C5	40	40	20	4ø16	8.04			1cø8
C6	30	30	15	16ø12	18.08			2+1cø8
C7	30	30	20	4ø16	8.04			1cø8
C8	30	30	15	4ø12	4.52			1cø8
				Bottom	*Area*	*Top*	*Area*	
B1	30	40	5	2ø12+2ø12	4.52	2ø12+5ø16	12.32	1cø6
B2	30	40	5	2ø12+2ø12	4.52	2ø12+7ø16	16.34	1cø6
B3	30	40	5	2ø12+2ø12	4.52	2ø12+6ø16	14.33	1cø6
B4	30	40	10	2ø12+4ø20	14.83	2ø20	6.28	1cø6
B5	30	40	5	2ø12+2ø20	8.55	2ø20+4ø20	18.85	1cø6
B6	30	40	5	2ø16+2ø20	10.30	2ø12+4ø20	14.83	1cø6

5.2 Numerical model

From the prototype building, the central frame indicated with dot lines in Fig. 5.1 (left) was selected. The beams of this frame P1 support the gravity loads transferred by the joists that form the one-way slab. This section describes in detail the numerical model developed to obtain nonlinear dynamic response of frame P1 under seismic loadings. Two types of numerical models are commonly used to study the seismic response of RC frame structures: fiber models and plastic hinge models. Fiber models (Spacone, Filippou, & Taucer, 1996) are the most general and fundamental models, capable of reproducing the axial-flexural coupling response under variable axial

load. This is a useful capability since the increase of axial load in columns, due to the overturning moment, can be considerable when adding brace-type dampers. In addition, the generality of fiber models is useful for us to study the effect of the proposed retrofitting solutions, such as the addition of SRP wire stripes and the confinement with FRP. In contrast, axial-flexural coupling in beams is not so relevant and plastic hinge models (lumped-plasticity models) are a computational efficient and simple approach. In addition, they can capture strength and stiffness deterioration (up to collapse) when defined with experimental calibrated parameters, such as the effects of the deterioration of the reinforcing bars due to buckling and low-cycle fatigue. Thus, in this study, a plastic hinge approach is defined for beams while a force-based element with nonlinear fiber sections at the ends is defined for columns. The platform OpenSEES (McKenna, Fenves, Scott, & Jeremic, 2000) is employed to carry out the analyses. A sketch of the frame modeled is shown in Figs. 5.2 and 5.3. Beams are modeled with elastic beam elements (elastic part) and plastic hinges (nonlinear springs) at the both ends (inelastic part), connected in series. The nonlinear springs of the beam elements are defined as part of the two-dimensional joint model developed by Altoontash (2004) and implemented as *Joint2D* in OpenSEES. This model incorporates an additional rotational spring to reproduce the shear behavior of the joint to which beams and columns are connected. Columns are modeled with force-based column elements that incorporate the plastic hinge length concept (Scott & Fenves,

2006). Thus, the springs of the model that correspond to the end of the columns (shown in Fig. 5.8 of the original model) remain unused.

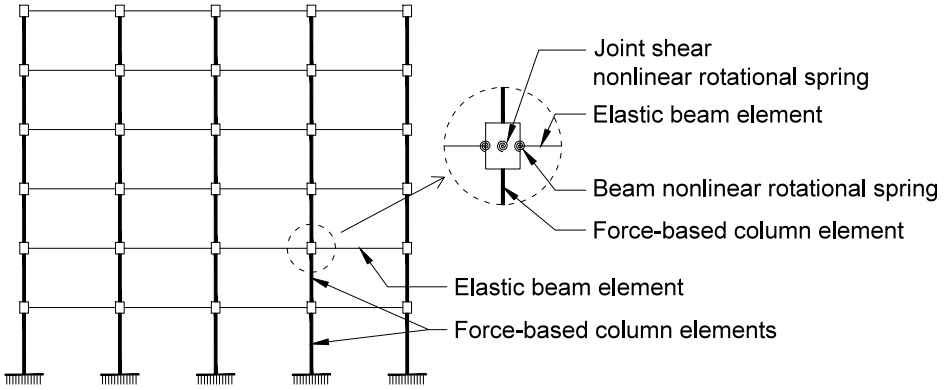

Fig. 5.2: Numerical model that represents the existing frame

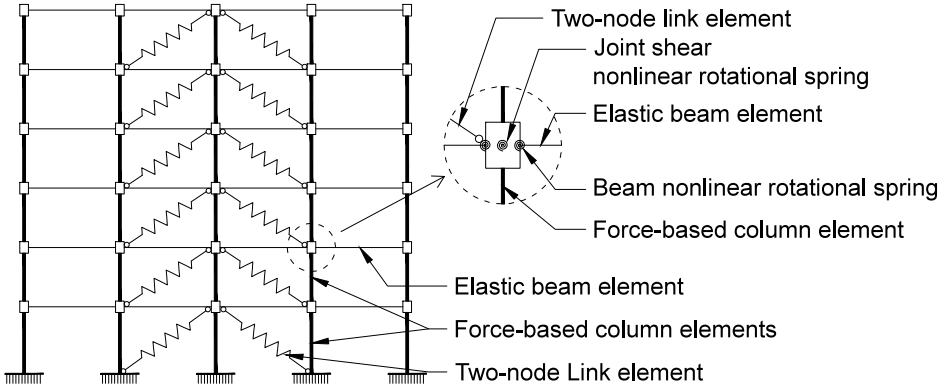

Fig. 5.3: Numerical model that represents the retrofitted existing frame

5.2.1.1 Characterization of the effective stiffness of the beam/column elements

For both columns and beams, the interior part of the element is considered elastic. For that purpose, an effective or reduced stiffness, EI_{eff}, for the members is used in order to take into account the concrete cracking. EI_{eff} is calculated with Eq. (5.1) proposed by Panagiotakos & Fardis (2001):

$$EI_{eff} = \frac{M_y L_s}{3\theta_y} \tag{5.1}$$

Here, M_y is the yield moment, $L_s = M/V$ is the shear span and θ_y is the chord rotation at member yielding. In the case of beams asymmetrically reinforced, the average value of EI_{eff} over the two ends and the two senses of bending was considered as the rigidity of the member (Fardis, 2009). The expressions for θ_y and M_y are Eqs. (5.5) and (5.12), respectively, and they are described in detail in section 5.2.1.3.

5.2.1.2 Force-based beam column elements for columns

Force-based beam column elements present several advantages over the displacement-based elements (Neuenhofer & Filippou, 1997). The force-based beam column elements used in this study employ an integration method that incorporates the plastic hinge length concept,

L_{pl}, and is based on modified Gauss-Radau quadrature (for details, see figure 5 in Scott & Fenves, 2006). This approach consists of applying the two-point Gauss-Radau integration rule over a length equal to $4L_{pl}$ at the element ends and two-point Gauss integration over the element interior (six element integration points). As a result, plastic curvature can be clearly related to plastic rotations through the specification of a physically meaningful plastic hinge length. The authors (Scott & Fenves, 2006) recommended the use of force-based beam-column elements, along with the described integration method, for the nonlinear analysis of frame structures suffering softening and degradation, even under cyclic loads.

The plastic hinge length, L_{pl}, was calculated with the following empirical expression proposed by Fardis (2009), for cyclic loading:

$$L_{pl} = 0.2h\left(1+\frac{3}{8}\min\left(9;\frac{L_s}{h}\right)\right) \tag{5.2}$$

where $L_s=M/V$ is the shear span and h is the depth of the column cross section.

Nonlinear fiber sections were defined at the element ends while the element interior was considered to be elastic, with an effective stiffness equal to EI_{eff}, as defined above. The constitutive models for the nonlinear fiber section corresponding to the original main frame without strengthening were: (a) the modified Kent-Scott-Park for

concrete with degraded linear unloading/reloading stiffness and no tensile strength (Karsan & Jirsa, 1969; Kent & Park, 1971; Scott, Park, & Priestley, 1982; Taucer, Spacone, & Filippou, 1991) and (b) the Giuffré-Menegotto-Pinto for steel with isotropic hardening (Filippou, Popov, & Bertero, 1983). In addition, an elastic uniaxial material was defined to take into account the area of SRP, bounded with a MinMax material (McKenna et al., 2000) to determine the threshold values for failure (as explained in sub-section 5.3.2, no compression strength and maximum deformation in tension equal to the design strain of the FRP wrapping reinforcement ε_{fd}). Finally, the confinement effect was considered by modifying the properties of the concrete material, as explained in sub-section 5.3.2.

5.2.1.3 Characterization of the beams

For beams, elastic frame elements with nonlinear springs at both ends connected in series were defined. This arrangement allows defining an empirical moment-rotation relation for the nonlinear springs, since the variation of axial load is not relevant for beams. As for the rotational stiffness of the compound member, K_{mem}, it was computed as an equivalent combination the sub-elements in series (Ibarra & Krawinkler, 2005):

$$K_{mem} = \frac{K_{ns} K_{bc}}{K_{ns} + K_{bc}} \tag{5.3}$$

where K_{ns} is the stiffness of the nonlinear springs, and K_{bc} is the stiffness of the elastic beam-column element. To avoid the numerical problems that arise when assigning an infinite initial stiffness to one of the sub-elements (either the plastic springs or the beam-column element), the elastic stiffness of the plastic hinges is set n times larger than the beam-column element stiffness, $K_{ns}=nK_{bc}$ (Ibarra & Krawinkler, 2005). The option of assigning a larger stiffness to the nonlinear springs instead of to the elastic beam element permits minimizing spurious damping effects, as explained in the following section. In this study, the value $n=10$ is taken, and the stiffness of the sub-elements is given by:

$$K_{bc}=\frac{n+1}{n}K_{mem};\quad K_{ns}=\left(n+1\right)K_{mem} \tag{5.4}$$

Thus, the elastic stiffness of the plastic hinge considered is large, $11K_{mem}$, while the elastic stiffness of the beam column element is $1.1K_{mem}$ (Haselton et al., 2008).

Accordingly, the properties of nonlinear springs need to be adjusted to reproduce the empirical moment-rotation behavior of the member. These modifications are explained in detail in (Ibarra & Krawinkler, 2005).

The response of the member-end non-linear springs is characterized by a trilinear monotonic backbone curve and hysteretic rules that govern the cyclic behavior under arbitrary loads. In this

study, the constitutive model proposed by (Ibarra, Medina, & Krawinkler, 2005) is used to define the moment-rotation of the member-end hinges. A remarkable capability of this model is the negative branch of the post-peak response, that allows modeling the strain-softening behavior due to concrete crushing, rebar buckling and bond failure.

The trilinear monotonic backbone curve is shown in Fig. 5.4 and it is determined by five parameters: (1) the yield chord rotation, θ_y; (2) the yield moment, M_y; (3) the chord rotation at the onset of strength loss (capping), θ_{cap}; (4) the hardening stiffness, K_s; (5) and the post-capping stiffness, K_c. Additional parameters, which depend on the ones already cited, are described in the figure: the capping moment, M_c; the plastic capping rotation, θ_{cap}^{pl}; the ultimate plastic rotation, θ_u; the ultimate plastic rotation from yield to point of 20% strength loss, θ_u^{pl}; and the initial stiffness, K_e. In the case of the beams with asymmetric reinforcement averaged values for K_e, K_s and K_c are considered over the two senses of bending (Fardis, 2009), while M_y and θ_{cap}^{pl}, were defined separately (i.e. asymmetrically) for each domain of loading.

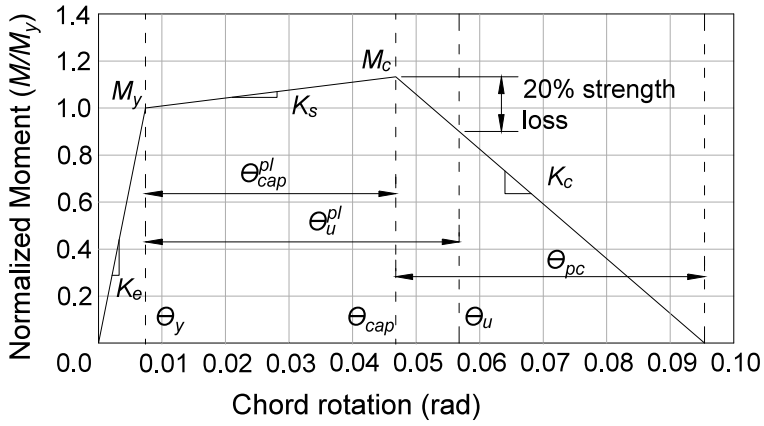

Fig. 5.4: Monotonic backbone curve used for characterizing the non-linear springs

θ_y, M_y and θ_u were calculated with the equations developed by Fardis (2009) and Panagiotakos & Fardis (2001). These equations were calibrated on the base of a large database of experimental tests on RC columns with and without FRP.

θ_y is given by the following expression:

$$\theta_y = \varphi_y \frac{L_s + a_v z}{3} + 0.0014\left(1 + 1.5\frac{h}{L_s}\right) + a_{sl}\frac{\varphi_y d_{bL} f_y}{8\sqrt{f_c}} \qquad (5.5)$$

where φ_y is the "theoretical" yield curvature multiplied by the correction factor 1.025; $L_s = M/V$, as defined before, is the shear span; $z = d - d_1$ is the length of the internal lever arm, being d the section effective depth and d_1, the distance of the center of the compression reinforcement from the extreme compression fiber; h is the depth of member cross section; d_{bL} is the mean tension bar diameter; f_y is the yield strength of tension reinforcement (in MPa); f_c is the compressive

strength of unconfined concrete based on standard cylinder test (in MPa); a_{sl} is a zero-one variable, being $a_{sl} = 1$ if slippage of longitudinal bars is considered and $a_{sl} = 0$ if not; a_v is a zero-one variable, being $a_v = 0$ if $V_{Rc} > V_{My} = M_y/L_s$ and $a_v = 1$ if $V_{Rc} \leq V_{My} = M_y/L_s$.

The shear force at diagonal cracking of the member, V_{Rc}, is calculated as equal to the shear resistance of members without shear reinforcement, given by Fardis (2009):

$$V_{R,c} = \left\{ \max\left[180\left(100\rho_1\right)^{1/3}, 35\sqrt{1+\sqrt{\frac{0.2}{d}}} f_c^{1/6} \right] \left(1+\sqrt{\frac{0.2}{d}} \right) f_c^{1/3} + 0.15\frac{N}{A_c} \right\} b_w d \tag{5.6}$$

where ρ_1 is the ratio of tension reinforcement area, N is the axial load taken positive for compression (but if N is tensile, then $V_{R,c} = 0$), A_c is the area of the cross section; b_w is the width of the web. If b_w and d are in m, f_c is in MPa and, N is in kN, then $V_{R,c}$ is in kN.

The "theoretical" yield curvature (Fardis, 2009), φ_y, is calculated as the minimum of the curvature at yielding of the tension steel, φ_{y1}, and the apparent yielding curvature, φ_{y2} (which appears in members with high axial load due to the sharp nonlinear behavior of the concrete in compression before the steel reinforcement yields):

$$\varphi_{y1} = \frac{f_{yL}}{E_s\left(1-\xi_y\right)d} \tag{5.7}$$

where f_{yL} is the yield stress of the longitudinal reinforcement, E_s is the elastic modulus of steel, ξ_y is the neutral axis depth at yielding normalized to d and defined as:

$$\xi_y = \left(\zeta^2 A^2 + 2\zeta B\right)^{1/2} - \zeta A \tag{5.8}$$

with $\zeta = E_s/E_c$, the ratio steel-to-concrete elastic moduli, and the parameters A and B calculated as follows:

$$A = \rho_1 + \rho_2 + \rho_v + \frac{N}{bdf_y};\quad B = \rho_1 + \rho_2\frac{d_1}{d} + \frac{\rho_v\left(1+\frac{d_1}{d}\right)}{2} + \frac{N}{bdf_y} \tag{5.9}$$

Here, ρ_1, ρ_2 and ρ_v are the ratios of tension, compression and "web" reinforcement area to bd, respectively and b is the width of the compression zone.

The apparent yielding curvature is calculated as:

$$\varphi_{y2} = \frac{1.8f_c}{E_c\xi_y d} \tag{5.10}$$

where ξ_y is calculated with Eq. (5.8) but the parameters A and B are calculated with different expressions:

$$A=\rho_1+\rho_2+\rho_v-\frac{N}{1.8\zeta bdf_c};\quad B=\rho_1+\rho_2\frac{d_1}{d}+\frac{\rho_v\left(1+\frac{d_1}{d}\right)}{2} \tag{5.11}$$

The yield moment, *My*, is given by (Fardis, 2009):

$$\frac{M_y}{bd^3}=\varphi_y\left\{E_c\frac{\xi_y^2}{2}\left(\frac{1+\frac{d_1}{d}}{2}-\frac{\xi_y}{3}\right)+\frac{E_s\left(1-\frac{d_1}{d}\right)}{2}\left[\left(1-\xi_y\right)\rho_1+\left(\xi_y-\frac{d_1}{d}\right)\rho_2+\frac{\rho_v}{6}\left(1-\frac{d_1}{d}\right)\right]\right\} \tag{5.12}$$

The ultimate chord rotation, θ_u, is calculated with the following empirical expression (Fardis, 2009):

$$\theta_u=\theta_y+\theta_u^{pl}=\theta_y+a_{st}^{pl}\left(1-0.52a_{cy}\right)\left(1+\frac{a_{sl}}{1.6}\right)\left(1-0.44a_{w,r}\right)\left(1-\frac{a_{w,nr}}{4}\right)\left(0.25\right)^{v}\left(\frac{\max\left(0.01;\omega_2\right)}{\max\left(0.01;\omega_1\right)}\right)^{0.3}f_c^{0.2}\left[\min\left(9;\frac{L_s}{h}\right)\right]^{0.35}25^{\left(\frac{a\rho_s f_{yw}}{f_c}\right)}1.275^{100\rho_d} \tag{5.13}$$

where a_{st}^{pl} is a coefficient for steel type, being $a_{st}^{pl}=0.0185$ for hot-rolled steel; a_{cy} is a zero-one variable for the type of loading, equal to $a_{cy}=0$ for monotonic loading and to $a_{cy}=1$ for cyclic loading; $a_{w,r}$ and $a_{w,nr}$ are zero-one variables for rectangular walls, being $a_{w,r}=0$

and $a_{w,nr}=0$ for other members; $v=N/bhf_c$ is the axial load ratio, with the axial force N positive for compression; $\omega_1=\left(\rho_1+\rho_v\right)f_{yL}/f_c$ is the mechanical ratio of tension and "web" longitudinal reinforcement; $\omega_2=\left(\rho_2\right)f_{yL}/f_c$ is the mechanical ratio of compression longitudinal reinforcement, with f_{yL} being the yield stress of the longitudinal bars; $a=a_n a_s$ is the effectiveness factor for confinement with $a_s=\left(1-\frac{s}{2b_{xo}}\right)\left(1-\frac{s}{2b_{yo}}\right)$ and $a_n=1-\frac{\sum b_i^2/6}{b_{xo}b_{yo}}$, being b_{xo} and b_{yo} equal to the centerline dimensions of the confining tie and b_i equal to the length between points laterally restrained by a cross-tie hook, for further details see figures in (Fardis, 2009); $\rho_s=A_{sh}/b_w s_h$ is the ratio of transverse reinforcement area, A_{sh}, parallel to the loading direction, with b_w being the width of the "web"; f_{yw} is the yield stress of transverse steel and; ρ_d is the steel ratio of diagonal reinforcement in each diagonal direction.

Since members considered lack seismic detailing (e.g., not closed stirrups), the plastic chord rotation of Eq. (5.13) is corrected through the following modification (Biskinis, 2007):

$$\theta_{u,old}=\theta_y+\theta^{pl}_{u,Eq.5.13}/1.2 \tag{5.14}$$

Finally, θ^{pl}_u is determined immediately as $\theta^{pl}_u=\theta^{pl}_{u,Eq.5.13}/1.2$.

The values of M_y, θ_y and $\theta_u=\theta_{u,old}$ obtained for the 6-story frame under study are shown in Fig. 5.5 and Fig. 5.6. Although they were used only for beams, we computed also these values for columns, to use them as a reference for comparison purposes.

	196.0 86.0	116.2 247.3		139.3 197.1	139.3 197.1		139.3 197.1	139.3 197.1		116.2 247.3	196.0 86.0	
54.3			46.5			46.5			46.5			54.3
	62.4 163.7	62.3 214.2		62.3 214.2	62.4 189.1		62.4 189.1	62.3 214.2		62.3 214.2	62.4 163.7	
69.6			67.1			67.1			67.1			69.6
	62.4 163.7	62.3 214.2		62.3 214.2	62.4 189.1		62.4 189.1	62.3 214.2		62.3 214.2	62.4 163.7	
103.5			103.8			103.8			103.8			103.5
	62.4 163.7	62.3 214.2		62.3 214.2	62.4 189.1		62.4 189.1	62.3 214.2		62.3 214.2	62.4 163.7	
103.7			201.1			172.0			201.1			103.7
	62.4 163.7	62.3 214.2		62.3 214.2	62.4 189.1		62.4 189.1	62.3 214.2		62.3 214.2	62.4 163.7	
188.3			227.9			227.9			227.9			188.3
	62.4 163.7	62.3 214.2		62.3 214.2	62.4 189.1		62.4 189.1	62.3 214.2		62.3 214.2	62.4 163.7	
205.4			279.6			259.8			279.6			205.4

Fig. 5.5: Values of M_y obtained for the 6-story main frame (kN m)

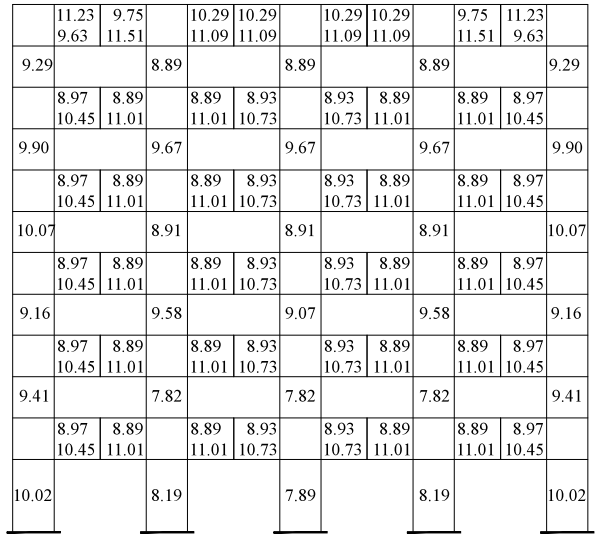

a)

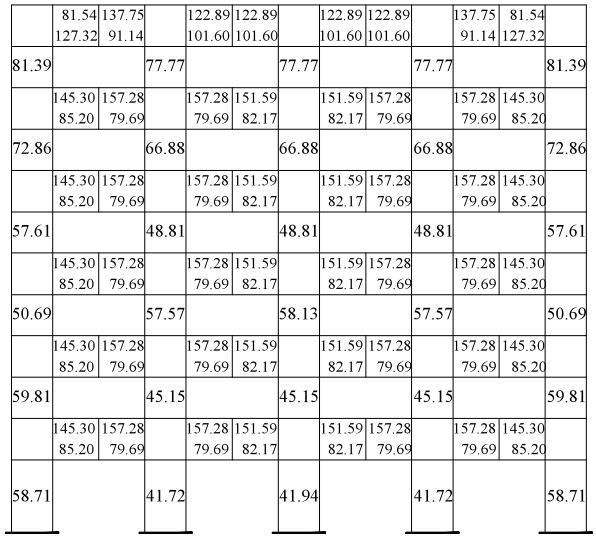

b)

Fig. 5.6: Values of θ_y and $\theta_u=\theta_{u,old}$ (10^{-3} rad) obtained for the 6-story main frame

As for the rotation at onset of strength loss (capping), it is defined as $\theta_{cap} = \theta_y / \theta_{cap}^{pl}$, where θ_{cap}^{pl} is calculated from the ultimate rotation (θ_u^{pl}) provided by Fardis (2009), taking into account that θ_u^{pl} is associated with a strength drop of 20%. Accordingly:

$$\theta_{cap}^{pl} = \theta_u^{pl} - 0.2 M_y / |K_c| \tag{5.15}$$

The hardening stiffness, K_s, is determined by assuming the simplified equation $K_s = M_c / M_y = 1.13$ recommended by Liel & Deierlein (2008).

The post-capping stiffness, K_c, is related to the post-capping rotation capacity θ_{pc} with the following expression (Liel & Deierlein, 2008):

$$K_c = -K_e \left(\theta_y / \theta_{pc}\right)\left(M_c / M_y\right) \tag{5.16}$$

The post-capping rotation capacity is determined from the following empirical equation:

$$\theta_{pc} = \left(0.76\right)\left(0.031\right)^{\nu}\left(0.02 + 40\rho_w\right)^{1.02} \leq 0.10 \tag{5.17}$$

with ρ_w is the area ratio of transverse reinforcement and ν is the axial load ratio.

Regarding the hysteretic rules, the model proposed by Ibarra et al. (2005) considers four modes of cyclic deterioration that are shown

in Fig. 5.7: (i) strength deterioration of the inelastic strain-hardening branch, (ii) strength deterioration of the post-peak strain-softening branch, (iii) accelerated reloading stiffness deterioration, and (iv) unloading stiffness deterioration. In the original proposal of Ibarra et al. (2005), these modes of cyclic deterioration are characterized by four pairs of parameters. However, for the sake of simplicity and following the approach of Liel & Deierlein (2008), these four pairs of parameters have been reduced to two parameters: (1) the normalized energy dissipation capacity, λ and (2) an exponent term to describe the variation of cyclic deterioration with the accumulation of damage, c. As in (Liel & Deierlein, 2008), c=1 was considered. The normalized energy dissipation capacity was calculated as:

$$\lambda = \left(170.7\right)\left(0.27\right)^{v}\left(0.10\right)^{s_h/d} \tag{5.18}$$

where s_h is the spacing of transverse reinforcement.

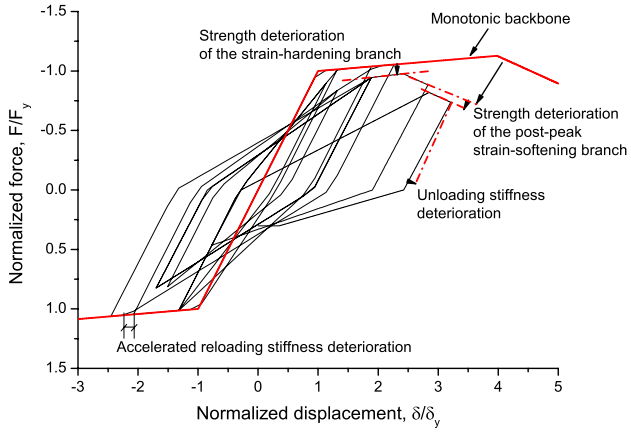

Fig. 5.7: SDOF response of the peak oriented model described with cyclic deterioration (Ibarra & Krawinkler, 2005).

5.2.1.4 Rayleigh damping

A time invariant Rayleigh matrix is used to represent the inherent damping of the structure. This matrix has two parts: the stiffness-proportional part and the mass-proportional part.

$$\mathbf{C} = \beta\mathbf{K} + \gamma\mathbf{M} \tag{5.19}$$

where $\mathbf{C}$ is the viscous damping matrix, $\mathbf{M}$ is the mass matrix, $\mathbf{K}$ is the initial stiffness matrix, β is the stiffness proportional factor and γ is the mass proportional factor.

If Rayleigh damping based on initial stiffness matrix is considered, unrealistic damping forces may appear at the inelastic hinges when yielding takes place (Zareian & Krawinkler, 2006; Zareian & Medina, 2010), causing abrupt velocity changes (Bernal, 1994). To avoid these spurious damping effects, the method proposed by Ibarra & Krawinkler (2005) and Zareian & Medina (2010) is used. This method consists basically on assigning zero stiffness-proportional damping to the plastic hinges (i.e. nonlinear springs), and thus building the damping matrix only with the elastic part of the members (i.e. elastic beam-column elements). A detailed description of the method and its practical application can be found in (Ibarra & Krawinkler, 2005; Medina & Krawinkler, 2004; Zareian & Medina, 2010).

Since no stiffness proportional damping is assigned to the nonlinear springs, the stiffness proportional damping term of elastic

elements, β, needs to be increased to compensate the lack of stiffness proportional damping corresponding to the nonlinear springs. For n=10, factor β must be multiplied by 1.1 (Ibarra & Krawinkler, 2005), as given by the following expression (Zareian & Medina, 2010):

$$\beta' = \frac{1+n}{n}\beta \tag{5.20}$$

Finally, the damping ratio considered is 5% and damping coefficients γ and β were computed by using the frequencies corresponding to the first and third mode.

5.2.1.5 Shear failure detected by postprocessing analysis results

Column shear failure was not directly reproduced in the model due to the difficulties to simulate it accurately (Elwood, 2004; Liel, Haselton, & Deierlein, 2011). For the sake of simplicity, results obtained from numerical analysis were postprocessed to detect shear failure. To this end, two verifications were carried out: (1) "brittle" failure mode, which takes place if shear failure precedes flexural yielding, and (2) "ductile shear" failure, which only occurs under cyclic loading, due to the degradation of shear strength after initial flexure yielding (Fardis, 2009).

The first failure mode, $V_{max} > V_{R,brittle}$, (1) was checked according to section 6.2.3. of Eurocode 2-Part 1 (EN 1992-1-1:2004, 2004). The "ductile shear" failure mode, $V_{max} > V_{R,ductile}$, was checked according to

A.3.3.1 of Eurocode 8-Part 3 (EN 1998-3:2005, 2005), and the cyclic shear resistance, $V_{R,ductile}$, (Fardis, 2009) is defined as (in MN and meters):

$$V_{R,ductile} = \frac{h-x}{2L_s}\min\left(N;0.55A_c f_c\right)+\left(1-0.05\min\left(5;\mu_\theta^{pl}\right)\right) \left[0.16\max\left(0.5;100\rho_{tot}\right)\left(1-0.16\min\left(5;\frac{L_s}{h}\right)\right)\sqrt{f_c}A_c+V_{Rs}\right] \quad (5.21)$$

where h, N, A_c, f_c, L_s were defined in previous section; ρ_{tot} is the total ratio of longitudinal steel and $x=\xi_y\, d$ is the neutral axis depth at flexural yielding with ξ_y from Eq. (5.8). Here, the shear resistance V_{Rs} is the contribution of transverse reinforcement to shear resistance for cross-sections with rectangular web $V_{Rs} = \rho_w\, b_w\, z\, f_{yw}$; ρ_w is the transverse reinforcement ratio, b_w is the width of the cross-section web, z is the length of the internal lever arm and f_{yw} is the yield stress of the transverse reinforcement. Finally, μ_θ^{pl} is the ratio of the plastic part of the chord rotation at ductile shear failure to the yield chord rotation, θ_y, from Eq. (5.5). It is worth mentioning that instantaneous values of N and μ_θ^{pl} were used to check the shear resistance of each member at each step of the analysis, as recommended by Fardis (2009).

5.2.1.6 Characterization of the nonlinear springs that represent the joint shear panel

Predicting the behavior of existing non-ductile RC frames under seismic loads requires special attention to the simulation of beam-column joints. Joint shear damage can contribute significantly to strength and stiffness deterioration in the absence of enough confinement and transverse reinforcement (Liel & Deierlein, 2008). In this study, the behavior of the joint shear panel is simulated with the two-dimensional joint model developed by Altoontash (2004), which simplified the model proposed by Lowes & Altoontash (2003). As explained before, the former model was implemented by its developers as *Joint2D* in OpenSees (McKenna et al., 2000). As shown in Fig. 5.8, the model consists of four zero-length rotational springs to reproduce the member-end rotations and an additional rotational spring to simulate the shear deformation of the joint panel.

The moment-rotation relationship of the joint panel was defined from the experimental relation of joint shear stress, τ_{jh}, and strain, γ_j, using the procedure proposed by Celik & Ellingwood (2008). The rotation of the joint panel rotational spring, θ_j, is considered equal to the joint shear strain γ_j.

The moment transferred through the rotational spring, M_j, was determined from the joint shear stress, τ_{jh}, by using the equations described in (Celik & Ellingwood, 2008) for the *Joint2D* model.

$$M_j = \tau_{jh} A_{jh} \frac{\eta}{\lambda}; \quad \eta = 1 - \frac{h_j}{L_c} - \frac{b_j}{L_b}; \quad \lambda = \frac{1 - b_j / L_b}{jd} - \frac{a}{L_c} \tag{5.22}$$

where a=1 for intermediate interior and exterior joints and a=2 for top interior and exterior joints, A_{jh} is the effective joint area calculated using Sec. 21.7.4 of ACI 318-11 (2011), jd is the internal moment arm of the joint, h_j is the height of the joint panel, b_j is the width of the joint panel, L_b is the total length of the left and the right beams and L_c is the total length of the top and bottom columns.

In the present study, a simplified approach of the shear-stress response of the joint, τ_{jh}–γ_j, is used by defining a linear elastic constitutive model. This model remains on the conservative side, since it does not take into account the energy dissipation capacity of the joints. The elastic stiffness was calculated as the quotient of the moment corresponding to the joint shear cracking, $\left(\overline{\tau}_{jh}\right)_{cr}$, and a lower bound value of the experimental data defined in (Celik & Ellingwood, 2008): 0.0001.

The joint shear cracking, $\left(\overline{\tau}_{jh}\right)_{cr}$, was defined with the following equation (Uzumeri, 1977), normalized in $\sqrt{psi}$ units as $\overline{\tau}_{jh} = \frac{\tau_{jh}}{\sqrt{f_c}}$:

$$\left(\overline{\tau}_{jh}\right)_{cr} = 3.5\sqrt{1 + 0.002\left(N / A_{jh}\right)} \tag{5.23}$$

with N/A_{jh} in psi. In addition, results were postprocessed in order to verify that the joint shear strength demand did not surpass the shear strength, $V_{R,ACI}$, prescribed in ACI 318-11 (2011) as follows: (a) $1.7\sqrt{f_c}A_{jh}$ for joints confined on all four faces (interior joints in the studied 2D frame) and (b) $1.2\sqrt{f_c}A_{jh}$ for joints confined on three faces (exterior joints in the studied 2D frame). It is worth mentioning that the maximum strength considered is regarded as an upper bound value, since it is defined for joints with a minimum amount of transverse reinforcement in the joint, as defined in ACI 318-11 (2011). However, this is not always the case of existing buildings. Significant efforts have been carried out to define a constitutive model for the panel zone that overcomes the limitation of the modified-compression field theory (MCFT) for joints with no transverse shear reinforcement (Lowes & Altoontash, 2003), though some of them are based on a limited set of experimental data (Celik & Ellingwood, 2008). However, they still need calibration and/or are rather complex (Mitra & Lowes, 2007). Thus, a complex simulation of the joint shear response is considered out of the scope of this study, and the linear elastic constitutive model is defined as a safe-side approach in terms of energy response.

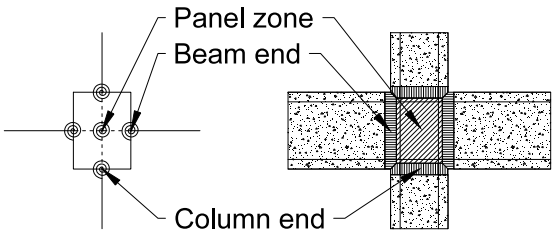

Fig. 5.8: The joint zones represented by rotational springs (Altoontash, 2004).

5.2.1.7 Modelization of the hysteretic dampers

The hysteretic damper is simulated in OpenSEES by using a two-node link element. In the local x-axis direction, a Giuffré-Menegotto-Pinto model with isotropic strain hardening is defined (Filippou et al., 1983), which is able to reproduce reasonably well the experimental results obtained by Benavent-Climent et. al (2011) for the hysteretic damper named WPD and developed by these authors. Fig. 5.9 compares the axial load-displacement curve obtained experimentally for the WPD, and the prediction provided by Giuffré-Menegotto-Pinto model calibrated with the following values of the parameters that control the strain hardening (b), the transition from elastic to plastic branches (R_o, ${}_cR_1$, ${}_cR_2$), and the isoptropic hardening (a_1, a_2, a_3, a_4): b=0.015, R_o=20, ${}_cR_1$=0.87, ${}_cR_2$=0.15, a_1=0.06, a_2=0.9, a_3=0.06, a_4=0.9).

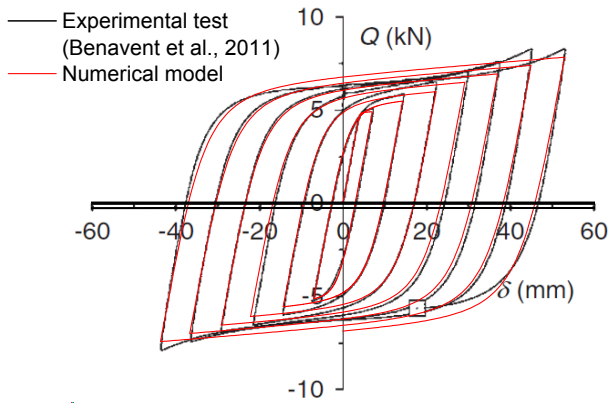

Fig. 5.9: Modelization of the hysteretic damper WPD.

5.2.1.8 Mass properties and gravitational loads

The inertial effects of the design seismic action was evaluated by taking all gravity loads appearing in the combinations of actions established by 3.2.4 of EN 1998-1:2004 (2004). Accordingly, the total mass considered in each story for calculating the hysteretic dampers and performing the dynamic response was obtained summing the dead loads and 0.3 times the life loads, giving 363835 kg for the roof, 375968 kg for the fifth and fourth floors, 380120 kg for the third floor, 387039 kg for the second floor and 391848 kg for the first floor. These masses included the corresponding mass of the columns at each floor. In the dynamic response analysis, the gravity loads were applied in the first step. Since there are five frames parallel to the direction of seismic loading, for the purpose of dynamic analyses, one fifth of the total masses indicated above are associated with each frame. The gravity loads used for second order effects and as initial axial forces in columns corresponded to the tributary area.

5.3 Design of the dampers and required level of strengthening with FRP/SRP

The prototype building is intended to be seismic upgraded in the direction of the main frames by installing hysteretic dampers in two spans of each frame and of each story, and strengthening the beams and/or columns with FRP/SRP. A similar upgrading would be required in the direction perpendicular to the main frames. As mentioned above, for the sake of simplicity, it is considered that the seismic loading in the direction of the main frames is distributed evenly among the five frames. Following is a description of how the proposed procedure was applied to the central main frame, to design the hysteretic dampers and the required FRP/SRP strengthening. The inherent damping ratio assumed for the structure is ξ=0.01. This low value of damping is sustained by the studies of Martinelli & Filippou (2009).

Step 1: The following three seismic hazard levels were defined to design the seismic upgrading solution for the existing structure:

- Frequent earthquake, associated to T_R=95years and characterized by V_D=42.65cm/s
- Design earthquake, associated to T_R=475years and characterized by V_D=98.10cm/s

- Design earthquake, associated to T_R=2475years and characterized by V_D=187.67cm/s

The values of V_D described above were calculated as follows. The new seismic hazard map of Spain (Instituto Geográfico Nacional, 2012) provides the PGA for four return periods: 95, 475, 975 and 2475years (for the site of Granada, they are 0.1g, 0.23g, 0.28g and 0.44g, respectively). From these PGA, the total input energy spectra in terms of equivalent velocity V_E-T was obtained as proposed by Benavent-Climent et al. (2002). It is worth mentioning that the V_E-T spectrum proposed by Benavent et al. was constructed by using 108 ground motion records obtained from 48 earthquakes in Spain, including near-fault and far-field signals. Finally, V_D was estimated from V_E by using the expression proposed by Akiyama (1999) that depends on the inherent damping ratio ξ. In this calculations, ξ=0.01 was adopted for the structure, and according to Akiyama's formulae, this gives V_D/V_E=0.87.

As for the other seismological parameters that characterize also the seismic hazard in the proposed method (i.e. I_d, T_{NH}, c_1 and c_2) two scenarios are considered: (a) a near-fault design earthquake with I_d=3, T_{NH}=0.51; c_1=0.23 and c_2=0.4; and (b) a far-field design earthquake with I_d=9, T_{NH}=0.33s; c_1=0.18 and c_2=0.6. These values of I_d and T_{NH} correspond approximately with the averaged values over the two sets of ground motion records used for the nonlinear time history analyses, as detailed below.

Step 2: The numerical model developed in section 7.2 was used, and the eigenvalue analysis provided the fundamental period ${}_fT_1$ and vibration modes $\boldsymbol{\phi}_n$ shown in Table 5.3.

Step 3: The static pushover analyses provided the ${}_fQ_i$-δ_i curves shown in Fig. 5.10 and Fig. 5.11 which were approximated with two segments to determine the yield strength ${}_fQ_{y,i}$, the yield displacement ${}_f\delta_{y,i}$ and the lateral stiffness ${}_fk_i$ for each story that are summarized in Table 5.3, for the main frame without SRP/FRP strengthening.

Step 4: The values obtained for ${}_f\alpha_i$ and χ_1 are shown in Tables 5.3, 5.5 and 5.6. The value of α_e is 0.283.

Step 5: The maximum ν_{1max} among the stories obtained with the iterative procedure with tentative values of $\nu_{1,i}$ is shown in Table 5.4 and Table 5.5, together with the required level of strengthening with SRP/FRP expressed in terms of required increase of the yielding interstory drift of the story i of the main frame $\Delta_f\delta_{yi}$.

Step 6: From ν_{1max}, the required shear force coefficients ${}_s\alpha_i$, stiffness ${}_sk_i$, yield strength ${}_sQ_{y,i}$ and normalized energy dissipation capacity η ($=\eta_i$) for the dampers to be installed in each story i, was determined and it is shown in Table 5.4 and Table 5.5.

5.3.1 Strengthening with SRP/FRP

To determine the properties of the main frame ${}_fk_i$, ${}_f\delta_{y,i}{}^o$, ${}_f\delta_{ui}{}^o$, a pushover analysis was performed by following the procedure described in Chapter 4. The force-displacement curves selected for each floor are shown in Fig. 5.10 and Fig. 5.11. The black thick bold line represents the original main frame without any strengthening, and the line with rectangle symbol represents the bilinear elastic-plastic model explained in Chapter 4.

For the case of far-field design, it was not necessary to strengthen the main frame with FRP/SRP to find a solution that made $\delta_{m,i}$ less than ${}_f\delta_{y,i}={}_f\delta_{y,i}{}^o$. In addition, predicted displacements for 95 and 2475years satisfied the acceptance criteria without the need of any strengthening, as shown in Table 5.4. Thus, the original main frame was used for the nonlinear time history analyses with far field records. Acceptance criteria for each performance level and damper design characteristics are summarized in Table 5.4.

On the other hand, for the case of near-fault design, it was not possible to find a solution so that $\delta_{m,i}$ was less than ${}_f\delta_{y,i}={}_f\delta_{y,i}{}^o$. In this case, maximum displacements were limited by the collapse of fifth floor, as observed in the pushover analysis (Fig. 5.10, Fig. 5.11 and Fig. 5.12). Thus, the internal columns of fifth floor were retrofitted with the minimum amount of SRP/FRP such that the attained

yielding displacements, ${}_f\delta_{y,i}={}_f\delta_{yi}{}^o+\Delta_f\delta_{yi,}$ were enough to find a solution for the design of the dampers (see Table 5.6). To this end, a SRP/FRP retrofitting solution was defined, as described in sub-section 5.3.2. The pushover response of the strengthen solution is shown with medium bold black line in Fig. 5.10 and Fig. 5.11. Fig. 5.12 shows a detail of the pushover analyses at 5th floor.

Following, predicted displacements for 95 years were found to satisfy the acceptance criteria, while those for 2475years did not. In the latter case, the ultimate deformation capacity of the global frame was controlled by the failure of the external columns of first floor under axial-moment interaction, due to the high overturning moment (Fig. 5.10). Thus, a CFRP retrofitting solution was designed for this columns, so that the observed ultimate displacements were enough to make $\delta_{m,i}$ less than ${}_f\delta_{ui}={}_f\delta_{ui}{}^o+\Delta_f\delta_{ui}$ (see Table 5.6). This retrofitting solution is described in detail in sub-section 5.3.2. The pushover response of the final strengthen solution is shown with dash black line in Fig. 5.10, Fig. 5.11 and Fig. 5.12.

In short, the original frame was considered for the nonlinear time history analyses with far-field records, while two strengthening solutions were considered for near-fault records: (i) 5th floor internal columns strengthen with SRP/FRP for T_R=95, 475years and (ii) FRP also added in 1st floor external columns for T_R=2475years.

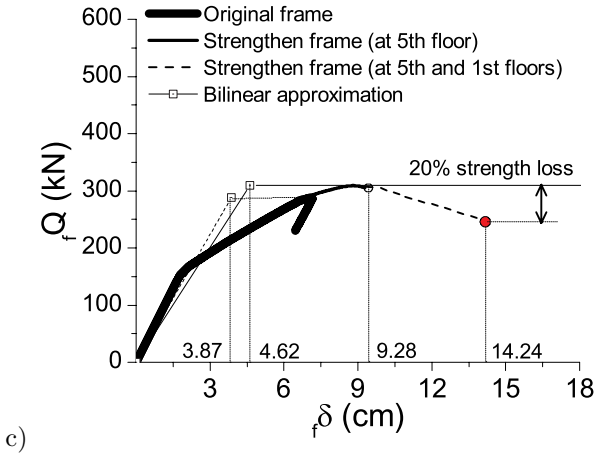

c)

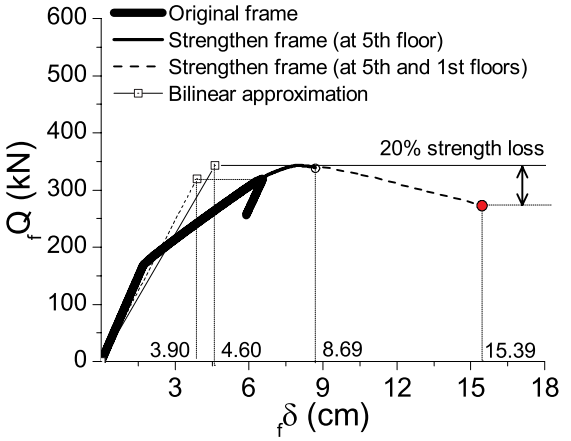

b)

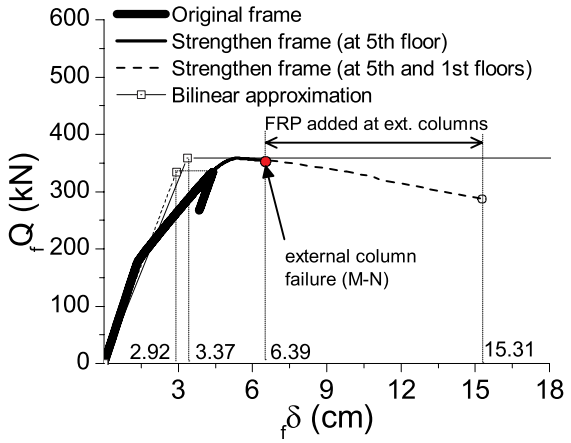

a)

Fig. 5.10: Pushover analyses: (a) first floor, (b) second floor, (c) third floor

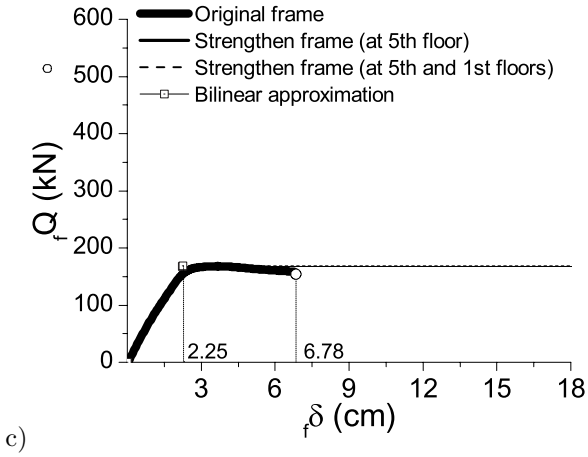

c)

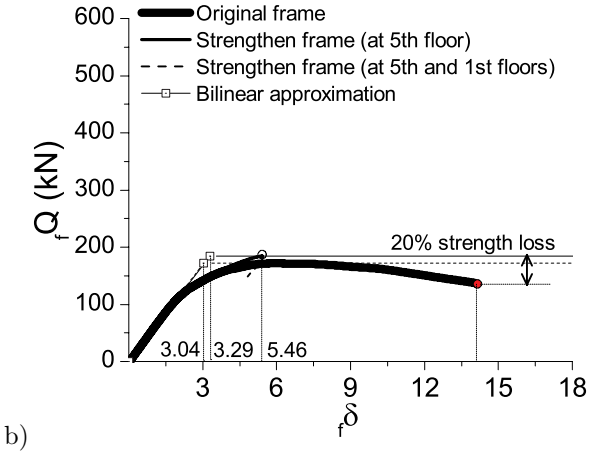

b)

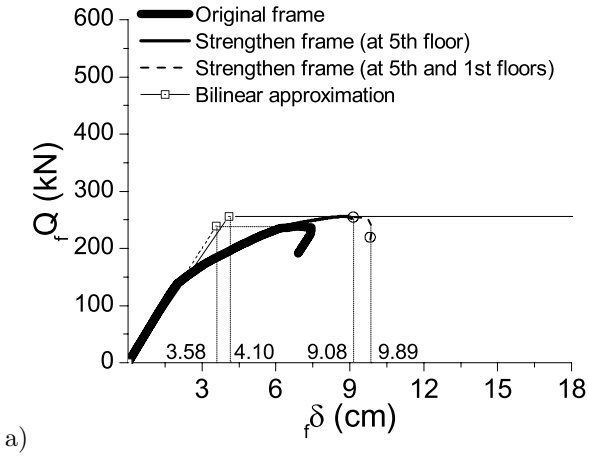

a)

Fig. 5.11: Pushover analyses: (a) fourth floor, (b) fifth floor and (c) sixth floor

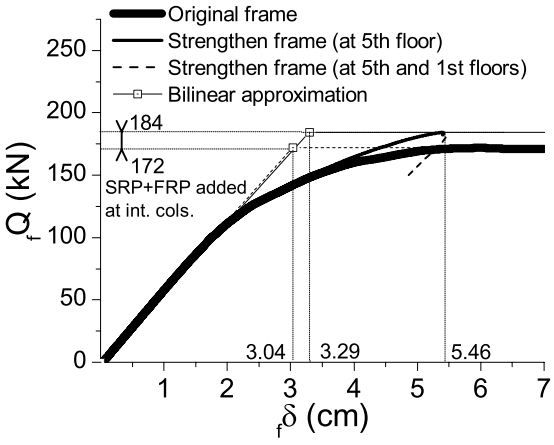

Fig. 5.12: Detail of the pushover analyses at 5th floor

Fig. 5.13 shows the collapse mode of the original main frame. Fig. 5.14 shows the collapse mode of (a) the main frame retrofitted with SRP/FRP at internal columns of 5th floor and (b) the main frame retrofitted with SRP/FRP at internal columns of 5th floor and FRP at external columns of 1st floor. For beams, numbers 0-3 are assigned to hinges with rotations corresponding to Limit States. The meaning of these numbers for beams is as follows: (0) Damage Limitation ($\theta<\theta_y$), (1) Significant Damage ($\theta_y<\theta<0.75\theta_u$), (2) Near Collapse ($0.75\theta_u<\theta<\theta_u$), and (3) Collapse ($\theta_u<\theta$). For columns (fiber sections), numbers 0-2 are assigned to fiber sections which showed yielding (1) or collapse (2). For the sections retrofitted with SRP, (0*) corresponds to an intermediate situation in which yielding of steel reinforcement is produced but SRP failure is not attained.

The damage level of the panel zone is identified with the number 0 or with letters A-C. The meaning is as follows: (0) means no

damage (elastic), (A) joint shear cracking, (B) maximum joint strength attained and (C) maximum joint strength overpassed more than 25%.

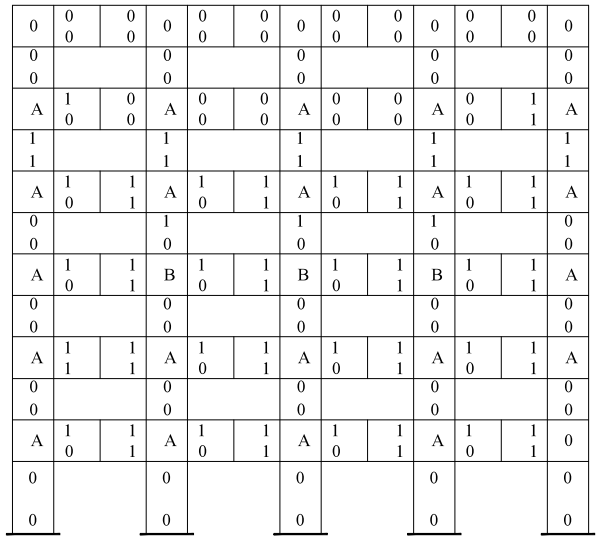

Fig. 5.13: Collapse mode of the original main frame.

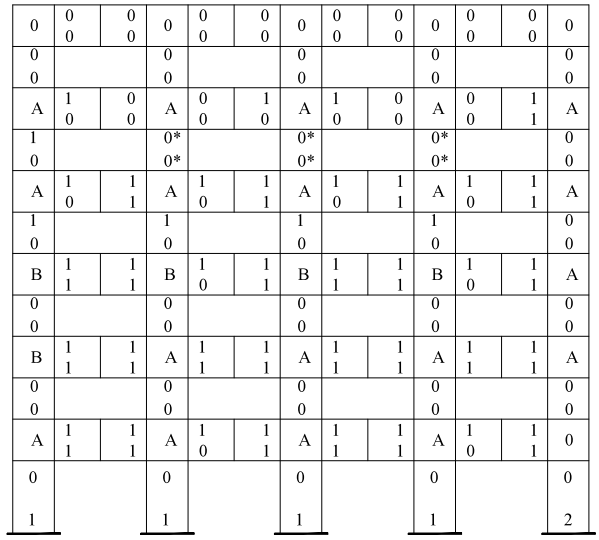

a)

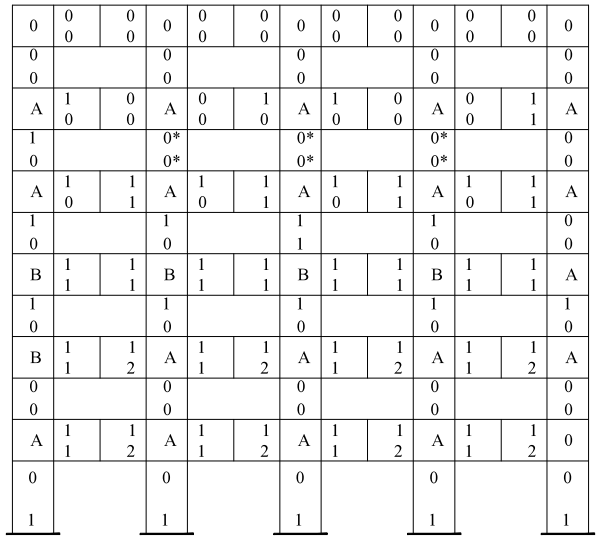

b)

Fig. 5.14: Collapse mode of (a) the main frame retrofitted with SRP/FRP at internal columns of 5th floor and (b) the main frame retrofitted with SRP/FRP at internal columns of 5th floor and FRP at external columns of 1st floor.

Table 5.3: Properties of the main frame

Story	${}_fk_i$ kN/cm	${}_f\delta_{yi}{}^o$ cm (%)	${}_f\alpha_i$	${}_f\delta_{ui}{}^o$ cm (%)	Vibration modes					
					ϕ_1	ϕ_2	ϕ_3	ϕ_4	ϕ_5	ϕ_6
6	74.90	2.25	0.24	6.76	1.00	1.00	-0.98	-0.46	0.16	0.01
5	56.61	3.04	0.12	14.07	0.89	0.25	0.85	1.00	-0.55	-0.07
4	66.70	3.58	0.11	7.44	0.72	-0.53	1.00	-0.51	1.00	0.25
3	74.35	3.87	0.10	7.15	0.53	-0.89	-0.20	-0.62	-0.92	-0.62
2	82.09	3.90	0.09	6.56	0.33	-0.80	-0.95	0.44	-0.05	1.00
1	114.45	2.92	0.07	4.39	0.15	-0.41	-0.70	0.65	0.84	-0.93
	χ_1=3.15			Period (s):	2.22	0.80	0.46	0.31	0.23	0.15

Table 5.4: Design of dampers for far-field design earthquake

Story	Predicted displacements						Dampers		
	T_R = 475years		T_R = 95years		T_R = 2475years		Far-field earthquake		
	$\delta_{m,i}$ cm (%)	*Accept. criteria*	$\delta_{m,i}$ cm (%)	*Accept. criteria*	$\delta_{m,i}$ cm (%)	*Accept. criteria*	${}_sk_i$ kN/cm	${}_s\alpha_i$	${}_sQ_{yi}$ kN
6	2.24 (0.72)	$< {}_f\delta_{yi}{}^o$	0.77 (0.25)	$< 0.5\%$	3.81 (1.23)	$< {}_f\delta_{ui}{}^o$	927.36	0.63	446.97
5	2.55 (0.82)	$< {}_f\delta_{yi}{}^o$	0.85 (0.27)	$< 0.5\%$	4.37 (1.41)	$< {}_f\delta_{ui}{}^o$	1338.30	0.47	681.32
4	3.28 (1.06)	$< {}_f\delta_{yi}{}^o$	1.11 (0.36)	$< 0.5\%$	5.60 (1.81)	$< {}_f\delta_{ui}{}^o$	1159.16	0.36	784.61
3	3.69 (1.19)	$< {}_f\delta_{yi}{}^o$	1.26 (0.41)	$< 0.5\%$	6.29 (2.03)	$< {}_f\delta_{ui}{}^o$	1118.78	0.30	865.95
2	3.70 (1.19)	$< {}_f\delta_{yi}{}^o$	1.26 (0.41)	$< 0.5\%$	6.30 (2.03)	$< {}_f\delta_{ui}{}^o$	1253.47	0.26	970.53
1	2.65 (0.76)	$< {}_f\delta_{yi}{}^o$	0.89 (0.25)	$< 0.5\%$	4.52 (1.29)	$< {}_f\delta_{ui}{}^o$	2079.54	0.25	1128.75
							η=6.504; ν_{1max}=0.186		

Table 5.5: Design of dampers for near-fault design earthquake

Story	${}_sk_i$ kN/cm	${}_s\alpha_i$	${}_sQ_{yi}$ kN
6	1022.53	0.67	474.77
5	1287.18	0.50	718.67
4	1055.86	0.38	827.93
3	981.10	0.31	913.98
2	1109.99	0.28	1024.48
1	1885.29	0.27	1191.51
	η=5.263		
	ν_{1max}=0.188		

Table 5.6: Predicted displacements for near-fault design earthquake

		Strengthening 5th floor		T_R = 475years		T_R = 95years		Stren. 5th & 1st fl.	T_R = 2475years	
	${}_fk_i$ kN/cm	${}_f\delta_{yi}{}^o+\Delta_f\delta_{yi}$ cm (%)	${}_f\alpha_i$	$\delta_{m,i}$ cm (%)	*Acc. Crit.*	$\delta_{m,i}$ cm (%)	*Acc. Crit.*	${}_f\delta_{ui}{}^o+\Delta_f\delta_{ui}$ cm (%)	$\delta_{m,i}$ cm (%)	*Acc. Crit.*
6	75.06	2.24 (0.72)	0.24	2.18 (0.70)	$<{}_f\delta_{yi}{}^o+\Delta_f\delta_y$	0.68 (0.22)	<0.5%	6.78 (2.19)	4.68 (1.51)	$<{}_f\delta_{ui}{}^o+\Delta_f\delta_{ui}$
5	55.97	3.29 (1.06)	0.13	2.78 (0.90)	$<{}_f\delta_{yi}{}^o+\Delta_f\delta_y$	0.83 (0.27)	<0.5%	5.46 (1.76)	6.02 (1.94)	$<{}_f\delta_{ui}{}^o+\Delta_f\delta_{ui}$
4	62.37	4.10 (1.32)	0.12	3.78 (1.22)	$<{}_f\delta_{yi}{}^o+\Delta_f\delta_y$	1.16 (0.37)	<0.5%	9.89 (3.19)	8.15 (2.63)	$<{}_f\delta_{ui}{}^o+\Delta_f\delta_{ui}$
3	66.89	4.62 (1.49)	0.11	4.42 (1.43)	$<{}_f\delta_{yi}{}^o+\Delta_f\delta_y$	1.36 (0.44)	<0.5%	14.24 (4.59)	9.49 (3.06)	$<{}_f\delta_{ui}{}^o+\Delta_f\delta_{ui}$
2	74.56	4.60 (1.48)	0.09	4.39 (1.41)	$<{}_f\delta_{yi}{}^o+\Delta_f\delta_y$	1.35 (0.44)	<0.5%	15.39 (4.96)	9.43 (3.04)	$<{}_f\delta_{ui}{}^o+\Delta_f\delta_{ui}$
1	106.48	3.37 (0.96)	0.08	3.07 (0.88)	$<{}_f\delta_{yi}{}^o+\Delta_f\delta_y$	0.93 (0.27)	<0.5%	15.31 (4.37)	6.61 (1.89)	$<{}_f\delta_{ui}{}^o+\Delta_f\delta_{ui}$
	χ_1=2.93									

5.3.2 Design of the strengthening solution with SRP/FRP

As explained before, two strengthening solutions were considered for the near-fault records: (i) the internal columns at 5th floor were strengthen with SRP/FRP for the analyses corresponding to return periods T_R=95, 475years and (ii) the external columns 1st floor were retrofitted with CFRP, for the return period T_R=2475years.

The strengthening solution with SRP/FRP has been designed to increase the flexural strength of section C8 (corresponding to internal columns at fifth floor, as referred in Fig. 5.1). At this floor, internal columns have a yielding rotation lower than the external ones (see Fig. 5.6). Experimental tests showed that retrofitting a reinforced concrete element with SRP can increase its flexural strength more than 40% (Cuzzilla, Di Ludovico, Prota, & Manfredi, 2011) or even over 100% (Huang, Birman, Nanni, & Tunis, 2005). Fig. 5.15 shows the retrofitting solution consisting on placing SRP wire stripes at each side of the retrofitted section and wrapping the section with CFRP to avoid the buckling of the SRP spikes (Cuzzilla et al., 2011).

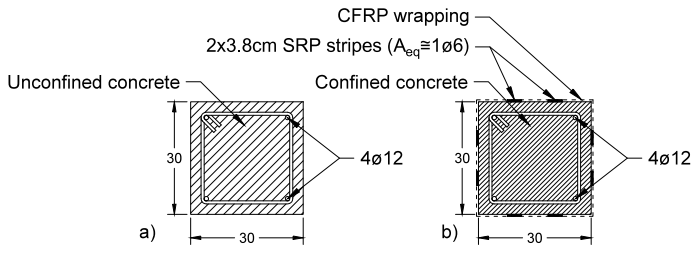

Fig. 5.15: Section C8 (a) and SRP/FRP retrofitting scheme (b)

The increase in flexural strength of the retrofitting solution was evaluated numerically through moment-curvature analysis on a fiber section (Fig. 5.16). To this end, a minimum equivalent load-resistant area of SRP equal to A_{eq}=28.26mm2 (=1ϕ6) was considered at each side of the section. This value of equivalent load-resistance area can be attained by placing two bands of 38mm-width of mono-directional steel fibre fabric (Mapei, 2010) with a load-resistant area per unit of width equal to 373.80 mm2/m. The constitutive material of SRP wire stripes was considered to be linear elastic, with elastic modulus E_f=190000MPa, maximum tensile strength of 2845MPa and zero-compression strength (as a safe-side approach, although buckling is avoided by the CFRP wrapping). These constitutive properties are similar to those defined in previous literature (Cuzzilla et al., 2011; Huang et al., 2005; Mapei, 2010). However, the maximum tension strain was limited to ε_{fd} = 1.2% to account for delamination failure. In this sense, a first approach was done by using the first member of Eq. 4.19 of CNR DT 200/2004 (2004), $\varepsilon_{fd} = \min\left(\eta_a \frac{\varepsilon_{fk}}{\gamma_f}; \varepsilon_{fdd}\right)$, where ε_{fk} = 1.6% is the characteristic strain at failure of the strengthening system, γ_f=1.1 and η_a= 0.85 are the coefficients defined in Table 3-2 and Table 3-4 of CNR DT 200/2004 (2004) for certified strengthening systems, rupture failure mode and external exposure condition; and ε_{fdd} is the maximum strain due to intermediate debonding. To increase the maximum design strength, ε_{fdd}, additional CFRP wrapping is disposed over the SRP wire stripes (as shown in Fig. 5.15). It is worth

mentioning that maximum SRP strain recorded in the nonlinear time history analyses was 0.9%. However, further research needs to be done in order to determine experimentally the maximum design strength of the proposed solution, which is out the scope of the present study. On the other hand, bond length equal to the optimal bonded length CNR DT 200/2004 (2004) is also defined $l_e = \sqrt{\frac{E_f t_f}{2 f_{ctm}}} = 133mm\left[length\,in\,mm\right]$, were t_f =0.37mm is the thickness of the SRP and f_{ctm}=2.02MPa is the average tensile strength of the concrete (EHE-08, 2008).

CFRP wrapping was also designed to avoid the buckling of the longitudinal SRP wire stripes by using the following equation (CNR-DT 200/2004, 2004; Dolce & Manfredi, 2011), $t_f \cong \frac{10nd}{E_{FRP}} = 0.026mm$, where n=2 is the number of longitudinal reinforcement subjected to buckling, d=300mm is the size of the cross section parallel to the bending plane and E_{FRP}=230000MPa is the Young modulus of CFRP reinforcement (Dolce & Manfredi, 2011; Huang et al., 2005).

Constitutive properties of the concrete material for the retrofitted section were also modified, to account for the confinement effect of the CFRP wrapping. With this purpose, the constitutive law of confined concrete defined in Appendix D of CNR-DT 200/2004 (2004) was assumed. First, the design ultimate strain of confined concrete, ε_{ccu}, was calculated as in CNR-DT 200/2004 by using the following

equation: $\varepsilon_{ccu} = 0.0035 + 0.015\sqrt{\frac{f_{1,eff}}{f_{cd}}} = 0.0048$, where $f_{1,eff}$ is the effective confinement pressure and f_{cd}=17.5MPa is the design strength of unconfined concrete. The effective confinement pressure is calculated as $f_{1,eff} = k_{eff}\, f_1$, where k_{eff} =0.55 is a coefficient of efficiency and f_1=0.25MPa is the confinement lateral pressure (a detailed description can be found in CNR-DT 200/2004. Second, the tangent modulus is calculated as $E_t = \frac{f_{ccd} - f_{cd}}{\varepsilon_{ccu}} = 372.56MPa$, where f_{ccd} =19.30MPa is the design strength of confined concrete, calculated in $\frac{f_{ccd}}{f_{cd}} = 1 + 2.6\left(\frac{f_{1,eff}}{f_{cd}}\right)^{2/3}$. This constitutive law was also used for the retrofitted section of external columns at first floor, as a minimum approach.

Moment curvature analysis of the retrofitted section are shown in Fig. 5.16. Pushover results of the retrofitted solution, are shown in Fig. 5.10 and Fig. 5.11. At fifth floor, the total increase in flexural strength of 7%, was proved sufficient to avoid the collapse of fifth floor, thus increasing the overall deformation capacity of the frame. The corresponding bilinear approximation and the attained values of ${}_f\delta_{yi}{}^o + \Delta_f\delta_{yi}$ are also shown in Fig. 5.10 and Fig. 5.11. The increment of ${}_f\delta_{yi}$ attained by this minimum reinforcement was enough to find a solution for the design of the dampers such that ($\delta_{mi} < {}_f\delta_{yi}{}^o + \Delta_f\delta_{yi}$), satisfying the acceptance criteria for T_R=475 years, as shown in Table

5.5. At ground floor, the minimum CFRP wrapping considered was proved enough to satisfy the acceptance criteria for T_R=2475 years shown in Table 5.5, ($\delta_{mi} < {}_f\delta_{ui}{}^o + \Delta_f\delta_{ui}$).

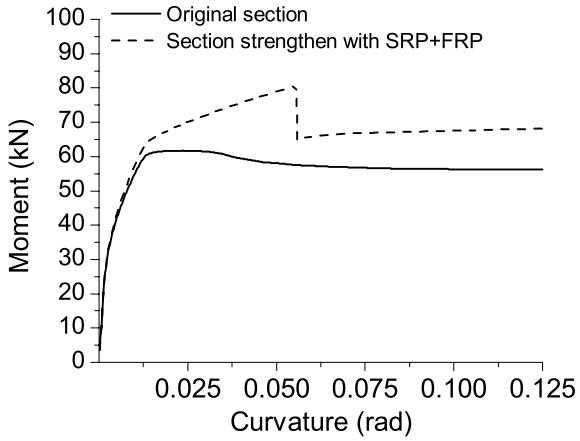

a)

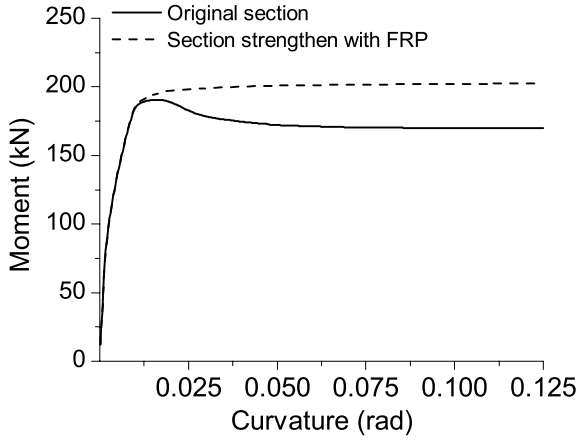

b)

Fig. 5.16: Moment-curvature analyses on a fiber section for (a) the internal columns at 5th floor strengthen with SRP and FRP and (b) the external columns at 1st floor strengthen with FRP.

5.4 Nonlinear dynamic response analyses

A series of non-linear dynamic response analyses were carried out with the frame equipped with hysteretic dampers and strengthened with FRP/SRP. To this end, two sets of 20 natural acceleration records were compiled from the PEER NGA-West2 database (Pacific Earthquake Engineering Research Center, 2013): (a) records taken in the near fault region with source-to-site distance $D_f < 12$ km and (b) records with $D_f > 12$ km. The intervals were defined according to (Decanini & Mollaioli, 1998, 2001), who consider the interval $D_f <$ 5km as proper to the near-fault area, and the interval 5km$< D_f <$ 12km as proper of sites where the effect of the closeness of the seismic source can still be significant. In particular, the closest distance from the recording site to the rupture plane D_f is used, since the epicentral distance D_e is considered to have a low correlation with the ground motion characteristics (Decanini & Mollaioli, 1998). Each set of records was subdivided into two sub-sets. The first set of records with $D_f < 12$ km was subdivided into (a.1) pulse-like and (a.2) no-pulse like records. This characterization was made according to the information provided by the PEER database (Pacific Earthquake Engineering Research Center, 2010, 2013), except for Lorca record, which was analyzed by (Rueda Nuñez, Mezcua Rodríguez, & Garcia Blanco, 2013). As for the second set of records, it was ordered by I_d, establishing two sub-sets: (b.1) I_d>9 and (b.2) I_d<9, being I_d=9 considered for the design of the dampers.

First, a selection of records was performed from the PEER database by comparing the spectral shape of the selected signals (see Annex A) with the design inelastic energy spectra, near the periods of interest (Bommer & Acevedo, 2004). For this purpose (EN 1998-1:2004, 2004), the range between $0.2T_1$ and $2T_1$ was considered, where T_1 is the fundamental period of the structure (approximated here as the fundamental period of the flexible part ${}_fT_1 = 2.22$s). In particular, special care was taken to select signals with T_G similar to the design spectra $T_G = 0.40$s.

Second, the empirical relation proposed by Fajfar, Vidic, & Fischinger (1990), $T_{NH} = 4.3\frac{v_g}{a_g}$, was used to calculate the initial period of medium period region in the Newmark-Hall spectrum, T_{NH}, where v_g is the peak ground velocity and a_g is the peak ground acceleration. This expression is adequate to describe elastic structural behavior (Fajfar et al., 1990). Here, it is used to calculate the ratio $\frac{T}{T_{NH}}$ (for $T < T_{NH}$) that characterizes the elastic response in the formula of equivalent number of cycles proposed by Manfredi (2001). It is worth recalling that the plastic response in Manfredi's expression (Eq. 4.15) is completely represented by (R–1) (Manfredi, 2001). Since the predominant period of the ground motion, T_G, is considered to be similar to the initial period of medium period region in the Newmark-Hall spectrum, T_{NH}, the selected records have an averaged value of

T_{NH} similar to the considered T_G =0.40s (Cosenza & Manfredi, 2000; Fajfar, Vidic, & Fischinger, 1992). For the fist set of records (D_f < 12 km) the averaged value of T_{NH} is 0.51s, ranging between 0.21 and 1.06s; and for the second set of records (D_f >12 km), the averaged value of T_{NH} is 0.33s, ranging between 0.18 and 0.55s. Third, signals with similar I_d were selected. For the ground motions with D_f < 12, I_d varies between 2.08 and 4.94, with an averaged value I_d = 3.45 and around the design value, I_d = 3. For the ground motions with D_f > 12, I_d varies between 6.77 and 12.83, with an averaged value I_d = 9.20 and around the design value, I_d = 9. Fourth, as recommended by Bommer & Acevedo (2004), the selection of earthquakes was also based on a particular earthquake scenario. In this sense, similar magnitude and site conditions were also considered. The magnitude (M_w) of the selected signals ranged between 5.10 and 7.51, around the expected maximum magnitude for the site of Granada: 6.7±0.4 (Instituto Geográfico Nacional, 2012). In addition, for the far-field set of records (D_f >12 km), soil conditions were restricted to medium soil, type C (180 m/s ≤ $v_{s,30}$ ≤ 360 m/s) (EN 1998-1:2004, 2004), as considered before for the design energy spectrum. To this end, the average shear wave velocity of top 30 meters of the site, $v_{s,30,}$ is used when available (Pacific Earthquake Engineering Research Center, 2013). For the near-fault set of records (D_f <12 km), a wider selection had to be made, ranging between 206 and 792 m/s.

In addition, the selected signals with $D_f < 12$ have the following characteristics: PGA ranges between 0.09g and 0.83g, PGV is between 7.95cm/s and 113.08cm/s. As for the selected signals with $D_f > 12$: PGA ranges between 0.08g and 0.45g, PGV is between 3.84cm/s and 33.89 cm/s. The selected signals and their characteristics are summarized in Tables II and III.

Finally, scaling factors were applied in an iterative process, so that the total energy input contributable to damage expressed in terms of equivalent velocity was V_{Dmax}= 98±2.45 cm/s at the end of the nonlinear time-history analysis (thus compensating mismatches with the earthquake magnitude, distance or soil conditions).

Table 5.7: Selected pulse-like ground motions with $D_f < 12$ km

Earthquake	Year	Station	M_w	D_f (Km)	PGA (g)	PGV (cm/s)	I_d	T_{NH} (s)	$V_{s,30}$ (cm/s)
Kobe, Japan	1995	Takarazuka	6.90	0.27	0.70	68.37	4.10	0.43	312.00
Coyote Lake	1979	Gilroy Array #2	5.74	9.02	0.26	31.92	3.99	0.55	270.84
Loma Prieta	1989	Gilroy - Historic Bldg.	6.93	10.97	0.29	43.37	3.71	0.67	308.55
Darfield, New Zealand	2010	LINC	7.00	7.11	0.46	108.69	3.42	1.03	263.20
Kocaeli, Turkey	1999	Gebze	7.51	10.92	0.26	44.60	3.00	0.75	792.00
Kalamata, Greece-02	1986	Kalamata (bsmt) (2nd trigger)	5.40	5.60	0.26	24.57	2.91	0.41	382.21
Parkfield-02, CA	2004	Parkfield - Stone Corral 1E	6.00	3.79	0.83	39.77	2.83	0.21	260.63
San Salvador	1986	Geotech Investig Center	5.80	6.30	0.70	79.88	2.81	0.50	489.34
Lorca	2011	Lorca	5.10	--*	0.37	34.88	2.62	0.42	--*
Imperial Valley-06	1979	El Centro Array #7	6.53	0.56	0.47	113.08	2.08	1.06	210.51

* Data not available. The epicentral distance is 4.7km.

Table 5.8: Selected non-pulse like ground motions with $D_f < 12$ km

Earthquake	**Year**	**Station**	M_w	D_f (Km)	**PGA** (g)	**PGV** (cm/s)	I_d	T_{NH} (s)	$V_{s,30}$ (cm/s)
Parkfield	1966	Cholame - Shandon Array #5	6.19	9.58	0.44	25.04	4.94	0.25	289.56
Morgan Hill	1984	Halls Valley	6.19	3.48	0.31	39.32	4.52	0.55	281.61
Duzce Turkey	1999	Duzce	7.14	6.58	0.51	84.19	4.30	0.72	281.86
Managua Nicaragua-02	1972	Managua ESSO	5.20	4.98	0.26	25.39	4.09	0.42	288.77
Coalinga-07	1983	Coalinga-14th & Elm (Old CHP)	5.21	10.89	0.68	35.47	3.77	0.23	286.41
Coalinga-05	1983	Coalinga-14th & Elm (Old CHP)	5.77	10.78	0.52	29.58	3.41	0.25	286.41
Imperial Valley-06	1979	El Centro Array #8	6.53	3.86	0.61	54.46	3.13	0.39	206.08
New Zealand-01	1984	Turangi Telephone Exchange	5.50	8.84	0.15	9.34	2.96	0.28	356.39
Erzican Turkey	1992	Erzincan	6.69	4.38	0.50	78.12	2.94	0.69	352.05
Drama Greece	1985	Drama	5.20	11.61	0.09	7.95	2.91	0.41	324.55

Table 5.9: Selected ground motions with $D_f > 12$ km and I_d>9

Earthquake	**Year**	**Station**	M_w	D_f	**PGA**	**PGV**	I_d	T_{NH}	$V_{s,30}$
				(Km)	(g)	(cm/s)		(s)	(cm/s)
Tabas Iran	1978	Boshrooyeh	7.35	28.79	0.11	13.30	12.83	0.55	324.57
Northern Calif-07	1975	Ferndale City Hall	5.20	19.90	0.09	6.30	12.32	0.30	219.31
Friuli Italy-01	1976	Codroipo	6.50	33.40	0.09	8.05	11.43	0.39	249.28
Hollister-01	1961	Hollister City Hall	5.60	19.56	0.11	9.88	11.15	0.38	198.77
Taiwan SMART1(5)	1981	SMART1 I06	5.90	26.40	0.09	4.71	10.54	0.23	309.41
Coalinga-01	1983	Parkfield - Cholame 1E	6.36	43.68	0.09	11.29	10.27	0.54	326.64
Imperial Valley-06	1979	Compuertas	6.53	15.30	0.19	13.77	9.98	0.32	259.86
San Fernando	1971	Whittier Narrows Dam	6.61	39.45	0.11	10.55	9.63	0.43	298.68
Coyote Lake	1979	San Juan Bautista 24 Polk St	5.74	19.70	0.11	7.11	9.22	0.28	335.50
Victoria Mexico	1980	SAHOP Casa Flores	6.33	39.30	0.10	8.51	9.05	0.37	259.59

Table 5.10: Selected ground motions with $D_f > 12$ km and I_d<9

Earthquake	**Year**	**Station**	M_w	D_f (Km)	**PGA** (g)	**PGV** (cm/s)	I_d	T_{NH} (s)	$V_{s,30}$ (cm/s)
Trinidad	1980	Rio Dell Overpass - FF	7.20	76.26	0.15	8.75	8.51	0.26	311.75
Westmorland	1981	Niland Fire Station	5.90	15.29	0.18	7.56	8.32	0.19	212.00
Northwest Calif-03	1951	Ferndale City Hall	5.80	53.77	0.11	7.86	8.14	0.31	219.31
Northern Calif-01	1941	Ferndale City Hall	6.40	44.68	0.12	6.76	8.00	0.24	219.31
Kobe, Japan	1995	Shin-Osaka	6.90	19.15	0.23	21.80	8.00	0.41	256.00
Parkfield	1966	Cholame - Shandon Array #8	6.19	12.90	0.27	11.36	7.91	0.18	256.82
Northern Calif-04	1960	Ferndale City Hall	5.70	57.21	0.08	3.84	7.73	0.22	219.31
Cape Mendocino	1992	Fortuna Fire Station	7.01	20.41	0.33	33.89	7.39	0.45	355.18
Anza (Horse Canyon)-01	1980	Rancho De Anza	5.19	21.32	0.09	5.94	6.85	0.28	329.00
Northridge-01	1994	LA - Centinela St	6.69	28.30	0.45	20.23	6.77	0.20	321.91

5.4.1 Results

The frame with dampers and FRP/SRP strengthening designed for each design earthquake (i.e. near-fault and far-field) was subjected to the corresponding set of acceleration records. The results of the analyses are shown in Figs. 5.17 to 5.52.

5.4.1.1 Maximum interstory drift

Figs. 5.17 to 5.22 show the maximum interstory drift, δ_i, for each floor in percentage of the story height, *IDR*. The bold dash-dot line shows the interstory drift ${}_f\delta_{y,i}$ —in percentage of the story height, ${}_fIDR_y$. The line with blue triangles shows the maximum predicted interstory drift in percentage of story height, $IDR_{predicted}$. The lines with symbols correspond to numerical simulations carried out with different records.

In all cases with T_R=475years (Fig. 5.17 and Fig. 5.18), the maximum interstory drift obtained from the response analyses remains mostly below the maximum allowed drift for this return period, which coincides with ${}_fIDR_y$. It is worth mentioning that while no significant difference is observed between pulse or no-pulse records for the case of near-fault records, a difference is observed between the two sub-sets of far-field records, being those with higher I_d the ones with lower response values.

Fig. 5.19 and Fig. 5.20 show the results for T_R=95years. The blue dot line with cross symbol expresses the maximum allowed drift for this return period, IDR = 0.5%. In cases corresponding to far-field records (Fig. 5.20), response values remain the maximum allowed drift. In cases corresponding to near-fault records (Fig. 5.19), and specially for pulse-like records (Fig. 5.19.a), intermediate floors, 3th and 4th, exceed the predicted values, but remained under 0.75% and far away from ${}_fIDR_y$.

Fig. 5.21 and Fig. 5.22 show the results for T_R=2475years. The blue cross symbol expresses the maximum allowed drift for this return period, ${}_fIDR_u$. In most cases, response values remain under the predicted values. In three cases of pulse-like records (Fig. 5.21.a), lower floors exceed the predicted values but remained far away from the maximum allowed drift, ${}_fIDR_u$.

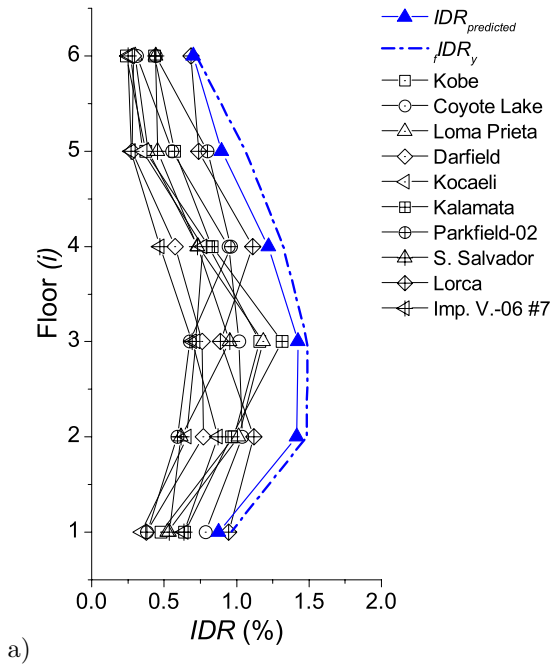

a)

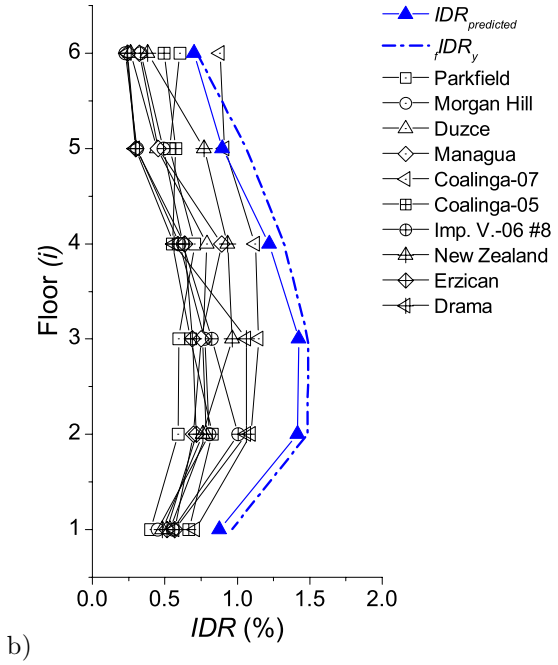

b)

Fig. 5.17: Maximum interstory drift for T_R= 475years and ground motions with $D_f < 12$ km, (a) pulse-like and (b) non-pulse like

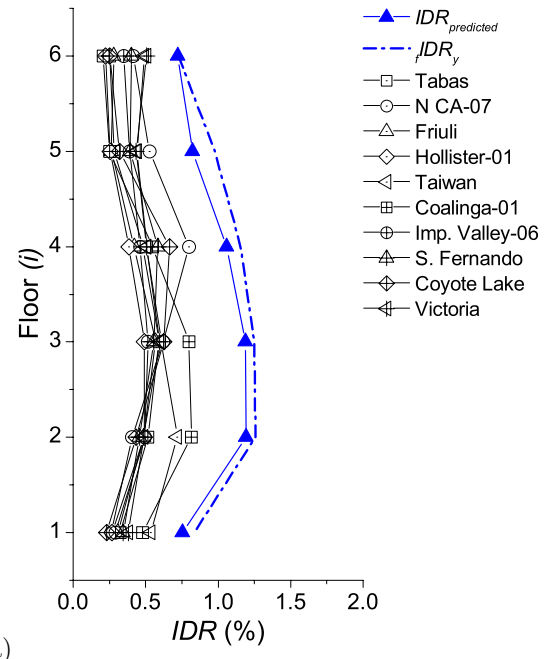

a)

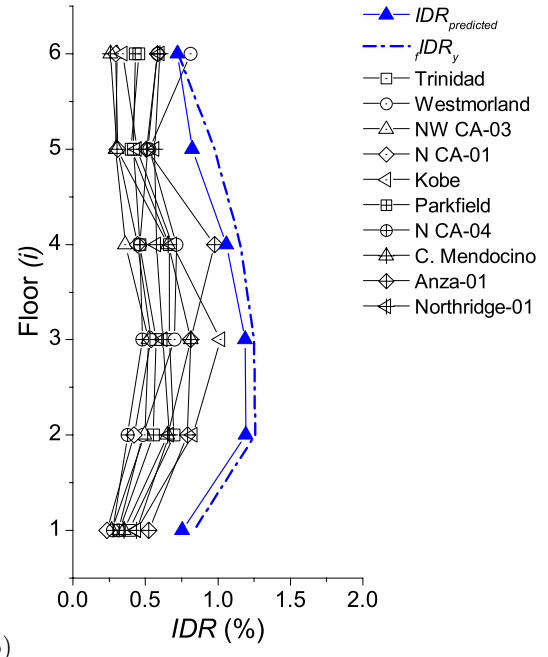

b)

Fig. 5.18: Maximum interstory drift for T_R= 475years and ground motions with D_f> 12, (a) I_d>9 and (b) I_d<9

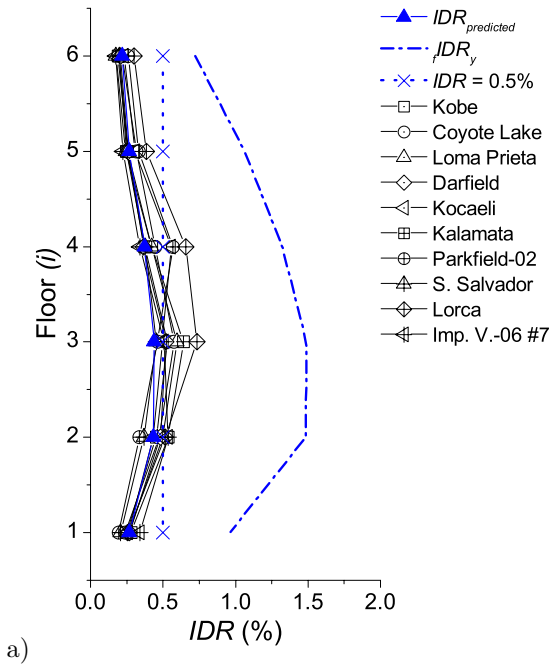

a)

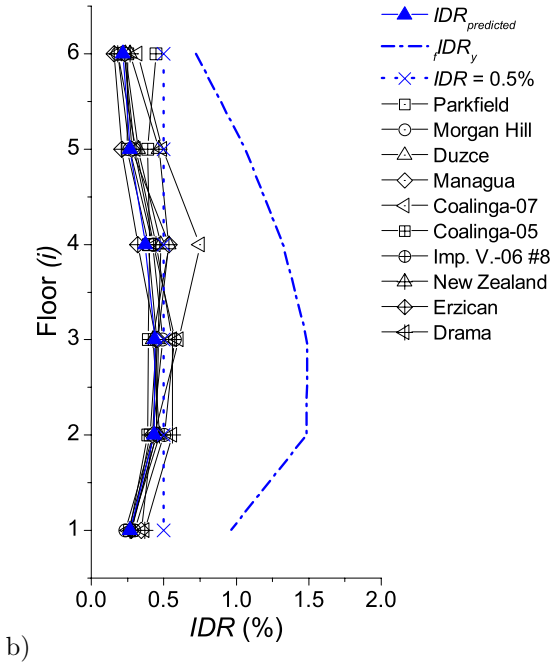

b)

Fig. 5.19: Maximum interstory drift for T_R= 95years and ground motions with $Df < 12$, (a) pulse-like and (b) non-pulse like

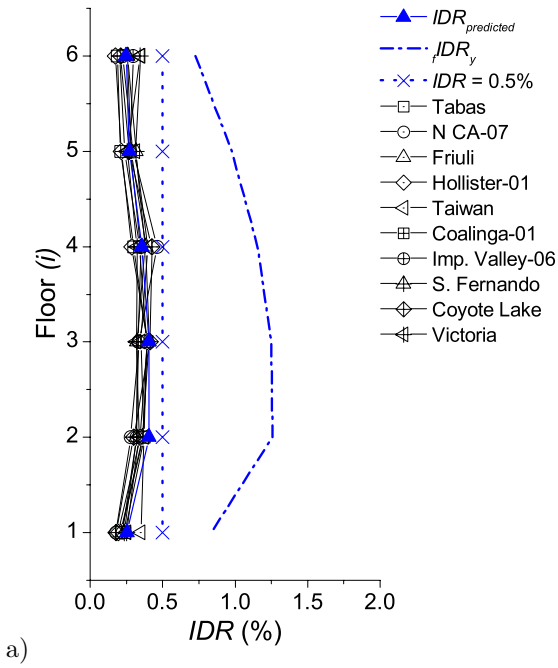

a)

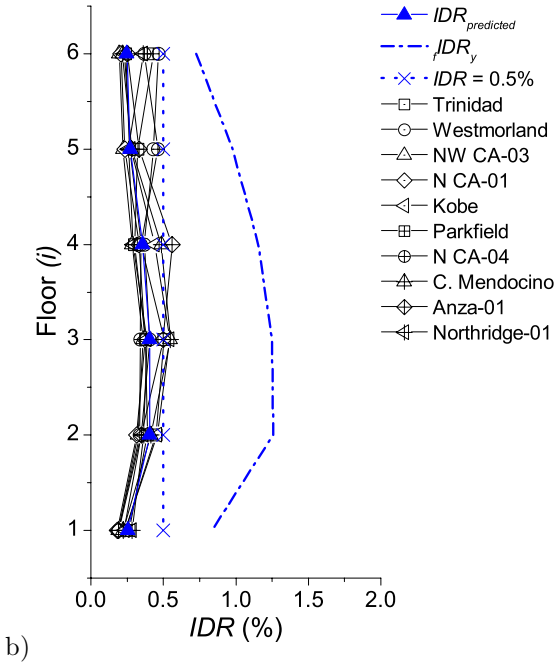

b)

Fig. 5.20: Maximum interstory drift for TR= 95years and ground motions with Df > 12 km, (a) Id>9 and (b) Id<9

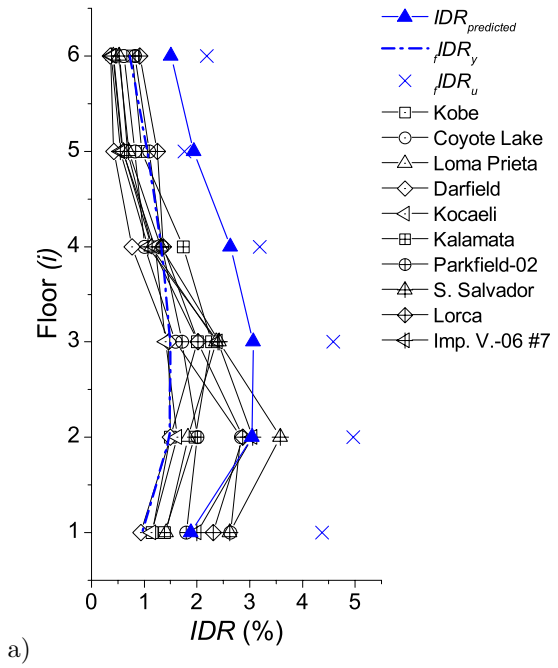

a)

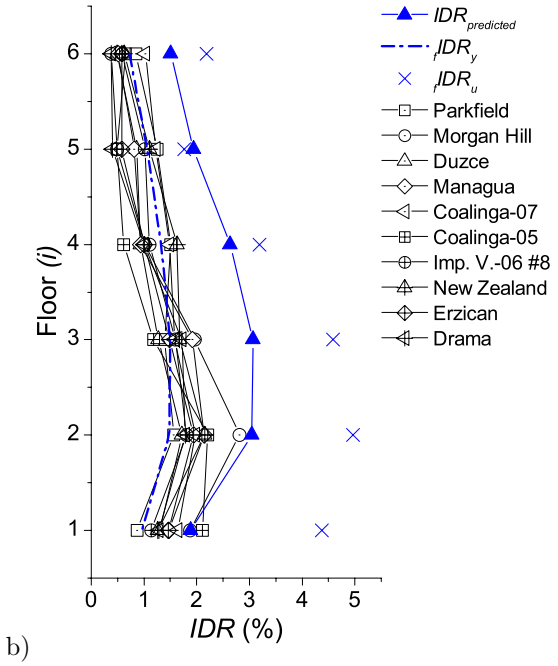

b)

Fig. 5.21: Maximum interstory drift for TR= 2475years and ground motions with Df < 12 km, (a) pulse-like and (b) non-pulse like

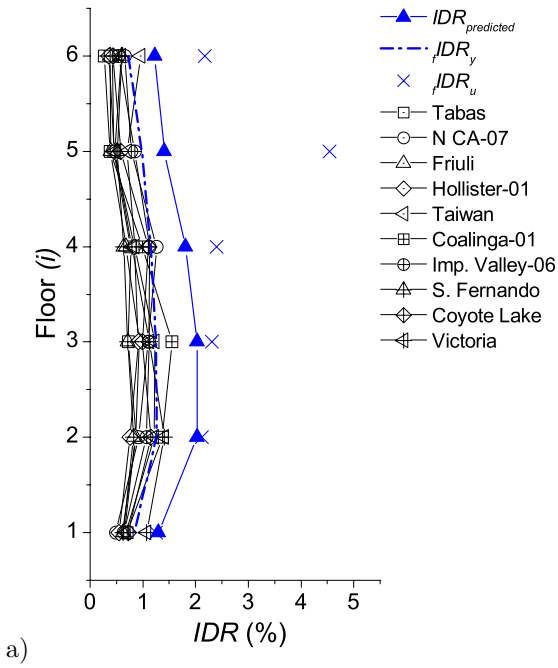

a)

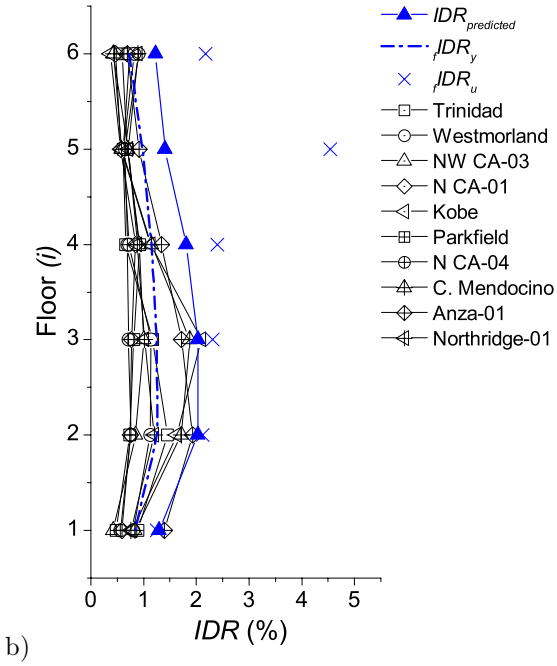

b)

Fig. 5.22: Maximum interstory drift for T_R= 2475years and ground motions with Df > 12 km, (a) Id>9 and (b) Id<9

5.4.1.2 Shear failure detected by postprocessing analysis results

As explained before, two verifications were carried out by postprocessing analysis results: (1) "brittle" failure mode (EN 1992-1-1:2004, 2004) and (2) "ductile shear" failure, which only occurs under cyclic loading (EN 1998-3:2005, 2005; Fardis, 2009). Shear failure was detected in columns of pier 2 and 4 at third floor, for some analyses corresponding to T_R=2475years, even if the angle between the concrete compression strut and the member axis, is considered as the minimum recommended by EN 1992-1-1:2004, i.e. 22º. These columns were constructed with section C4, as referred in Fig. 5.1. As shown in Table 5.2, this section has the greatest spacing of stirrups, s_h=30cm, of the floor. Maximum values attained and computed values of shear resistance are shown in Table 5.11. For this members, CFRP wrapping should be designed, in order to increase their shear capacity (EN 1998-3:2005, 2005).

Table 5.11: Shear failure detected by postprocessing analysis results for T_R=2475years (units in kN)

			Columns at third floor				Ductile failure A.3.3.1. Ec8-Part3		Brittle failure EC2
		Earthquake name	V_{max} Pier 2	Failure	V_{max} Pier 4	Failure	$V_{R,ductile}$ Pier2	$V_{R,ductile}$ Pier4	
Near-Fault	*Pulse*	Lorca	114.22	brittle	107.96	-	170.70	200.10	108.76
		Kobe	86.55	-	111.53	brittle	95.07	185.40	
		Kocaeli	110.20	brittle	88.59	-	180.30	101.60	
		Parkfield	118.26	brittle	90.26	-	179.40	197.20	
		Kalamata	110.37	brittle	110.68	brittle	183.60	195.70	
	No pulse	Coalinga-05	83.35	-	119.70	brittle	93.80	188.60	108.76
		Coalinga-07	109.31	brittle	76.39	-	196.40	86.75	
		Erzican	104.76	-	112.37	brittle	189.60	188.70	
		Managua	103.10	-	116.88	brittle	188.10	170.30	
Far-field		Kobe	94.43	-	111.99	brittle	184.90	180.20	108.76
		Anza (Horse Canyon)-01	114.53	brittle	92.59	-	183.20	100.20	

5.4.1.3 Maximum joint shear detected by postprocessing analysis results

Table 5.12 resumes the elements that attained the moment, $M_{jR\ ACI}$, corresponding to the maximum joint shear strength, $V_{R,ACI}$, (surpassing it no more than a 2.5%). It only occurred for the nonlinear time history analyses with T_R=2475years and near fault records. Not any element exceeded this limit over a 2.5% during the numerical simulations described in section 7.5, as shown in the sixth column. Position of the elements is described according to Fig. 5.1.

Table 5.12: Maximum joint shear detected by postprocessing analysis results for T_R=2475years and near fault records (units in kN)

	Earthquake name	*Position*	$M_{j,max}$ (kN m)	$M_{jR\ ACI}$ (kN m)	*% exceeded*
Pulse	Lorca	Second floor – left external joint	145.70	144.06	1.14
	Coyote Lake	Second floor – left external joint	147.14	144.06	2.14
	Imp. Valley-06 #7	Second floor – left external joint	144.53	144.06	0.33
No pulse	Morgan Hill	Second floor – right external joint	144.19	144.06	0.09

5.4.1.4 Normalized cumulative plastic strain energy, η_i

Figs. 5.23 to 5.28 show the variation of η_i. The continuous line with blue triangles shows the predicted value of η_i,. The lines with symbols correspond to numerical simulations carried out with different records. The discontinuous line with white triangles shows the mean value of η_i, computed over the numerical simulations shown in the graph. It can be seen that the mean value of the η_i obtained in the dynamic response analyses is very close to the predicted value.

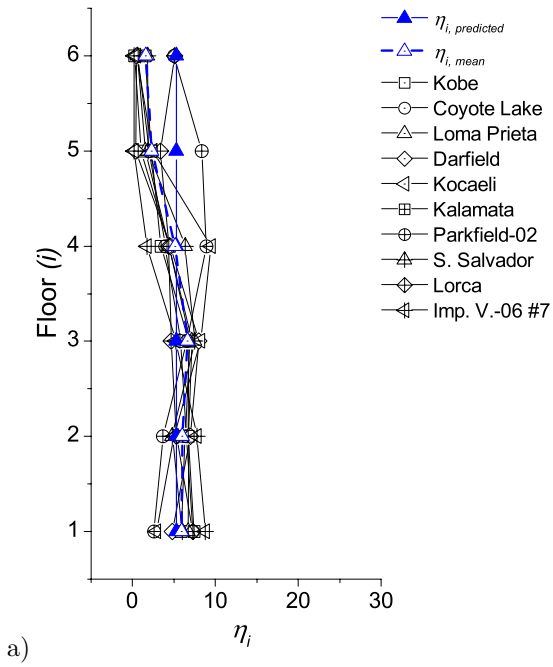

a)

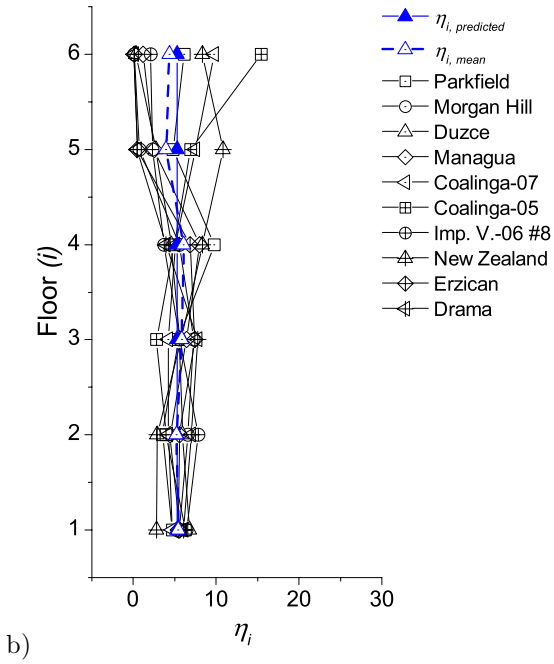

b)

Fig. 5.23: Variation of η_i for T_R= 475years and ground motions with D_f < 12 km, (a) pulse-like and (b) non-pulse like

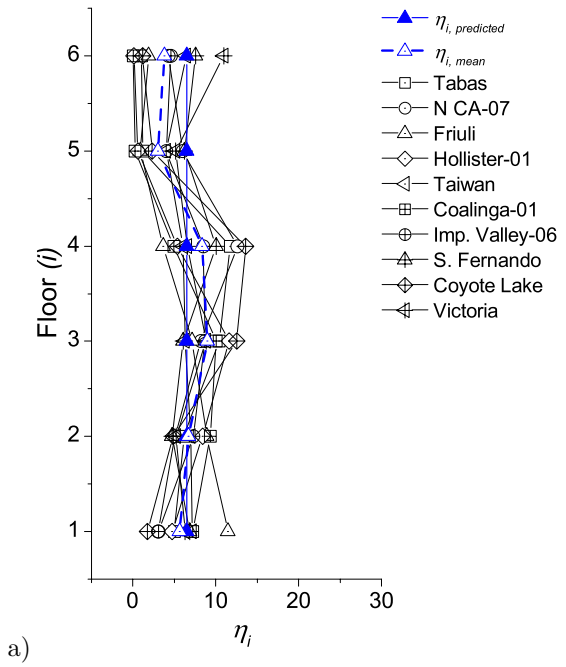

a)

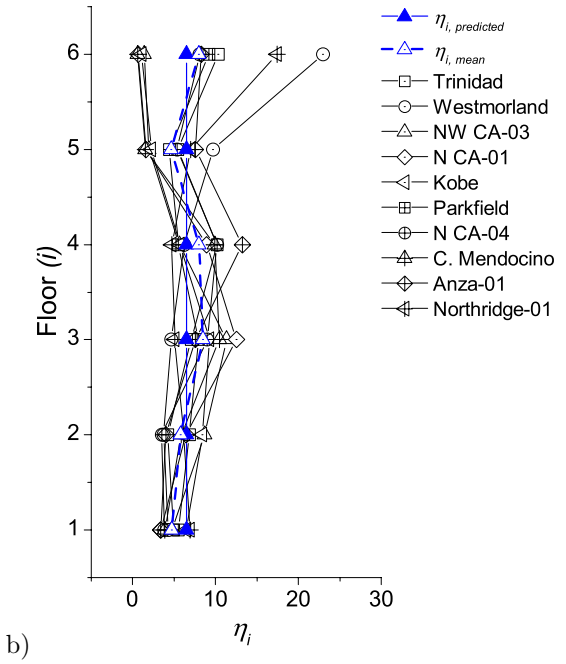

b)

Fig. 5.24: Variation of η_i for T_R= 475years and ground motions with D_f > 12 km, (a) I_d>9 and (b) I_d<9

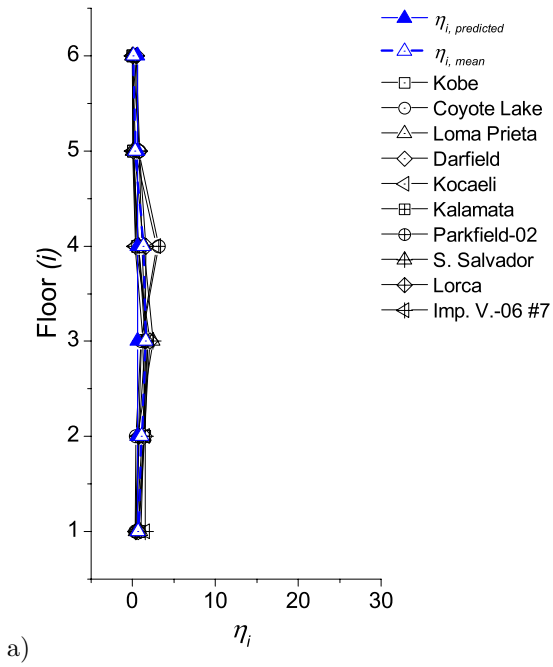

a)

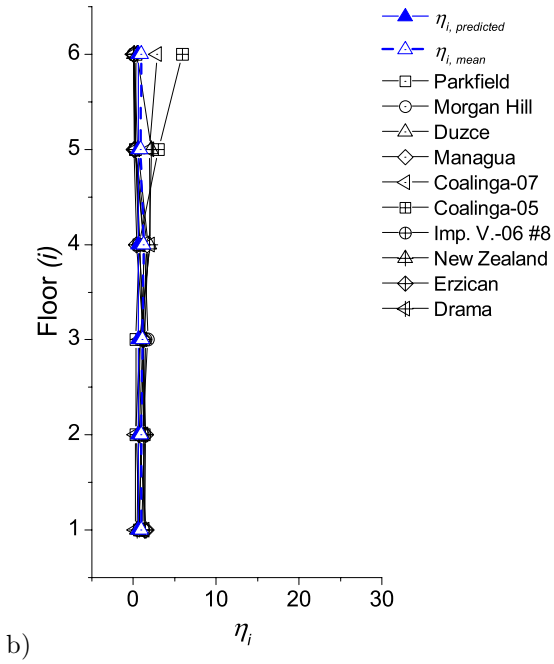

b)

Fig. 5.25: Variation of η_i for T_R= 95years and ground motions with $D_f <$ 12 km, (a) pulse-like and (b) non-pulse like

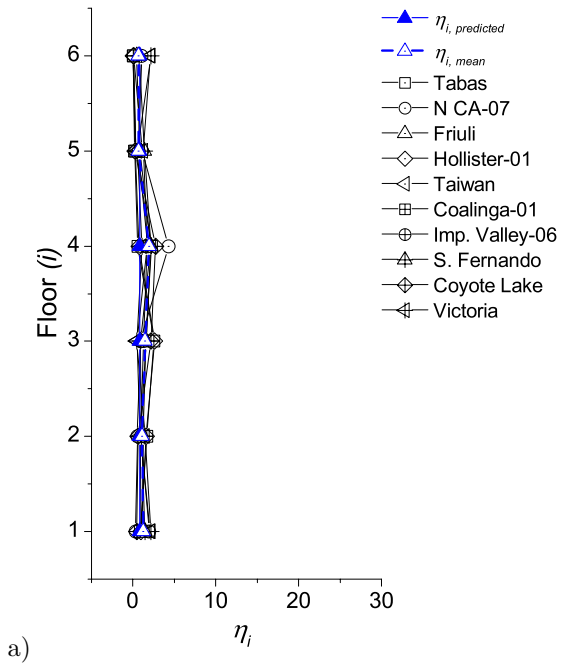

a)

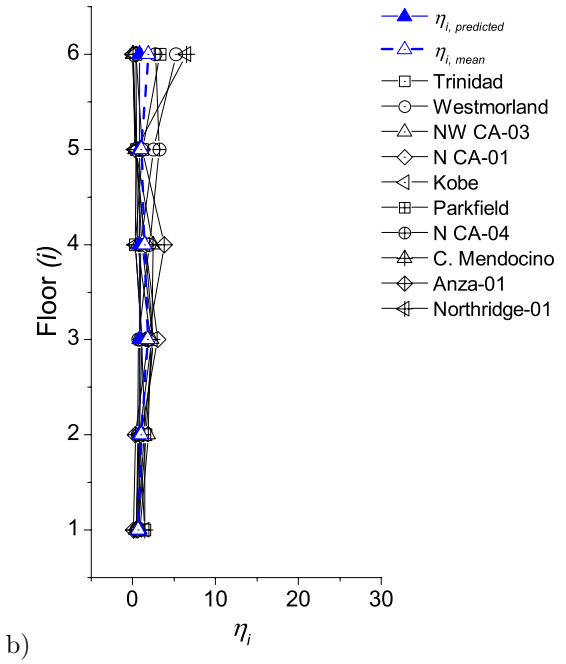

b)

Fig. 5.26: Variation of η_i for T_R= 95years and ground motions with $D_f >$ 12 km, (a) I_d>9 and (b) I_d<9

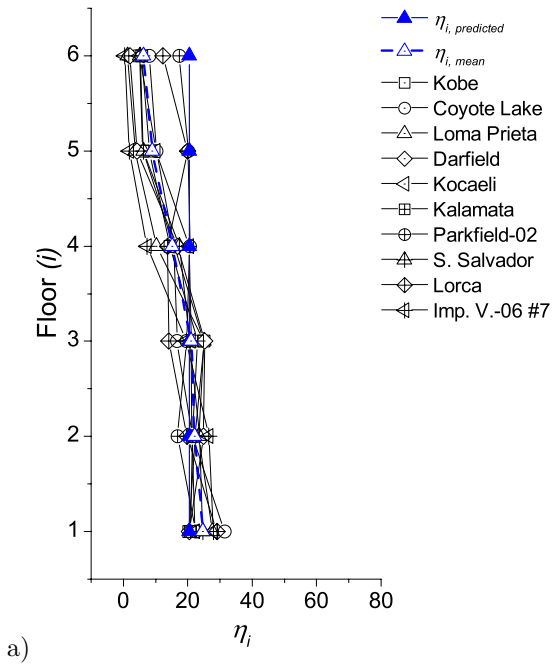

a)

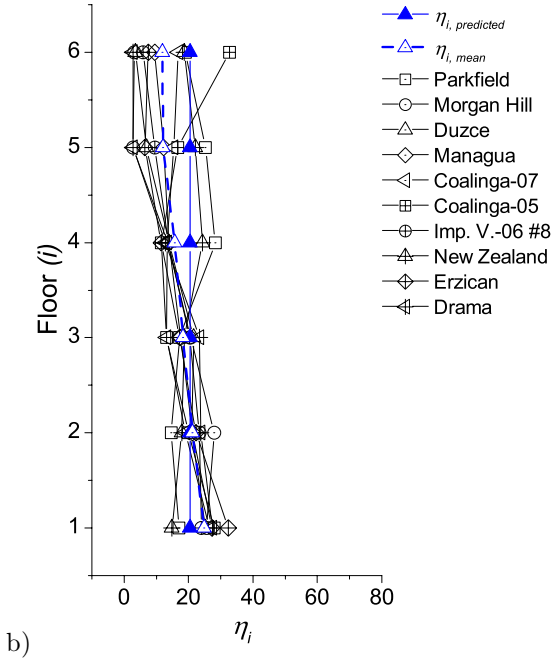

b)

Fig. 5.27: Variation of η_i for T_R= 2475years and ground motions with D_f < 12 km, (a) pulse-like and (b) non-pulse like

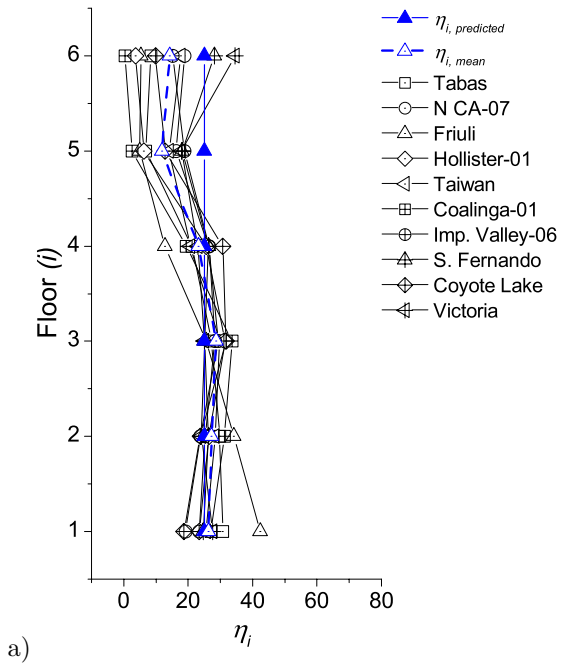

a)

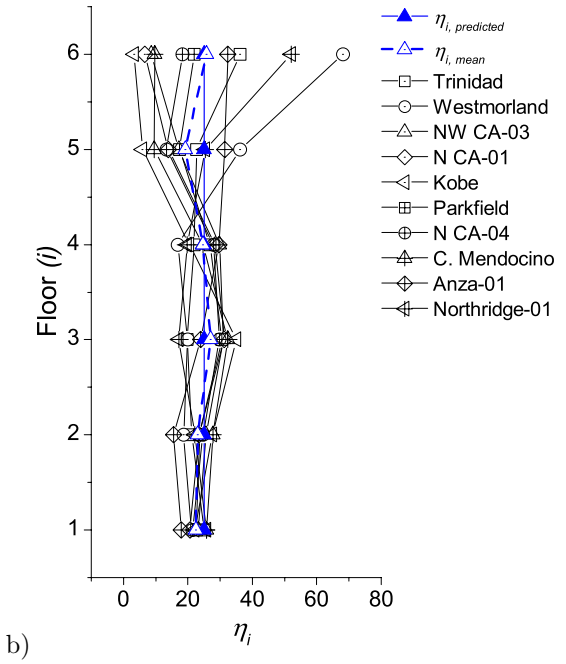

b)

Fig. 5.28: Variation of η_i for T_R= 2475years and ground motions with D_f > 12 km, (a) I_d>9 and (b) I_d<9

5.4.1.5 Maximum plastic deformation ratio, $\mu_{m,i}$

Figs. 5.29 to 5.34 show the variation of $\mu_{m,i}$. The continuous line with blue triangles shows the predicted value of $\mu_{m,i}$. The lines with symbols correspond to numerical simulations carried out with different records. It can be seen that the actual ductility demand characterized with $\mu_{m,i}$, obtained in the dynamic response analyses, is in most cases lower than the prediction. It can be also observed that the responses for T_R=95 years are very stable (i.e. the derivations from the mean are small), and the prediction is close to the mean value.

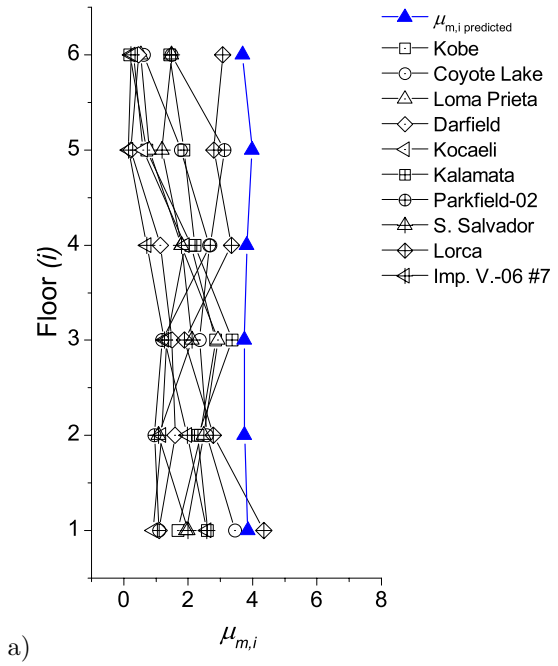

a)

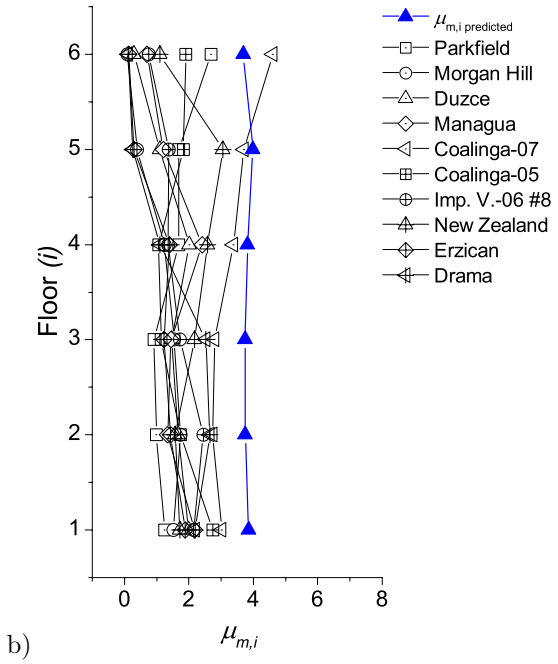

b)

Fig. 5.29: Variation of $\mu_{m,i}$ for T_R= 475years and ground motions with D_f < 12 km, (a) pulse-like and (b) non-pulse like

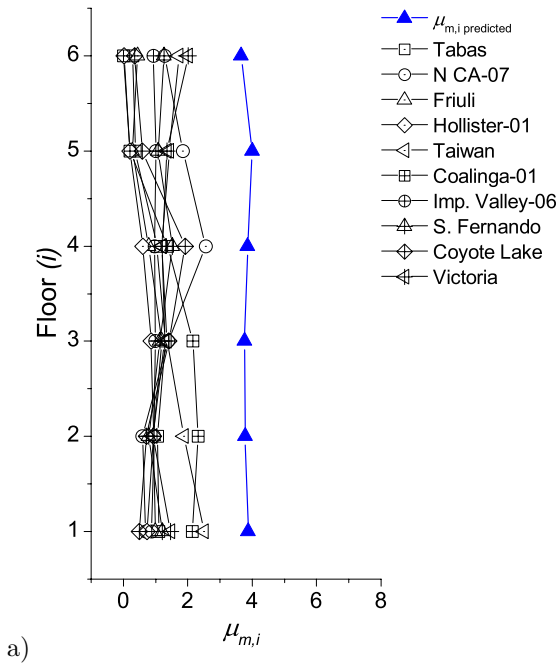

a)

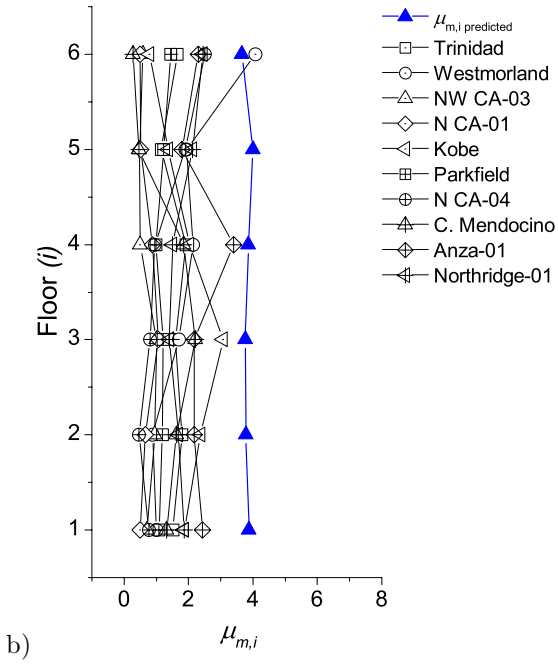

b)

Fig. 5.30: Variation of $\mu_{m,i}$ for T_R= 475years and ground motions with D_f > 12 km, (a) I_d>9 and (b) I_d<9

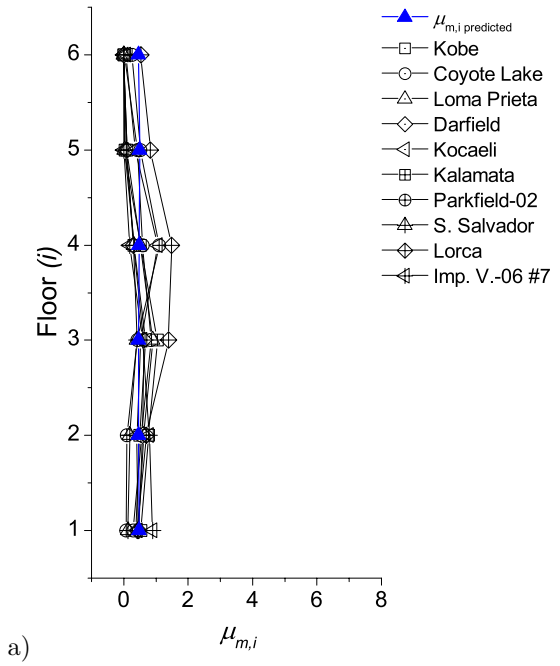

a)

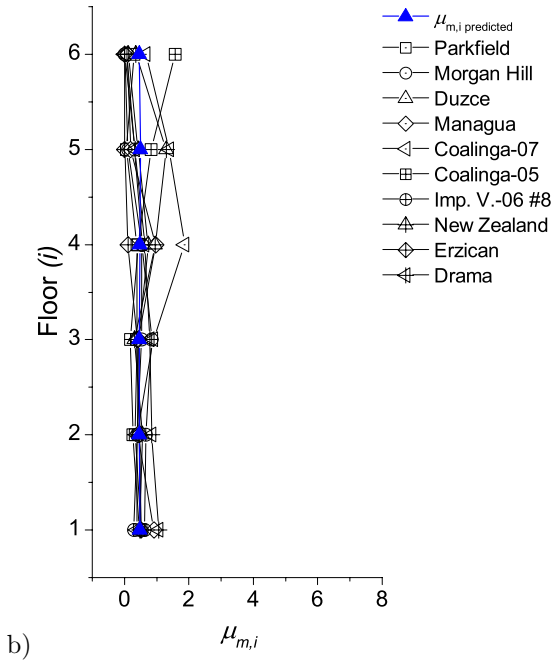

b)

Fig. 5.31: Variation of $\mu_{m,i}$ for T_R= 95years and ground motions with D_f < 12 km, (a) pulse-like and (b) non-pulse like

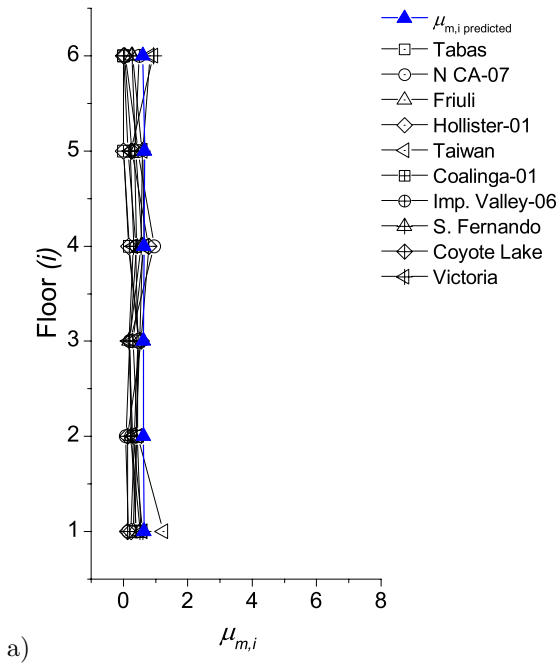

a)

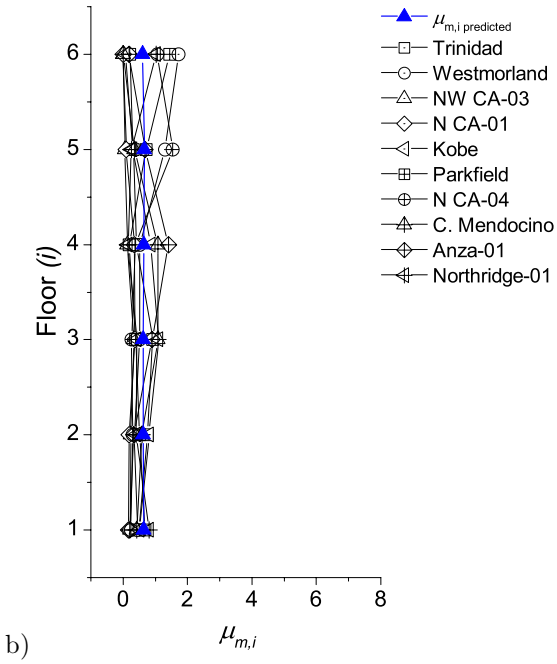

b)

Fig. 5.32: Variation of $\mu_{m,i}$ for T_R= 95years and ground motions with D_f > 12 km, (a) I_d>9 and (b) I_d<9

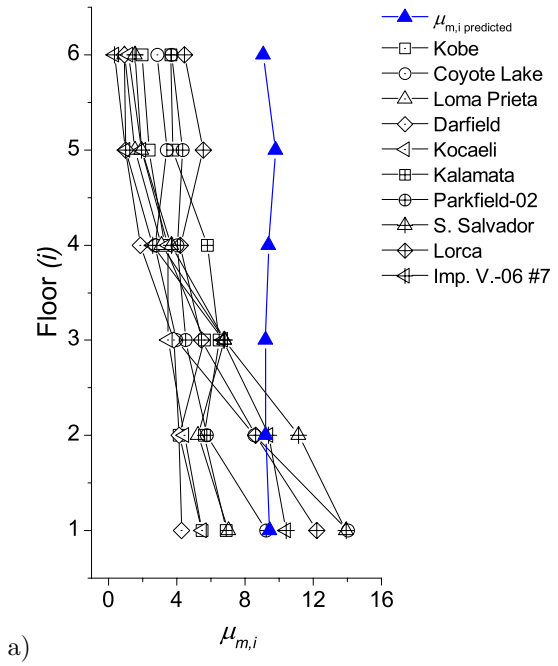

a)

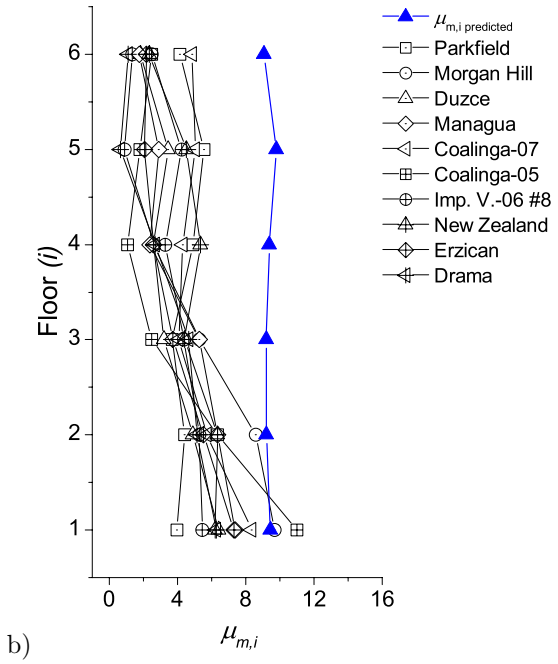

b)

Fig. 5.33: Variation of $\mu_{m,i}$ for T_R= 2475years and ground motions with $D_f <$ 12 km, (a) pulse-like and (b) non-pulse like

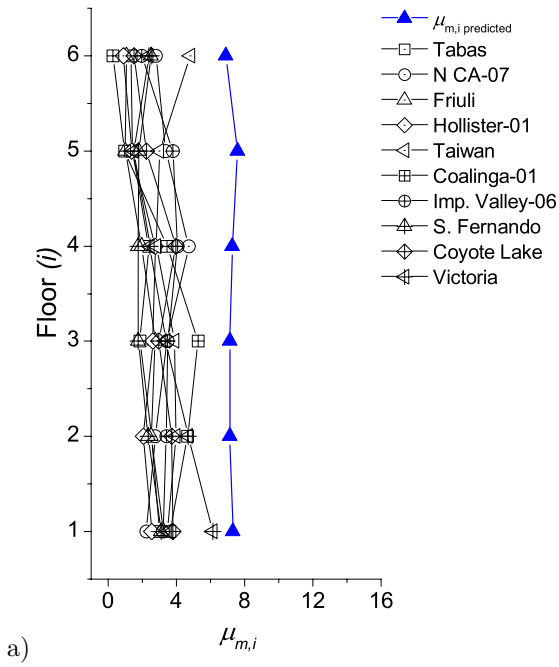

a)

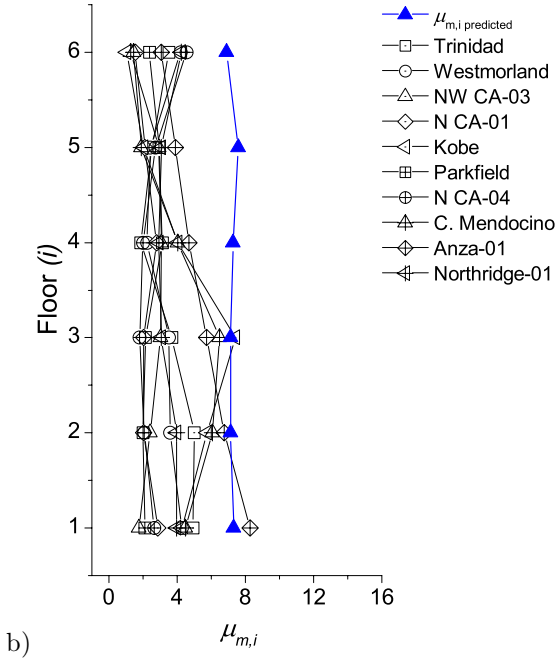

b)

Fig. 5.34: Variation of $\mu_{m,i}$ for T_R= 2475years and ground motions with $D_f > 12$ km, (a) I_d>9 and (b) I_d<9

5.4.1.6 Equivalent number of plastic cycles, $n_{e,i}$

Figs. 5.35 to 5.4 show the variation of $n_{e,i}=\eta_i/\mu_{m,i}$. The continuous line with blue triangles shows the predicted value of $n_{e,i}$. The lines with symbols correspond to numerical simulations carried out with different records. It can be observed that the values of $\eta_i/\mu_{m,i}$ used in the design procedure (i.e. the predicted $\eta_i/\mu_{m,i}$) are approximately a lower bound of the actual values provided by the dynamic response analyses. This means that the prediction of the ratio $\eta_i/\mu_{m,i}$ adopted for the procedure is on the safe side.

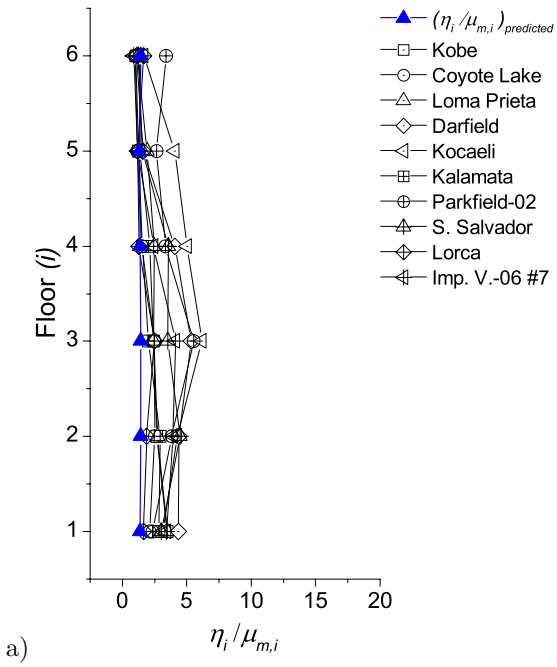

a)

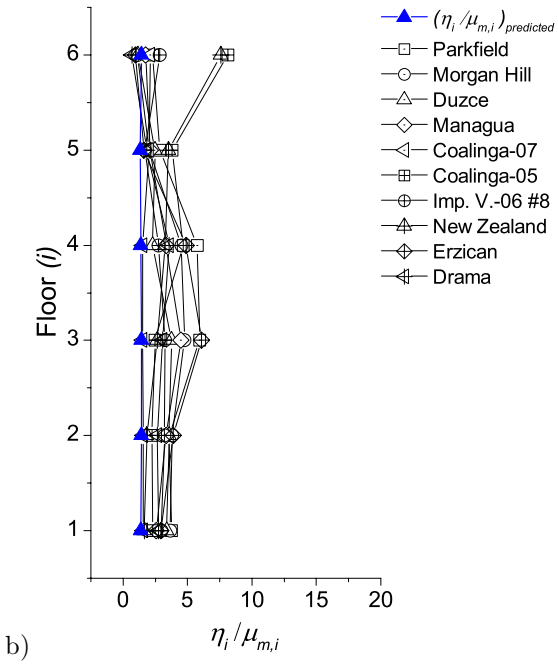

b)

Fig. 5.35: Variation of $\eta_i/\mu_{m,i}$ for T_R= 475years and ground motions with $D_f < 12$ km, (a) pulse-like and (b) non-pulse like

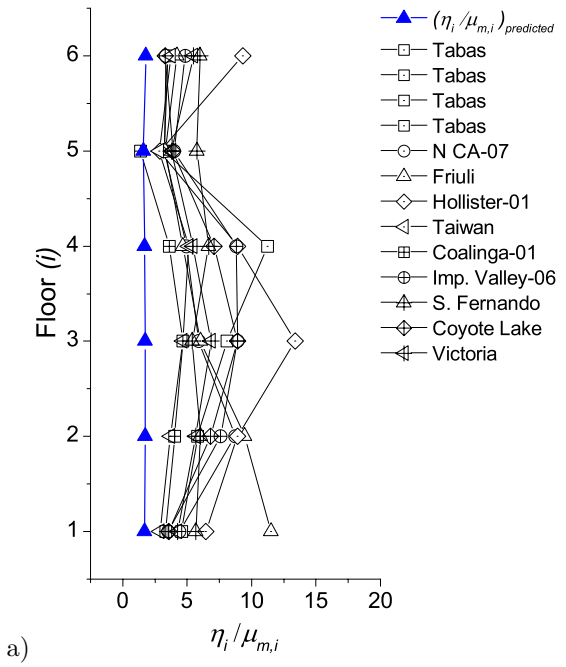

a)

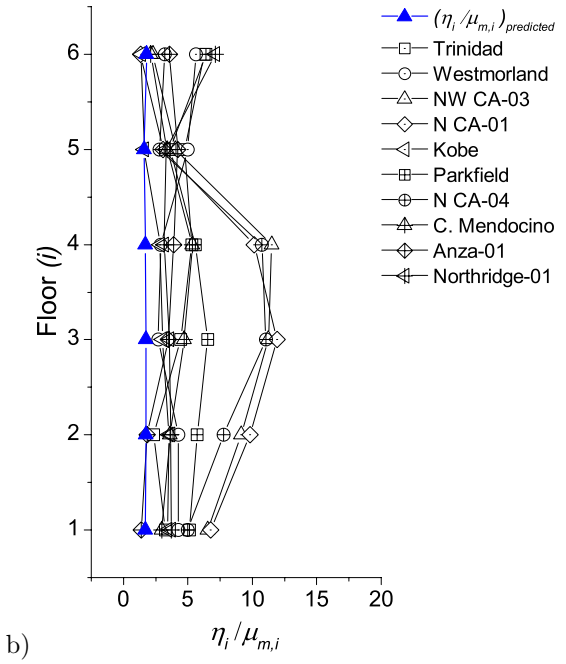

b)

Fig. 5.36: Variation of $\eta_i/\mu_{m,i}$ for T_R= 475years and ground motions with $D_f >$ 12 km, (a) I_d>9 and (b) I_d<9

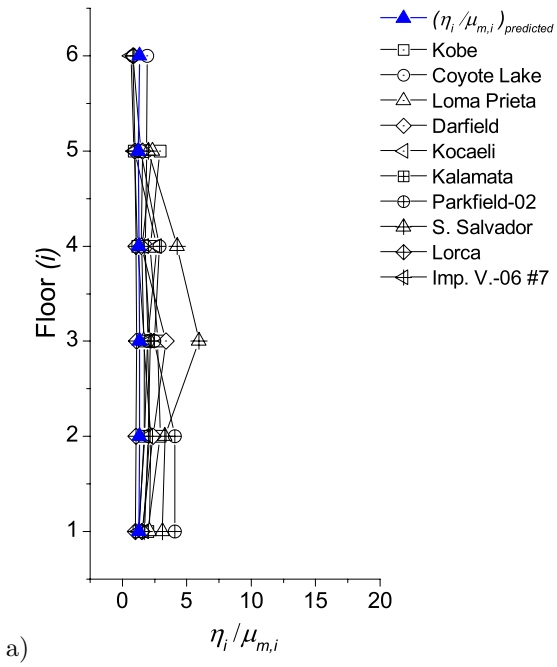

a)

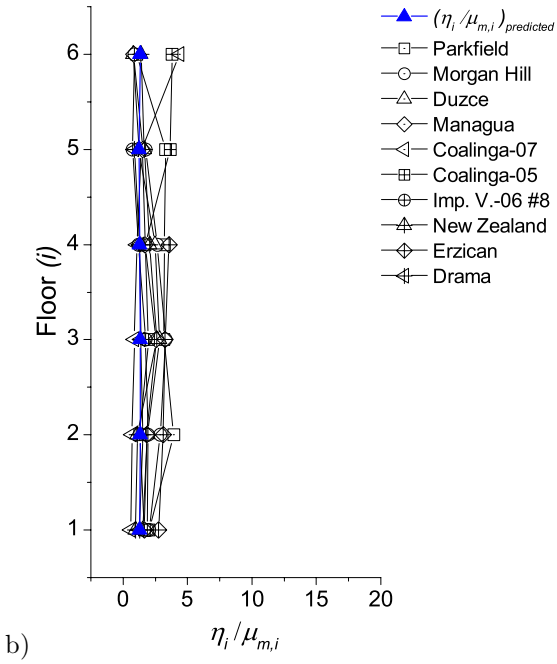

b)

Fig. 5.37: Variation of $\eta_i/\mu_{m,i}$ for T_R= 95years and ground motions with D_f< 12 km, (a) pulse-like and (b) non-pulse like

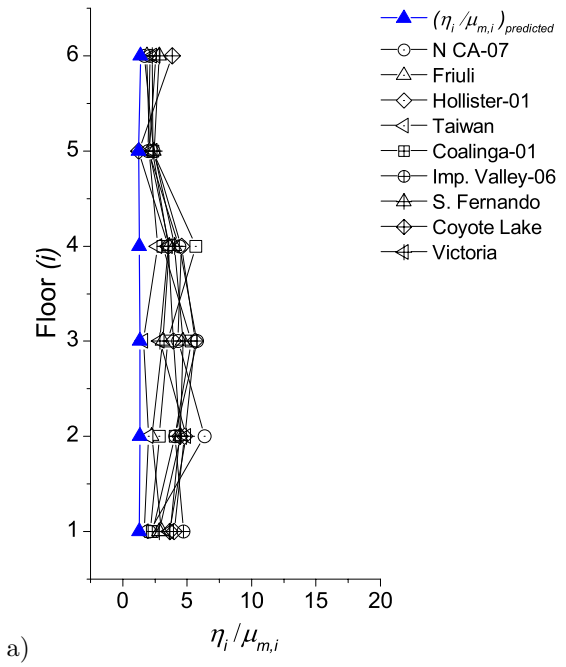

a)

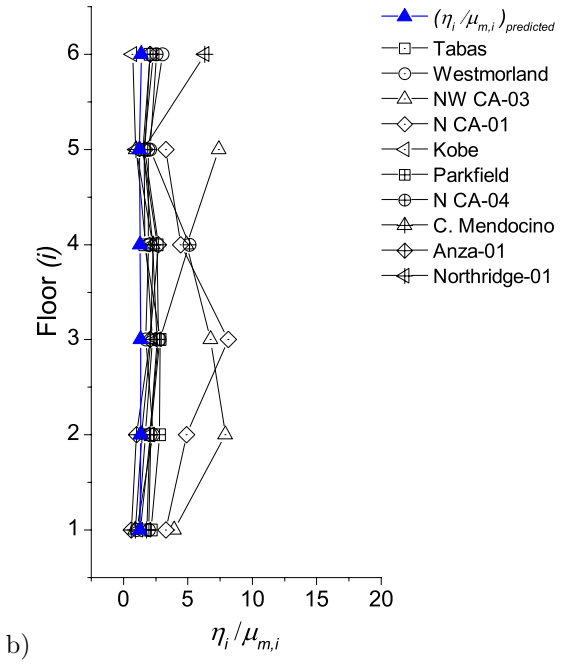

b)

Fig. 5.38: Variation of $\eta_i/\mu_{m,i}$ for T_R= 95years and ground motions with $D_f > 12$ km, (a) I_d>9 and (b) I_d<9

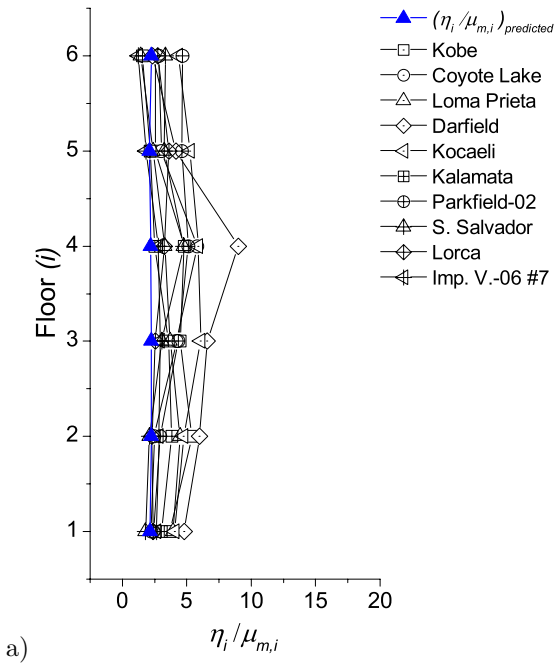

a)

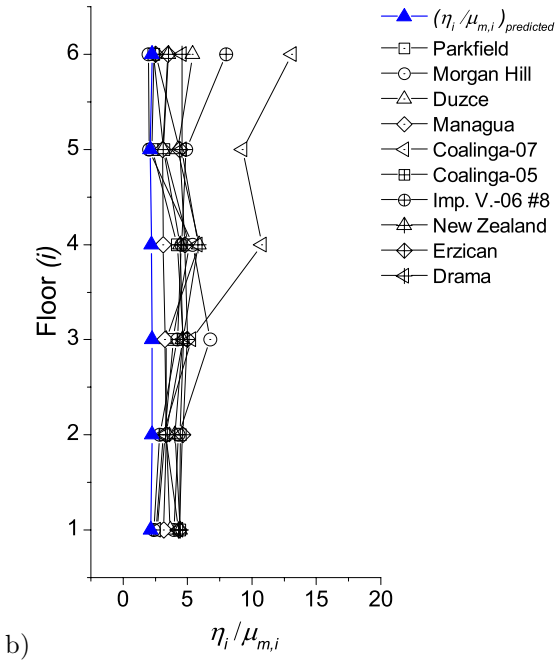

b)

Fig. 5.39: Variation of $\eta_i/\mu_{m,i}$ for T_R= 2475years and ground motions with $D_f < 12$ km, (a) pulse-like and (b) non-pulse like

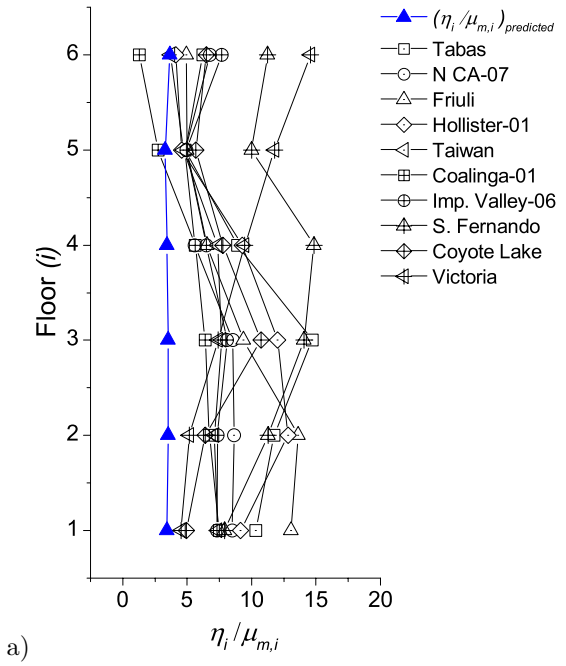

a)

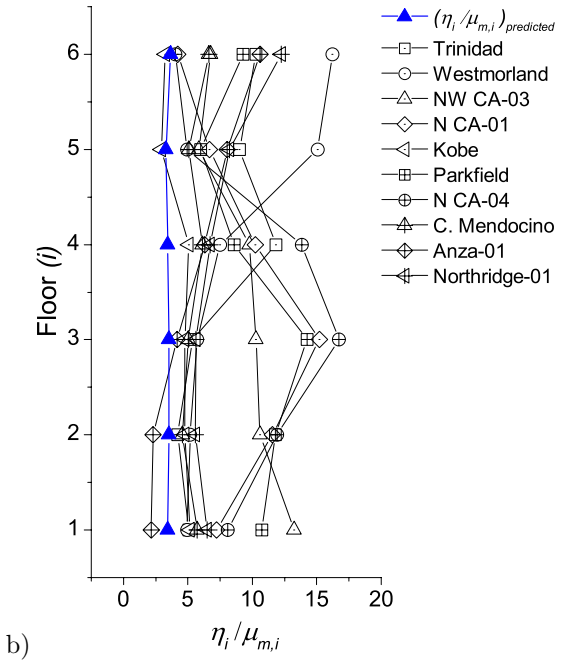

b)

Fig. 5.40: Variation of $\eta_i/\mu_{m,i}$ for T_R= 2475years and ground motions with $D_f > 12$ km, (a) I_d>9 and (b) I_d<9

5.4.1.7 Fraction of plastic strain energy dissipated by the dampers in relation to the total plastic strain energy dissipated at each floor, ${}_sE_{hi}/E_{hi}$

Figs. 5.41 to 5.46 show, for each story, the fraction of energy dissipated by the dampers in relation to the total energy dissipated at each floor (i.e. by the dampers and by the main frame), ${}_sE_{hi}/E_{hi}$. The dash dot blue line shows the maximum relative value of 1. The lines with symbols correspond to numerical simulations carried out with different records. In all cases, it can be seen that most of the "damaging" plastic strain energy is dissipated by the dampers (between 85% and 100% approximately).

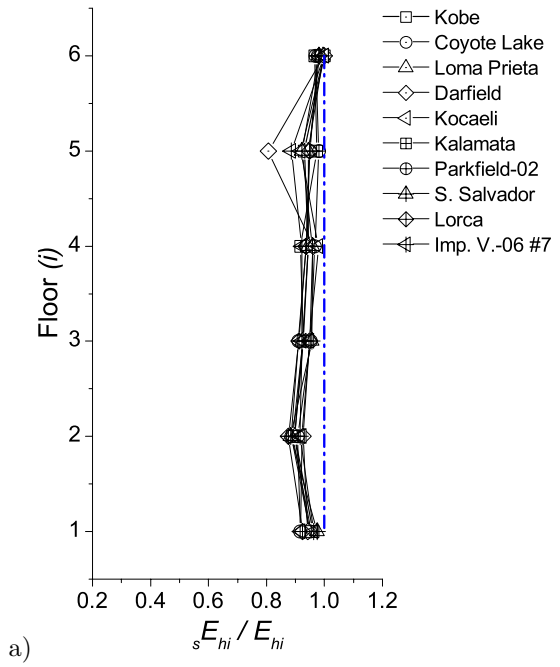

a)

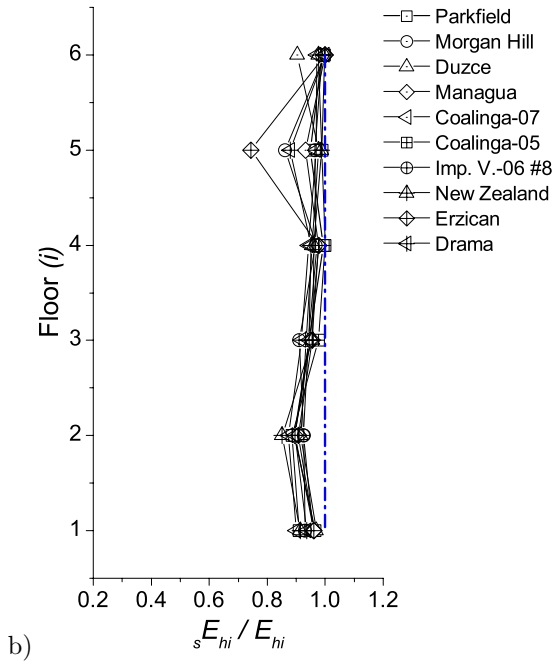

b)

Fig. 5.41: Variation of $_sE_{hi}/E_{hi}$ for T_R= 475years and ground motions with D_f< 12 km, (a) pulse-like and (b) non-pulse like

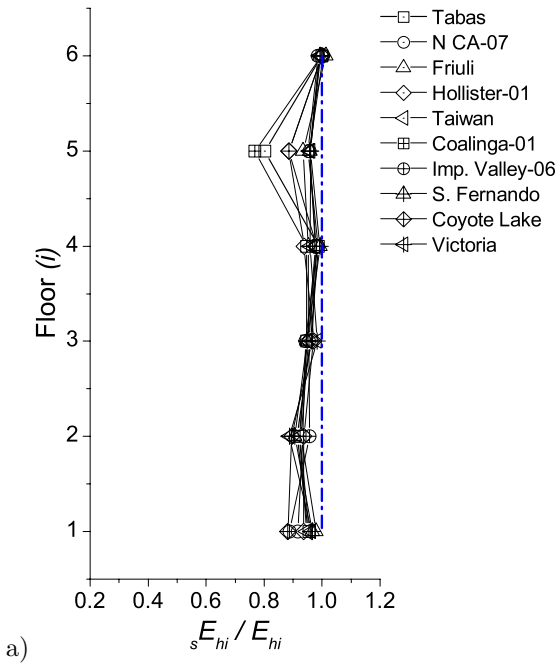

a)

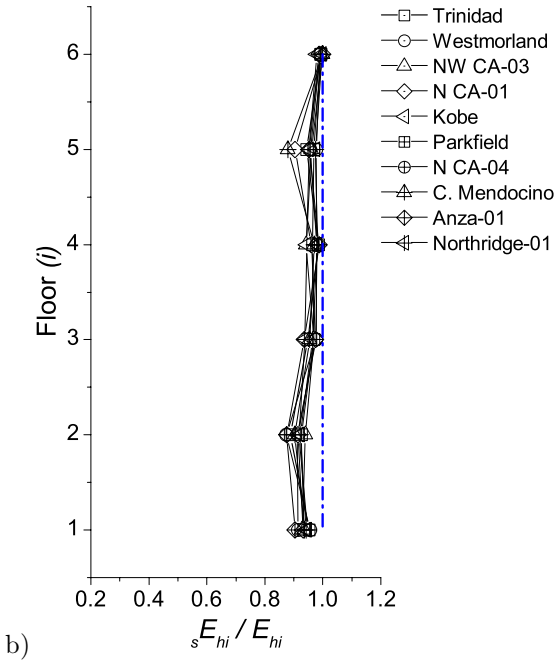

b)

Fig. 5.42: Variation of $_sE_{hi}/E_{hi}$ for T_R= 475years and ground motions with $D_f >$ 12 km, (a) I_d>9 and (b) I_d<9

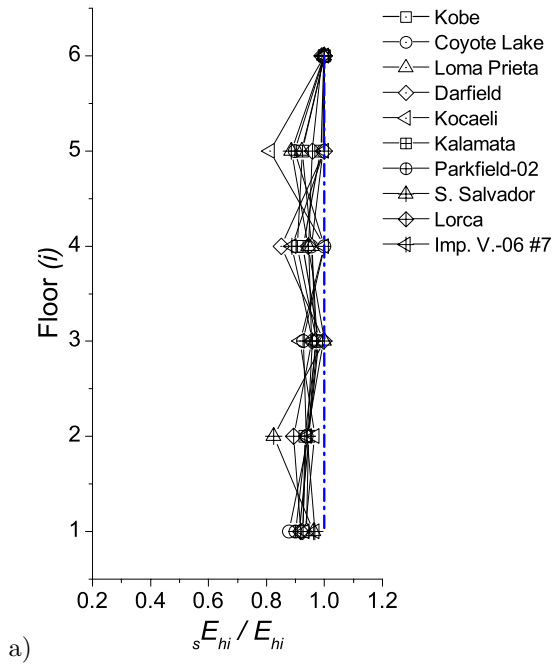

a)

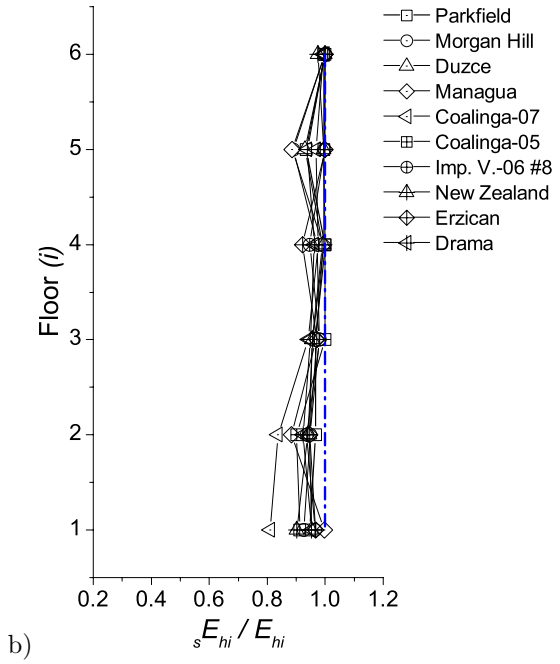

b)

Fig. 5.43: Variation of ${}_sE_{hi}/E_{hi}$ for T_R= 95years and ground motions with $D_f < 12$ km, (a) pulse-like and (b) non-pulse like

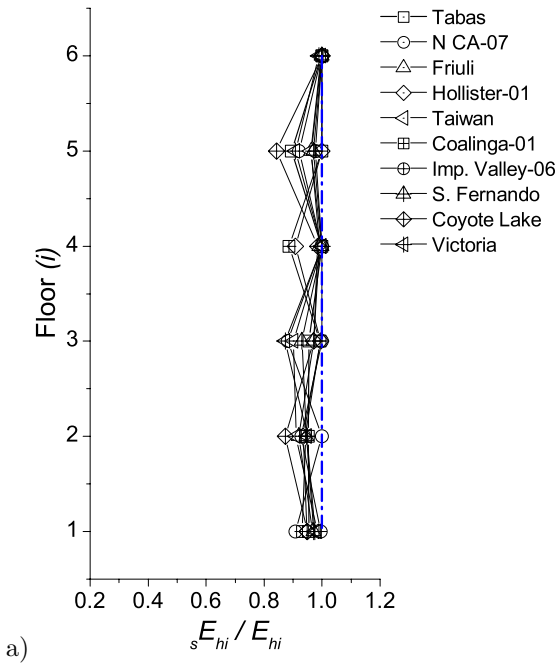

a)

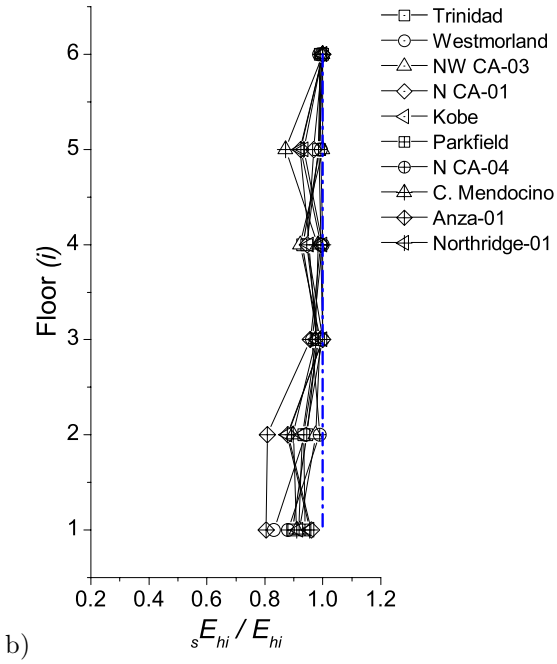

b)

Fig. 5.44: Variation of $_sE_{hi}/E_{hi}$ for T_R= 95years and ground motions with $D_f >$ 12 km, (a) I_d>9 and (b) I_d<9

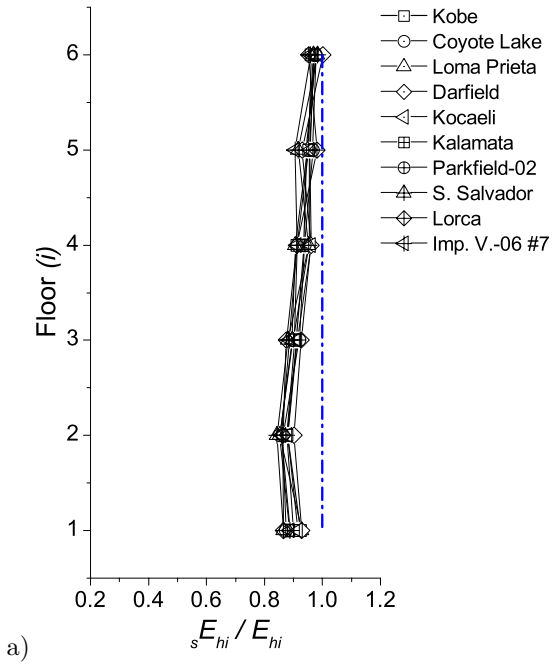

a)

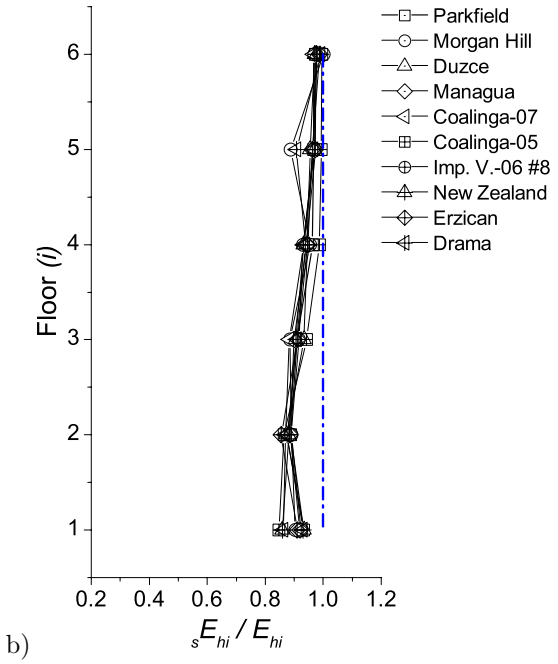

b)

Fig. 5.45: Variation of $_sE_{hi}/E_{hi}$ for T_R= 2475years and ground motions with $D_f < 12$ km, (a) pulse-like and (b) non-pulse like

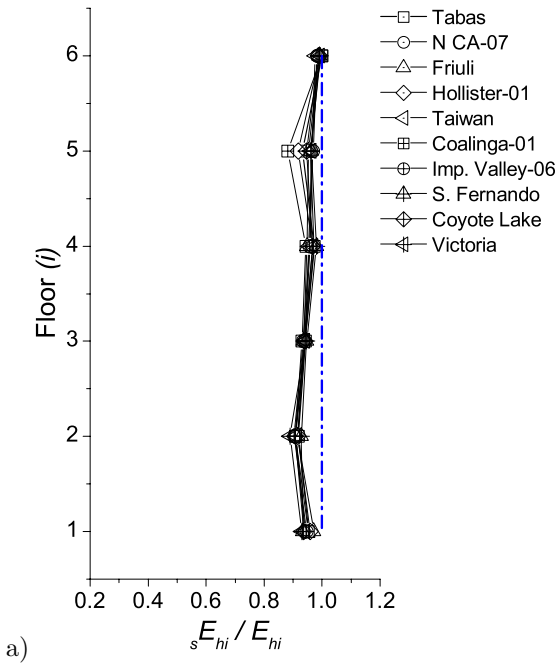

a)

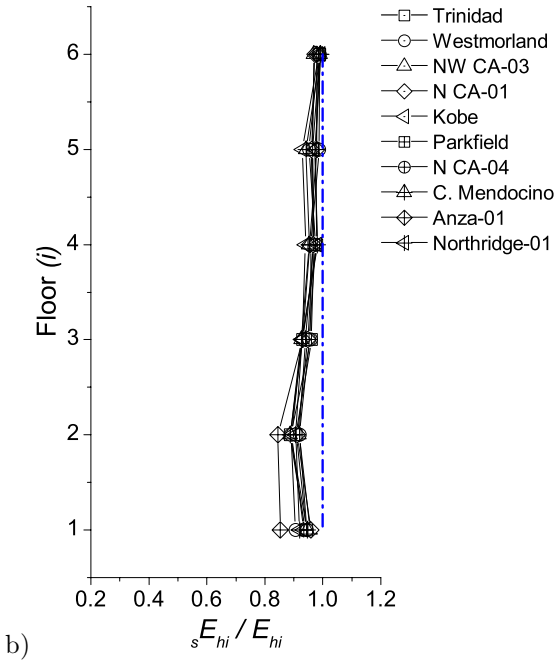

b)

Fig. 5.46: Variation of $_sE_{hi}/E_{hi}$ for T_R= 2475years and ground motions with $D_f > 12$ km, (a) I_d>9 and (b) I_d<9

5.4.1.8 *Fraction of plastic strain energy dissipated by the dampers in relation to the total plastic strain energy dissipated by the whole structure, ${}_sE_{hi}/E_{ht}$*

Figs. 5.47 to 5.52 show, for each story, the fraction of plastic strain (hysteretic) energy dissipated by the dampers in relation to the total plastic strain (hysteretic) energy dissipated by the whole structure, ${}_sE_{hi}/E_{ht}$. The continuous line with blue triangles shows the predicted value of ${}_sE_{hi}/E_{ht}$. The lines with symbols correspond to numerical simulations carried out with different records. The discontinuous line with white triangles shows the mean value of ${}_sE_{hi}/E_{ht}$, computed over the numerical simulations shown in the graph. It can be observed that the distribution curve assumed in the proposed procedure (i.e. the curve called "Predicted") is very close to the mean curve obtained from the dynamic response analyses.

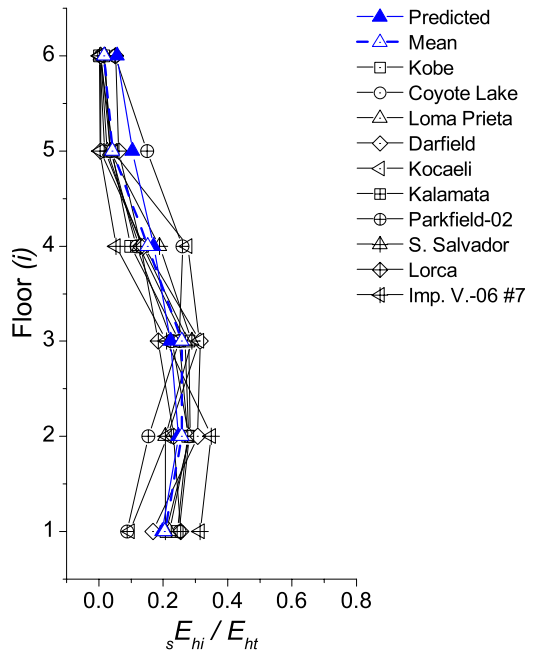

a)

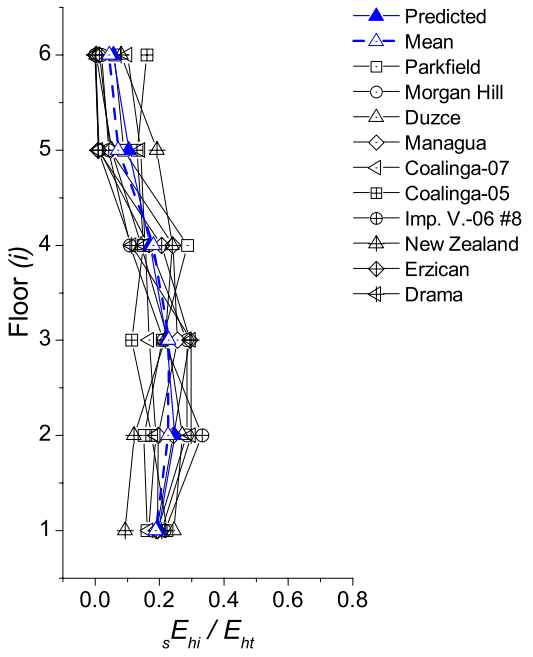

b)

Fig. 5.47: Variation of $_sE_{hi}/E_{ht}$ for T_R= 475years and ground motions with D_f< 12 km, (a) pulse-like and (b) non-pulse like

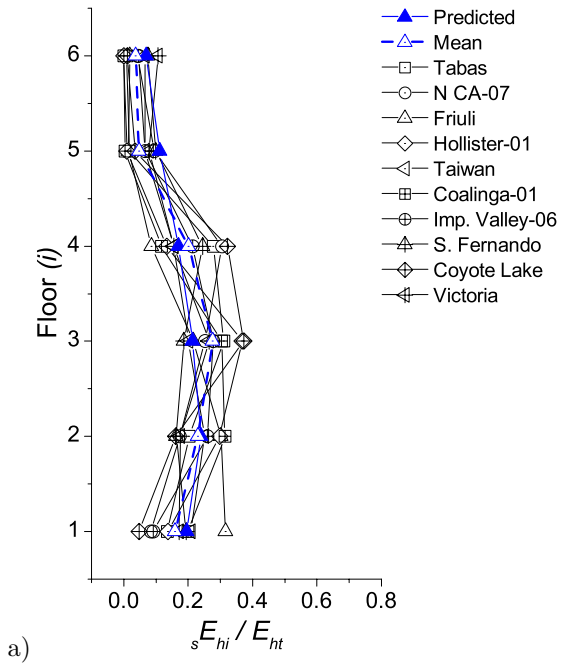

a)

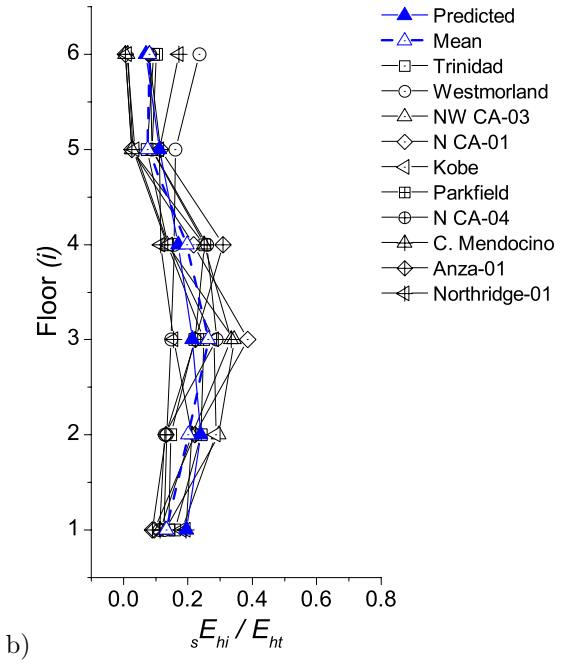

b)

Fig. 5.48: Variation of $_sE_{hi}/E_{ht}$ for T_R= 475years and ground motions with D_f> 12 km, (a) I_d>9 and (b) I_d<9

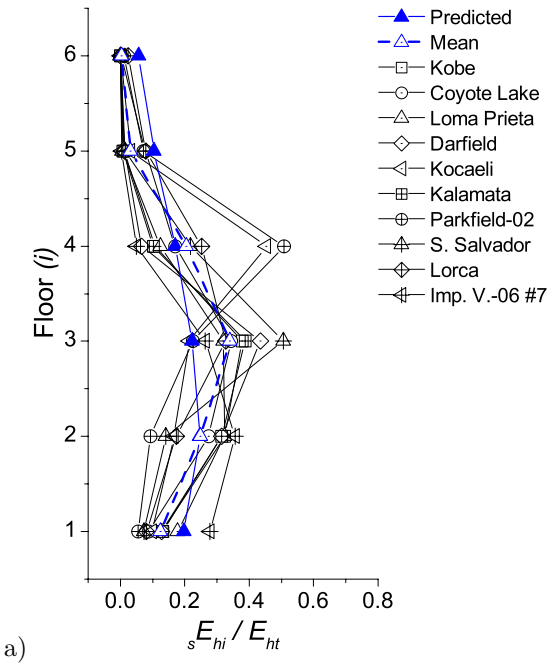

a)

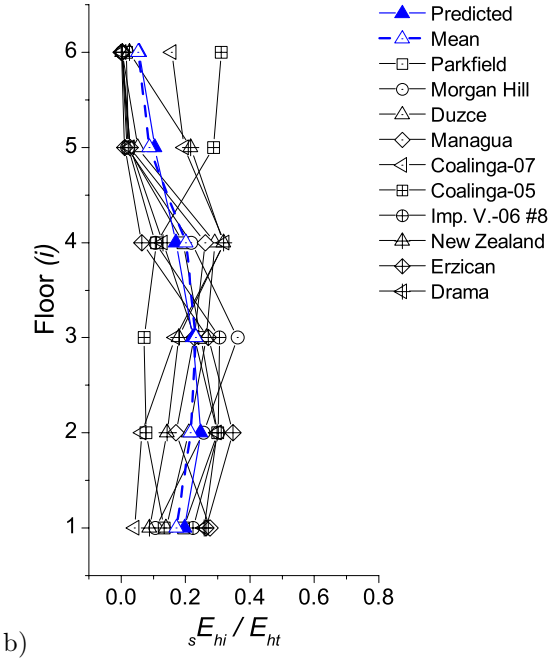

b)

Fig. 5.49: Variation of $_sE_{hi}/E_{ht}$ for T_R= 95years and ground motions with D_f< 12 km, (a) pulse-like and (b) non-pulse like

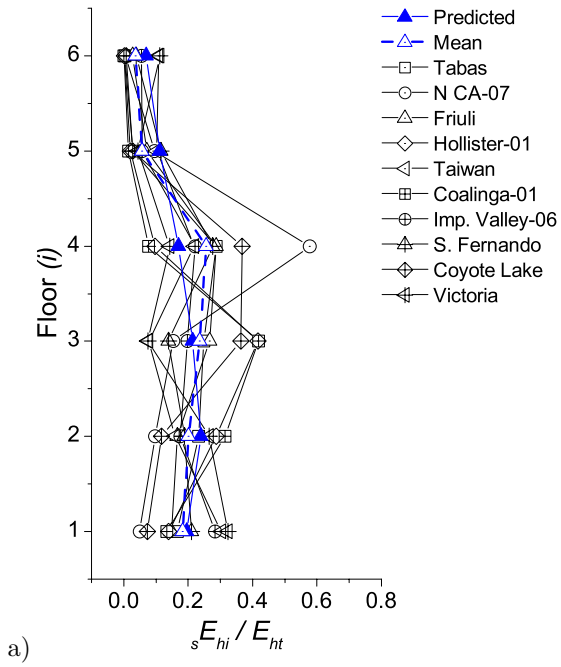

a)

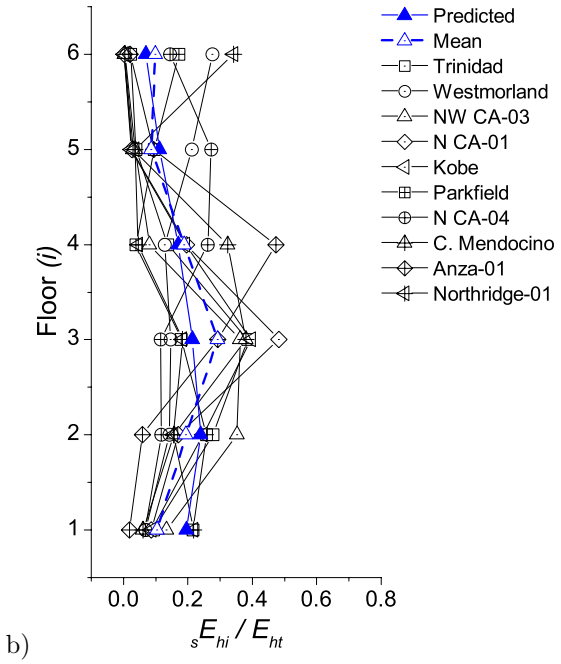

b)

Fig. 5.50: Variation of $_sE_{hi}/E_{ht}$ for T_R= 95years and ground motions with $D_f >$ 12 km, (a) I_d>9 and (b) I_d<9

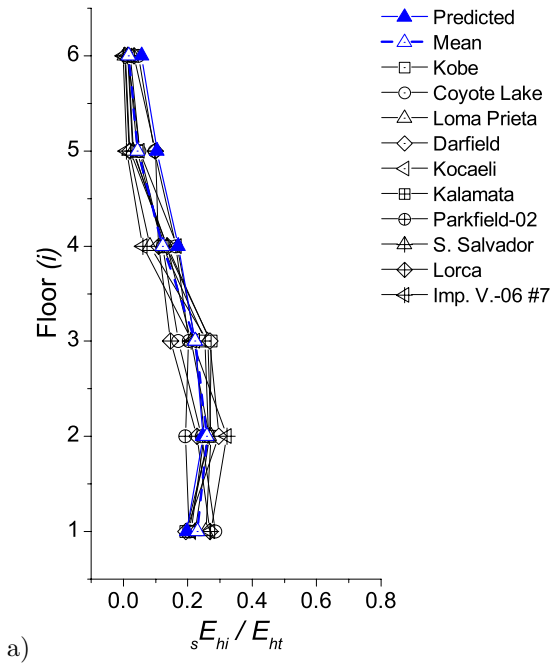

a)

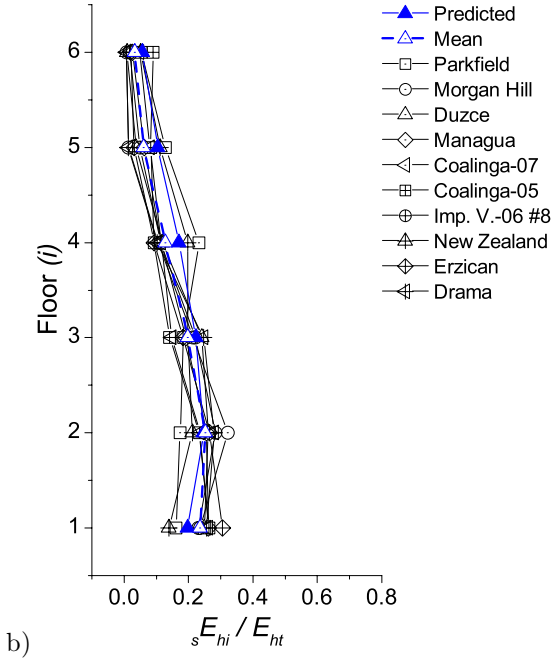

b)

Fig. 5.51: Variation of ${}_sE_{hi}/E_{ht}$ for T_R= 2475years and ground motions with $D_f <$ 12 km, (a) pulse-like and (b) non-pulse like

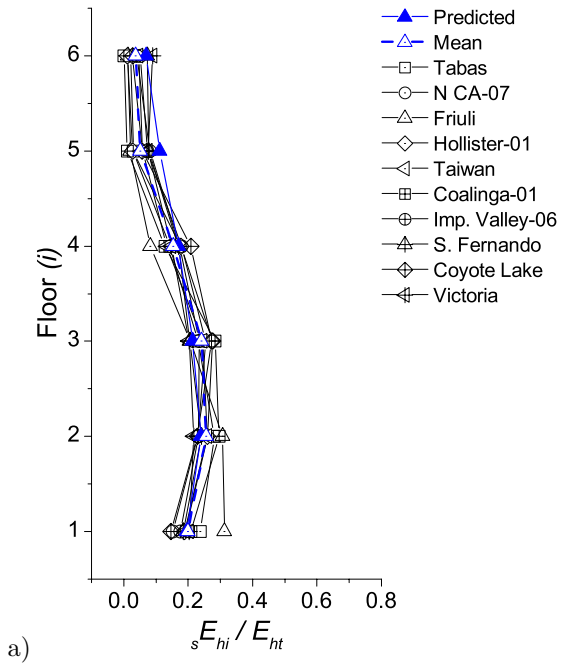

a)

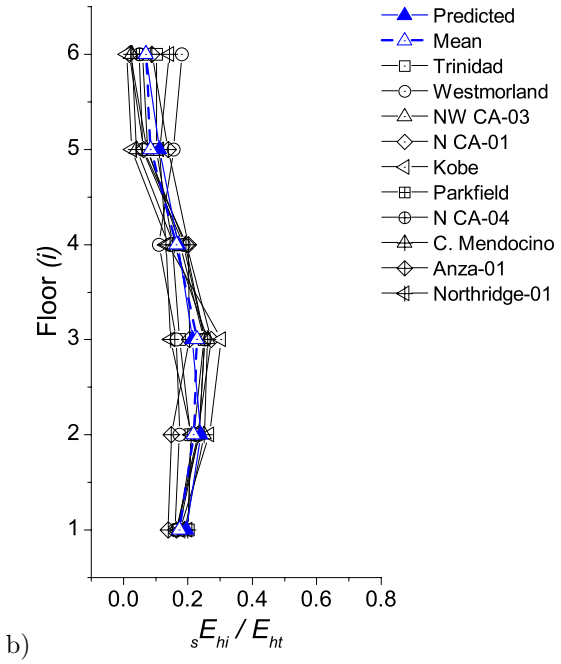

b)

Fig. 5.52: Variation of ${}_sE_{hi}/E_{ht}$ for T_R= 2475years and ground motions with $D_f > 12$ km, (a) I_d>9 and (b) I_d<9

6

Conclusions

1. The present Thesis has investigated a retrofitting solution for under-designed RC frame buildings that combines hysteretic-type energy dissipation devices (dampers) with member strengthening by means of composite materials (FRP and SRP). The dampers are installed like conventional diagonal braces (brace-type hysteretic dampers). Adding energy dissipation devices provides the structure not only the strength and deformation necessary to ensure life safety, but also the supplemental energy dissipation capacity required to reduce structural and non-structural damage. However, when retrofitting an under-designed RC frame structure with brace-type hysteretic dampers, two particular problems have been identified: (i)

the connection of the brace-type dampers with the existing frame is a matter of major concern, since the steel brace may develop high axial loads; and (ii) the existing main frame may not have enough lateral deformation capacity for the dampers to deform in the plastic range and to develop efficiently their inherent energy dissipation capacity.

2. A new solution for connecting concentric braces to beam-column joints of existing reinforced concrete frames has been proposed, suitable for connecting either a conventional concentric steel brace or a brace-type hysteretic damper. The connection consists of two shear-key steel plates fixed to the concrete with anchor bolts, and a device for minimizing the friction between these shear-key plates and the end-plates of the brace. The addition of a low-friction device practically eliminates tension forces on the anchor bolts and reduces bending moments on the shear-key plates. As a result, thinner plates without stiffeners can be used as shear-key plates; brittle failure modes on the anchors are avoided; and reduced number of anchors and effective anchorage depth are required.
3. A 3D finite element model has been developed to clarify: (1) the influence of initial gaps, t_g, between the shear-key plates and the end-plate of the brace, and (2) the thickness

of the Teflon sheets, t_t. The performance of the proposed connection was satisfactory for all combinations of t_g and t_t. The thickness of the Teflon sheets, t_t, showed no influence on the behavior, whereas the initial gap, t_g, increased the lateral displacement required to mobilize the damper, although this was relatively small even for the largest value of t_g considered.

4. Execution provisions have been proposed for the new brace-frame connection, which are summarized as follows: (1) a clearance up to 2mm shall be allowed between the diameter of the holes and the diameter of the anchor bolts, and this clearance should be filled with epoxy or high strength cement grout; (2) the width t_g of the initial gap between the shear-key plates and the end-plate of the brace must be less than 2mm and must satisfy the limits established from the geometrical relationships described between the thickness of the shear-key plate and the relative distance t_g. This ensures that he thickness of the shear-key plates is large enough to remove the risk of the brace "running away", when it is subjected to high axial tension forces. In addition, the flexural deformations of beams and columns have a beneficial fastening effect when the damper is in tension that also reduces this risk.
5. Design criteria of the brace-frame connection have been proposed. Expressions for the shear and axial forces acting

on each anchor, and the bending moment acting on the fixture, have been derived by decomposing the maximum axial force developed by the brace. However, the proposed beam-frame connection cannot be applied if the quality of the concrete is too poor, and thus, the anchorage of the shear-key plate to the concrete members cannot be guaranteed.

6. The efficiency and validity of the proposed brace-frame connection has been evaluated by means of shaking-table tests conducted on a 3x3x3 m^3 scaled reinforced concrete frame retrofitted with brace-type hysteretic dampers. The main conclusions reached for these tests are as follows:
   a. The braces installed with the proposed brace-frame connection successfully controlled the damage on the main frame. On one hand, the retrofitted structure exhibited seismic performance levels of “immediate occupancy”, for the design ground motions associated with a mean return period up to 500 years, and of “life safety”, for more severe earthquakes with longer mean return periods (1435, 2032, and 2828 years).
   b. The RC frame remained basically elastic. It experienced minor plastic deformations (small damage), excluding the bottom ends of the columns when the structure was subjected to the most severe earthquakes. For the design ground motions associated

with a mean return period up to 500 years, the rotation demand was far below yielding, and the Park and Ang damage index was very small. During seismic simulations corresponding to earthquakes with longer mean return periods (1435, 2032, and 2828 years), the rotation demand slightly exceeded the yield rotation and the Park and Ang damage index was very small, except at the bottom end of the columns.

c. The shear values attained during the tests were considerably lower than the shear resistance of the columns calculated without shear reinforcement, showing that there was no need to increase the global shear resistance of the existing columns.

d. The sum of the plastic and elastic strain energy dissipated by the RC frame was negligible in comparison with the energy dissipated by the EDDs, as expected.

e. The response of the hysteretic dampers was stable and the proposed brace-frame connection was effective in mobilizing the energy dissipation capacity of the hysteretic dampers. On the other hand, although the dampers remained elastic for the earthquakes with mean return periods lower than 500years, the dampers suffered large plastic deformations for the severe earthquakes with longer mean return periods.

f. The damage suffered by the hysteretic dampers was characterized by the index $\overline{ID}$ proposed by Benavent-Climent (2007), showing that the dampers approached their ultimate capacity at the end of the most severe simulation (2828 years).

g. The relative movements between the end-plates of the damper and the beam-column joints to which they were fastened were negligible.

h. The addition of low-friction material at the contact surface between the end-plate of the brace and the horizontal shear-key plate increased the normal stresses in the latter at the vicinity of the contact surface —in comparison to the brace-frame connection without low-friction material. The relative displacements and rotations were similar, yet small.

7. An energy-based seismic design procedure has been proposed, based on the method developed by Benavent-Climent (2011) for the retrofitting of existing RC frame structures with hysteretic dampers. The new procedure considers the possibility of locally strengthening the main frame (e.g. by adding FRP/SRP). This ensures the existence of a solution for the design of the dampers that meets the drift requirements at each floor, for different performance objectives.

8. The retrofitting solution and the energy-based seismic design procedure have been validated by means of nonlinear time history analysis. To this end, an upgrading solution with hysteretic dampers and local strengthening with FRP/SRP was designed, by following the proposed energy-based seismic design procedure. Thus, a six-story prototype RC frame structure —representative of pre-70 residential buildings was upgraded for different types of earthquakes (near-fault and far-field), and three levels of seismic hazard (corresponding to mean return periods 95, 475 and 2475 years). Afterwards, a numerical model capable of reproducing the performance of the under-designed RC frame structure, upgraded with the proposed solution, was developed, and subjected to two sets of 20 natural acceleration records —far-field and near-fault.
    a. In general, good agreement was found between the overall performance obtained from the dynamic response analysis, and the behavior anticipated in the design. However, further research should be carried out in the future to improve the response for the case of near-fault pulse-like records and high seismic hazard levels corresponding to T_R=2475years. Future research should deepen in the consideration of a non-perfectly elastic flexible part.

b. As intended in the design procedure, the normalized cumulative plastic deformation energy (represented by parameter η_i) was almost constant among the stories, and the small variations occurred smoothly over the different floors of the building. This indicated that there was no concentration of damage. In addition, although the predicted values of η_i varied with respect to the observed values for the individual simulations, the average value at each floor level matched reasonably well the predicted ones.

c. In most cases, the predicted values of the normalized maximum deformation (represented by parameter $\mu_{m,i}$) were greater than those obtained in the numerical analyses. The few exceptions occurred in the lower floors of pulse-like records and T_R=2475years. This gives a safe-side estimation of the maximum interstory drift.

d. For most cases, the predicted values of the ratio $n_{e,i.}=\eta_i / \mu_{m,i}$ were lower than the observed ones, which were considered a safe-side approach (since maximum displacements $\delta_{m,i}$ were inversely proportional to $n_{e,I}$).

e. At each story level, the observed ratio of energy dissipated by dampers to total energy dissipated in the story, ${}_sE_{hi}/E_{hi}$ were near 1 for all cases, thus indicating

that the dampers (stiff-part) dissipated most of the energy dissipated at each floor.

f. The ratio of plastic strain energy at each story level to the total plastic strain energy dissipated by the whole building, ${}_sE_{hi}/E_{ht}$, averaged over the different ground motions, matched reasonably well the predicted distribution.

7

Recommendations for future work

- Conduct further experimental tests to verify the influence of some parameters on the performance of the proposed brace-connection and to further develop practical application guidelines. In particular, the factors that require special attention are:
    - the strength of the concrete base;
    - the initial gap between the steel plates;
    - the thickness of the Teflon sheets;
    - the friction coefficient of the Teflon sheets;
    - the type of anchoring system (mechanical and chemical anchors); and
    - the presence of local strengthening (e.g. adding FRP/SRP).

- Deepen the study on the "best" combination of hysteretic dampers with member strengthening with FRP/SRP. In this sense, a simplified procedure for selecting the optimum solution in terms of economic efficiency and practical purposes must be developed by
    - performing an extensive parametric study over the set of valid solutions;
    - performing an economic assessment of the different retrofitting solutions and expressing options in terms that enable stakeholders to make informed decisions; and
    - integrating the design procedure into a performance-based probabilistic approach that quantifies the uncertainties associated to the prediction of the response and allows to assess its behavior in terms that also fit the necessities of the skateholders.
- Improve the response of the retrofitting solution for the case of near-fault pulse-like records and high seismic hazard levels (i.e. T_R=2475years) by
    - incorporating the consideration of a non-perfectly elastic flexible part in the proposed energy-based method; and

- identifying the influence of the seismic parameters that are characteristic of pulse-like records, on the estimation of $\delta_{m,i}$.

- Deepen the study of the influence of I_d on the prediction of the $\delta_{m,i}$ to narrow the validity of the proposed solution for a specific earthquake scenario.
- Test the validity and efficiency of the proposed hybrid retrofitting solution on a shake-table by
  - designing a retrofitting solution for a prototype structure upgraded with hysteretic dampers and local strengthening (i.e. FRP/SRP); and
  - subjecting the specimen to different types of natural records (near-fault and far-field) and increasing intensity level.

Annex A: Elastic response spectra of the accelerograms used in the analyses

A. 1 Selected ground motions with $D_f < 12km$

A. 1. 1 Pulse-like

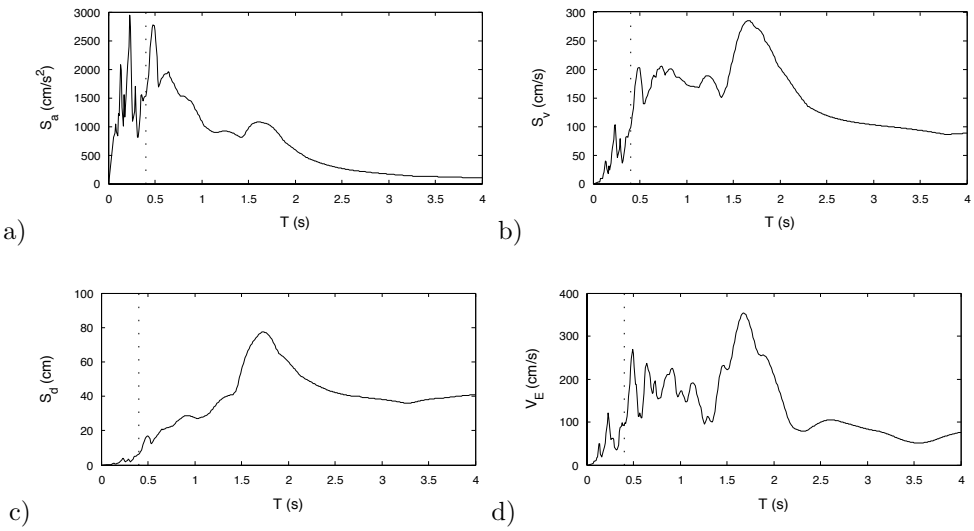

Fig. A.1 Kobe, Japan (Takarazuka, 1995). Elastic response spectra (a) absolute acceleration, b) relative velocity c) relative displacement and d) input energy (damping 1%)

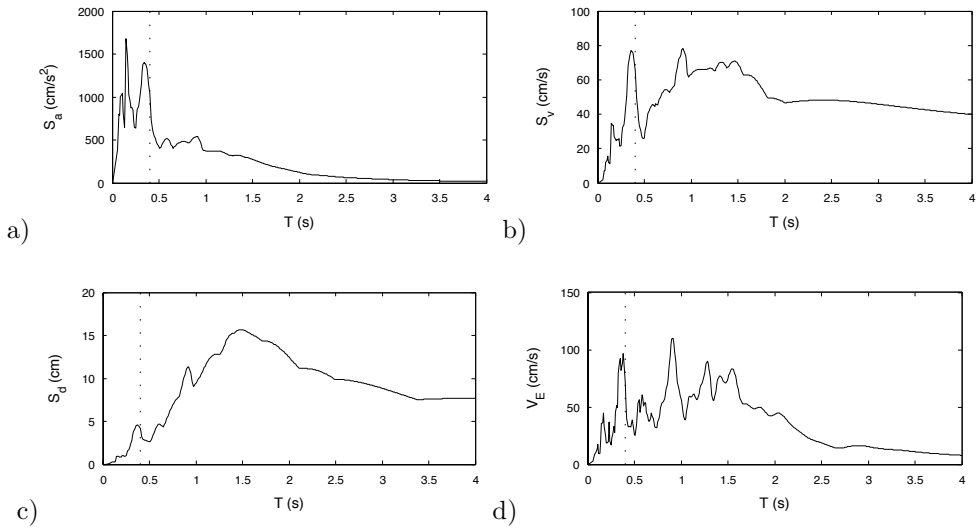

Fig. A.2 Coyote Lake (Gilroy Array #2, 1979). Elastic response spectra: (a) absolute acceleration, b) relative velocity c) relative displacement and d) input energy (damping 1%)

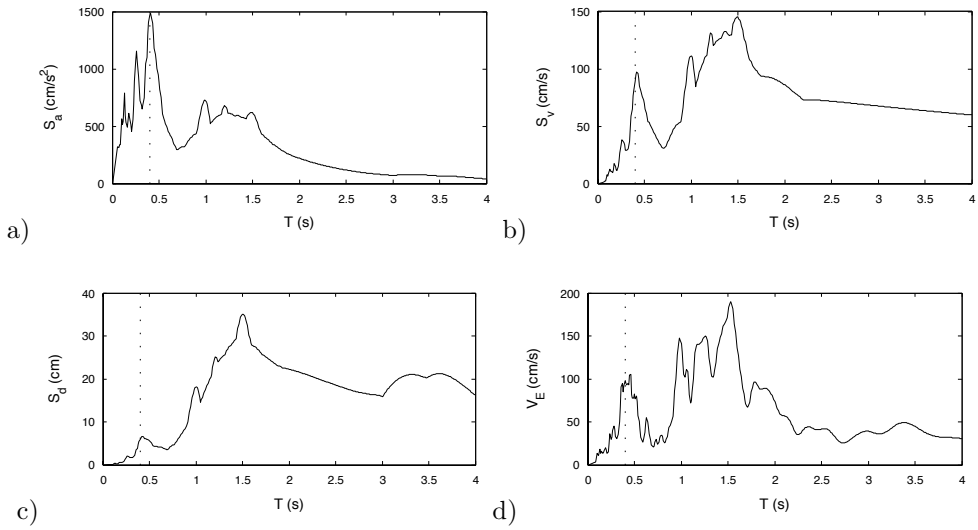

Fig. A.3 Loma Prieta (Gilroy-Historic Bldg, 1989). Elastic response spectra: (a) absolute acceleration, b) relative velocity c) relative displacement and d) input energy (damping 1%)

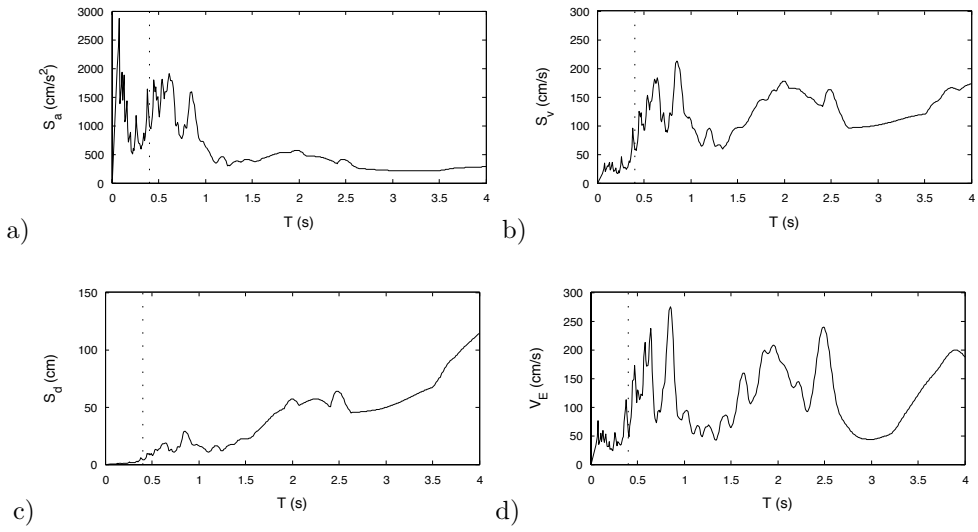

Fig. A.4 Darfield, New Zealand (LINC, 2010). Elastic response spectra: (a) absolute acceleration, b) relative velocity c) relative displacement and d) input energy (damping 1%)

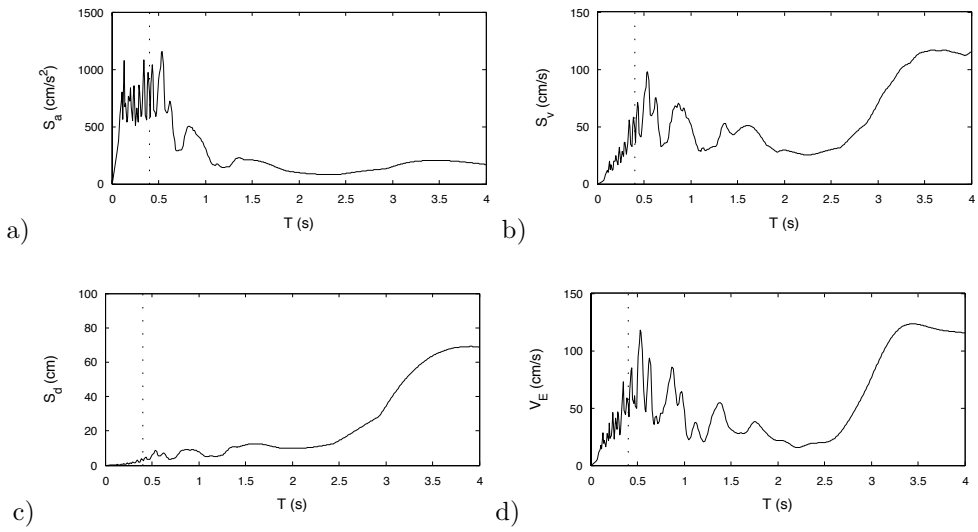

Fig. A.5 Kocaeli, Turkey (Gebze, 1999). Elastic response spectra: (a) absolute acceleration, b) relative velocity c) relative displacement and d) input energy (damping 1%)

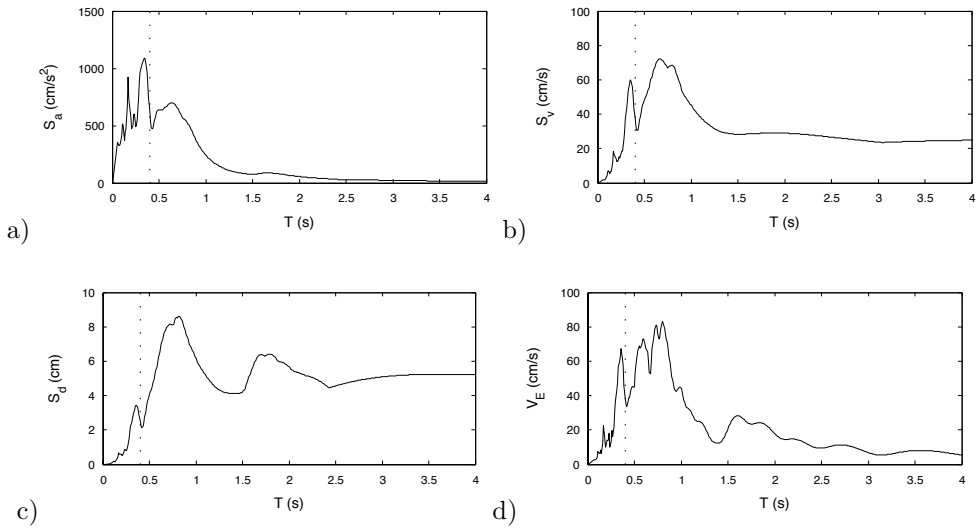

Fig. A.6 Kalamata, Greece (1986). Elastic response spectra: (a) absolute acceleration, b) relative velocity c) relative displacement and d) input energy (damping 1%)

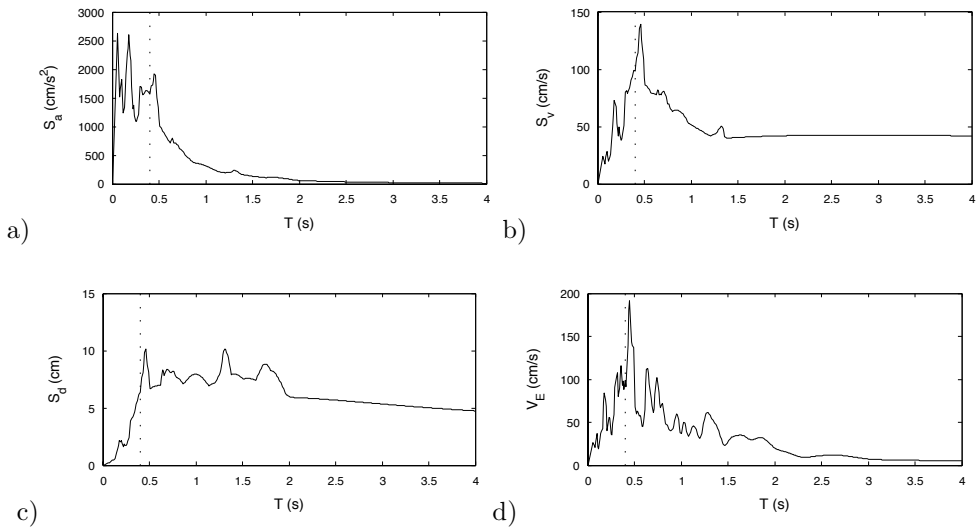

Fig. A.7 Parkfield-02, CA (Parkfield-Stone Corral 1E, 2004). Elastic response spectra: (a) absolute acceleration, b) relative velocity c) relative displacement and d) input energy (damping 1%)

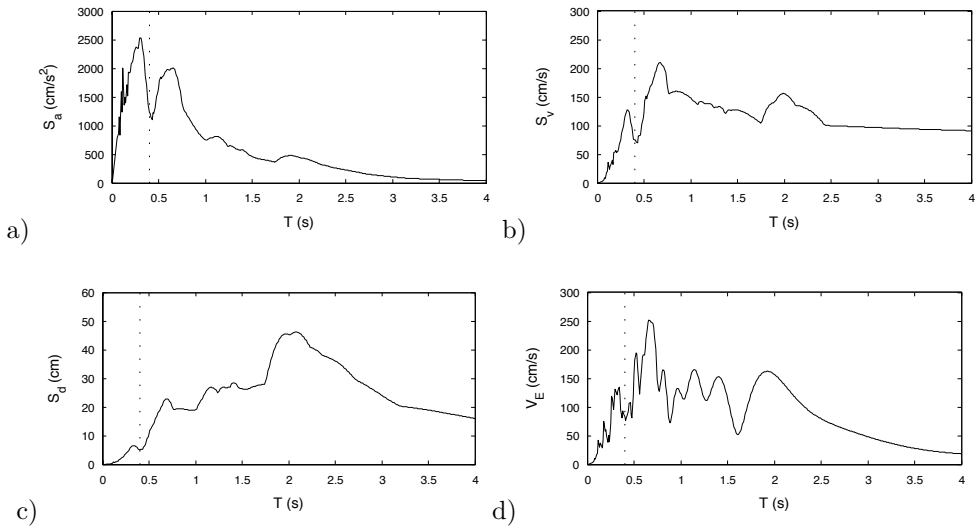

Fig. A.8 San Salvador (Geotech Investig Center, 1986). Elastic response spectra: (a) absolute acceleration, b) relative velocity c) relative displacement and d) input energy (damping 1%)

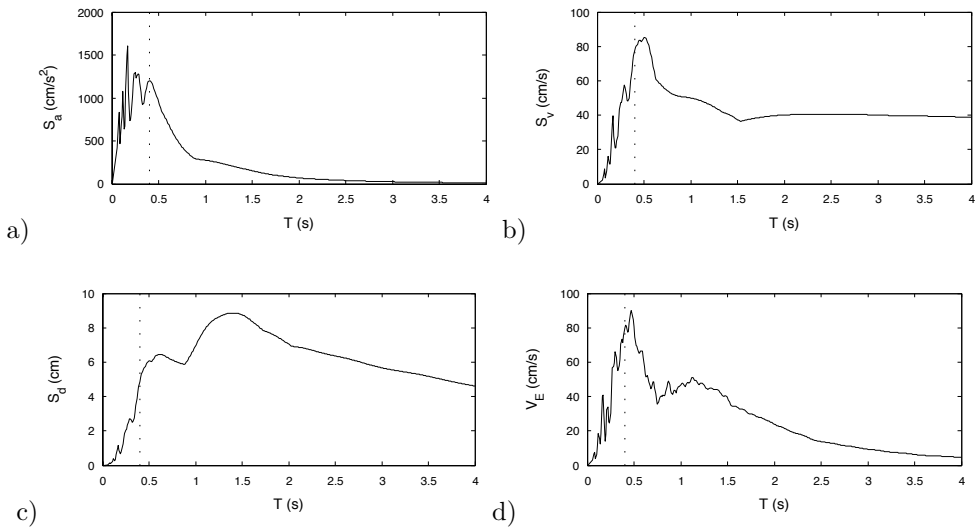

Fig. A.9 Lorca, Spain (2011). Elastic response spectra: (a) absolute acceleration, b) relative velocity c) relative displacement and d) input energy (damping 1%)

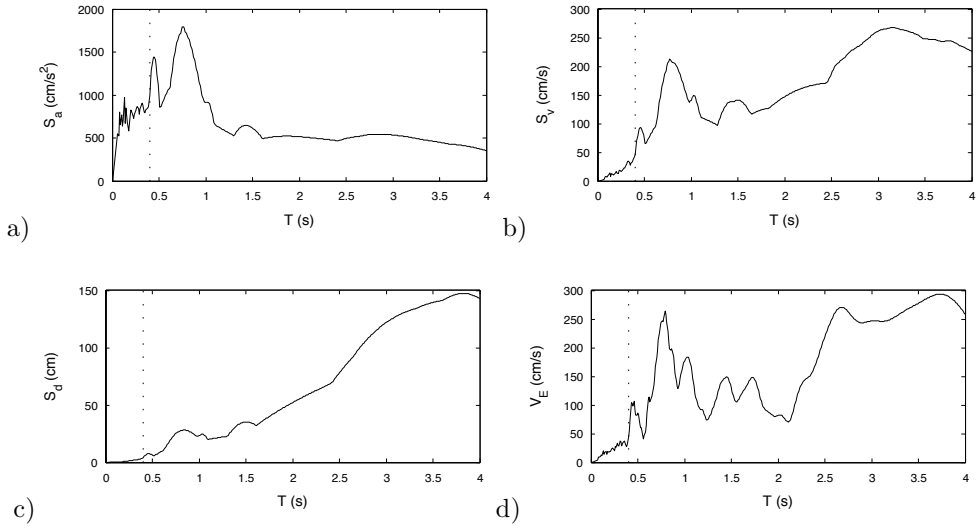

Fig. A.10 Imperial Valley-06 (El Centro Array #7, 1979). Elastic response spectra: (a) absolute acceleration, b) relative velocity c) relative displacement and d) input energy (damping 1%)

A.1.2 Non-pulse like

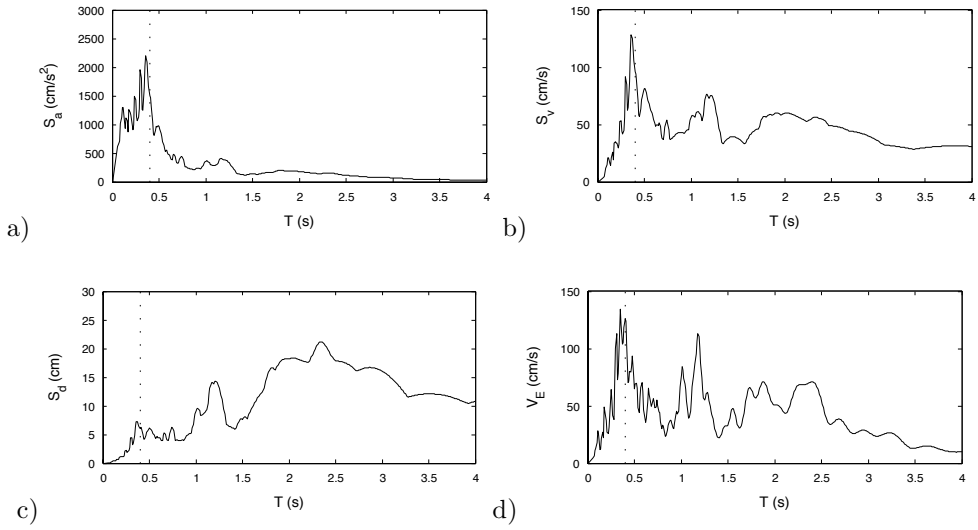

Fig. A.11 Parkfield (Cholame-Shandon Array #5, 1966). Elastic response spectra (a) absolute acceleration, b) relative velocity c) relative displacement and d) input energy (damping 1%)

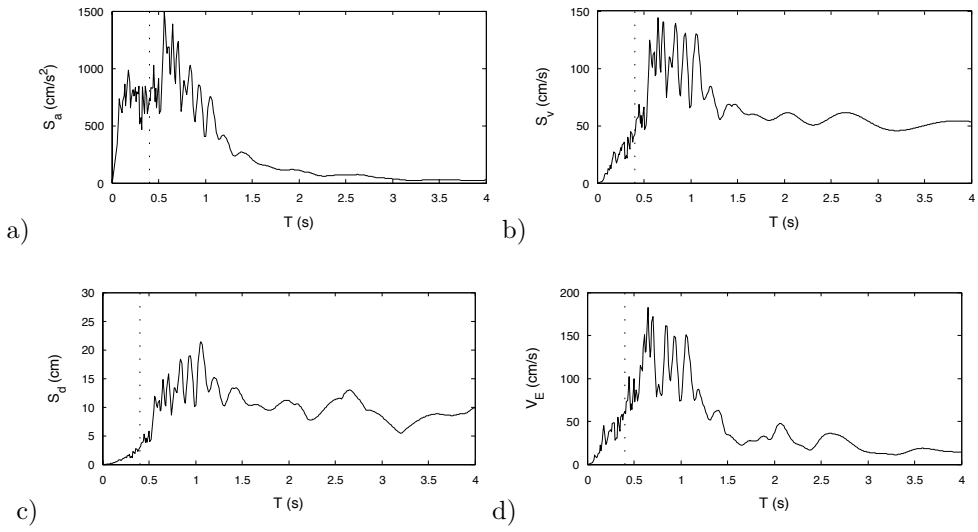

Fig. A.12 Morgan Hill (Halls Valley, 1984). Elastic response spectra: (a) absolute acceleration, b) relative velocity c) relative displacement and d) input energy (damping 1%)

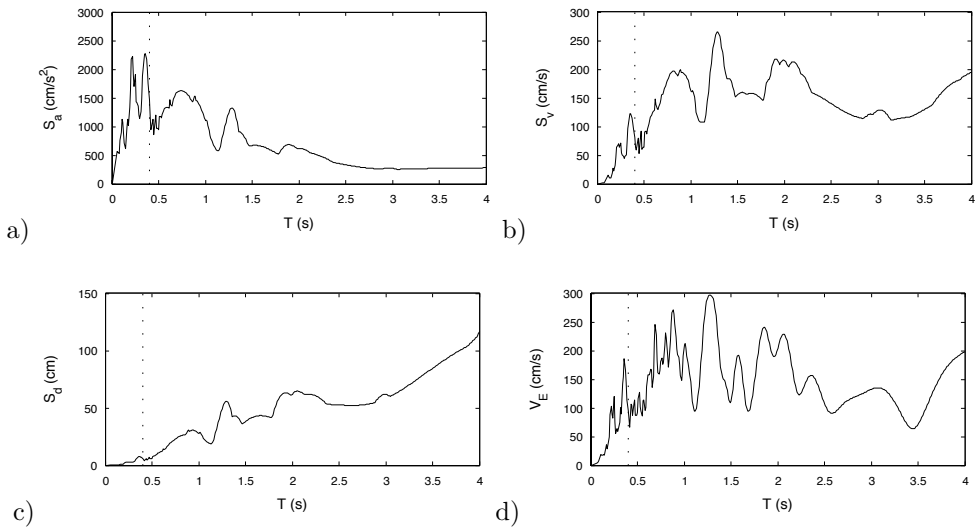

Fig. A.13 Duzce Turkey (1999). Elastic response spectra: (a) absolute acceleration, b) relative velocity c) relative displacement and d) input energy (damping 1%)

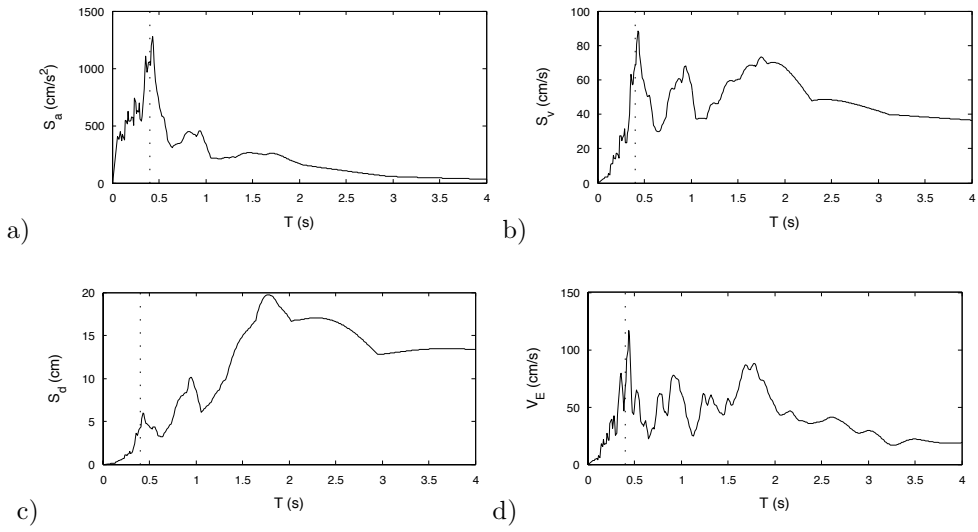

Fig. A.14 Managua Nicaragua-02 (ESSO, 1972). Elastic response spectra: (a) absolute acceleration, b) relative velocity c) relative displacement and d) input energy (damping 1%)

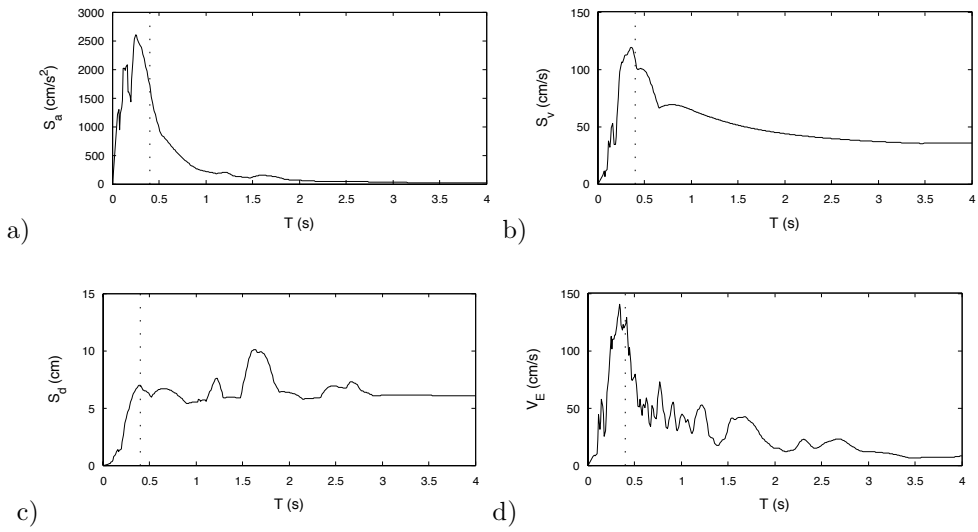

Fig. A.15 Coalinga-07 (Coalinga-14th & Elm Old CHP, 1983). Elastic response spectra: (a) absolute acceleration, b) relative velocity c) relative displacement and d) input energy (damping 1%)

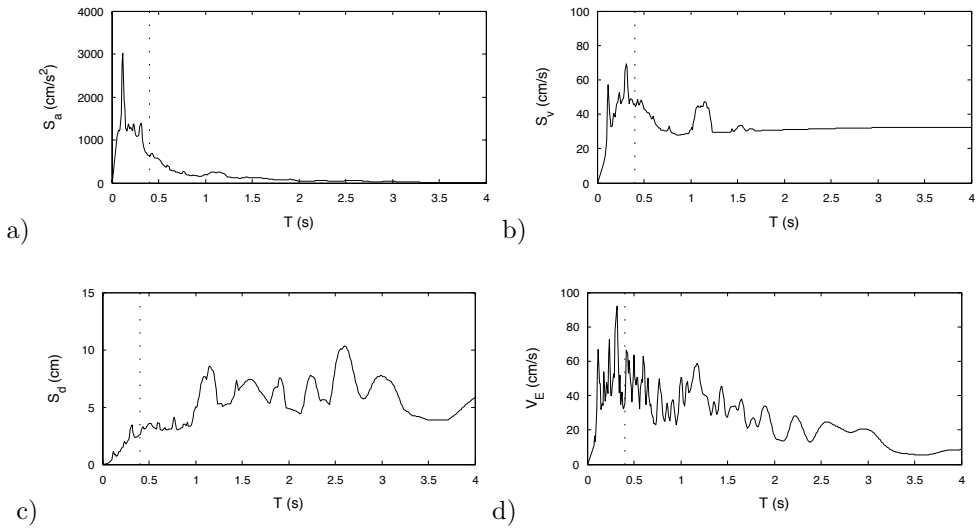

Fig. A.16 Coalinga-05 (Coalinga-14th & Elm Old CHP, 1983). Elastic response spectra: (a) absolute acceleration, b) relative velocity c) relative displacement and d) input energy (damping 1%)

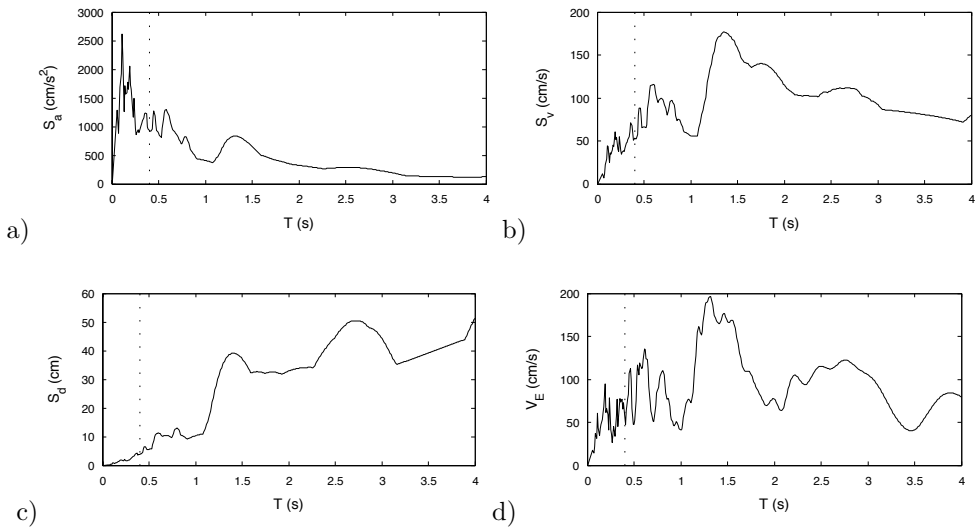

Fig. A.17 Imperial Valley-06 (El Centro Array #8, 1979). Elastic response spectra: (a) absolute acceleration, b) relative velocity c) relative displacement and d) input energy (damping 1%)

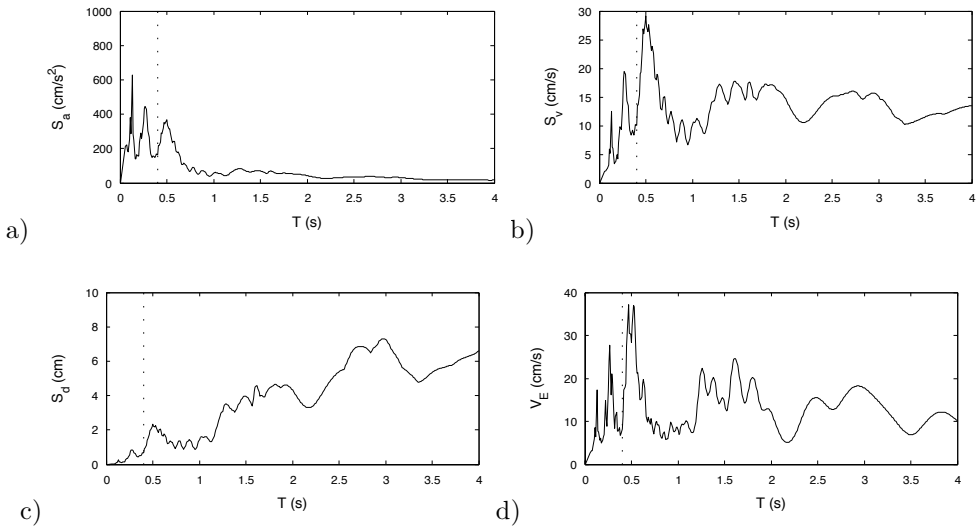

Fig. A.18 New Zealand-01 (Turangi Telephone Exchange, 1984). Elastic response spectra: (a) absolute acceleration, b) relative velocity c) relative displacement and d) input energy (damping 1%)

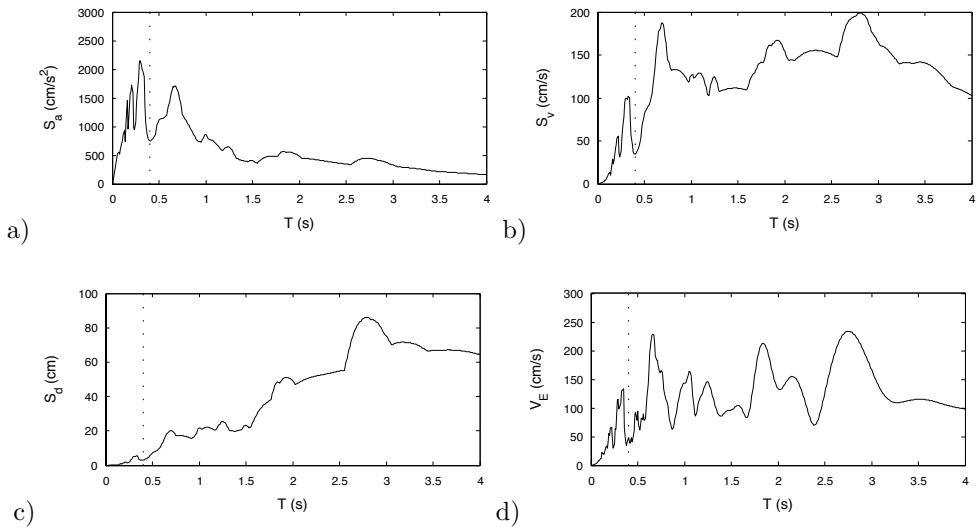

Fig. A.19 Erzican, Turkey (1992). Elastic response spectra: (a) absolute acceleration, b) relative velocity c) relative displacement and d) input energy (damping 1%)

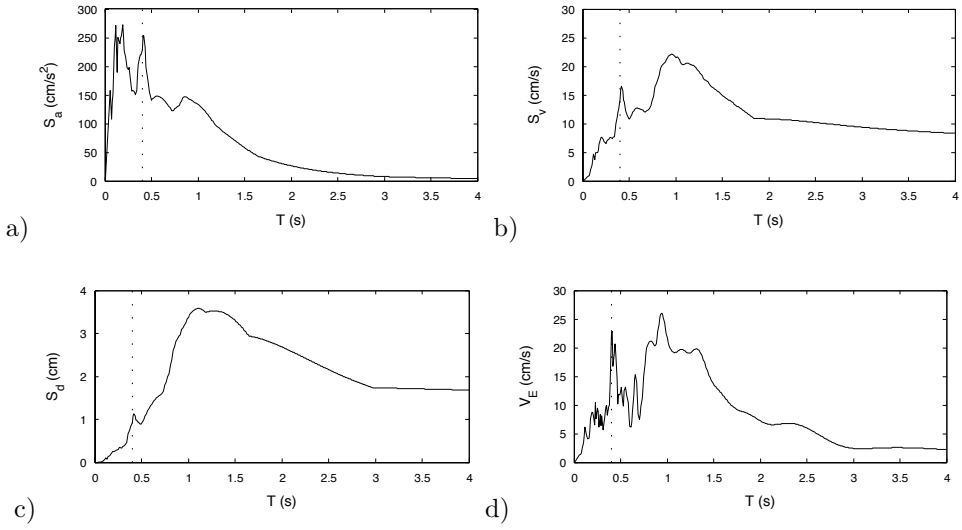

Fig. A.20 Drama, Greece (1985). Elastic response spectra: (a) absolute acceleration, b) relative velocity c) relative displacement and d) input energy (damping 1%)

A. 2 Selected ground motions with $D_f > 12$km

A.2.1 Selected ground motions with $I_d > 9$

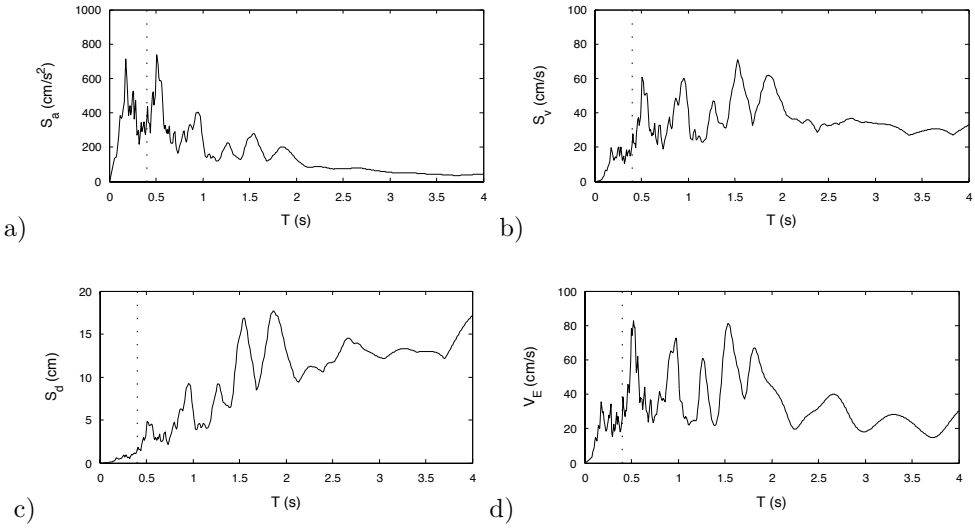

Fig. A.21 Tabas, Iran (Boshrooyeh, 1978). Elastic response spectra (a) absolute acceleration, b) relative velocity c) relative displacement and d) input energy (damping 1%)

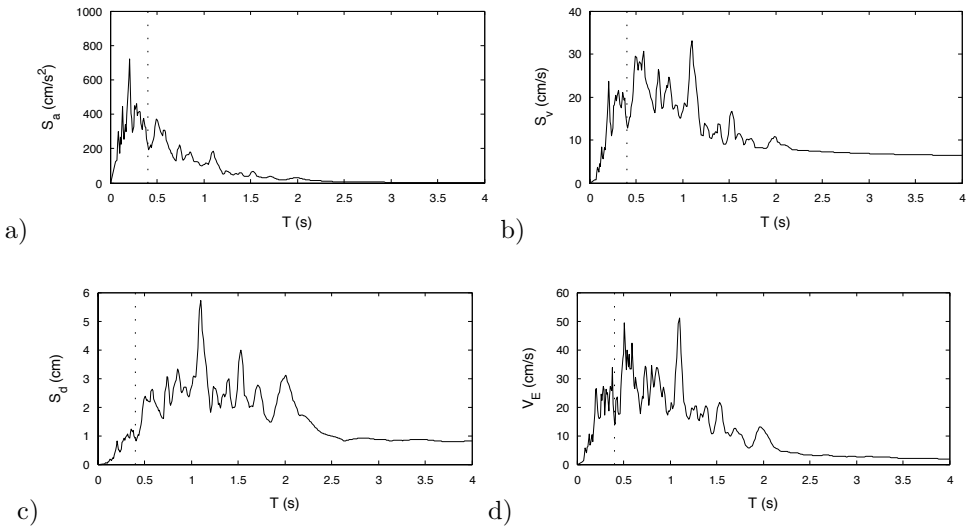

Fig. A.22 Northern Calif-07 (Ferndale City Hall, 1975). Elastic response spectra: (a) absolute acceleration, b) relative velocity c) relative displacement and d) input energy (damping 1%)

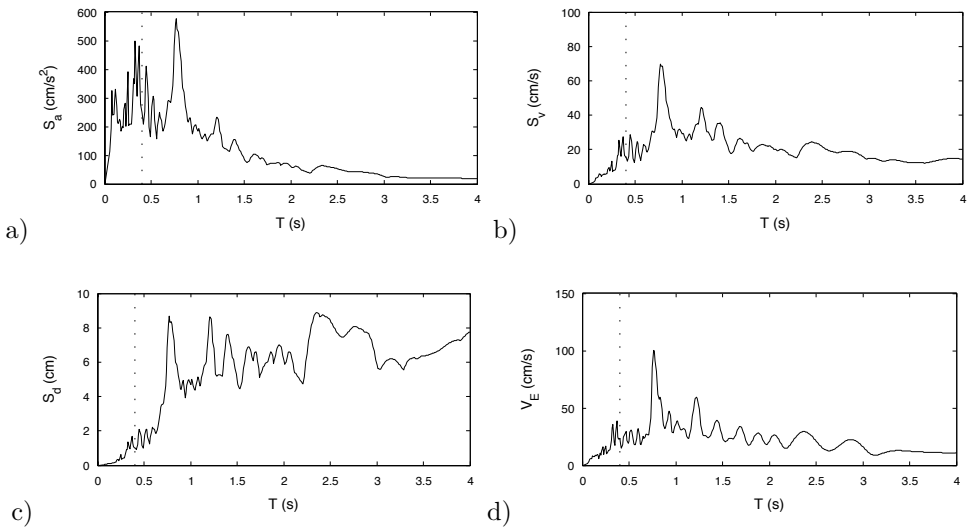

Fig. A.23 Friuli Italy-01 (Codroipo, 1976). Elastic response spectra: (a) absolute acceleration, b) relative velocity c) relative displacement and d) input energy (damping 1%)

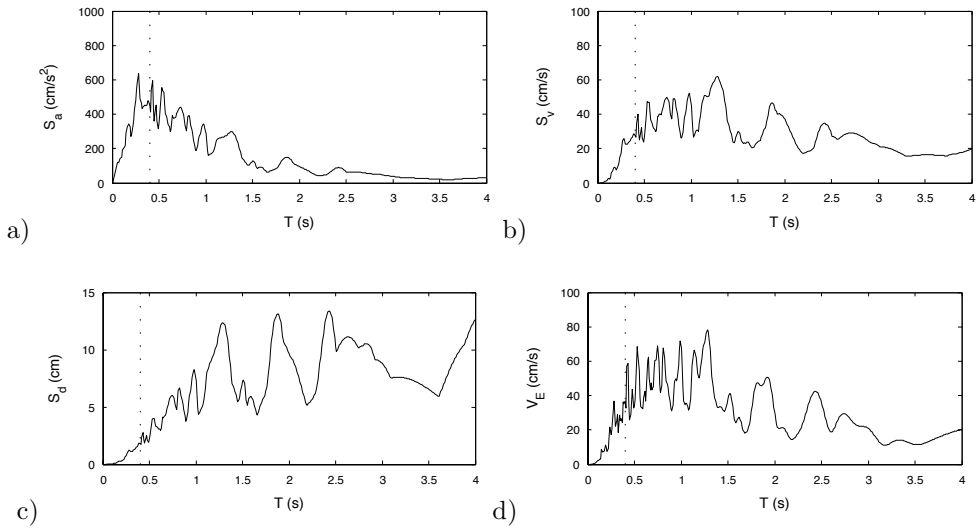

Fig. A.24 Hollister-01, New Zealand (Hollister City Hall, 1961). Elastic response spectra: (a) absolute acceleration, b) relative velocity c) relative displacement and d) input energy (damping 1%)

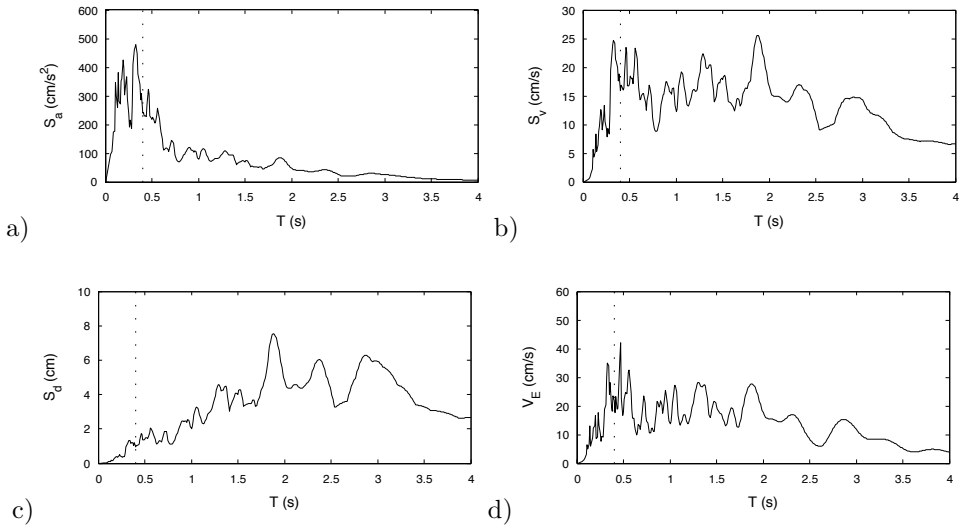

Fig. A.25 Taiwan SMART1-5 (SMART1 I06, 1981). Elastic response spectra: (a) absolute acceleration, b) relative velocity c) relative displacement and d) input energy (damping 1%)

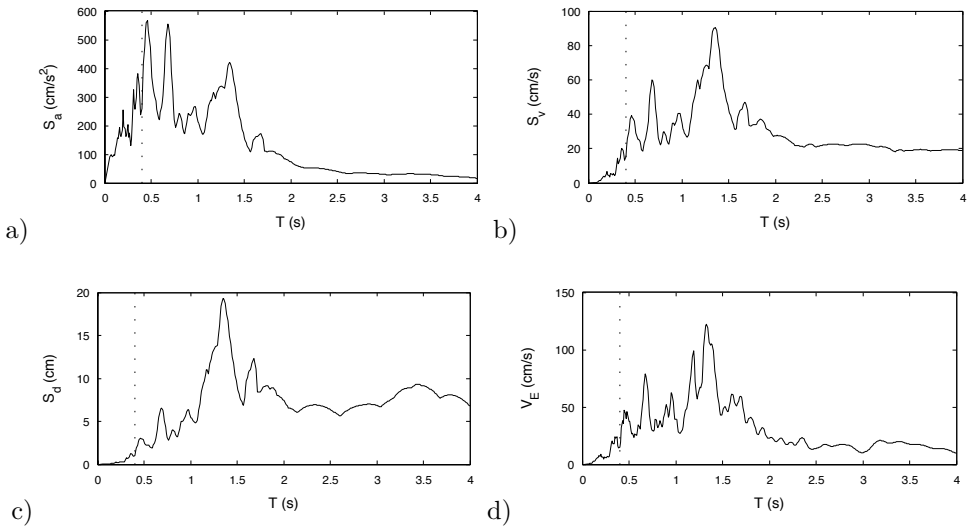

Fig. A.26 Coalinga-01 (Parkfield-Cholame 1E, 1983). Elastic response spectra: (a) absolute acceleration, b) relative velocity c) relative displacement and d) input energy (damping 1%)

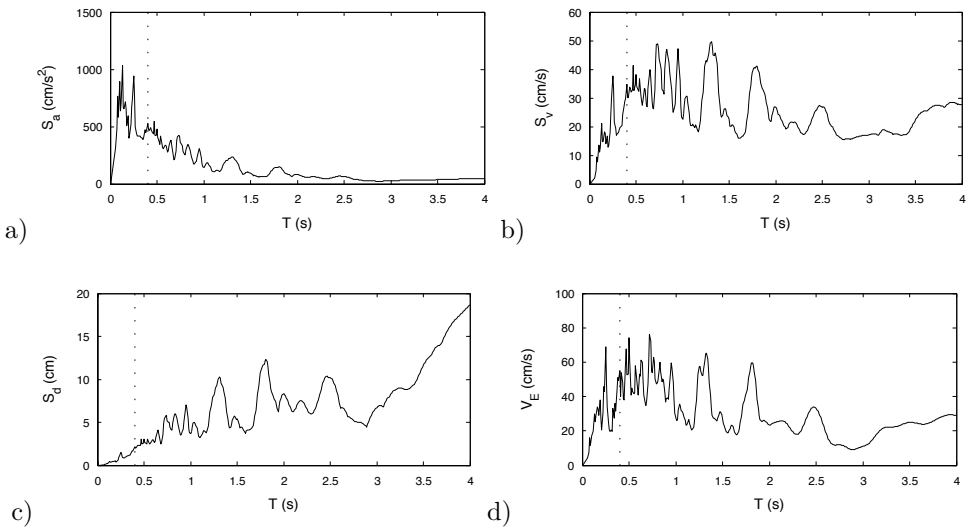

Fig. A.27 Imperial Valley-06 (Compuertas, 1979). Elastic response spectra: (a) absolute acceleration, b) relative velocity c) relative displacement and d) input energy (damping 1%)

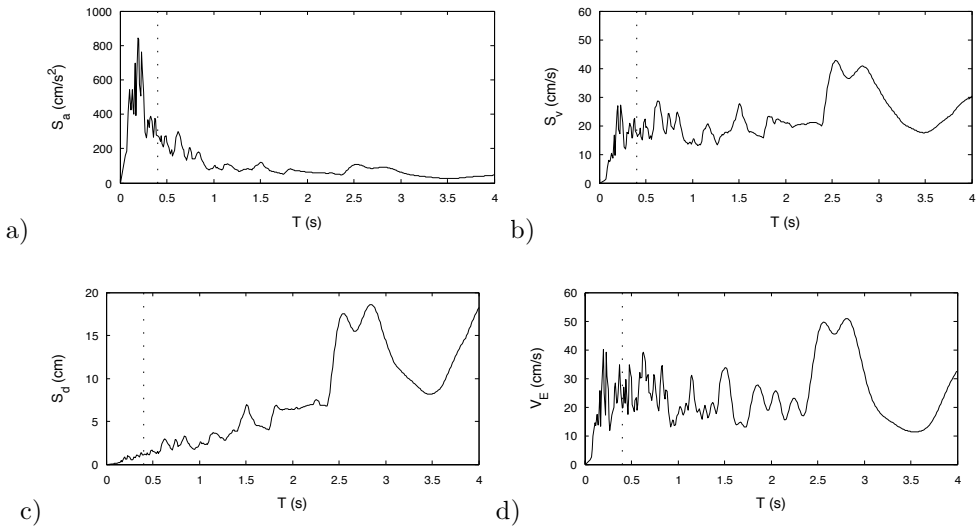

Fig. A.28 San Fernando (Whittier Narrows Dam, 1971). Elastic response spectra: (a) absolute acceleration, b) relative velocity c) relative displacement and d) input energy (damping 1%)

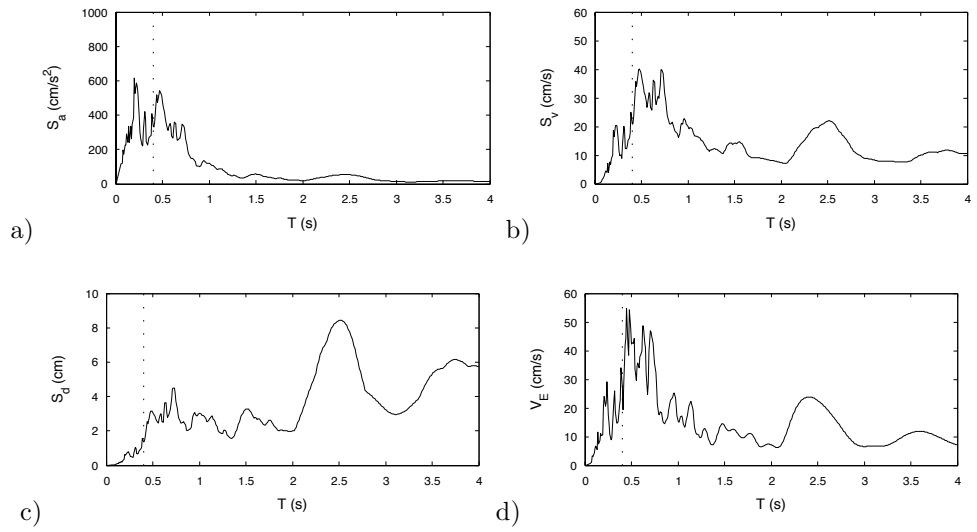

Fig. A.29 Coyote Lake (San Juan Bautista 24 Polk St, 1979). Elastic response spectra: (a) absolute acceleration, b) relative velocity c) relative displacement and d) input energy (damping 1%)

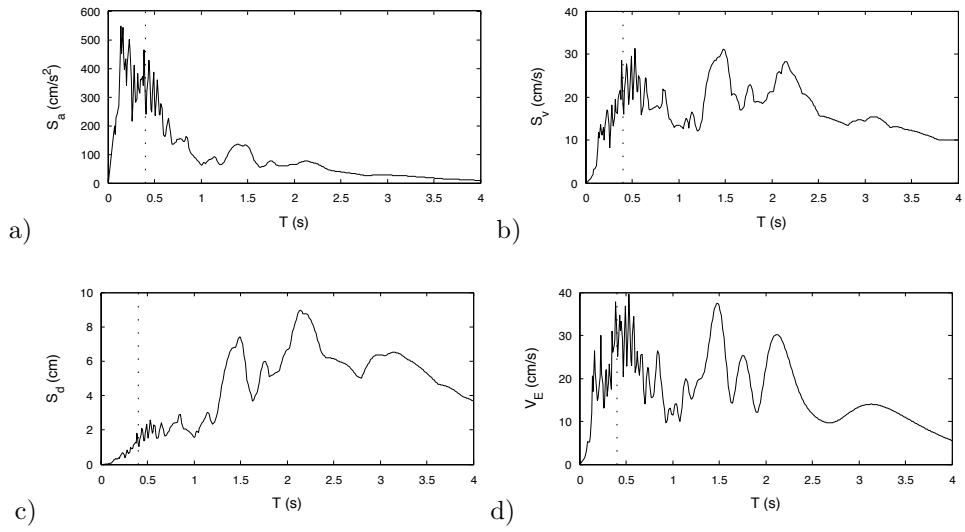

Fig. A.30 Victoria Mexico (SAHOP Casa Flores, 1980). Elastic response spectra: (a) absolute acceleration, b) relative velocity c) relative displacement and d) input energy (damping 1%)

A.2.2 Selected ground motions with $I_d < 9$

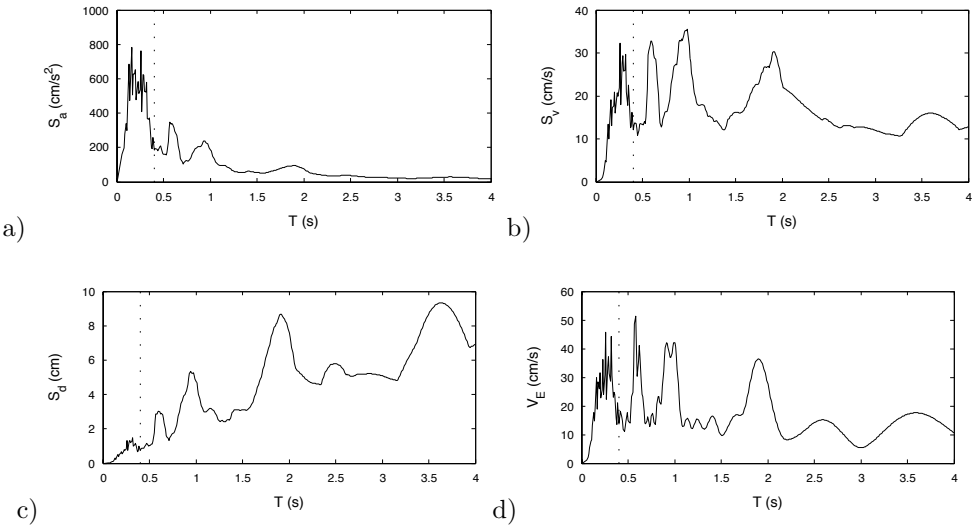

Fig. A.31 Trinidad (Rio Dell Overpass-FF, 1980). Elastic response spectra (a) absolute acceleration, b) relative velocity c) relative displacement and d) input energy (damping 1%)

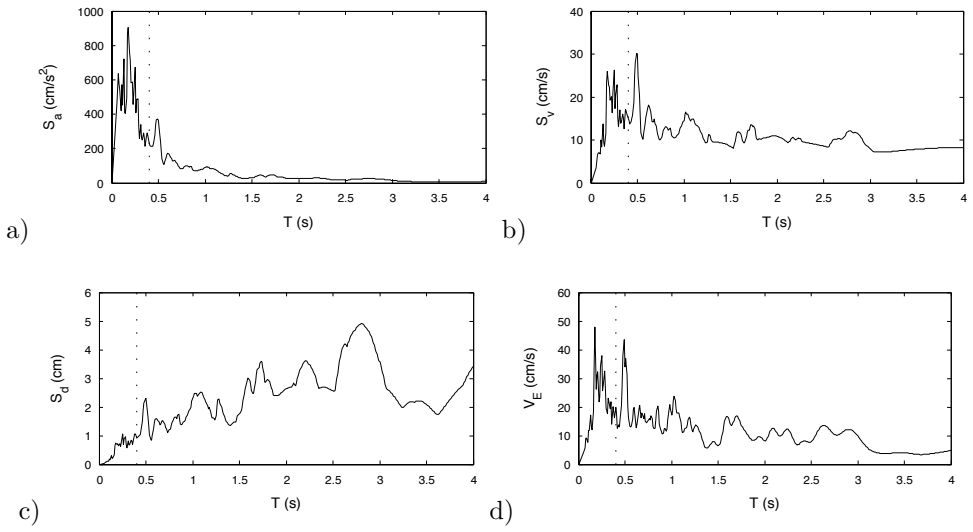

Fig. A.32 Westmorland (Niland Fire Station, 1981). Elastic response spectra: (a) absolute acceleration, b) relative velocity c) relative displacement and d) input energy (damping 1%)

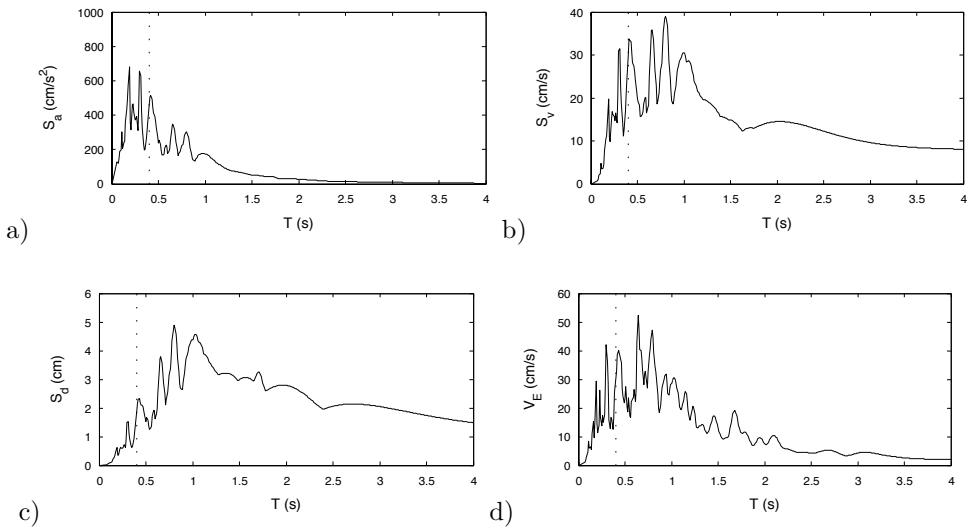

Fig. A.33 Northwest Calif-03 (Ferndale City Hall, 1951). Elastic response spectra: (a) absolute acceleration, b) relative velocity c) relative displacement and d) input energy (damping 1%)

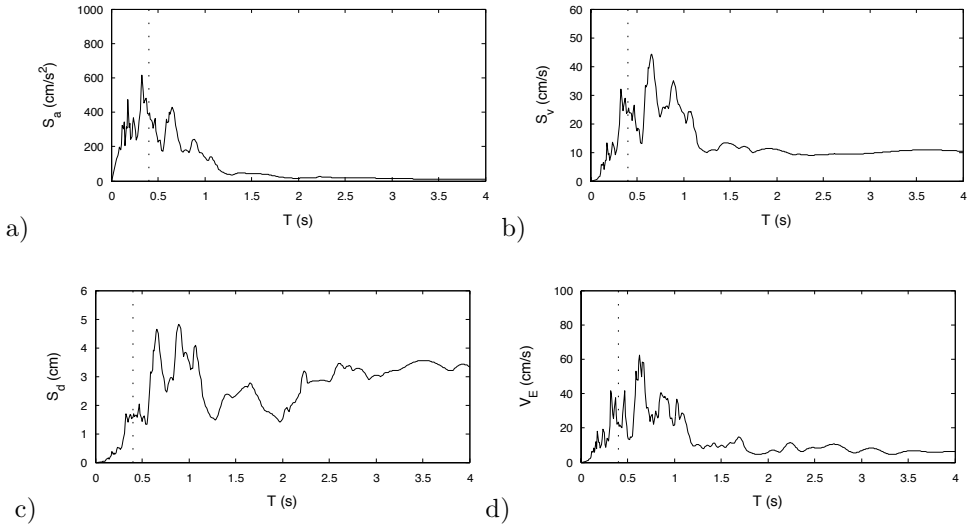

Fig. A.34 Northern Calif-01 (Ferndale City Hall, 1941). Elastic response spectra: (a) absolute acceleration, b) relative velocity c) relative displacement and d) input energy (damping 1%)

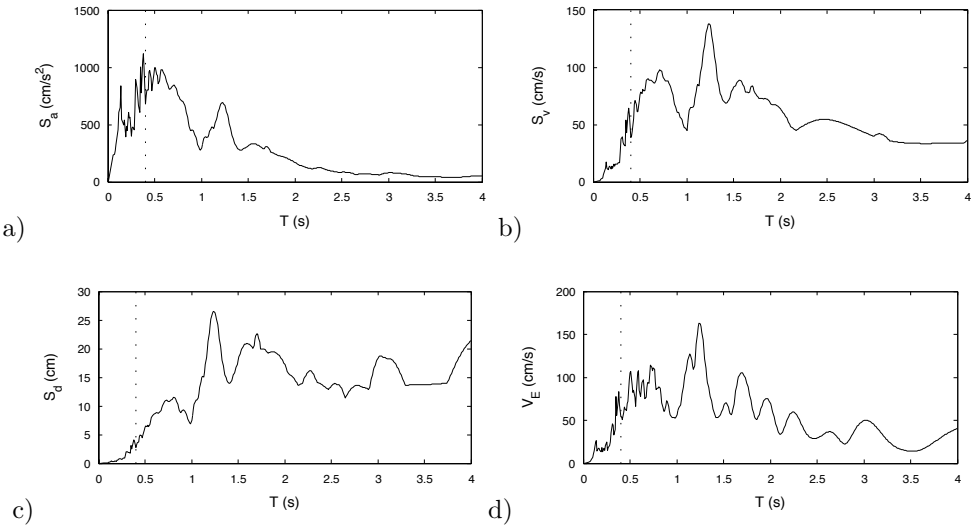

Fig. A.35 Kobe, Japan (Shin-Osaka, 1995). Elastic response spectra: (a) absolute acceleration, b) relative velocity c) relative displacement and d) input energy (damping 1%)

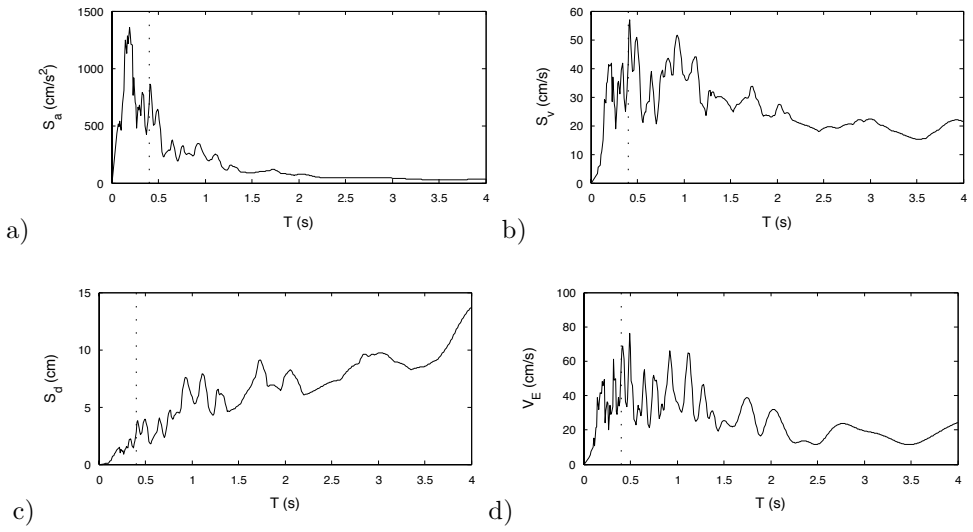

Fig. A.36 Parkfield (Cholame Shandon Array #8, 1966). Elastic response spectra: (a) absolute acceleration, b) relative velocity c) relative displacement and d) input energy (damping 1%)

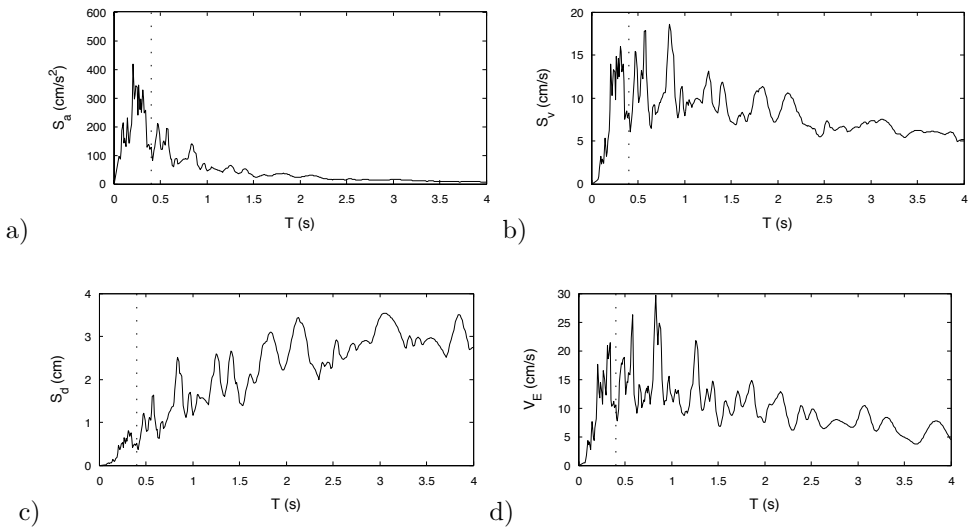

Fig. A.37 Northern Calif-04 (Ferndale City Hall, 1960). Elastic response spectra: (a) absolute acceleration, b) relative velocity c) relative displacement and d) input energy (damping 1%)

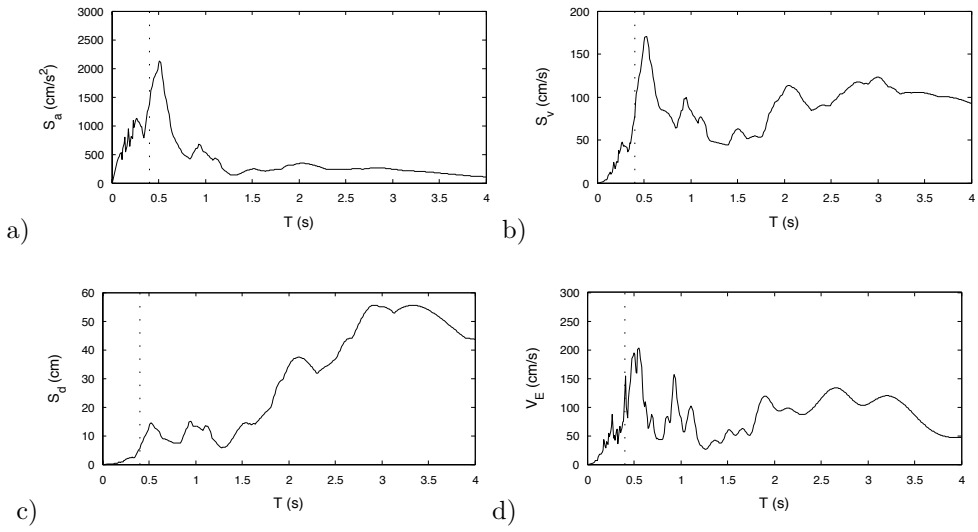

Fig. A.38 Cape Mendocino (Fortuna Fire Station, 1992). Elastic response spectra: (a) absolute acceleration, b) relative velocity c) relative displacement and d) input energy (damping 1%)

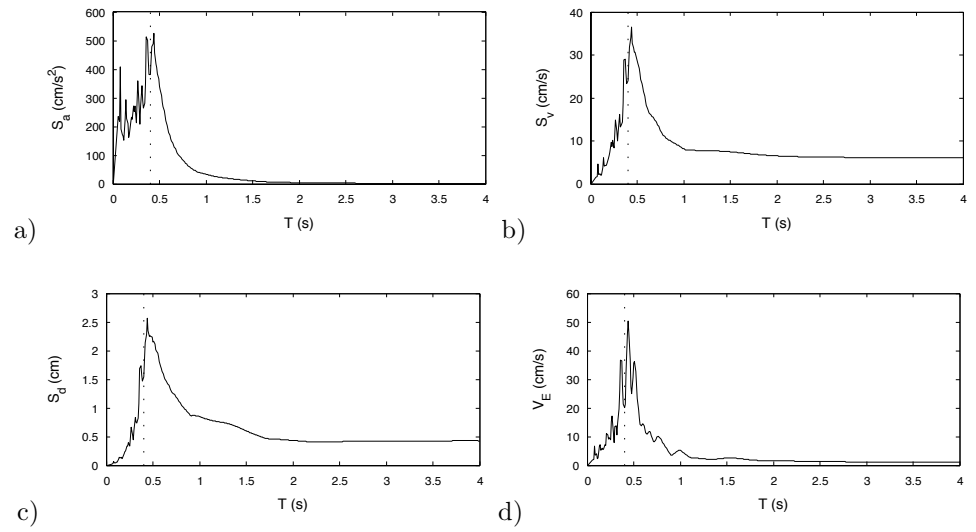

Fig. A.39 Anza Horse Canyon-01 (Rancho de Anza, 1980). Elastic response spectra: (a) absolute acceleration, b) relative velocity c) relative displacement and d) input energy (damping 1%)

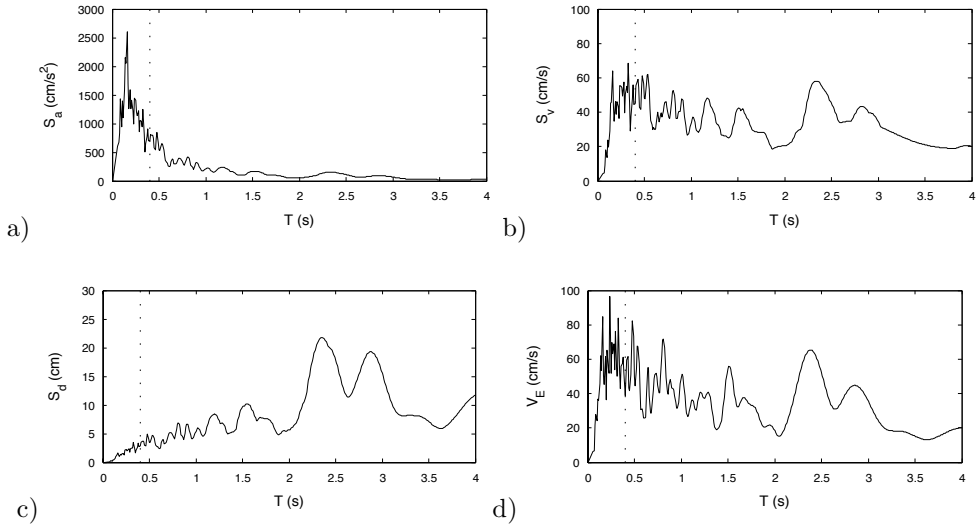

Fig. A.40 Northridge-01 (LA Centinela St, 1994). Elastic response spectra: (a) absolute acceleration, b) relative velocity c) relative displacement and d) input energy (damping 1%)

List of figures

List of tables

List of symbols

a_b	reference peak ground acceleration prescribed by the Spanish seismic code NCSE-02
A_c	area of the cross section
a_c	design ground acceleration prescribed by the Spanish seismic code NCSE-02
a_{cy}	zero-one variable for the type of loading (cyclic or monotonic)
A_{eq}	equivalent load-resistant area of SRP reinforcement
AI	Arias intensity
A_{jh}	effective cross-sectional area within a joint in a plane parallel to plane of reinforcement generating shear in the joint
a_{rms}	root-mean square acceleration
A_s	anchor cross-section area
a_{sl}	zero-one variable that accounts for slippage of longitudinal bars
a_{st}^{pl}	coefficient for steel type
a_v	zero-one variable, being $a_v = 0$ if $V_{Rc} > V_{My} = M_y/L_s$ and $a_v = 1$ if $V_{Rc} \leq V_{My} = M_y/L_s$
b	width of compression zone
b_j	width of the joint panel
b_w	width of the web
${}_BW_u^+$	area enveloped by the positive domain of loading in the Bauschinger curve
${}_BW_u^-$	area enveloped by the negative domain of loading in the Bauschinger curve
${}_B\eta$	ultimate cumulative plastic deformation ratio on the Bauschinger Part
C	damping coefficient

$\mathbf{C}$	damping matrix
c_1	seismological parameter
c_2	seismological parameter
d	effective depth of the cross section
d_1	distance of the center of compression reinforcement from the extreme compression fiber
d_{bL}	mean tension bar diameter
D_f	closest distance from the recording site to the rupture plane
D_i	index of damage proposed by Darwin and Nmai
DI_{PA}	index of damage proposed by Park and Ang
D_s	significant duration of the ground motion
E	total (relative) input energy
E_c	elastic modulus of concrete
E_f	elastic modulus of SRP reinforcement
E_{hi}	total plastic strain (hysteretic) energy dissipated at each floor (i.e. by the dampers and by the main frame)
EI_{eff}	effective elastic stiffness
e_N	eccentricity of the force, $\mu_c V$, normal to the shear-key plate and measured as prescribed by ETAG-001
${}_{ep}\eta$	apparent ultimate cumulative plastic deformation ratio on the Skeleton Part
E_s	elastic modulus of steel
${}_f\alpha_i$	shear force coefficient representing ${}_fQ_{y,i}$ normalized by the total weight of the upper stories
${}_f\delta_{ui}$	ultimate interstory drift of the main frame without dampers
${}_f\delta_{y,i}$	yielding interstory drift of the i-th story of the main structure (without dampers)

${}_f\delta_{yi}{}^o$	initial yielding interstory drift of the i-th story of the main frame (before local strengthening)
f_c	uniaxial compressive strength of unconfined concrete based on standard cylinder test
f_{ck}	characteristic compression strength of concrete
${}_fIDR_u$	ultimate interstory drift of the i-th story of the main frame, ${}_f\delta_{ui}$, in percentage of the story height
${}_fIDR_y$	yielding interstory drift of the i-th story of the main frame, ${}_f\delta_{y,i}$, in percentage of the story height
${}_fk_i$	lateral stiffness of the i-th story of the main structure (without dampers)
${}_fk_N$	lateral stiffness of the uppermost N-th story of the main structure (without dampers)
${}_fQ_i$	restoring shear force at the i-th story of the main structure (without dampers)
${}_f\overline{Q}_{m,i}$	mean value of the maximum shear force sustained by the i-th story of the main frame in the positive and negative domains
${}_fQ_{y,i}$	yield shear force at the i-th story of the main structure (without dampers)
${}_fQ_{yi}{}^o$	initial yield shear force at the i-th story of the main frame (before local strengthening)
${}_fT_1$	fundamental period of the main structure (without dampers)
${}_fT_n$	n-th natural period of vibration of the main structure (without dampers)
$F_{I,B}$	total shear force $F_{I,B}$ exerted by the inertial force of the SDOF system $\left(=m\ddot{y}^t\right)$
F_u	maximum axial force to be developed by the brace
f_{uk}	characteristic ultimate tensile strength of steel

F_y	lateral force corresponding to the yielding of the brace
f_y	yield stress of steel
f_{yL}	yield stress of the longitudinal reinforcement
f_{yw}	yield stress of the transverse reinforcement
g	acceleration of gravity
h	depth of member cross section
H	total height of the frame
h_{ef}	effective anchorage depth of the anchor
h_j	height of the joint panel
i	story level
ID	maximum interstory drift ratio
I_d	damage factor proposed by Cosenza and Manfredi
$\overline{ID}$	damage index for structural steel components defined as the ratio of the total dissipated energy to the ultimate energy dissipation capacity, proposed by Benavent-Climent
ID_r	residual interstory drift ratio
$IDR_{predicted}$	predicted interstory drift, $\delta_{m,i}$, in percentage of the story height
jd	internal moment arm of the joint
$\mathbf{K}$	stiffness matrix
K_{bc}	stiffness of the elastic beam-column element
K_c	post-capping stiffness of the monotonic backbone curve used for characterizing the nonlinear springs
K_D	initial lateral stiffness of the brace-damper
K_e	initial stiffness of the monotonic backbone curve used for characterizing the nonlinear springs
k_{eq}	stiffness of an equivalent SDOF system of mass $M=\Sigma m_i$ and period equal to the fundamental period of the main structure (without dampers), ${}_fT_1$, i.e. $k_{eq}=4\pi^2 M/{}_fT_1{}^2$

K_f	initial lateral stiffness of the reinforced concrete frame (without dampers)
K_i	stiffness ratio at the i-th story ($={}_sk_i/{}_fk_i$)
K_{mem}	total stiffness of the elastic beam element with nonlinear springs at the both ends, connected in series
K_{ns}	stiffness of the nonlinear springs
K_s	hardening stiffness of the monotonic backbone curve used for characterizing the nonlinear springs
K_T	initial lateral stiffness of the entire building-device structure
K_{td}	tangent stiffness of the hysteretic damper
L_b	total length of the left and the right beams of the beam-column joint
L_c	total length of the top and bottom columns of the beam-column joint
L_{pl}	plastic hinge length
L_s	shear span of a member ($=M/V$)
m	mass of the SDOF system
M	total mass of the building
$\mathbf{M}$	mass matrix
M_c	capping moment of the monotonic backbone curve used for characterizing the nonlinear springs
m_i	lumped mass of the i-th story
M_j	moment transferred through the joint panel rotational spring
$M_{jR\ ACI}$	moment transferred through the joint panel rotational spring corresponding to the maximum joint shear strength, $V_{R,ACI}$
M_w	earthquake magnitude
M_y	yield moment of the cross section
N	axial force

N_{D1}	axial force in Damper 1
N_{D2}	axial force in Damper 2
$n_{e,i}$	equivalent number of plastic cycles at the maximum value of plastic excursion that an equivalent SDOF system must develop to dissipate the total hysteretic energy input by the earthquake $(=W_{p,i}/[{}_sQ_{y,i}(\delta_{m,i}-{}_s\delta_{y,i})]=\eta_i/\mu_{m,i}$
N_i	tension forces acting on the anchor bolts
PGA	peak ground acceleration
PGV	peak ground velocity
$\mathbf{Q}(t)$	restoring force vector
Q_B	restoring force exerted by the SDOF structure
Q_{Bd}	apparent maximum strength of the hysteretic damper
Q_y	yield strength of the SDOF system
Q_{yd}	yield strength of the hysteretic damper
Q_{yi}	yield shear force at the i-th story of the entire building-device structure (main structure with dampers)
$\mathbf{r}$	displacement vector resulting from a unit support displacement
R	strength reduction factor
$r_{q,i}$	shear strength ratio at the i-th story $(= {}_fQ_{m,i}/{}_sQ_{y,i})$
${}_s\alpha_i$	shear force coefficient representing ${}_sQ_{y,i}$ normalized by the total weight of the upper stories
S_a	spectral absolute response acceleration
S_d	spectral relative displacement
${}_sE_{hi}$	plastic strain (hysteretic) energy dissipated by the dampers at each floor
s_h	spacing of transverse reinforcement
SI	Housner's spectrum intensity

S_i	scale factor defined as the quotient between the value of quantity i in the prototype and the value of quantity i in the model
${}_sk$	lateral stiffness of the hysteretic damper
${}_sk_i$	initial lateral stiffness of the dampers of the i-th story
${}_sQ_{yi}$	lateral yield shear force of the dampers of the i-th story
S_v	spectral relative velocity
${}_sW_u^+$	area enveloped by the positive domain of loading in the Skeleton curve
${}_sW_u^-$	area enveloped by the negative domain of loading in the Skeleton curve
${}_s\eta$	ultimate cumulative plastic deformation ratio on the Skeleton Part
${}_s\delta_{y,i}$	lateral yielding interstory drift of the dampers of the i-th story
${}_s\delta_u^+$	maximum displacement attained in the positive domain of loading in the Skeleton Part
${}_s\delta_u^-$	maximum displacement attained in the negative domain of loading in the Skeleton Part
T	period of vibration
t	time
T_1	fundamental period of the entire building-device structure
t_g	initial gap width between the end-plates of the dampers and the shear-key plates
T_G	predominant period of the ground motion
T_{NH}	initial period of medium period region in the Newmark and Hall spectral representation
t_o	instant when the ground motion fades away
t_p	thickness of the shear-key plate

T_R	mean return period
t_t	thickness of the Teflon sheet
V_a	equivalent velocity converted from the absorbed energy
V_c	contact forces perpendicular to the plane of the shear-key plate
$V_{D,p}$	equivalent velocity V_D used to design the prototype building
V_D	equivalent velocity converted from the energy that contributes to damage ($=W_e+W_p$)
V_{Dmax}	maximum value of V_D in the V_D-T design spectrum
V_E	equivalent velocity converted from the total input energy
V_i	shear forces acting on the anchor bolts
V_{max}	maximum shear value attained in columns during the numerical simulations
$V_{R,ACI}$	joint shear strength prescribed in ACI 318-11
$V_{R,brittle}$	shear resistance defined in section 6.2.3. of Eurocode 2-Part 1
$V_{R,ductile}$	cyclic shear resistance according to A.3.3.1 of Eurocode 8-Part 3
V_{Rc}	shear force at diagonal cracking of the member
V_{Rs}	contribution of transverse reinforcement to shear resistance for cross-sections with rectangular web
$v_{s,30}$	average shear wave velocity of top 30 meters of the site
W_ξ	damping energy
$W_{C,k}$	energy absorbed/dissipated at given plastic hinge k by the concrete material
W_e	elastic vibrational energy
W_k	kinetic energy
$W_{p,i}$	plastic strain energy (hysteretic energy) accumulated at the i-th story
W_p	irrecoverable plastic strain energy

$W_{S,k}$	energy absorbed/dissipated at given plastic hinge k by the steel material
W_s	absorbed energy
W_{se}	recoverable elastic strain energy
x	neutral axis depth at flexural yielding
y	relative horizontal displacement
$\dot{y}$	relative horizontal velocity
$\ddot{y}$	relative horizontal acceleration
$\ddot{y}^t$	absolute acceleration
$\ddot{y}^t_{\max}$	maximum absolute acceleration
$\mathbf{y}(t)$	relative displacement vector
$\dot{\mathbf{y}}(t)$	relative velocity vector
$\ddot{\mathbf{y}}(t)$	relative acceleration vector
z	length of the internal lever arm ($=d-d_1$)
$\ddot{z}_g$	ground acceleration

α	angle that the axis of the brace forms with the horizontal
α_e	base shear force coefficient that the main structure should have in order to absorb by itself (i.e. without hysteretic dampers) the amount of energy that contributes to damage supplied by the earthquake
α_i	shear-force coefficient representing $Q_{y,i}$ normalized by the total weight of the upper stories
$\bar{\alpha}_i$	lateral strength distribution of the entire building-device structure expressed as α_i/α_1
β	stiffness proportional factor
β_i	shear strength ratio at the i-th story ($={}_sQ_{y,i}/({}_sQ_{y,i}/{}_fQ_{y,i})$

$\beta_{opt,i}$	optimum value for β_i which which maximizes the equivalent viscous damping ratio of the entire structural system (i.e. frame+dampers)
γ	mass proportional factor
γ_j	joint shear strain
γ_1	ratio of W_p to W_{p1}
δ_i	interstory drift of the i-th story
δ_{max}	maximum allowed interstory drift
$\delta_{m,i}$	maximum interstory drift of the entire building-device structure at the i-th story
δ_T	horizontal displacement of the center of mass of the floor diaphragm of the SDOF structure
δ_{yd}	yield displacement of the hysteretic damper
ε_c	uniaxial strain at f_c
ε_{fd}	design strain of FRP reinforcement
ε_{max}	normalized maximum strain measured in the longitudinal bars located at the member end sections of columns and beams
ε_y	yield strain of the steel
ζ	ratio steel-to-concrete elastic moduli ($= E_s/E_c$)
η	normalized cumulated plastic strain energy (equal for all stories)
η_i	normalized plastic strain energy accumulated at the i-th story ($= W_{p,i}/({}_sQ_{y,i}\ {}_s\delta_{y,i})$
η_u	normalized ultimate energy dissipation capacity of the dampers
η_{ui}	normalized ultimate energy dissipation capacity of the dampers at the i-th story
θ_{cap}	chord rotation at the onset of the strength loss (capping)
θ_{cap}^{pl}	plastic part of the capping rotation, θ_{cap}
θ_j	rotation of the joint panel rotational spring

θ_m	maximum chord rotation demand
θ_{pc}	post-capping rotation capacity
θ_u	ultimate chord rotation
θ_u^{pl}	ultimate plastic rotation from yield to point of 20% strength loss
$\theta_{u,old}$	ultimate chord rotation, corrected to consider the lack of seismic detailing
θ_y	chord rotation at member yielding
λ	normalized energy dissipation capacity used to characterize the cyclic deterioration in the hysteretic model proposed by Ibarra et al.
μ	ductility factor (defned as the ratio of ultimate displacement to yield displacement)
μ_c	friction coefficient of the device inserted between the end-plates and the shear-key plates
$\mu_{m,i}$	plastic deformation ratio at the i-th story $(=(\delta_{m,i}-{}_s\delta_{y,i})/{}_s\delta_{y,i})$
μ_θ^{pl}	ratio of the plastic part of the chord rotation normalized to the yield chord rotation
ν	normalized axial load ratio $(=N/(A_c f_c))$
$\nu_{1,i}$	yield displacement ratio required on the dampers of the first story so that the maximum interstory drift at the i-th story meets ${}_f\delta_{y,i}$
$\nu_{1,max}$	maximum of the $\nu_{1,i}$, which gives the required yield displacement ratio for the dampers of the first story
ν_i	yield deformation ratio at the i-th story $(={}_s\delta_{y,i}/{}_f\delta_{y,i})$
ξ	damping ratio
ξ_y	neutral axis depth at yielding normalized to d
ρ_1	ratio of tension reinforcement area to bd

ρ_2	ratio of compression reinforcement area to bd
ρ_d	ratio of diagonal reinforcement in each diagonal direction
ρ_s	ratio of transverse reinforcement area to $b_w s_h$ (parallel to the loading direction)
ρ_{tot}	ratio of total longitudinal reinforcement area to bd
ρ_v	ratio of "web" reinforcement area to bd
ρ_w	ratio of transverse reinforcement area to bd
$\sigma_{N,plate}$	normal stress in the cross-section of the shear-key plate
τ_{jh}	joint shear stress
$\left(\overline{\tau}_{jh}\right)_{cr}$	joint shear cracking stress
$\boldsymbol{\phi}_n$	n-th natural mode shape of vibration
χ_1	stiffness ratio of ${}_f k_1$ to k_{eq}
φ_y	"theoretical" yield curvature
φ_{y1}	curvature at yielding of the tension steel
φ_{y2}	apparent yielding curvature
ω_1	mechanical ratio of tension and "web" longitudinal reinforcement
ω_2	mechanical ratio of compression longitudinal reinforcement

References

Aboutaha, R. S., Engelhardt, M. U., Jirsa, J. O., & Kreger, M. F. (1996). Retrofit of concrete columns with inadequate lap splices by the use of rectangular steel jackets. *Earthquake Spectra*, *12*(4), 693–714. doi:10.1193/1.1585906

ACI 318-11. (2011). *Building code requirements for structural concrete and commentary*. Farmington Hills, MI: American Concrete Institute.

ACI 440R-96. (1996). *State-of-the-art report on fiber reinforced plastic (FRP) reinforcement for concrete structures*. Farmington Hills, MI: American Concrete Institute.

Akiyama, H. (1985). *Earthquake resistant limit-state design for buildings*. Japan: University of Tokyo Press.

Akiyama, H. (1999). *Earthquake-resistant design method for buildings based on energy balance*. Gihodo-shuppan.

Altoontash, A. (2004). *Simulation and damage models for performance assessment of reinforced concrete beam-column joints* (Doctoral dissertation). Department of Civil and Environmental Engineering, Stanford University, CA. Retrieved from http://opensees.berkeley.edu/OpenSees/doc/Altoontash_Dissertation.pdf

Álvarez Cabal, R., Díaz-Pavón Cuaresma, E., & Rodríguez Escribano, R. (2013). *El terremoto de Lorca. Efectos en los edificios*. Consorcio de compensación de seguros.

ANSYS. (2007). *Programmer's manual for ANSYS. ANSYS Release 11.0*. ANSYS, Inc.

Architectural Institute of Japan (1994). *Structural design guidelines for reinforced concrete buildings*. Tokyo.

Arias, A. (1970). A measure of earthquake intensity. In R. J. Hansen (Ed.), *Seismic design for nuclear power plants* (pp. 438–483). Cambridge, MA: The M.I.T. Press.

ASCE/SEI 31-03. (2002). *Seismic evaluation of existing buildings*. Reston, VA: American Society of Civil Engineers.

ASCE/SEI 41-13. (2014). *Seismic evaluation and retrofit of existing buildings*. Reston, VA: American Society of Civil Engineers.

ATC-40. (1996). *Seismic evaluation and retrofit of concrete buildings* (No. SSC 96-01). Redwood City, CA: Applied Technology Council.

Barbat, A. H., Pujades, L. G., & Lantada, N. (2006). Performance of buildings under earthquakes in Barcelona, Spain. *Computer-Aided Civil and Infrastructure Engineering*, *21*(8), 573–593. doi:10.1111/j.1467-8667.2006.00450.x

Benavent-Climent, A. (2007). An energy-based damage model for seismic response of steel structures. *Earthquake Engineering and Structural Dynamics*, *36*(8), 1049–1064. doi:10.1002/eqe.671

Benavent-Climent, A. (2008). Development and application of passive structural control systems in the moderate-seismicity mediterranean area: the case of spain. *Proceedings of the 14th World Conference on Earthquake Engineering*. Beijing, China.

Benavent-Climent, A. (2010a). A brace-type seismic damper based on yielding the walls of hollow structural sections. *Engineering Structures*, *32*(4), 1113–1122. doi:10.1016/j.engstruct.2009.12.037

Benavent-Climent, A. (2010b). *Estructuras sismorresistentes*. Madrid: Maia ediciones.

Benavent-Climent, A. (2011). An energy-based method for seismic retrofit of existing frames using hysteretic dampers. *Soil Dynamics and Earthquake Engineering*, *31*(10), 1385–1396. doi:10.1016/j.soildyn.2011.05.015

Benavent-Climent, A., Akiyama, H., Lopez-Almansa, F., & Pujades, L. (2004). Prediction of ultimate earthquake resistance of gravity-load designed RC buildings. *Engineering Structures*, *26*(8), 1103–1113. doi:10.1016/j.engstruct.2004.03.011

Benavent-Climent, A., Escobedo, A., Donaire-Avila, J., Oliver-Saiz, E., & Ramírez-Márquez, A. L. (2013). Assessment of expected damage on buildings subjected to Lorca earthquake through an energy-based seismic index method and nonlinear dynamic response analyses. *Bulletin of Earthquake Engineering*, *12*(5), 2049–2073. doi:10.1007/s10518-013-9513-9

Benavent-Climent, A., Morillas, L., & Escolano-Margarit, D. (2014). Seismic performance and damage evaluation of a reinforced concrete frame with hysteretic dampers through shake-table tests. *Earthquake Engineering & Structural Dynamics*, *43*(15), 2399–2417. doi:10.1002/eqe.2459

Benavent-Climent, A., Morillas, L., & Vico, J. M. (2011). A study on using wide-flange section web under out-of-plane flexure for passive energy dissipation. *Earthquake Engineering & Structural Dynamics*, *40*(5), 473–490. doi:10.1002/eqe.1031

Benavent-Climent, A., Oh, S.-H., & Akiyama, H. (1998). Ultimate energy absorption capacity of slit-type steel plates subjected to shear deformations. *Journal of Structural and Construction Engineering, Transactions of Architectural Institute of Japan*, (503), 139–147.

Benavent-Climent, A., Oliver-Saiz, E., & Donaire-Avila, J. (2002). New connection between reinforced concrete building frames and concentric braces: Shaking table tests. *Engineering Structures*, *96*, 7-21. doi:10.1016/j.engstruct.2015.03.023

Benavent-Climent, A., Pujades, L. G., & Lopez-Almansa, F. (2002). Design energy input spectra for moderate-seismicity regions. *Earthquake Engineering & Structural Dynamics*, *31*(5), 1151–1172. doi:10.1002/eqe.153

Bergman, D., & Goel, S. (1987). *Evaluation of cyclic testing of steel plate devices for added damping and stiffness* (No. UMCE87-10). Ann Arbor, MI: The University of Michigan.

Bernal, D. (1994). Viscous damping in inelastic structural response. *Journal of Structural Engineering*, *120*(4), 1240–1254. doi:10.1061/(ASCE)0733-9445(1994)120:4(1240)

Bertero, R. D., & Bertero, V. V. (2002). Performance-based seismic engineering: the need for a reliable conceptual comprehensive approach. *Earthquake Engineering and Structural Dynamics*, *31*(3), 627–652. doi:10.1002/eqe.146

Bertero, V. V. (1992a). Major issues and future directions in earthquake-resistant design. *Proceedings of the 10th World Conference on Earthquake Engineering*. Madrid, Spain.

Bertero, V. V. (1992b). Seismic upgrading of existing structures. *Proceedings of the 10th World Conference on Earthquake Engineering*. Madrid, Spain.

Bertero, V. V. (1995). State of the art report on: design criteria. *Proceedings of the 11th World Conference on Earthquake Engineering*. Acapulco, Mexico.

Bertero, V. V. (2000). Performance-based seismic engineering: conventional vs. innovative approaches. *Proceedings of the 12th World Conference on Earthquake Engineering*. Auckland, New Zealand.

Bertero, V. V., & Bozorgnia, Y. (2004). *Earthquake engineering: from engineering seismology to performance-based engineering*. Boca Raton, FL: CRC Press.

Biskinis, D. (2007). *Resistance and deformation capacity of concrete members with or without retrofitting* (Doctoral dissertation). Civil Engineering Department, University of Patras.

Blázquez Martínez, R. (1997). Enfoque y avances conceptuales de la nueva norma española de construcción sismorresistente NCSE-94. *Informes de la construcción*, *48*(447), 39–45. doi: 10.3989/ic.1997.v48.i447.974

Bommer, J. J., & Acevedo, A. B. (2004). The use of real earthquake accelerograms as input to dynamic analysis. *Journal of Earthquake Engineering*, *8*(S1), 43–91. doi:10.1080/13632460409350521

Bournas, D., & Triantafillou, T. (2010). Innovative seismic retrofitting of RC columns using advanced composites. In M.N. Fardis (Ed.) *Advances in performance-based earthquake engineering* (pp. 383–393), *Geotechnical, Geological, and Earthquake Engineering 13*, Dordrecht: Springer Netherlands. doi: 10.1007/978-90-481-8746-1_36

BSL. (2009). *The building standard law of Japan*. Tokyo: The Building Center of Japan.

Cabañas, L., Carreño, E., Izquierdo, A., Martínez, J. M., Capote, R., Martínez, J., … Murphy, P. (2011). *Informe del sismo de Lorca del 11 de mayo de 2011*. Madrid: Instituto Geográfico Nacional, Universidad Complutense De Madrid, Universidad Politécnica De Madrid, Instituto Geológico Y Minero De España and Asociación Española De Ingeniería Sísmica. Retrieved from http://www.ign.es/ign/resources/sismologia/Lorca.pdf

Celik, O. C., & Ellingwood, B. R. (2008). Modeling beam-column joints in fragility assessment of gravity load designed reinforced concrete frames. *Journal of Earthquake Engineering*, *12*(3), 357–381. doi:10.1080/13632460701457215

Chan, R. W. K., & Albermani, F. (2008). Experimental study of steel slit damper for passive energy dissipation. *Engineering Structures*, *30*(4), 1058–1066. doi:10.1016/j.engstruct.2007.07.005

Chou, C. C., & Uang, C.-M. (2000). Establishing absorbed energy spectra - An attenuation approach. *Earthquake Engineering and Structural Dynamics*, *29*(10), 1441–1455. doi:10.1002/1096-9845(200010)29:10<1441::AID-EQE967>3.0.CO;2-E

CNR-DT 200/2004. (2004). *Guide for the design and construction of externally bonded FRP systems for strengthening existing structures*. National Research Council - Advisory Committee on Technical Recommendations for Construction.

Cosenza, E., & Manfredi, G. (1997). The improvement of the seismic-resistant design for existing and new structures using damage criteria. In P. Fajfar & H. Krawinkler (Eds.), *Seismic design methodologies for the next generation of codes* (pp. 119–30). Rotterdam: Balkema.

Cosenza, E., & Manfredi, G. (2000). Damage incides and damage measures. *Progress in structural engineering and materials*, *2*(1), 50-59. doi: 10.1002/(sici)1528-2716(200001/03)2:1<50::aid-pse7>3.0.co;2-s

Crowley, H., Colombi, M., Borzi, B., Faravelli, M., Onida, M., Lopez, M., … Pinho, R. (2009). A comparison of seismic risk maps for Italy. *Bulletin of Earthquake Engineering*, *7*(1), 149–180. doi:10.1007/s10518-008-9100-7

Cuzzilla, R., Di Ludovico, M., Prota, A., & Manfredi, G. (2011). Seismic rehabilitation of RC bridges by using FRP and SRP : case study of a bridge in the south of Italy. In Y. J. Kim (Ed.), *Recent advances in maintenance and repair of concrete bridges* (pp. 1–20), *ACI Special Publication, SP-277*-1, American Concrete Institute. doi:10.14359/51682366

Dargush, G. F., & Sant, R. S. (2005). Evolutionary aseismic design and retrofit of structures with passive energy dissipation. *Earthquake Engineering and Structural Dynamics*, *34*(13), 1601–1626. doi:10.1002/eqe.497

Darwin, D., & Nmai, C. (1986). Energy dissipation in RC beams under cyclic load. *Journal of Structural Engineering*, *112*(8), 1829–1846. doi:10.1061/(ASCE)0733-9445(1986)112:8(1829)

De Luca, F., Verderame, G. M., Gómez-Martínez, F., & Pérez-García, A. (2013). The structural role played by masonry infills on RC building performances after the 2011 Lorca, Spain, earthquake. *Bulletin of Earthquake Engineering*, *12*(5), 1999-2026. doi:10.1007/s10518-013-9500-1

Decanini, L. D., De Sortis, A., Goretti, A., Liberatore, L., Mollaioli, F., & Bazzurro, P. (2004). Performance of reinforced concrete buildings during the 2002 Molise, Italy, earthquake. *Earthquake Spectra*, *20*(S1), S221–S255. doi:10.1193/1.1765107

Decanini, L. D., & Mollaioli, F. (1998). Formulation of elastic earthquake input energy spectra. *Earthquake Engineering & Structural Dynamics*, *27*(12), 1503–1522. doi:10.1002/(SICI)1096-9845(199812)27:12<1503::AID-EQE797>3.0.CO;2-A

Decanini, L. D., & Mollaioli, F. (2001). An energy-based methodology for the assessment of seismic demand. *Soil Dynamics and Earthquake Engineering*, *21*(2), 113–137. doi:10.1016/S0267-7261(00)00102-0

Di Ludovico, M., Prota, A., Manfredi, G., & Cosenza, E. (2008). Seismic strengthening of an under-designed RC structure with FRP. *Earthquake Engineering and Structural Dynamics*, *37*(1), 141–162. doi:10.1002/eqe.749

Di Sarno, L., & Manfredi, G. (2012). Experimental tests on full-scale RC unretrofitted frame and retrofitted with buckling-restrained braces. *Earthquake Engineering and Structural Dynamics*, *41*(2), 315–333. doi:10.1002/eqe.1131

Di Sarno, L., & Manfredi, G. (2008). Seismic assessment of a RC school building retrofitted with innovative braces. In M. G. Alexander, H. D. Beushausen , F. Dehn , and P. Moyo (Eds.) *Concrete Repair, Rehabilitation and Retrofitting II* (pp. 409–410). Boca Raton, FL: CRC Press. doi: 10.1201/9781439828403.ch162

Dolce, M., Cardone, D., & Croatto, F. (2005). Frictional behavior of steel-PTFE interfaces for seismic isolation. *Bulletin of Earthquake Engineering*, *3*(1), 75–99. doi:10.1007/s10518-005-0187-9

Dolce, M., & Manfredi, G. (2011). *Linee Guida per riparazione e rafforzamento di elementi strutturali, tamponature e partizioni*. Rete dei Laboratori Universitari di Ingegneria Sismica (ReLUIS). Retrieved from http://www.reluis.it/doc/pdf/Linee_guida1.pdf

Donaire-Ávila, J., Benavent-Climent, A., Escobedo, A., Oliver-Saiz, E., Ramirez-Marquez, A. L., & Feriche, M. (2012). Damage assessment on building structures subjected to the recent near-fault earthquake in Lorca (Spain). *Proceedings of the 15th World Conference on Earthquake Engineering*. Lisbon, Portugal.

Dove, R., & Bennett, J. (1986). *Scale modeling of reinforced concrete category I structures subjected to seismic loading* (No. LA-10624-MS). Los Alamos, NM: Los Alamos National Laboratory.

EH-91. (1991). *Instrucción para el proyecto y la ejecución de obras de hormigón en masa o armado* (RD 1039/1991 de 28 de Junio). Madrid: Ministerio de Obras Públicas y Transportes.

EHE-08. (2008). *Instrucción de Hormigón Estructural* (RD 1247/2008 de 18 de Julio). Madrid: Ministerio de la Presidencia.

EHE-98. (1998). *Instrucción de Hormigón Estructural* (RD 2661/1998 de 11 de Diciembre). Madrid: Ministerio de Fomento.

Elwood, K. J. (2004). Modelling failures in existing reinforced concrete columns. *Canadian Journal of Civil Engineering*, *31*(5), 846–859. doi:10.1139/l04-040

EN 15129:2009 (2009). *Anti-seismic devices*. Brussels: European Committee for Standardization.

EN 1992-1-1:2004. (2004). *Eurocode 2: Design of concrete structures - Part 1-1: General rules and rules for buildings*. Brussels: European Commitee for Standardization.

EN 1998-1:2004 (2004) *Eurocode 8: Design of Structures for earthquake resistance – Part 1: General rules, seismic actions and rules for buildings*. Brussels: European Committee for Standardization.

EN 1998-3:2005. (2005). *Eurocode 8: Design of structures for earthquake resistance - Part 3: Assessment and retrofitting of buildings*. Brussels: European Commitee for Standardization.

ETAG 001. (1997). *Guideline for European Technical Approval of metal anchors for use in concrete*. Brussels: European Organisation for Technical Approvals.

Fajfar, P., & Vidic, T. (1994). Consistent inelastic design spectra: hysteretic and input energy. *Earthquake Engineering & Structural Dynamics*, *23*(5), 523–537. doi:10.1002/eqe.4290230505

Fajfar, P., Vidic, T., & Fischinger, M. (1990). A measure of earthquake motion capacity to damage medium-period structures. *Soil Dynamics*

and Earthquake Engineering, *9*(5), 236–242. doi:10.1016/S0267-7261(05)80002-8

Fajfar, P., Vidic, T., & Fischinger, M. (1992). On energy demand and supply in SDOF systems. In P. Fajfar & H. Krawinkler (Eds.) *Nonlinear seismic analisis and design of reinforced concrete buildings* (pp. 48–71). New York, NY: Elsevier Applied Science.

Fardis, M. N. (2009). *Seismic design, assessment and retrofitting of concrete buildings: based on EN-Eurocode 8* (Vol. 8). In A. Ansal (Series Ed.), *Geotechnical, Geological and Earthquake Engineering*. Dordrecht: Springer Netherlands. doi:10.1007/978-1-4020-9842-0

Fardis, M. N. (2010). *Advances in performance-based earthquake engineering* (Vol. 13). In A. Ansal (Series Ed.), *Geotechnical, geological and earthquake engineering*. Dordrecht: Springer Netherlands. doi:10.1007/978-90-481-8746-1

FEMA 154. (2002). *Rapid visual screening of buildings for potential seismic hazards: a handbook*. Washington, DC: prepared by the Applied Technology Council (Report No. ATC- 21, 1988) for the Federal Emergency Management Agency.

FEMA 178. (1992) *NEHRP Handbook for the seismic evaluation of existing buildings*. Washington, DC: prepared by the Building Seismic Safety Council for the Federal Emergency Management Agency.

FEMA 273. (1997). *NEHRP Guidelines for the seismic rehabilitation of buildings*. Washington, DC: prepared by the Applied Technology Council for the Building Seismic Safety Council, published by the Federal Emergency Management Agency.

FEMA 274. (1997). *NEHRP Commentary on the guidelines for the seismic rehabilitation of buildings*. Washington, DC: prepared by the Applied Technology Council, for the Building Seismic Safety Council, published by the Federal Emergency Management Agency.

FEMA 302. (1997). *NEHRP Recommended provisions for seismic regulations for new buildings and other structures*. Washington, DC:

prepared by the Building Seismic Safety Council for the Federal Emergency Management Agency.

FEMA 343. (1999). *Case studies: an assessment of the NEHRP guidelines for the seismic rehabilitation of buildings*. Washington, DC: prepared by the Building Seismic Safety Council for the Federal Emergency Management Agency.

FEMA 356. (2000). *Prestandard and commentary for the seismic rehabilitation of buildings*. Washington, DC: prepared by the American Society of Civil Engineers for the Federal Emergency Management Agency.

FEMA 445. (2006). *Next-generation performance-based seismic design guidelines: program plan for new and existing buildings*. Washington, DC: prepared by the Applied Technology Council for the Federal Emergency Management Agency.

FEMA 547. (2006). *Techniques for the seismic rehabilitation of existing buildings*. Washington, DC: prepared by Rutherford & Chekene (R & C) Consulting Engineers for the National Institute of Standards and Technology, published by the Federal Emergency Management Agency.

FEMA P-58-1. (2012). *Methodology* (Vol. 1). In *Seismic performance assessment of buildings.* Washington, DC: prepared by the Applied Technology Council for the Federal Emergency Management Agency.

FEMA P-58-2. (2012). *Implementation guide* (Vol. 2). In *Seismic performance assessment of buildings.* Washington, DC: prepared by the Applied Technology Council for the Federal Emergency Management Agency.

Feriche, M., Vidal, F., Alguacil, G., Navarro, M., & Aranda, C. (2012). Vulnerabilidad y daño en el terremoto de Lorca de 2011. *Actas de la 7ª Asamblea hispano-portuguesa de Geodesia y Geofísica.* San Sebastián, España.

Filippou, F. C., Popov, E. P., & Bertero, V. V. (1983). *Effects of bond deterioration on hysteretic behaviour of reinforced concrete joints* (No.

UCB/EERC-83/19). Berkeley, CA: Earthquake Engineering Research Center, College of Engineering, University of California.

Frosch, R. J., Li, W., Jirsa, J. O., & Kreger, M. E. (1996). Retrofit of non-ductile moment-resisting frames using precast infill wall panels. *Earthquake Spectra*, *12*(4), 741–760. doi:10.1193/1.1585908

Galal, K., Arafa, A., & Ghobarah, A. (2005). Retrofit of RC square short columns. *Engineering Structures*, *27*(5), 801–813. doi:10.1016/j.engstruct.2005.01.003

Gluck, N., Reinhorn, A. M., Gluck, J., & Levy, R. (1996). Design of supplemental dampers for control of structures. *Journal of Structural Engineering*, *122*(12), 1394–1399. doi:10.1061/(ASCE)0733-9445(1996)122:12(1394)

Goel, S. C., & Masri, A. C. (1996). Seismic strengthening of an RC slab-column frames with ductile steel bracing. *Proceedings of the 11th World Conference on Earthquake Engineering.* Acapulco, Mexico.

Harris, H., & Sabnis, G. (1999). *Structural modeling and experimental techniques* (2nd ed.). Boca Raton, FL: CRC Press.

Haselton, C. B., Goulet, C. A., Mitrani-Reiser, J., Beck, J. L., Deierlein, G. G., Porter, K. A., … Taciroglu, E. (2008). *An assessment to benchmark the seismic performance of a code-conforming reinforced concrete moment-frame building* (No. PEER 2007/12). Berkeley, CA: Pacific Earthquake Engineering Research Center, College of Engineering, University of California.

Housner, G. W. (1956). Limit design of structures to resist earthquakes. *Proceedings of the 1st World Conference on Earthquake Engineering.* Berkeley, CA.

Huang, X., Birman, V., Nanni, A., & Tunis, G. (2005). Properties and potential for application of steel reinforced polymer and steel reinforced grout composites. *Composites Part B: Engineering*, *36*(1), 73–82. doi:10.1016/S1359-8368(03)00080-5

Ibarra, L. F., & Krawinkler, H. (2005). *Global collapse of frame structures under seismic excitations* (No. PEER 2005/06). Berkeley, CA: Pacific Earthquake Engineering Research Center, College of Engineering, University of California.

Ibarra, L. F., Medina, R. A., & Krawinkler, H. (2005). Hysteretic models that incorporate strength and stiffness deterioration. *Earthquake Engineering & Structural Dynamics*, *34*(12), 1489–1511. doi:10.1002/eqe.495

Ichikawa, Y., Okayasu, T., Nakamura, H., Yamada, S., & Wada, A. (2005). Experimental study on joint of seismic retrofitting brace for steel structure using shear-key plate adhered to concrete slab. *Journal of Structural and Construction Engineering, AIJ*, (596), 133–140.

Instituto Nacional de Estadística. (2013). *Censos de Población y Viviendas 2011. Edificios y viviendas. Datos provisionales*. Retrieved from http://www.ine.es/prensa/np775.pdf

Inoue, K., & Kuwahara, S. (1998). Optimum strength ratio of hysteretic damper. *Earthquake Engineering & Structural Dynamics*, *27*(6), 577–588. doi:10.1002/(SICI)1096-9845(199806)27:6<577::AID-EQE743>3.0.CO;2-U

Instituto Geográfico Nacional. (2012). *Actualización de mapas de peligrosidad sísmica de España 2012*. Madrid: Centro Nacional de Información Geográfica.

Ioannou, I., Borg, R., Novelli, V., Melo, J., Alexander, D., Kongar, I., … Rossetto, T. (2012) *The 29th May 2012 Emilia Romagna Earthquake* (No. EPI-FO-290512). London: UCL EPICentre.

Istituto Nazionale di Statistica. (1991). *13º Censimento generale della popolazione e delle abitazioni.*

JBDPA. (2005). *Recent development of seismic retrofit methods in Japan*. Tokyo: Japan Building Disaster Prevention Association. Retrieved from http://www.kenchiku-bosai.or.jp/files/2013/11/srm.pdf

JBDPA. (2001). *Standard for seismic evaluation of existing reinforced concrete buildings*. Tokyo: Japan Building Disaster Prevention Association.

JBDPA. (1977). *Standard for seismic capacity evaluation of existing reinforced concrete buildings*. Tokyo: Japan Building Disaster Prevention Association.

Jirsa, J. O., & Kreger, M. E. (1989). Recent research on repair and strengthening of reinforced concrete structures. In C. A. Kircher & A. K. Chopra (Eds.) *Seismic engineering, research and practice*. New York, NY: American Society of Civil Engineers

Kachlakev, D., Miller, T., Yim, S., Chansawat, K., & Potisuk, T. (2001). *Finite element modeling of reinforced concrete structures strengthened with FRP laminates* (No. SPR 316). Salem, OR: Oregon Department of Transportation. Retrieved from http://ntl.bts.gov/lib/18000/18100/18175/PB2001107345.pdf

Karabinis, a. I., & Rousakis, T. C. (2002). Concrete confined by FRP material: a plasticity approach. *Engineering Structures*, *24*(7), 923–932. doi:10.1016/S0141-0296(02)00011-1

Karami Mohammadi, R., El Naggar, M. H., & Moghaddam, H. (2004). Optimum strength distribution for seismic resistant shear buildings. *International Journal of Solids and Structures*, *41*(22-23), 6597–6612. doi:10.1016/j.ijsolstr.2004.05.012

Karayannis, C. G., Chalioris, C. E., & Sirkelis, G. M. (2008). Local retrofit of exterior RC beam-column joints using thin RC jackets - An experimental study. *Earthquake Engineering and Structural Dynamics*, *37*(5), 727–746. doi:10.1002/eqe.783

Karsan, I. D., & Jirsa, J. O. (1969). Behavior of concrete under compressive loading. *Journal of the Structural Division, 95*(12), 2543–2563.

Kent, D. C., & Park, R. (1971). Flexural members with confined concrete. *Journal of the Structural Division*, *97*(7), 1969–1990.

Khampanit, A., Leelataviwat, S., Kochanin, J., & Warnitchai, P. (2014). Energy-based seismic strengthening design of non-ductile reinforced concrete frames using buckling-restrained braces. *Engineering Structures*, *81*, 110–122. doi:10.1016/j.engstruct.2014.09.033

Kobori, T., Miura, Y., Fukuzawa, E., Yamada, T., Arita, T., Takenaka, Y., … Fukumoto, T. (1992). Development and application of hysteresis steel dampers. *Proceedings of the 10th World Conference on Earthquake Engineering*. Madrid, Spain.

Kunnath, S. K., & Chai, Y. H. (2004). Cumulative damage-based inelastic cyclic demand spectrum. *Earthquake Engineering and Structural Dynamics*, *33*(4), 499–520. doi:10.1002/eqe.363

Kuwamura, H., & Galambos, T. V. (1989). Earthquake load for structural reliability. *Journal of Structural Engineering*, *115*(6), 1446–1462. doi:10.1061/(ASCE)0733-9445(1989)115:6(1446)

Liel, A. B., & Deierlein, G. G. (2008). *Assessing the collapse risk of California's existing reinforced concrete frame structures: metrics for seismic safety decisions* (Report No. 166). Stanford, CA: The John A. Blume Earthquake Engineering Center.

Liel, A. B., Haselton, C. B., & Deierlein, G. G. (2011). Seismic collapse safety of reinforced concrete buildings. II: comparative assessment of nonductile and ductile moment frames. *Journal of Structural Engineering*, *137*(4), 492–502. doi:10.1061/(ASCE)ST.1943-541X.0000275

Lowes, L. N., & Altoontash, A. (2003). Modeling reinforced-concrete beam-column joints subjected to cyclic loading. *Journal of Structural Engineering*, *129*(12), 1686–1697. doi:10.1061/(ASCE)0733-9445(2003)129:12(1686)

M. V. 101-1962. (1963). *Acciones en la edificación* (D 195/1963 de 17 de enero). Madrid: Ministerio de la vivienda.

Maekawa, K., Pimanmas, A., & Okamura, H. (2003). *Nonlinear mechanics of reinforced concrete*. New York, NY: Spon Press.

Manfredi, G. (2001). Evaluation of seismic energy demand. *Earthquake Engineering & Structural Dynamics*, *30*(4), 485–499. doi:10.1002/eqe.17

Manfredi, G., Polese, M., & Cosenza, E. (2003). Cumulative demand of the earthquake ground motions in the near source. *Earthquake Engineering & Structural Dynamics*, *32*(12), 1853–1865. doi:10.1002/eqe.305

Mapei. (2010). *MapeWrap S Fabric – Technical data sheet*. Retrieved from http://www.mapei.com/public/COM/products/1038_mapewrap_s_fabric_gb.pdf

Martinelli, P., & Filippou, F. C. (2009). Simulation of the shaking table test of a seven-story shear wall building. *Earthquake Engineering & Structural Dynamics*, *38*(5), 587–607. doi:10.1002/eqe.897

Martinez-Rueda, J. E. (2002). On the evolution of energy dissipation devices for seismic design. *Earthquake Spectra*, *18*(2), 309–346. doi:10.1193/1.1494434

Masi, A. (2003). Seismic vulnerability assessment of gravity load designed R/C frames. *Bulletin of Earthquake Engineering*, *1*(3), 371–395. doi:10.1023/B:BEEE.0000021426.31223.60

Matsagar, V. A., & Jangid, R. S. (2008). Base isolation for seismic retrofitting of structures. *Practice Periodical on Structural Design and Construction*, *13*(4), 175–185. doi:10.1061/(ASCE)1084-0680(2008)13:4(175)

Mazza, F. (2014). Displacement-based seismic design of hysteretic damped braces for retrofitting in-plan irregular r.c. framed structures. *Soil Dynamics and Earthquake Engineering*, *66*, 231–240. doi:10.1016/j.soildyn.2014.07.001

McKenna, F., Fenves, G. L., Scott, M. H., & Jeremic, B. (2000). OpenSees: Open System for Earthquake Engineering Simulation [Computer software]. Berkeley (CA): Pacific Earthquake Engineering Research Center, University of California. Retrieved from http://opensees.berkeley.edu

Medeot, R. (2014). Application and revision of the european Norm EN 15129 on anti-seismic devices. *Proceedings of the 2nd European Conference on Earthquake Engineering and Seismology*. Istanbul, Turkey.

Medina, R., & Krawinkler, H. (2004). *Seismic demands for nondeteriorating frame structures and their dependence on ground motions* (No. PEER 2003/15). Berkeley, CA: Pacific Earthquake Engineering Research Center, College of Engineering, University of California.

Mirmiran, A., & Shahawy, M. (1997). Behavior of concrete columns confined by fiber composites. *Journal of Structural Engineerin*, *123*(5), 583–590. doi: 10.1061/(ASCE)0733-9445(1997)123:5(583)

Mitra, N., & Lowes, L. N. (2007). Evaluation, calibration, and verification of a reinforced concrete beam-column joint model. *Journal of Structural Engineering*, *133*(1), 105–120. doi: 10.1061/(ASCE)0733-9445(2007)133:1(105)

Moehle, J., & Deierlein, G. G. (2004). A framework methodology for performance-based earthquake engineering. *Proceedings of the 13th World Conference on Earthquake Engineering*. Vancouver, Canada.

Moehle, J. P. (2000). State of research on seismic retrofit of concrete building structures in the US. *US-Japan Symposium and Workshop on Seismic Retrofit of Concrete Structures – State of research and practice*.

Monjo Carrió, J. (2005). La evolución de los sistemas constructivos en la edificación. Procedimientos para su industrialización. *Informes de La Construcción*, *57*(499–500), 37-54. doi:10.3989/ic.2005.v57.i499-500.481

Moreschi, L. M., & Singh, M. P. (2003). Design of yielding metallic and friction dampers for optimal seismic performance. *Earthquake Engineering and Structural Dynamics*, *32*(8), 1291–1311. doi:10.1002/eqe.275

Nakashima, M., Iwai, S., Iwata, M., Takeuchi, T., Konomi, S., Akazawa, T., & Saburi, K. (1994). Energy dissipation behaviour of shear panels made of low yield steel. *Earthquake Engineering & Structural Dynamics*, *23*(12), 1299–1313. doi:10.1002/eqe.4290231203

NBE AE-88. (1988). *Acciones en la edificación* (RD 1370/1988 de 11 de Noviembre). Madrid: Ministerio de Obras Públicas y Urbanismo.

NCSE-02. (2002). *Norma de Construcción Sismorresistente: parte general y edificación* (RD 997/2002 de 27 de Septiembre). Madrid: Ministerio de Fomento.

NCSE-94. (1994). *Norma de Construcción Sismorresistente: parte general y edificación* (RD 2543/1994 de 29 de Diciembre). Madrid: Ministerio de Obras Públicas, Transportes y Medio Ambiente.

Neuenhofer, A., & Filippou, F. C. (1997). Evaluation of nonlinear frame finite element models. *Journal of Structural Engineering, 123*(7), 958-966. doi: 10.1061/(ASCE)0733-9445(1997)123:7(958)

Newmark, N., & Hall, W. (1982). *Earthquake spectra and design. Earthquake* (Vol. 3). In M. S. Agbabian (Series Ed.), *Engineering Monographs on Earthquake Criteria, Structural Design, and Strogn Motion Records.* Berkeley, CA: Earthquake Engineering Research Institute.

NTC 2008. (2008). *Norme Tecniche per le Costruzioni* (D.M. 14 Gennaio 2008). Ministero delle Infrastrutture.

Observatorio ITE. (2013). *Informe estadístico anual / 2013*. Valladolid: Instituto de la Construcción de Castilla y León. Retrieved April 10, 2015 from http://www.iteweb.es/estadisticasAnuales

Observatorio ITE. (2014). *Informe estadístico anual / 2014*. Valladolid: Instituto de la Construcción de Castilla y León. Retrieved April 10, 2015 from http://www.iteweb.es/estadisticasAnuales

Oh, S.-H., Kim, Y.-J., & Ryu, H.-S. (2009). Seismic performance of steel structures with slit dampers. *Engineering Structures*, *31*(9), 1997–2008. doi:10.1016/j.engstruct.2009.03.003

Otani, S., Kaneko, T., & Shiohara, H. (2003). Strain rate effect on performance of reinforced concrete members. In *Proceedings of the FIB Symposium on Concrete Structures in Seismic Regions.* Athens, Greece.

Oviedo A., J. A., Midorikawa, M., & Asari, T. (2010). Earthquake response of ten-story story-drift-controlled reinforced concrete frames with hysteretic dampers. *Engineering Structures*, *32*(6), 1735–1746. doi:10.1016/j.engstruct.2010.02.025

Ozaki, H., Harada, H., & Murakami, K. (2008). Challenging applications of seismic dampers for retrofit of tall building. *Proceedings of the 14th World Conference on Earthquake Engineering*. Beijing, China.

Pacific Earthquake Engineering Research Center. (2013). *PEER NGA-West2 Ground Motion Database*. Retrieved from http://ngawest2.berkeley.edu

Pacific Earthquake Engineering Research Center. (2010). *Technical report for the peer ground motion database web application*. Retrieved from http://ngawest2.berkeley.edu/Technical_Report.pdf

Panagiotakos, T., & Fardis, M. N. (2001). Deformations of reinforced concrete members at yielding and ultimate. *ACI Structural Journal*, *98*(2), 135–148. doi:10.14359/10181

Park, H., & Eom, T. (2006). A simplified method for estimating the amount of energy dissipated by flexure-dominated reinforced concrete members for moderate cyclic deformations. *Earthquake Spectra*, *22*(2), 459–490. doi:10.1193/1.2197547

Park, R., & Paulay, T. (1975). *Reinforced concrete structures*. New York, NY: Wiley-Interscience.

Park, Y., & Ang, A. (1985). Mechanistic seismic damage model for reinforced concrete. *Journal of Structural Engineering*, *111*(4), 722–739. doi:10.1061/(ASCE)0733-9445(1985)111:4(722)

PDS-1. (1974). *Norma sismorresistente* (D 3209/1974 de 30 de Agosto). Madrid: Ministerio de Planificación del Desarrollo.

Pekelnicky, R., & Poland, C. (2012). ASCE 41-13: Seismic evaluation and retrofit of existing buildings. *Proceedings of the SEAOC 2012 Convention*. Santa Fe, New Mexico.

PGS-1. (1968). *Norma sismorresistente* (D 106/1969 de 16 de Enero). Madrid.

Priestley, M. J. N. (1993). Myths and fallacies in earthquake engineering – conflicts between design and reality. *Bulletin of the New Zealand Society for Earthquake Engineering*, *26*(3), 329–341.

Priestley, M. J. N. (2007a). Fundamentals of direct displacement-based seismic design and assessment. In A. Pecker (Ed.) *Advanced Earthquake Engineering Analysis* (pp. 133–154). Vienna: Springer. doi:.1007/978-3-211-74214-3_8

Priestley, M. J. N. (2007b). The need for displacement-based design and analysis. In A. Pecker (Ed.) *Advanced Earthquake Engineering Analysis* (pp. 121–132). Vienna: Springer. doi:10.1007/978-3-211-74214-3_7

Priestley, M. J. N., Calvi, G. M., & Kowalsky, M. J. (2007). *Displacement-based seismic design of structures*. Pavia: IUSS Press.

Rae, P. J., & Dattelbaum, D. M. (2004). The properties of poly(tetrafluoroethylene) (PTFE) in compression. *Polymer*, *45*(22), 7615–7625. doi:10.1016/j.polymer.2004.08.064

Ricci, P., de Luca, F., & Verderame, G. M. (2011). 6th April 2009 L'Aquila earthquake, Italy: reinforced concrete building performance. *Bulletin of Earthquake Engineering*, *9*(1), 285–305. doi:10.1007/s10518-010-9204-8

Rueda Nuñez, J., Mezcua Rodríguez, J., & Garcia Blanco, R. M. (2013). Directividad de la fuente sísmica en el terremoto de Lorca del 11 de mayo de 2011. *Física de La Tierra*, *24*, 83–111. doi:10.5209/rev_FITE.2012.v24.40133

Ruiz-García, J., & Miranda, E. (2003). Inelastic displacement ratios for evaluation of existing structures. *Earthquake Engineering and Structural Dynamics*, *32*(8), 1237–1258. doi:10.1002/eqe.271

Scott, B. D., Park, R., & Priestley, M. J. N. (1982). Stress-strain behavior of concrete confined by overlapping hoops at low and high strain rates. *ACI Journal Proceedings*, *79*(1), 13–27. doi: 10.14359/10875

Scott, M. H., & Fenves, G. L. (2006). Plastic hinge integration methods for force-based beam–column elements. *Journal of Structural Engineering*, *132*(2), 244–252. doi:10.1061/(ASCE)0733-9445(2006)132:2(244)

SEAOC Vision 2000 Committee (1995). *Performance-Based Seismic Engineering*. Sacramento, CA: Report prepared by Structural Engineers Association of California.

Soong, T. T., & Spencer Jr, B. F. (2002). Supplemental energy dissipation: state-of-the-art and state-of-the- practice, *Engineering Structures, 24*(3), 243–259. doi: 10.1016/S0141-0296(01)00092-X

Spacone, E., Filippou, F. C., & Taucer, F. F. (1996). Fibre beam-column model for non-linear analysis of R/C frames: Part I. Formulation. *Earthquake Engineering & Structural Dynamics*, *25*(7), 711–725. doi:10.1002/(SICI)1096-9845(199607)25:7<711::AID-EQE576>3.0.CO;2-9

Symans, M. D., Charney, F. A., Whittaker, A. S., Constantinou, M. C., Kircher, C. A., Johnson, M. W., & McNamara, R. J. (2008). Energy dissipation systems for seismic applications: current practice and recent developments. *Journal of Structural Engineering*, *134*(1), 3-21. doi:10.1061/(ASCE)0733-9445(2008)134:1(3)

Taucer, F. F., Spacone, E., & Filippou, F. C. (1991). *A fiber beam-column element for seismic response analysis of reinforced concrete structures* (No. UCB/EERC-91/17). Berkeley, CA: Earthquake Engineering Research Center, College of Engineering, University of California.

Trifunac, M., & Brady, A. (1975). A study on the duration of strong earthquake ground motion. *Bulletin of the Seismological Society of America*, *65*(3), 581–626.

Tsai, K. C., Chen, H. W., Hong, C. P., & Su, Y. F. (1993). Design of steel triangular plate energy absorbers for seismic-resistant construction. *Earthquake Spectra, 9*(3), 505–528. doi:10.1193/1.1585727

Uang, C. M., & Bertero, V. V. (1990). Evaluation of seismic energy in structures. *Earthquake Engineering & Structural Dynamics*, *19*(1), 77–90. doi:10.1002/eqe.4290190108

Uetani, K., Tsuji, M., & Takewaki, I. (2003). Application of an optimum design method to practical building frames with viscous dampers and hysteretic dampers. *Engineering Structures*, *25*(5), 579–592. doi:10.1016/S0141-0296(02)00168-2

Uzumeri, S. M. (1977). Strength and ductility of cast-in-place beam-column joints. In N. M. Hawkins and D. Mitchell (Eds.), *Reinforced concrete structures in seismic zones* (pp. 293–350), *ACI Special Publication, SP-53-12*, American Concrete Institute. doi: 10.14359/17701

Veletsos, A. S., & Newmark, N. M. (1960). Effect of inelastic behavior on the response of simple systems to earthquake motions. *Proceedings of the 2nd World Conference on Earthquake Engineering*. Japan.

Verderame, G. M., De Luca, F., Ricci, P., & Manfredi, G. (2011). Preliminary analysis of a soft-storey mechanism after the 2009 L'Aquila earthquake. *Earthquake Engineering and Structural Dynamics*, *40*(8), 925–944. doi:10.1002/eqe.1069

Verderame, G. M., Ricci, P., De Luca, F., Del Gaudio, C., & De Risi, M. T. (2014). Damage scenarios for RC buildings during the 2012 Emilia (Italy) earthquake. *Soil Dynamics and Earthquake Engineering*, *66*, 385–400. doi:10.1016/j.soildyn.2014.06.034

Villaverde, R. (2007). Methods to assess the seismic collapse capacity of building structures: state of the art. *Journal of Structural Engineering*, *133*(1), 57–66. doi: 10.1061/(ASCE)0733-9445(2007)133:1(57)

Watanabe, A., Hitomi, Y., Saeki, E., Wada, A., & Fujimoto, M. (1988). Properties of brace encased in buckling-restraining concrete and steel tube. *Proceedings of the 9th World Conference on Earthquake Engineering*. Tokyo-Kyoto, Japan.

Xie, Q. (2005). State of the art of buckling-restrained braces in Asia. *Journal of Constructional Steel Research*, *61*(6), 727–748. doi:10.1016/j.jcsr.2004.11.005

Zareian, F., & Krawinkler, H. (2006). *Simplified performance-based earthquake engineering* (Report No. 169). Stanford, CA: The John A. Blume Earthquake Engineering Center.

Zareian, F., & Medina, R. A. (2010). A practical method for proper modeling of structural damping in inelastic plane structural systems. *Computers & Structures*, *88*(1-2), 45–53. doi:10.1016/j.compstruc.2009.08.001

Zia, P., White, R. N., & Vanhorn, D. A. (1970). Principles of model analysis. In R. N. White (Ed.), *Models of concrete structures* (pp. 19–40), *ACI Special Publication, SP-24-02*, American Concrete Institute. doi:10.14359/17583